

Drivers of plant nutrient acquisition and allocation strategies and their influence
on plant responses to environmental change

by

Evan A. Perkowski, B.S.

A Dissertation

In

Biological Sciences

Submitted to the Graduate Faculty
of Texas Tech University in
Partial Fulfillment of
the Requirements for
the Degree of

Doctor of Philosophy

Approved

Nicholas G. Smith, Ph.D.
Chair of Committee

Aimée T. Classen, Ph.D.

Natasja van Gestel, Ph.D.

Lindsey C. Slaughter, Ph.D.

Dylan W. Schwilk, Ph.D.

Mark Sheridan, Ph.D.
Dean of the Graduate School

May 2023

Copyright 2023, Evan A. Perkowski

Acknowledgements

This dissertation was made possible by the mentorship, collaboration, and friendship of many people. I am so thankful to be surrounded by such supportive and helpful mentors, peers, and friends that have made navigating through graduate school and finishing this dissertation an enjoyable experience. Specifically, I am thankful for the incredible mentorship of my advisor and committee chair, Dr. Nick Smith, who provided invaluable insight and tools that have helped shape me into the plant ecophysiological I claim to be today. I am also indebted to my committee members, Drs. Aimée Classen, Natasja van Gestel, Dylan Schwilk, and Lindsey Slaughter, for useful feedback, invaluable support, and encouragement as I planned and implemented experiments.

I am also thankful for past and present members of the EcoHealth lab for encouragement, support, and extracurricular activities that made time inside and outside the lab enjoyable and memorable. Particular thanks go to Dr. Lizz Waring, Dr. Xiulin Gao, Helen Scott, and Risa McNellis, Billi Jean Petermann, and the late Dr. Kris Petterson, all of whom were invaluable to helping me navigate my first year. I am especially thankful for the mentorship and friendship of Dr. Lizz Waring, as our weekly coffee chats were instrumental for helping me feel welcome in Lubbock and acclimate to life as a graduate student. I am also grateful for the friendship of Billi Jean Petermann and the late Dr. Kris Petterson for their encouragement and willingness to discuss microbial symbioses over coffee on random Saturday mornings.

Additional thanks go out to Isa Beltran, Snehanjana Chatterjee, Jeff Chi-

eppa, Peter Eludini, Zinny Ezekannagha, Hannah German, Eve Gray, Monika Kelley, Azaj Mahmud, Jorge Ochoa, Brad Posch, Avery Schoenherr, and Jose Villeda for help with experiments or for lending an ear over puzzling results. I am also thankful for collaborators Dr. Christy Goodale and Dave Frey, who provided invaluable insight for the second experimental chapter.

I would like to thank my undergraduate advisor, Dr. Janice Krumm, for continued mentorship and friendship and for insightful advice about navigating graduate school, but most of all for helping me realize my career aspirations and pushing me to pursue this endeavor. Additional thanks go out to my family, particularly my parents, partner, and dog for continued support and distractions outside the lab. The experiments included here would not have been possible without their emotional and monetary support.

This work was made possible from funding by the NSF, USDA, Braun and Gresham, PLLC., and was a contribution to the LEMONTREE (Land Ecosystem Models based On New Theory, obseRvations and ExperimEnts) project. The LEMONTREE project is funded through the generosity of Eric and Wendy Schmidt by recommendation of the Schmidt Futures programme and the Imperial College initiative on Grand Challenges in Ecosystems and the Environment. This work was also funded by graduate student research awards from Texas Tech University and the Botanical Society of America.

I have inevitably missed mentioning folks that were instrumental to the completion of these experiments and contributed to my development as a plant physiological ecologist. Please know that I am grateful and appreciative of our interactions.

Table of Contents

Acknowledgements	ii
Abstract	ix
List of Tables	xi
List of Figures	xv
1. Introduction	1
2. Structural carbon costs to acquire nitrogen are determined by nitrogen and light availability in two species with different nitrogen acquisition strategies	7
2.1 Introduction	7
2.2 Methods	11
2.2.1 <i>Experiment setup</i>	11
2.2.2 <i>Plant measurements and calculations</i>	12
2.2.3 <i>Statistical analyses</i>	13
2.3 Results	15
2.3.1 <i>Carbon costs to acquire nitrogen</i>	15
2.3.2 <i>Whole plant nitrogen biomass</i>	18
2.3.3 <i>Root carbon biomass</i>	20
2.3.4 <i>Root nodule biomass</i>	22
2.4 Discussion	26
2.4.1 <i>Carbon costs to acquire nitrogen increase with light availability and decrease with fertilization</i>	26
2.4.2 <i>Modeling implications</i>	28
2.4.3 <i>Study limitations</i>	30
2.4.4 <i>Conclusions</i>	32
3. Soil nitrogen availability modifies leaf nitrogen economies in mature temperate deciduous forests: a direct test of photosynthetic least-cost theory	34
3.1 Introduction	34

3.2	Methods	38
3.2.1	<i>Study site description</i>	38
3.2.2	<i>Experimental design</i>	39
3.2.3	<i>Leaf gas exchange and trait measurements</i>	39
3.2.4	A_{net}/C_i curve-fitting and parameter estimation	42
3.2.5	<i>Proportion of leaf nitrogen allocated to photosynthesis and structure</i>	44
3.2.6	<i>Tradeoffs between nitrogen and water use</i>	45
3.2.7	<i>Soil nitrogen availability and pH</i>	46
3.2.8	<i>Statistical analyses</i>	48
3.3	Results	50
3.3.1	<i>Leaf nitrogen content</i>	50
3.3.2	<i>Net photosynthesis and leaf biochemistry</i>	53
3.3.3	<i>Leaf nitrogen allocation</i>	56
3.3.4	<i>Tradeoffs between nitrogen and water use</i>	59
3.4	Discussion	62
3.4.1	<i>Soil nitrogen availability modifies tradeoffs between nitrogen and water use</i>	63
3.4.2	<i>Soil pH did not modify tradeoffs between nitrogen and water usage</i>	65
3.4.3	<i>Species identity explains a large amount of variation in leaf and whole plant traits</i>	66
3.4.4	<i>Implications for photosynthetic least-cost theory model development</i>	67
3.4.5	<i>Conclusions</i>	69
4.	The relative cost of resource use for photosynthesis drives variance in leaf nitrogen content across a climate and soil resource availability gradient	70
4.1	Introduction	70
4.2	Methods	76
4.2.1	<i>Site descriptions and sampling methodology</i>	76

4.2.2 <i>Leaf trait measurements</i>	77
4.2.3 <i>Site climate data</i>	82
4.2.4 <i>Site edaphic characteristics</i>	82
4.2.5 <i>Plant functional group assignments</i>	84
4.2.6 <i>Data analysis</i>	85
4.3 Results	88
4.3.1 <i>Cost to acquire nitrogen relative to water</i>	88
4.3.2 <i>Leaf $C_i:C_a$</i>	91
4.3.3 <i>Leaf nitrogen content</i>	94
4.3.4 <i>Structural equation model</i>	98
4.4 Discussion	101
4.4.1 <i>Negative effects of leaf $C_i:C_a$ on N_{area} are driven by reductions in M_{area}, not N_{mass}</i>	101
4.4.2 <i>Soil nitrogen availability increases N_{area} through changes in β</i>	103
4.4.3 <i>Soil moisture increases N_{area} by facilitating increases in soil nitrogen availability</i>	104
4.4.4 <i>Indirect effects of climate on N_{area} are mediated through changes in leaf $C_i:C_a$ and β</i>	105
4.4.5 <i>Species identity traits modify effects of the environment on β, leaf $C_i:C_a$, and N_{area}</i>	106
4.4.6 <i>Next steps for optimality model development</i>	107
4.4.7 <i>Conclusions</i>	108
5. Optimal resource investment to photosynthetic capacity maximizes nutrient allocation to whole plant growth under elevated CO₂	109
5.1 Introduction	109
5.2 Methods	114
5.2.1 <i>Seed treatments and experimental design</i>	114
5.2.2 <i>Growth chamber conditions</i>	115
5.2.3 <i>Leaf gas exchange measurements</i>	117

5.2.4 <i>Leaf trait measurements</i>	118
5.2.5 <i>A/C_i curve fitting and parameter estimation</i>	120
5.2.6 Stomatal limitation	120
5.2.7 <i>Proportion of leaf nitrogen allocated to photosynthesis and structure</i>	121
5.2.8 <i>Whole plant traits</i>	123
5.2.9 <i>Statistical analyses</i>	125
5.3 Results	127
5.3.1 <i>Leaf nitrogen and chlorophyll content</i>	127
5.3.2 <i>Leaf biochemistry and stomatal conductance</i>	131
5.3.3 <i>Leaf nitrogen allocation</i>	135
5.3.4 <i>Whole plant traits</i>	139
5.3.5 <i>Nitrogen fixation</i>	143
5.4 Discussion	147
5.4.1 <i>Soil nitrogen fertilization has divergent effects on leaf and whole plant acclimation responses to CO₂</i>	148
5.4.2 <i>Implications for future model development</i>	152
5.4.3 <i>Study limitations and future directions</i>	153
5.4.4 <i>Conclusions</i>	155
6. Conclusions	157
References	168
Appendix A: Supplemental material for "Structural carbon costs to acquire nitrogen are determined by nitrogen and light availability in two species with different nitrogen acquisition strategies"	205
Appendix B: Supplemental material for "Soil nitrogen availability modifies leaf nitrogen economies in mature temperate deciduous forests: a direct test of photosynthetic least-cost theory"	209

Appendix C: Supplemental material for "The relative cost of resource use for photosynthesis drives variance in leaf nitrogen content across a climate and soil resource availability gradient"	214
Appendix D: Supplemental material for "Optimal resource investment to photosynthetic capacity maximizes nutrient allocation to whole plant growth under elevated CO₂" . . .	221

Abstract

Photosynthesis is the largest carbon flux between the atmosphere and is constrained by ecosystem carbon and nutrient cycle dynamics, which causes terrestrial biosphere models to be sensitive to the formulation of photosynthetic processes. Terrestrial biosphere models exhibit high divergence in simulated carbon and nitrogen fluxes under future environmental conditions, which may be due to uncertainty in the acclimation response of photosynthetic processes to environmental change. Photosynthetic least-cost theory provides a promising framework for understanding effects of climatic and edaphic factors on photosynthetic acclimation responses to changing environments. Yet, empirical tests of the theory are rare, limiting our ability to assess whether the theory is suitable for implementation in next-generation terrestrial biosphere models.

Here, I present four experiments designed to test assumptions of photosynthetic least-cost theory using a combination of greenhouse, growth chamber, field manipulation, and field gradient experiments. Experiment chapters are flanked by a general introduction chapter and conclusions chapter. The first experimental chapter quantifies structural carbon costs to acquire nitrogen in *Glycine max* and *Gossypium hirsutum* grown under four nitrogen fertilization levels and four light availability levels in a full factorial greenhouse experiment. I find that carbon costs to acquire nitrogen in both species increase with increasing light availability and decrease with increasing fertilization, though responses to fertilization in *G. max* were markedly less than *G. hirsutum*. The second experimental chapter quantifies leaf nitrogen and photosynthetic traits in upper canopy leaves of deciduous trees

growing in a 9-year nitrogen-by-sulfur field manipulation experiment. I find strong evidence for nitrogen-water use tradeoffs with increasing soil nitrogen availability, evidenced through a strong negative relationship between leaf nitrogen content and leaf $C_i:C_a$ and stronger increase in leaf nitrogen content with increasing soil nitrogen availability than leaf $C_i:C_a$. The third experiment investigates variance in leaf nitrogen content across a climate and soil resource availability gradient in Texan grasslands, showing that effects of soil resource availability and climate on leaf nitrogen content are driven by changes in leaf $C_i:C_a$. Finally, the fourth experiment quantifies leaf and whole plant acclimation responses in *G. max* grown under two atmospheric CO₂ levels, with and without inoculation with *Bradyrhizobium japonicum*, and across nine nitrogen fertilization treatments in a full factorial growth chamber experiment. I find that leaf acclimation responses to CO₂ were independent of soil nitrogen fertilization or inoculation treatment, though stimulations in whole plant growth under elevated CO₂ were enhanced with increasing soil nitrogen fertilization and in inoculated pots under low nitrogen fertilization.

Experiments included in this dissertation provide consistent support for patterns expected from photosynthetic least-cost theory. The use of multiple experimental approaches allowed me to examine mechanisms driving patterns expected from the theory and investigate whether these patterns occur naturally across environmental gradients. Findings from these chapters challenge common paradigms in plant ecophysiology, providing evidence that including photosynthetic least-cost frameworks in next-generation terrestrial biosphere models may improve the observed divergence in simulated outcomes across terrestrial biosphere model products.

List of Tables

2.1 Analysis of variance results exploring species-specific effects of light availability, nitrogen fertilization, and their interactions on carbon costs to acquire nitrogen, whole-plant nitrogen biomass, and root carbon biomass	16
2.2 Analysis of variance results exploring effects of light availability, nitrogen fertilization, and their interactions on <i>G. max</i> root nodule biomass (g) and the ratio of root nodule biomass to root biomass (g g^{-1})	23
2.3 Slopes of the regression line describing the relationship between each dependent variable and nitrogen fertilization at each light level	24
3.1 Effects of soil nitrogen availability, soil pH, and species on leaf nitrogen content per unit leaf area, leaf nitrogen content per unit leaf mass, and leaf mass per unit leaf area	51
3.2 Effects of soil nitrogen availability, soil pH, species, and N_{area} on net photosynthesis, the maximum rate of Rubisco carboxylation, the maximum rate of RuBP regeneration, and the ratio of the maximum rate of RuBP regeneration to the maximum rate of Rubisco carboxylation	54
3.3 Effects of soil nitrogen availability, soil pH, and species on the proportion of leaf nitrogen content allocated to photosynthesis, Rubisco, bioenergetics, and structure	57

3.4 Effects of soil nitrogen availability, soil pH, species, and N_{area} on χ , photosynthetic nitrogen use efficiency, leaf nitrogen content per unit χ , and maximum Rubisco carboxylation rate per unit χ	60
4.1 Site locality information, sampling year, 2006-2020 mean annual precipitation, mean annual temperature, and water holding capacity	80
4.2 Effects of soil moisture, soil nitrogen availability, and plant functional group on β	89
4.3 Effects of soil moisture, soil nitrogen availability, and plant functional group on leaf $C_i:C_a$	92
4.4 Effects of soil moisture, soil nitrogen availability, plant functional group, and leaf $C_i:C_a$ on leaf nitrogen content per unit leaf area, leaf nitrogen content per unit leaf biomass, and leaf biomass per unit leaf area	96
4.5 Structural equation model results investigating direct effects of climatic and soil resource availability on leaf nitrogen content	99
5.1 Effects of soil nitrogen fertilization, inoculation, and CO_2 treatments on N_{area} , N_{mass} , M_{area} , and Chl_{area}	129
5.2 Effects of soil nitrogen fertilization, inoculation, and CO_2 on leaf biochemistry	133
5.3 Effects of soil N availability, soil pH, species, and N_{area} on leaf nitrogen allocation	137

5.4 Effects of soil N availability, soil pH, species, and N_{area} on total leaf area, whole plant biomass, and carbon costs to acquire nitrogen	141
5.5 Effects of soil N availability, soil pH, species, and N_{area} on root nodule biomass and plant investments in symbiotic nitrogen fixation	145
A1 Summary table containing volumes of compounds used to create modified Hoagland's solutions for each soil nitrogen fertilization treatment. All volumes are expressed as milliliters per liter (mL/L)	205
A2 Analysis of variance results exploring species-specific effects of light availability, nitrogen fertilization, and their interactions on the ratio of whole plant biomass to pot volume	206
A3 Slopes of the regression line describing the relationship between each dependent variable and nitrogen fertilization at each light level*	207
B1 Sample sizes of each species, abbreviated by their USDA NRCS PLANTS database code, within each plot at each site	209
B2 Analysis of variance results exploring the linear effect of leaf temperature on net photosynthesis rate and stomatal conductance measured at $400 \mu\text{mol mol}^{-1} \text{CO}_2$	210
B3 Second order log-polynomial regression coefficients that described the effect of leaf temperature on net photosynthesis and stomatal conductance measured at $400 \mu\text{mol mol}^{-1} \text{CO}_2$	211
B4 Mean, standard error, and 95% confidence interval ranges of soil nitrogen availability estimates across all measured plots. All units are expressed as $\mu\text{g N g}^{-1} \text{resin d}^{-1}$	212

C1	List of sampled species and their plant functional group assignment	216
C2	List of sampled species and their plant functional group assignment (cont.)	217
C3	List of sampled species and their plant functional group assignment (cont.)	218
C4	Model selection results for soil moisture, air temperature, and vapor pressure deficit. Soil moisture was used in a bivariate regression against β , while vapor pressure deficit was used in bivariate regressions against leaf $C_i:C_a^*$	219
D1	Summary table containing volumes of compounds used to create modified Hoagland's solutions for each soil nitrogen fertilization treatment. All volumes are expressed as milliliters per liter (mL/L)	221
D2	Summary of the daily growth chamber growing condition program	222

List of Figures

2.1 Relationships between soil nitrogen fertilization and light availability on carbon costs to acquire nitrogen in <i>G. hirsutum</i> and <i>G. max</i>	17
2.2 Relationships between soil nitrogen fertilization and light availability on whole-plant nitrogen biomass in <i>G. hirsutum</i> and <i>G. max</i>	19
2.3 Relationships between soil nitrogen fertilization and light availability on root carbon biomass in <i>G. hirsutum</i> and <i>G. max</i>	21
2.4 Effects of shade cover and nitrogen fertilization on root nodule biomass and the ratio of root nodule biomass to root biomass in <i>G. max</i>	25
3.1 Effects of soil nitrogen availability and species on leaf nitrogen content per unit leaf area, leaf nitrogen content per unit leaf biomass, and leaf mass per leaf area	52
3.2 Effects of soil nitrogen availability, species, and leaf nitrogen content on net photosynthesis, maximum Rubisco carboxylation rate, and maximum RuBP regeneration rate	55
3.3 Effects of soil nitrogen availability, species, and leaf nitrogen content on the fraction of leaf nitrogen allocated to photosynthesis and structure	58
3.4 Effects of soil N availability, species, and leaf N content on tradeoffs between nitrogen and water use	61

4.1	Site locations along 2006-2020 mean annual precipitation and mean annual temperature gradients in Texas, USA.	81
4.2	Effects of soil nitrogen availability and soil moisture on the cost of acquiring and using nitrogen	90
4.3	Effects of 4-day mean vapor pressure deficit, 2-day soil moisture (per water holding capacity), and soil nitrogen availability on leaf $C_i:C_a$	93
4.4	Effects of leaf $C_i:C_a$, soil nitrogen availability, and soil moisture on leaf nitrogen content per unit leaf area, leaf nitrogen content per unit leaf biomass, and leaf mass per area.	97
4.5	Structural equation model results exploring drivers of N_{area}	100
5.1	Effects of CO_2 , fertilization, and inoculation on leaf nitrogen per unit leaf area, leaf nitrogen content, leaf mass per unit leaf area, and chlorophyll content per unit leaf area.	130
5.2	Effects of CO_2 , fertilization, and inoculation on maximum rate of Rubisco carboxylation, the maximum rate of RuBP regeneration, and the ratio of the maximum rate of RuBP regeneration to the maximum rate of Rubisco carboxylation leaf mass per unit leaf area, dark respiration, stomatal conductance, and stomatal limitation. .	134
5.3	Effects of CO_2 , fertilization, and inoculation on the relative fraction of leaf nitrogen allocated to photosynthesis and the fraction of leaf nitrogen allocated to structure.	138

5.4	Effects of CO ₂ , fertilization, and inoculation on total leaf area, total biomass, and structural carbon costs to acquire nitrogen.	142
5.5	Effects of CO ₂ , fertilization, and inoculation on nodule biomass, nodule: root biomass, and percent nitrogen fixed from the atmosphere.	146
A1	Effects of shade cover and nitrogen fertilization on the ratio of plant biomass to rooting volume in <i>G. hirsutum</i> and <i>G. max</i>	208
B1	Effects of leaf temperature on net photosynthesis rate and stomatal conductance values when measured at 400 $\mu\text{mol mol}^{-1}$ CO ₂ . . .	213
C1	Model selection results exploring relevant timescales for soil moisture and vapor pressure deficit	220
D1	Relationships between area-based leaf nitrogen content, mass-based leaf nitrogen content, and leaf mass per unit leaf area measured on the focal leaf used to generate A_{net}/C_i curves and leaf nitrogen content measured on the leaf used for chlorophyll extractions . . .	223
D2	Effects of CO ₂ , fertilization, and inoculation on the ratio of whole plant biomass to pot volume	224

1 **Chapter 1**
2 **Introduction**

3 Photosynthesis represents the largest carbon flux between the atmosphere
4 and biosphere, and is regulated by complex ecosystem carbon and nutrient cy-
5 cles (Hungate et al. 2003; IPCC 2021). As a result, the inclusion of robust,
6 empirically tested representations of photosynthetic processes is critical in order
7 for terrestrial biosphere models to accurately and reliably simulate carbon and
8 nutrient fluxes between the atmosphere and terrestrial biosphere (Oreskes et al.
9 1994; Smith and Dukes 2013; Prentice et al. 2015; Wieder et al. 2015). Despite
10 evidence that the inclusion of coupled carbon and nutrient cycles can improve
11 model uncertainty, widespread divergence in predicted carbon and nutrient fluxes
12 is still apparent across model products (Friedlingstein et al. 2014; Arora et al.
13 2020; Davies-Barnard et al. 2020). Divergence in predicted carbon and nutrient
14 fluxes across terrestrial biosphere models may be due to an incomplete under-
15 standing of how plants acclimate to changing environments (Smith and Dukes
16 2013; Davies-Barnard et al. 2020), as terrestrial biosphere models are sensitive to
17 the formulation of photosynthetic processes (Bonan et al. 2011; Ziehn et al. 2011;
18 Booth et al. 2012; Smith et al. 2016; Smith et al. 2017; Rogers et al. 2017).

19 Many terrestrial biosphere models predict leaf-level photosynthesis through
20 linear relationships between area-based leaf nitrogen content and the maximum
21 rate of Ribulose-1,5-bisphosphate carboxylase/oxygenase ("Rubisco"), following
22 the idea that large fractions of leaf nitrogen content are allocated to the con-
23 struction and maintenance of Rubisco and other photosynthetic enzymes (Evans

24 1989). The inclusion of coupled carbon and nutrient cycles in terrestrial bio-
25 sphere models (Shi et al. 2016; Braghieri et al. 2022) allows for the prediction
26 of leaf nitrogen content through soil nitrogen availability, which causes models to
27 indirectly predict photosynthetic processes through shifts in soil nitrogen avail-
28 ability (Smith et al. 2014; Lawrence et al. 2019). While these patterns are
29 commonly observed in ecosystems globally (Brix 1971; Evans 1989; Firn et al.
30 2019; Liang et al. 2020), this formulation does not allow for the prediction of
31 leaf and whole plant acclimation responses to changing environments (Smith and
32 Dukes 2013; Rogers et al. 2017; Harrison et al. 2021), and suggests that constant
33 leaf nitrogen-photosynthesis relationships are ubiquitous across ecosystems.

34 Photosynthetic least-cost theory (Prentice et al. 2014; Wang et al. 2017;
35 Smith et al. 2019; Scott and Smith 2022; Harrison et al. 2021) provides a con-
36 temporary framework for predicting leaf and whole plant acclimation responses
37 to environmental change. The theory, which unifies photosynthetic optimal coor-
38 dination (Chen et al. 1993; Maire et al. 2012) and least-cost (Wright et al. 2003)
39 theories, posits that plants optimize photosynthetic processes by minimizing the
40 summed cost of nutrient and water use (referred to here and in the rest of this
41 dissertation as β). The summed cost of nutrient and water use is predicted to
42 be positively correlated with the ratio of intercellular CO₂ to atmospheric CO₂
43 (referred to here and in the rest of this dissertation as leaf $C_i:C_a$). Leaf $C_i:C_a$ is
44 determined by factors that influence leaf nutrient demand, such as CO₂, temper-
45 ature, vapor pressure deficit, and light availability (Prentice et al. 2014; Wang
46 et al. 2017; Smith et al. 2019; Stocker et al. 2020), and may change in response to
47 changing edaphic characteristics through changes in β . Photosynthetic processes

48 are optimized such that nutrients are allocated to photosynthetic enzymes to allow
49 net photosynthesis rates to be equally co-limited by the maximum rate of Rubisco
50 carboxylation and the maximum rate of Ribulose-1,5-bisphosphate (RuBP) regen-
51 eration (Chen et al. 1993; Maire et al. 2012). The theory indicates that costs
52 of nutrient and water use are substitutable such that, in a given environment,
53 optimal photosynthesis rates can be achieved by sacrificing inefficient use of a
54 relatively more abundant (and less costly to acquire) resource for more efficient
55 use of a relatively less abundant (and more costly to acquire) resource.

56 Optimality models leveraging patterns expected from photosynthetic least-
57 cost theory have been developed for both C₃ (Wang et al. 2017; Smith et al. 2019;
58 Stocker et al. 2020) and more recently for C₄ species (Scott and Smith 2022). Such
59 models show broad agreement with patterns observed across environmental gradi-
60 ents (Smith et al. 2019; Paillassa et al. 2020; Querejeta et al. 2022; Westerband
61 et al. 2023), and are capable of reconciling dynamic leaf nitrogen-photosynthesis
62 relationships and acclimation responses to elevated CO₂, temperature, light avail-
63 ability, and vapor pressure deficit (Dong et al. 2017; Dong et al. 2020; Smith
64 and Keenan 2020; Luo et al. 2021; Peng et al. 2021; Dong et al. 2022; Dong
65 et al. 2022; Querejeta et al. 2022; Westerband et al. 2023). Current versions of
66 optimality models that invoke patterns expected from photosynthetic least-cost
67 theory hold β constant across growing environments. As growing evidence sug-
68 gests that costs of nutrient use change across resource availability and climatic
69 gradients in species with different nutrient acquisition strategies (Fisher et al.
70 2010; Brzostek et al. 2014; Terrer et al. 2018; Allen et al. 2020), one might
71 expect that β should dynamically change across environments and in species with

72 different nutrient acquisition strategies.

73 Despite recent recognition that patterns expected from photosynthetic
74 least-cost theory occur across broad environmental gradients, no study has investi-
75 gated how β varies across edaphic and climatic gradients aside from a single study
76 investigating variance in β due to soil water stress (Lavergne et al. 2020). Further-
77 more, no previous study has investigated whether β varies in species with different
78 nutrient acquisition strategies, or if changes in β due to changes in edaphic char-
79 acteristics scale to influence leaf or whole plant acclimation responses to changing
80 environments. The lack of these studies provided motivation for the experimental
81 chapters included in this dissertation.

82 In this dissertation, I use a combination of greenhouse, field manipulation,
83 environmental gradient, and growth chamber experiments to quantify leaf and
84 whole plant acclimation responses across various climatic and edaphic conditions
85 and different nutrient acquisition strategies. Together, these experiments eval-
86 uate patterns expected from photosynthetic least-cost theory and test mechanisms
87 predicted to drive responses expected from theory. The empirical data collected
88 in these experiments will also provide important information needed to refine ex-
89 isting optimality models that include photosynthetic least-cost frameworks, and
90 could help determine whether such models are suitable for implementing in next-
91 generation terrestrial biosphere models. While theory suggests that plants accli-
92 mate across environments by minimizing the summed cost of nutrients relative
93 to water, I choose to isolate effects of soil nitrogen availability on costs of nitro-
94 gen acquisition relative to water for the sake of brevity. Though, I acknowledge
95 that patterns expected from theory may be modified by other nutrients (e.g.,

96 phosphorus) or edaphic characteristics, and, though not included here, should be
97 investigated.

98 In the first experimental chapter, I re-analyze data from a greenhouse ex-
99 periment that grew *Glycine max* and *Gossypium hirsutum* seedlings under full-
100 factorial combinations of four light treatments and four fertilization treatments
101 to examine effects of nitrogen and light availability on structural carbon costs to
102 acquire nitrogen. In the second experimental chapter, I measure leaf physiological
103 traits in the upper canopy of mature trees growing in a 9-year nitrogen-by-pH
104 field manipulation experiment to assess whether changes in soil nitrogen availabil-
105 ity or soil pH modify nitrogen-water use trade-offs expected from photosynthetic
106 least-cost theory. The third experimental chapter leverages a broad precipitation
107 and soil nutrient availability gradient in Texan grasslands to investigate primary
108 drivers of leaf nitrogen content. In the fourth experimental chapter, I use growth
109 chambers to quantify leaf and whole plant acclimation responses to CO₂ across
110 a soil nitrogen fertilization gradient, while also manipulating nutrient acquisition
111 strategy by controlling whether seedlings were able to form associations with sym-
112 biotic nitrogen-fixing bacteria.

113 Across experiments, I find strong and consistent support for patterns ex-
114 pected from photosynthetic least-cost theory, showing that shifts in edaphic char-
115 acteristics predictably alter β , and that shifts in β facilitate changes in leaf
116 nitrogen-water use tradeoffs and leaf nitrogen-photosynthesis relationships. I also
117 show that costs of nitrogen acquisition vary in species with different nitrogen
118 acquisition strategies. Finally, I show strong evidence suggesting that leaf accli-
119 mation responses to elevated CO₂ are decoupled from soil nitrogen availability and

120 inoculation with symbiotic nitrogen-fixing bacteria. It is my hope that these ex-
121 periments will encourage future iterations of optimality models that adopt photo-
122 synthetic least-cost frameworks to consider frameworks for implementing dynamic
123 β values across soil resource availability gradients and in species with different nu-
124 trient acquisition strategies.

125 Finally, the four experimental chapters presented in this dissertation are
126 presented either as previously published journal articles (copyright clearance avail-
127 able upon request) or as manuscript drafts currently in preparation for journal
128 submission. Specifically, the first experimental chapter was published in *Journal*
129 *of Experimental Botany* in 2021 and the second chapter is currently in review,
130 while the third and fourth chapters are each in preparation for journal submis-
131 sion. This dissertation concludes with a sixth chapter that summarizes experiment
132 findings and briefly synthesizes common themes observed across experiments.

133

Chapter 2

134

Structural carbon costs to acquire nitrogen are determined by
135 nitrogen and light availability in two species with different nitrogen
136 acquisition strategies

137 2.1 Introduction

138 Carbon and nitrogen cycles are tightly coupled in terrestrial ecosystems. This
139 tight coupling influences photosynthesis (Walker et al. 2014; Rogers et al. 2017),
140 net primary productivity (LeBauer and Treseder 2008; Thomas et al. 2013), de-
141 composition (Cornwell et al. 2008; Bonan et al. 2013; Sulman et al. 2019), and
142 plant resource competition (Gill and Finzi 2016; Xu-Ri and Prentice 2017). Ter-
143 restrial biosphere models are beginning to include connected carbon and nitrogen
144 cycles to improve the realism of their simulations (Fisher et al. 2010; Brzostek
145 et al. 2014; Wieder et al. 2015; Shi et al. 2016; Zhu et al. 2019). Simula-
146 tions from these models indicate that coupling carbon and nitrogen cycles can
147 drastically influence future biosphere-atmosphere feedbacks under global change,
148 such as elevated carbon dioxide or nitrogen deposition (Thornton et al. 2007;
149 Goll et al. 2012; Wieder et al. 2015; Wieder et al. 2019). Nonetheless, there
150 are still limitations in our quantitative understanding of connected carbon and
151 nitrogen dynamics (Thomas et al. 2015; Meyerholt et al. 2016; Rogers et al.
152 2017; Exbrayat et al. 2018; Shi et al. 2019), forcing models to make potentially
153 unreliable assumptions.

154

Plant nitrogen acquisition is a process in terrestrial ecosystems by which
155 carbon and nitrogen are tightly coupled (Vitousek and Howarth 1991; Delaire
156 et al. 2005; Brzostek et al. 2014). Plants must allocate photosynthetically de-

157 rived carbon belowground to produce and maintain root systems or exchange with
158 symbiotic soil microbes in order to acquire nitrogen (Högberg et al. 2008; Hög-
159 berg et al. 2010). Thus, plants have an inherent carbon cost associated with
160 acquiring nitrogen, which can include both direct energetic costs associated with
161 nitrogen acquisition and indirect costs associated with building structures that
162 support nitrogen acquisition (Gutschick 1981; Rastetter et al. 2001; Vitousek
163 et al. 2002; Menge et al. 2008). Model simulations (Fisher et al. 2010; Brzostek
164 et al. 2014; Shi et al. 2016; Allen et al. 2020) and meta-analyses (Terrer et al.
165 2018) suggest that these carbon costs vary between species, particularly those
166 with different nitrogen acquisition strategies. For example, simulations using iter-
167 ations of the Fixation and Uptake of Nitrogen (FUN) model indicate that species
168 that acquire nitrogen from non-symbiotic active uptake pathways (e.g. mass flow)
169 generally have larger carbon costs to acquire nitrogen than species that acquire
170 nitrogen through symbiotic associations with nitrogen-fixing bacteria (Brzostek
171 et al. 2014; Allen et al. 2020).

172 Carbon costs to acquire nitrogen likely vary in response to changes in soil
173 nitrogen availability. For example, if the primary mode of nitrogen acquisition
174 is through non-symbiotic active uptake, then nitrogen availability could decrease
175 carbon costs to acquire nitrogen as a result of increased per-root nitrogen up-
176 take (Franklin et al. 2009; Wang et al. 2018). However, if the primary mode of
177 nitrogen acquisition is through symbiotic active uptake, then nitrogen availabil-
178 ity may incur additional carbon costs to acquire nitrogen if it causes microbial
179 symbionts to shift toward parasitism along the parasitism–mutualism continuum
180 (Johnson et al. 1997; Hoek et al. 2016; Friel and Friesen 2019) or if it reduces

181 the nitrogen acquisition capacity of a microbial symbiont (van Diepen et al. 2007;
182 Soudzilovskaia et al. 2015; Muñoz et al. 2016). Species may respond to shifts in
183 soil nitrogen availability by switching their primary mode of nitrogen acquisition
184 to a strategy with lower carbon costs to acquire nitrogen in order to maximize
185 the magnitude of nitrogen acquired from a belowground carbon investment and
186 outcompete other individuals for soil resources (Rastetter et al. 2001; Menge et al.
187 2008).

188 Environmental conditions that affect demand to acquire nitrogen to sup-
189 port new and existing tissues could also be a source of variance in plant carbon
190 costs to acquire nitrogen. For example, an increase in plant nitrogen demand could
191 increase carbon costs to acquire nitrogen if this increases the carbon that must be
192 allocated belowground to acquire a proportional amount of nitrogen (Kulmatiski
193 et al. 2017; Noyce et al. 2019). This could be driven by a temporary state of
194 diminishing return associated with investing carbon toward building and main-
195 taining structures that are necessary to support enhanced nitrogen uptake, such
196 as fine roots (Matamala and Schlesinger 2000; Norby et al. 2004; Arndal et al.
197 2018), mycorrhizal hyphae (Saleh et al. 2020), or root nodules (Parvin et al.
198 2020). Alternatively, if the environmental factor that increases plant nitrogen de-
199 mand causes nitrogen to become more limiting in the system (e.g. atmospheric
200 CO₂) (Luo et al. 2004; LeBauer and Treseder 2008; Vitousek et al. 2010; Liang
201 et al. 2016), species might switch their primary mode of nitrogen acquisition to
202 a strategy with lower relative carbon costs to acquire nitrogen in order to gain a
203 competitive advantage over species with either different or more limited modes of
204 nitrogen acquisition (Ainsworth and Long 2005; Taylor and Menge 2018).

205 Using a plant economics approach, I examined the influence of plant ni-
206 trogen demand and soil nitrogen availability on plant carbon costs to acquire
207 nitrogen. This was done by growing a species capable of forming associations
208 with nitrogen-fixing bacteria (*Glycine max* L. (Merr)) and a species not capable
209 of forming these associations (*Gossypium hirsutum* L.) under four levels of light
210 availability (plant nitrogen demand proxy) and four levels of soil nitrogen fertil-
211 ization (soil nitrogen availability proxy) in a full-factorial, controlled greenhouse
212 experiment. I used this experimental set-up to test the following hypotheses:

- 213 1. An increase in plant nitrogen demand due to increasing light availability will
214 increase carbon costs to acquire nitrogen through a proportionally larger
215 increase in belowground carbon than whole-plant nitrogen acquisition. This
216 will be the result of an increased investment of carbon toward belowground
217 structures that support enhanced nitrogen uptake, but at a lower nitrogen
218 return.
- 219 2. An increase in soil nitrogen availability will decrease carbon costs to acquire
220 nitrogen as a result of increased per root nitrogen uptake in *G. hirsutum*.
221 However, soil nitrogen availability will not affect carbon costs to acquire
222 nitrogen in *G. max* because of the already high return of nitrogen supplied
223 through nitrogen fixation.

224 2.2 Methods

225 2.2.1 *Experiment setup*

226 *Gossypium hirsutum* and *G. max* were planted in individual 3 liter pots (NS-300; **227** Nursery Supplies, Orange, CA, USA) containing a 3:1 mix of unfertilized potting **228** mix (Sungro Sunshine Mix #2, Agawam, MA, USA) to native soil extracted from **229** an agricultural field most recently planted with *G. max* at the USDA-ARS Lab-**230** oratory in Lubbock, TX, USA (33.59°N, -101.90°W). The field soil was classified **231** as Amarillo fine sandy loam (75% sand, 10% silt, 15% clay). Upon planting, **232** all *G. max* pots were inoculated with *Bradyrhizobium japonicum* (Verdesian N-**233** Dure™ Soybean, Cary, NC, USA) to stimulate root nodulation. Individuals of **234** both species were grown under similar, unshaded, ambient greenhouse conditions **235** for 2 weeks to germinate and begin vegetative growth.

236 Three blocks were set up in the greenhouse, each containing four light **237** treatments created using shade cloth that reduced incoming radiation by either 0 **238** (full sun), 30, 50, or 80%. Two weeks post-germination, individuals were randomly **239** placed in the four light treatments in each block. Individuals received one of four **240** nitrogen fertilization doses as 100ml of a modified Hoagland solution (Hoagland **241** and Arnon 1950) equivalent to either 0, 70, 210, or 630 ppm N twice per week **242** within each light treatment. Nitrogen fertilization doses were received as topical **243** agents to the soil surface. Each Hoagland solution was modified to keep concen-**244** trations of other macro- and micronutrients equivalent (Table A1). Plants were **245** routinely well watered to eliminate water stress.

246 2.2.2 *Plant measurements and calculations*

247 Each individual was harvested after 5 weeks of treatment, and biomass was sepa-
248 rated by organ type (leaves, stems, and roots). Nodules on *G. max* roots were also
249 harvested. Except for the 0% shade cover and 630 ppm N treatment combination,
250 all treatment combinations in both species had lower average dry biomass:pot vol-
251 ume ratios than the 1:1 ratio recommended by Poorter et al. (2012) to minimize
252 the likelihood of pot volume-induced growth limitation (Table A2; Table A3; Fig.
253 A1).

254 All harvested material was dried, weighed, and ground by organ type.
255 Carbon and nitrogen content (g g^{-1}) was determined by subsampling from ground
256 and homogenized biomass of each organ type using an elemental analyzer (Costech
257 4010; Costech, Inc., Valencia, CA, USA). I scaled these values to total leaf, stem,
258 and root carbon and nitrogen biomass (g) by multiplying dry biomass of each
259 organ type by carbon or nitrogen content of each corresponding organ type. Whole
260 plant nitrogen biomass (g) was calculated as the sum of total leaf (g), stem (g),
261 and root (g) nitrogen biomass. Root nodule carbon biomass was not included in
262 the calculation of root carbon biomass; however, relative plant investment toward
263 root or root nodule standing stock was estimated as the ratio of root biomass to
264 root nodule biomass (g g^{-1}), following similar metrics to those adopted by Dovrat
265 et al. (2018) and Dovrat et al. (2020).

266 Carbon costs to acquire nitrogen (N_{cost} ; gC gN^{-1}) were estimated as the
267 ratio of total root carbon biomass (C_{bg} ; gC) to whole-plant nitrogen biomass
268 (N_{wp} ; gN). This calculation quantifies the relationship between carbon spent on
269 nitrogen acquisition and whole plant nitrogen acquisition by using root carbon

270 biomass as a proxy for estimating the magnitude of carbon allocated toward ni-
271 trogen acquisition. This calculation therefore assumes that the magnitude of root
272 carbon standing stock is proportional to carbon transferred to root nodules or my-
273 corrhizae, or lost through root exudation or turnover. The assumption has been
274 supported in species that associate with ectomycorrhizal fungi (Hobbie 2006; Hob-
275 bie and Hobbie 2008), but is less clear in species that acquire nitrogen through
276 non-symbiotic active uptake or symbiotic nitrogen fixation. It is also unclear
277 whether relationships between root carbon standing stock and carbon transfer to
278 root nodules are similar in magnitude to carbon lost through exudation or when
279 allocated toward other active uptake pathways. Thus, because of the way mea-
280 surements were calculated, proximal values of carbon costs to acquire nitrogen are
281 underestimates.

282 2.2.3 *Statistical analyses*

283 I explored the effects of light and nitrogen availability on carbon costs to acquire
284 nitrogen using separate linear mixed-effects models for each species. Models in-
285 cluded shade cover, nitrogen fertilization, and interactions between shade cover
286 and nitrogen fertilization as continuous fixed effects, and also included block as a
287 random intercept term. Three separate models for each species were built with
288 this independent variable structure for three different dependent variables: (i)
289 carbon costs to acquire nitrogen (gC gN^{-1}); (ii) whole plant nitrogen biomass
290 (denominator of carbon cost to acquire nitrogen; gN); and (iii) belowground car-
291 bon biomass (numerator of carbon cost to acquire nitrogen; gC). I constructed two
292 additional models for *G. max* with the same model structure described above to

293 investigate the effects of light availability and nitrogen fertilization on root nodule
294 biomass (g) and the ratio of root nodule biomass to root biomass (unitless).

295 I used Shapiro–Wilk tests of normality to determine whether species spe-
296 cific linear mixed-effects model residuals followed a normal distribution. Zero
297 models satisfied residual normality assumptions when models were fit using un-
298 transformed data (Shapiro–Wilk: $p < 0.05$ in all cases). I attempted to satisfy
299 residual normality assumptions by first fitting models using dependent variables
300 that were natural-log transformed. If residual normality assumptions were still
301 not met (Shapiro–Wilk: $p < 0.05$), then models were fit using dependent variables
302 that were square root transformed. All residual normality assumptions were satis-
303 fied when models were fit with either a natural-log or square root transformation
304 (Shapiro–Wilk: $p > 0.05$ in all cases). Specifically, I natural-log transformed *G.*
305 *hirsutum* carbon costs to acquire nitrogen and *G. hirsutum* whole-plant nitrogen
306 biomass. I also square root transformed *G. max* carbon costs to acquire nitrogen,
307 *G. max* whole-plant nitrogen biomass, root carbon biomass in both species, *G.*
308 *max* root nodule biomass, and the *G. max* ratio of root nodule biomass to root
309 biomass. I used the ‘lmer’ function in the ‘lme4’ R package (Bates et al. 2015) to
310 fit each model and the ‘Anova’ function in the ‘car’ R package (Fox and Weisberg
311 2019) to calculate Wald’s χ^2 to determine the significance ($\alpha = 0.05$) of each fixed
312 effect coefficient. Finally, I used the ‘emmeans’ R package (Lenth 2019) to conduct
313 post-hoc comparisons of our treatment combinations using Tukey’s tests. Degrees
314 of freedom for all Tukey’s tests were approximated using the Kenward–Roger ap-
315 proach (Kenward and Roger 1997). All analyses and plots were conducted in R
316 version 4.0.1 (R Core Team 2021).

317 2.3 Results

318 2.3.1 *Carbon costs to acquire nitrogen*

319 Carbon costs to acquire nitrogen in *G. hirsutum* increased with increasing light
320 availability ($p<0.001$; Table 2.1; Fig. 2.1) and decreased with increasing nitrogen
321 fertilization ($p<0.001$; Table 2.1; Fig. 2.1). There was no interaction between
322 light availability and nitrogen fertilization ($p=0.486$, Table 2.1; Fig. 2.1).

323 Carbon costs to acquire nitrogen in *G. max* also increased with increasing
324 light availability ($p<0.001$, Table 2.1; Fig. 2.1) and decreased with increasing
325 nitrogen fertilization ($p<0.001$; Table 2.1; Fig. 2.1). There was no interaction
326 between light availability and nitrogen fertilization ($p=0.261$, Table 2.1; Fig. 2.1).

Table 2.1. Analysis of variance results exploring species-specific effects of light availability, nitrogen fertilization, and their interactions on carbon costs to acquire nitrogen (N_{cost} ; gC gN $^{-1}$), whole plant nitrogen biomass (N_{wp} ; gN), and root carbon biomass (C_{bg} ; gC)

	N_{cost}			N_{wp}			C_{bg}			
	df	Coefficient	χ^2	p	Coefficient	χ^2	p	Coefficient	χ^2	p
<i>G. hirsutum</i>										
Intercept		1.594	-	-	-3.232	-	-	0.432	-	-
Light (L)	1	-1.09E-02	56.494	<0.001	-6.41E-03	91.275	<0.001	-2.62E-03	169.608	<0.001
Nitrogen (N)	1	-1.34E-03	54.925	<0.001	1.83E-03	118.784	<0.001	1.15E-04	2.901	0.089
L*N	1	3.88E-06	0.485	0.486	-1.34E-05	10.721	0.001	-1.67E-06	3.140	0.076
<i>G. max</i>										
Intercept		1.877	-	-	0.239	-	-	0.438	-	-
Light (L)	1	-7.67E-03	174.156	<0.001	-6.72E-04	39.799	<0.001	-2.55E-03	194.548	<0.001
Nitrogen (N)	1	-2.35E-04	21.948	<0.001	1.55E-04	70.771	<0.001	2.52E-04	19.458	<0.001
L*N	1	-2.89E-06	1.262	0.261	-6.32E-07	1.435	0.231	-3.16E-06	10.803	0.001

327 *Significance determined using Wald's χ^2 tests ($p=0.05$). P -values less than 0.05 are in bold and p -values between
 328 0.05 and 0.1 are italicized. Negative coefficients for light treatments indicate a positive effect of increasing light
 329 availability on all response variables, as light availability is treated as percent shade cover in all linear mixed-effects
 330 models.

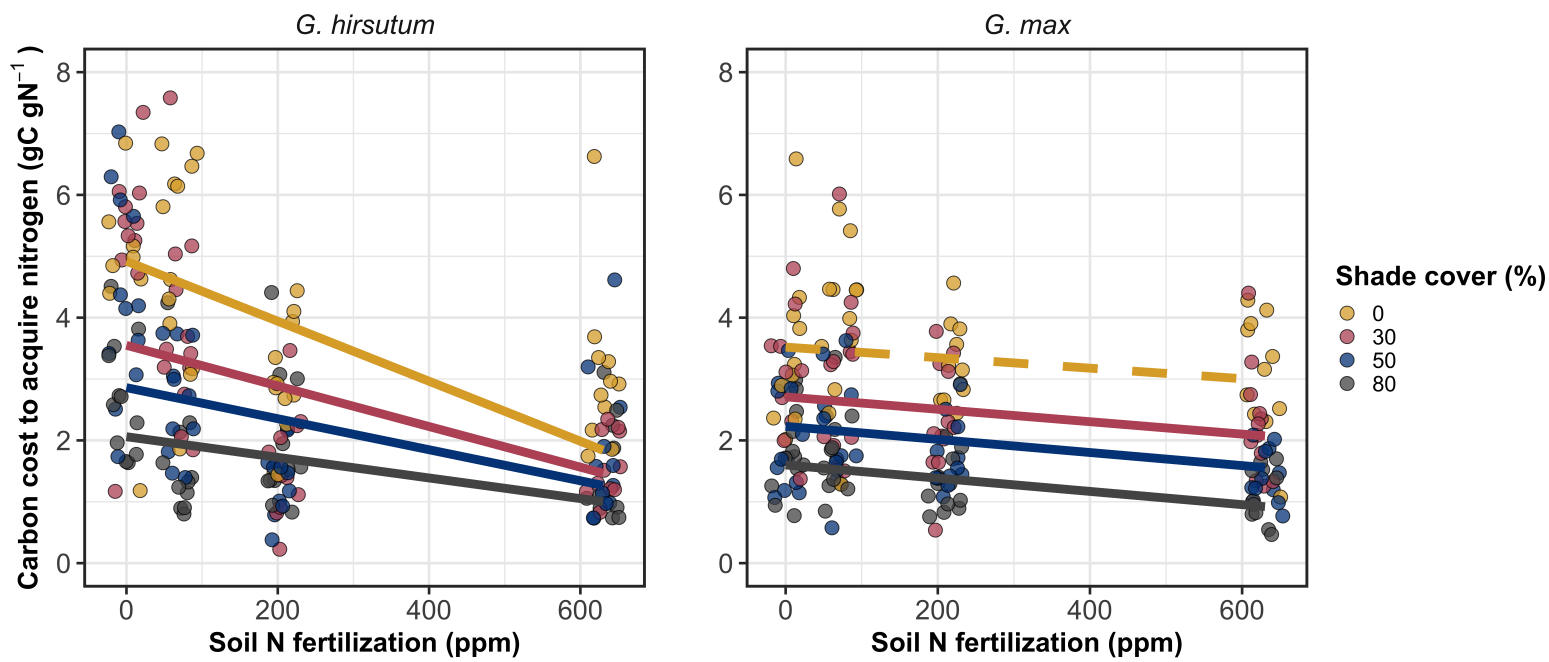


Figure 2.1. Relationships between soil nutrient fertilization and light availability on carbon costs to acquire nitrogen in *G. hirsutum* and *G. max*. Nitrogen fertilization treatments are represented on the x-axis. Shade cover treatments are represented through colored points and trendlines. Trendlines were created by back-transforming marginal mean slopes and intercepts from species-specific linear mixed-effects models. These values were calculated using the ‘emtrends’ and ‘emmeans’ functions in the ‘emmeans’ R package (Lenth, 2019). Yellow points and trendlines represent the 0% shade cover treatment, red points and trendlines represent the 30% shade cover treatment, blue points and trendlines represent the 50% shade cover treatment, and gray points and trendlines represent the 80% shade cover treatment. Solid trendlines indicate slopes that are significantly different from zero (Tukey: $p < 0.05$), while dashed trendlines indicate slopes that are not statistically different from zero.

331 2.3.2 *Whole plant nitrogen biomass*

332 Whole plant nitrogen biomass in *G. hirsutum* was driven by an interaction between
333 light availability and nitrogen fertilization ($p=0.001$; Table 2.1; Fig. 2.2). This
334 interaction indicated a greater stimulation of whole-plant nitrogen biomass by
335 nitrogen fertilization as light levels increased (Table 2.1; Fig. 2.2).

336 Whole plant nitrogen biomass in *G. max* increased with increasing light
337 availability ($p<0.001$) and nitrogen fertilization ($p<0.001$), with no interaction
338 between light availability and nitrogen fertilization ($p=0.231$; Table 2.1; Fig. 2.2).

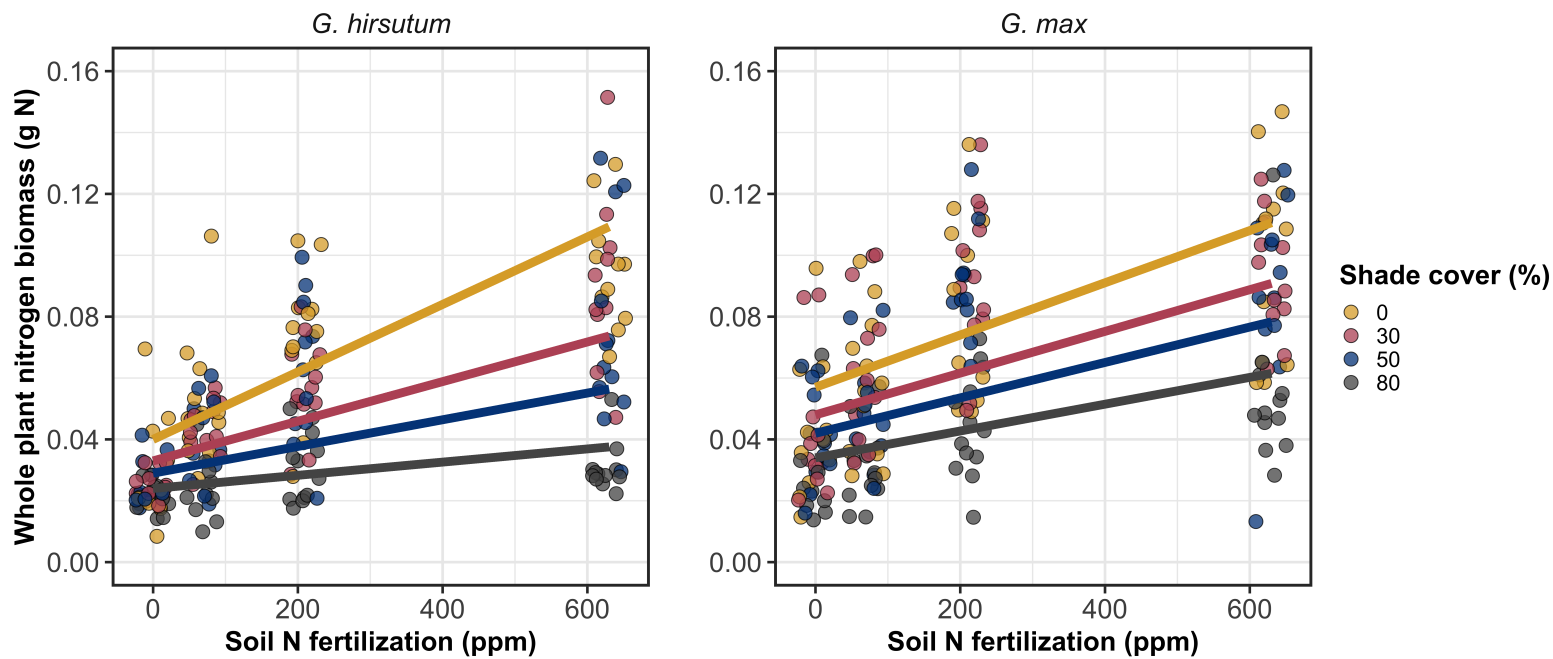


Figure 2.2. Relationships between soil nutrient fertilization and light availability on whole-plant nitrogen biomass in *G. hirsutum* and *G. max*. Whole-plant nitrogen biomass is the denominator of the carbon cost to acquire nitrogen calculation. Nitrogen fertilization treatments are represented on the x-axis. Shade cover treatments are represented through colored points and trendlines. Trendlines were created by back-transforming marginal mean slopes and intercepts from species-specific linear mixed-effects models. These values were calculated using the ‘emtrends’ and ‘emmeans’ functions in the ‘emmeans’ R package (Lenth 2019). Points are jittered for visibility. Colored points and trendlines are as explained in Fig. 2.1. Solid trendlines indicate slopes that are significantly different from zero (Tukey: $p < 0.05$), while dashed trendlines indicate slopes that are not statistically different from zero.

339 2.3.3 *Root carbon biomass*

340 Root carbon biomass in *G. hirsutum* significantly increased with increasing light
341 availability ($p<0.001$; Table 2.1; Fig. 2.3) and marginally increased with nitrogen
342 fertilization ($p=0.089$; Table 2.1; Fig. 2.3). There was also a marginal interaction
343 between light availability and nitrogen fertilization ($p=0.076$; Table 2.1), driven by
344 an increase in the positive response of root carbon biomass to increasing nitrogen
345 fertilization as light availability increased (Table 2.3). This resulted in significantly
346 positive trends between root carbon biomass and nitrogen fertilization in the two
347 highest light treatments (Tukey: $p<0.05$ in both cases; Table 2.3; Fig. 2.3) and no
348 effect of nitrogen fertilization in the two lowest light treatments (Tukey: $p>0.05$
349 in both cases; Table 2.3; Fig. 2.3).

350 There was an interaction between light availability and nitrogen fertiliza-
351 tion on root carbon biomass in *G. max* ($p=0.001$; Table 2.1; Fig. 2.3). Post-hoc
352 analyses indicated that the positive effects of nitrogen fertilization on *G. max*
353 root carbon biomass increased with increasing light availability (Table 2.3; Fig.
354 2.3). There were also positive individual effects of increasing nitrogen fertilization
355 ($p<0.001$) and light availability ($p<0.001$) on *G. max* root carbon biomass (Table
356 2.1; Fig. 2.3).

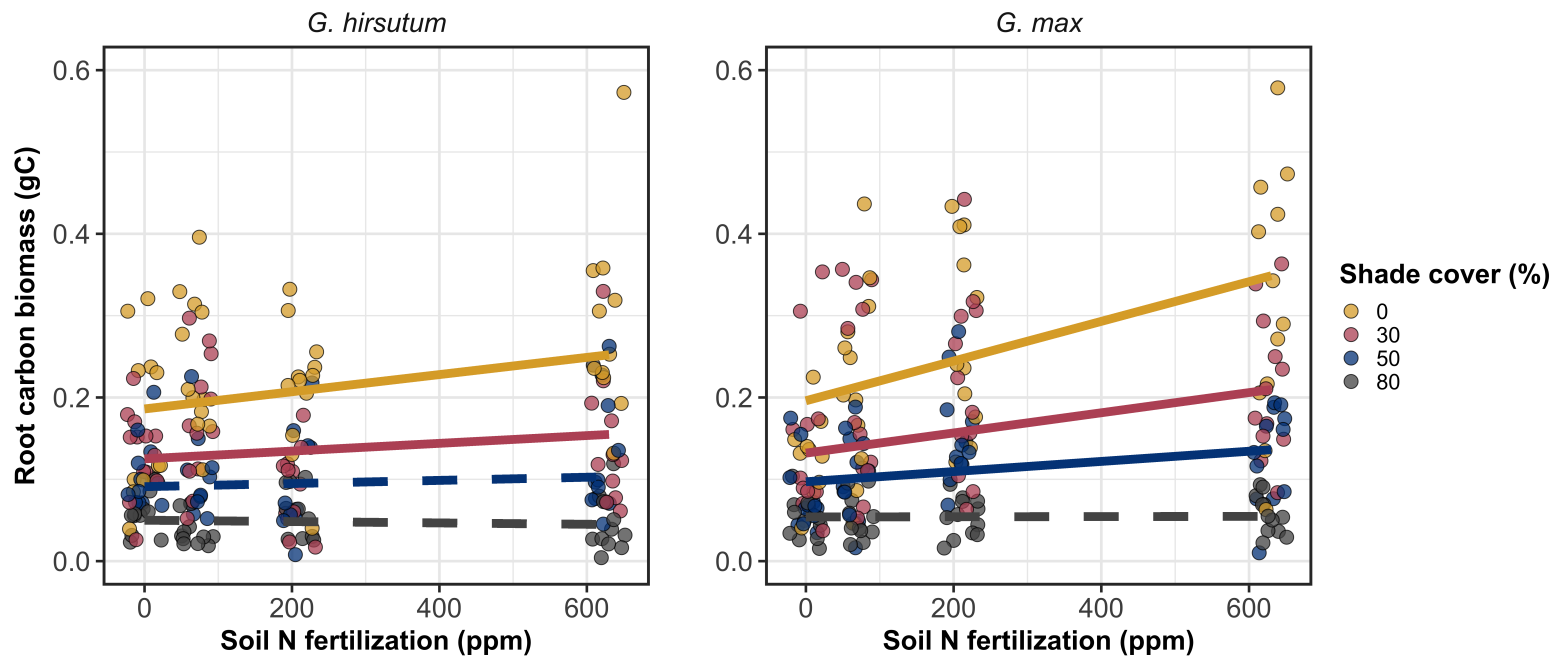


Figure 2.3. Relationships between soil nutrient fertilization and light availability on root carbon biomass in *G. hirsutum* and *G. max*. Root carbon biomass is the numerator of the carbon cost to acquire nitrogen calculation. Nitrogen fertilization treatments are represented on the x-axis. Colored points and trendlines are as explained in Fig. 2.1. Trendlines were created by back-transforming marginal mean slopes and intercepts from species-specific linear mixed-effects models. These values were calculated using the ‘emtrends’ and ‘emmeans’ functions in the ‘emmeans’ R package (Lenth 2019). Points are jittered for visibility. Colored points and trendlines are as explained in Fig. 2.1.

357 2.3.4 *Root nodule biomass*

358 Root nodule biomass in *G. max* increased with increasing light availability ($p<0.001$);
359 Table 2.2; Fig. 2.4a) and decreased with increasing nitrogen fertilization ($p<0.001$;
360 Table 2.2; Fig. 2.4a). There was no interaction between nitrogen fertilization and
361 light availability ($p=0.133$; Table 2.2; Fig. 2.4a). The ratio of root nodule biomass
362 to root biomass did not change in response to light availability ($p=0.481$; Table
363 2.2; Fig. 2.4b) but decreased with increasing nitrogen fertilization ($p<0.001$; Ta-
364 ble 2.2; Fig. 2.4b). There was no interaction between nitrogen fertilization and
365 light availability on the ratio of root nodule biomass to root biomass ($p=0.621$;
366 Table 2.2; Fig. 2.4b).

Table 2.2. Analysis of variance results exploring effects of light availability, nitrogen fertilization, and their interactions on *G. max* root nodule biomass and the ratio of root nodule biomass to root biomass*

	Nodule biomass			Nodule biomass: root biomass			<i>p</i>
	df	Coefficient	χ^2	<i>p</i>	Coefficient	χ^2	
(Intercept)		0.302	-	-	0.448	-	-
Light (L)	1	-1.81E-03	72.964	<0.001	-8.76E-05	0.496	0.481
Nitrogen (N)	1	-2.83E-04	115.377	<0.001	-5.09E-04	156.476	<0.001
L*N	1	1.14E-06	2.226	0.133	-7.30E-07	0.244	0.621

367 *Significance determined using Wald's χ^2 tests ($\alpha=0.05$). *P*-values less than 0.05 are in bold. Negative coefficients for
 368 light treatments indicate a positive effect of increasing light availability on all response variables, as light availability
 369 is treated as percent shade cover in all linear mixed-effects models. Root nodule biomass and nodule biomass: root
 370 biomass models were only constructed for *G. max* because *G. hirsutum* was not inoculated with *B. japonicum* and
 371 is not capable of forming root nodules.

Table 2.3. Slopes of the regression line describing the relationship between each dependent variable and nitrogen fertilization at each light level*

Shade cover	Carbon cost to acquire nitrogen	Whole plant nitrogen biomass	Belowground carbon biomass	Root nodule biomass	Nodule biomass: root biomass
<i>G. hirsutum</i>					
0%	-1.34E-03^a	1.83E-03^a	1.15E-04^b	-	-
30%	-1.22E-03^a	1.43E-03^a	1.17E-04^b	-	-
50%	-1.14E-03^a	1.17E-03^a	3.12E-05 ^b	-	-
80%	-1.02E-03^a	7.66E-04^a	-1.89E-06 ^b	-	-
<i>G. max</i>					
0%	-2.35E-04 ^b	1.55E-05^b	2.51E-04^b	-2.83E-04^b	-5.09E-04^b
30%	-3.22E-04^b	1.35E-05^b	1.57E-04^b	-2.49E-04^b	-5.31E-04^b
50%	-3.80E-04^b	1.23E-05^b	9.37E-05^b	-2.26E-04^b	-5.45E-04^b
80%	-4.66E-04^b	1.04E-05^b	-9.95E-07 ^b	-1.92E-04^b	-5.67E-04^b

24

372 * Slopes represent estimated marginal mean slopes from linear mixed-effects models described in the Methods. Slopes
373 were calculated using the ‘emmeans’ R package (Lenth 2019). Superscripts indicate slopes fit to natural-log (^a) or
374 square root (^b) transformed data. Slopes statistically different from zero (Tukey: $p<0.05$) are indicated in bold.
375 Marginally significant slopes (Tukey: $0.05<p<0.1$) are italicized.

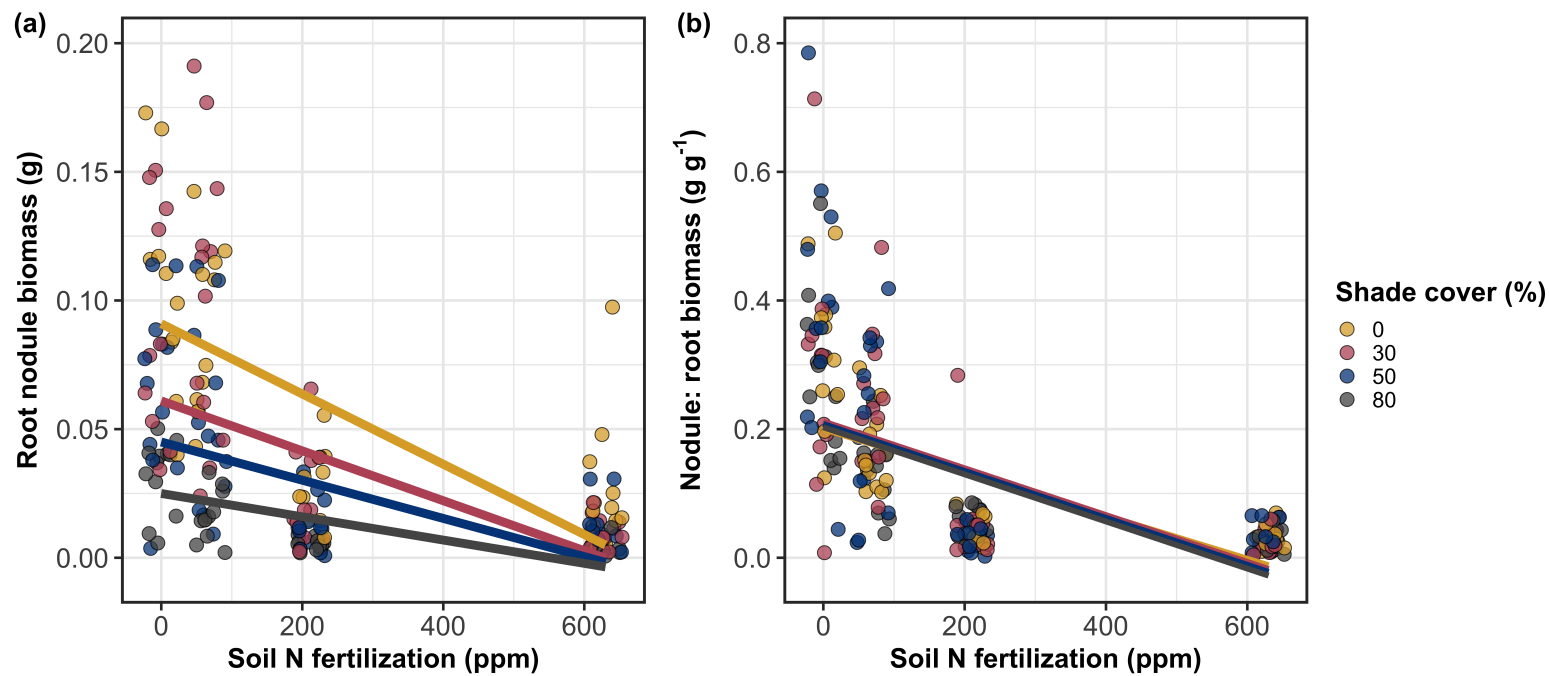


Figure 2.4. Effects of shade cover and nitrogen fertilization on root nodule biomass (a) and the ratio of root nodule biomass to root biomass (b) in *G. max*. Nitrogen fertilization treatments are represented on the x-axis. Shade cover treatments are represented through colored points and trendlines. Trendlines were created by back-transforming marginal mean slopes and intercepts from species-specific linear mixed-effects models. These values were calculated using the ‘emtrends’ and ‘emmmeans’ functions in the ‘emmeans’ R package (Lenth 2019). Points are jittered for visibility. Yellow points and trendlines represent the 0% shade cover treatment, blue points and trendlines represent the 30% shade cover treatment, green points and trendlines represent the 50% shade cover treatment, and purple points and trendlines represent the 80% shade cover treatment. Solid trendlines indicate slopes that are significantly different from zero (Tukey: $p < 0.05$), while dashed trendlines indicate slopes that are not statistically different from zero.

376 2.4 Discussion

377 In this chapter, I determined the effects of light availability and soil nitrogen
378 fertilization on root mass carbon costs to acquire nitrogen in *G. hirsutum* and *G.*
379 *max*. In support of my hypotheses, I found that carbon costs to acquire nitrogen
380 generally increased with increasing light availability and decreased with increasing
381 soil nitrogen fertilization in both species. These findings suggest that carbon costs
382 to acquire nitrogen are determined by factors that influence plant nitrogen demand
383 and soil nitrogen availability. In contrast to my second hypothesis, root nodulation
384 data suggested that *G. max* and *G. hirsutum* achieved similar directional carbon
385 cost responses to nitrogen fertilization despite a likely shift in *G. max* allocation
386 from nodulation to root biomass along the nitrogen fertilization gradient.

387 2.4.1 *Carbon costs to acquire nitrogen increase with light availability and*
388 *decrease with fertilization*

389 Both *G. max* and *G. hirsutum* experienced an increase in carbon costs to ac-
390 quire nitrogen due to increasing light availability. These patterns were driven by
391 a larger increase in root carbon biomass than whole-plant nitrogen biomass. In-
392 creases in root carbon biomass due to factors that increase plant nitrogen demand
393 are a commonly observed pattern, as carbon allocated belowground provides sub-
394 strate needed to produce and maintain structures that satisfy aboveground plant
395 nitrogen demand (Nadelhoffer and Raich 1992; Giardina et al. 2005; Raich et al.
396 2014). Findings suggest that plants allocate relatively more carbon for acquiring
397 nitrogen when demand increases over short temporal scales, which may cause a
398 temporary state of diminishing return due to asynchrony between belowground

399 carbon and whole-plant nitrogen responses to plant nitrogen demand (Kulmatiski
400 et al. 2017; Noyce et al. 2019). These responses might be attributed to a temporal
401 lag associated with producing structures that enhance nitrogen acquisition. For
402 example, fine roots (Matamala and Schlesinger 2000; Norby et al. 2004; Arndal
403 et al. 2018) and root nodules (Parvin et al. 2020) take time to build and first
404 require the construction of coarse roots. Thus, full nitrogen returns from these
405 investments may not occur immediately (Kayler et al. 2010; Kayler et al. 2017),
406 and may vary by species acquisition strategy. I speculate that increases in ni-
407 trogen acquisition from a given carbon investment may occur beyond the 5-week
408 scope of this experiment. A similar study conducted over a longer temporal scale
409 would address this.

410 Increasing soil nitrogen fertilization generally decreased carbon costs to
411 acquire nitrogen in both species. These patterns were driven by a larger increase
412 in whole-plant nitrogen biomass than root carbon biomass. In *G. hirsutum*, re-
413 ductions in carbon costs to acquire nitrogen may have been due to an increase in
414 per-root nitrogen uptake, allowing individuals to maximize the amount of nitro-
415 gen acquired from a belowground carbon investment. Interestingly, increased soil
416 nitrogen fertilization increased whole-plant nitrogen biomass in *G. max* despite
417 reductions in root nodule biomass that likely reduced the nitrogen-fixing capac-
418 ity of *G. max* (Andersen et al. 2005; Muñoz et al. 2016). While reductions in
419 root nodulation due to increased soil nitrogen availability are commonly observed
420 (Gibson and Harper 1985; Fujikake et al. 2003), root nodulation responses were
421 observed in tandem with increased root carbon biomass, implying that *G. max*
422 shifted relative carbon allocation from nitrogen fixation to soil nitrogen acquisition

423 (Markham and Zekveld 2007; Dovrat et al. 2020). This was likely because there
424 was a reduction in the carbon cost advantage of acquiring fixed nitrogen relative
425 to soil nitrogen, and suggests that species capable of associating with symbiotic
426 nitrogen-fixing bacteria shift their relative nitrogen acquisition pathway to opti-
427 mize nitrogen uptake (Rastetter et al. 2001). Future studies should investigate
428 these patterns with a larger quantity of phylogenetically related species, or differ-
429 ent varieties of a single species that differ in their ability to form associations with
430 symbiotic nitrogen-fixing bacteria to more directly test the impact of nitrogen
431 fixation on the patterns observed in this study.

432 2.4.2 *Modeling implications*

433 Carbon costs to acquire nitrogen are subsumed in the general discussion of eco-
434 nomic analogies to plant resource uptake (Bloom et al. 1985; Rastetter et al.
435 2001; Vitousek et al. 2002; Phillips et al. 2013; Terrer et al. 2018; Henneron
436 et al. 2020). Despite this, terrestrial biosphere models rarely include costs of
437 nitrogen acquisition within their framework for predicting plant nitrogen uptake.
438 There is currently one plant resource uptake model, FUN, that quantitatively
439 predicts carbon costs to acquire nitrogen within a framework for predicting plant
440 nitrogen uptake for different nitrogen acquisition strategies (Fisher et al. 2010;
441 Brzostek et al. 2014). Iterations of FUN are currently coupled to two terrestrial
442 biosphere models: the Community Land Model 5.0 and the Joint UK Land En-
443 vironment Simulator (Shi et al. 2016; Lawrence et al. 2019; Clark et al. 2011).
444 Recent work suggests that coupling FUN to CLM 5.0 caused a large overpredic-
445 tion of plant nitrogen uptake associated with nitrogen fixation (Davies-Barnard

446 et al. 2020) compared to other terrestrial biosphere model products. Thus, em-
447 pirical data from manipulative experiments that explicitly quantify carbon costs
448 to acquire nitrogen in species capable of associating with nitrogen-fixing bacteria
449 across different environmental contexts is an important step toward identifying
450 potential biases in models such as FUN.

451 These findings broadly support the FUN formulation of carbon costs to
452 acquire nitrogen in response to soil nitrogen availability. FUN calculates carbon
453 costs to acquire nitrogen based on the sum of carbon costs to acquire nitrogen
454 via nitrogen fixation, mycorrhizal active uptake, non-mycorrhizal active uptake,
455 and retranslocation (Fisher et al. 2010; Brzostek et al. 2014). Carbon costs to
456 acquire nitrogen via mycorrhizal or non-mycorrhizal active uptake pathways are
457 derived as a function of nitrogen availability, root biomass, and two parameterized
458 values based on nitrogen acquisition strategy (Brzostek et al. 2014). Due to this,
459 FUN simulates a net decrease in carbon costs to acquire nitrogen with increasing
460 nitrogen availability for mycorrhizal and non-mycorrhizal active uptake pathways,
461 assuming constant root biomass. This was a pattern I observed in *G. hirsutum* re-
462 gardless of light availability. In contrast, FUN would not simulate a net change in
463 carbon costs to acquire nitrogen via nitrogen fixation due to nitrogen availability.
464 This is because carbon costs to acquire nitrogen via nitrogen fixation are derived
465 from a well established function of soil temperature, which is independent of soil
466 nitrogen availability (Houlton et al. 2008; Fisher et al. 2010). I observed a net
467 reduction in carbon costs to acquire nitrogen in *G. max*, except when individu-
468 als were grown under 0% shade cover. While a net reduction of carbon costs in
469 response to nitrogen fertilization runs counter to nitrogen fixation carbon costs

470 simulated by FUN, these patterns were likely because *G. max* individuals switched
471 their primary mode of nitrogen acquisition from symbiotic nitrogen fixation to a
472 non-symbiotic active uptake pathway.

473 2.4.3 *Study limitations*

474 It should be noted that the metric used in this study to determine carbon costs
475 to acquire nitrogen has several limitations. Most notably, this metric uses root
476 carbon biomass as a proxy for estimating the amount of carbon spent on nitrogen
477 acquisition. While it is true that most carbon allocated belowground has at least
478 an indirect structural role in acquiring soil resources, it remains unclear whether
479 this assumption holds true for species that acquire nitrogen via symbiotic nitro-
480 gen fixation. I also cannot quantify carbon lost through root exudates or root
481 turnover, which may increase due to factors that increase plant nitrogen demand
482 (Tingey et al. 2000; Phillips et al. 2011), and can increase the magnitude of
483 available nitrogen from soil organic matter through priming effects on soil micro-
484 bial communities (Uselman et al. 2000; Bengtson et al. 2012). It is also not
485 clear whether these assumptions hold under all environmental conditions, such
486 as those that shift belowground carbon allocation toward a different mode of ni-
487 trogen acquisition (Taylor and Menge 2018; Friel and Friesen 2019) or between
488 species with different acquisition strategies. In this study, increasing soil nitrogen
489 fertilization increased carbon investment to roots relative to carbon transferred to
490 root nodules. By assuming that carbon allocated to root carbon was proportional
491 to carbon allocated to root nodules across all treatment combinations, these ob-
492 served responses to soil nitrogen fertilization were likely to be overestimated in *G.*

493 *max*. I encourage future research to quantify these carbon fates independently.

494 Researchers conducting pot experiments must carefully choose pot volume
495 to minimize the likelihood of growth limitations induced by pot volume (Poorter
496 et al. 2012). Poorter et al. (2012) indicate that researchers are likely to avoid
497 growth limitations associated with pot volume if measurements are collected when
498 the plant biomass:pot volume ratio is less than 1 g L^{-1} . In this experiment, all
499 treatment combinations in both species had biomass:pot volume ratios less than
500 1 g L^{-1} except for *G. max* and *G. hirsutum* that were grown under 0% shade
501 cover and had received 630 ppm N. Specifically, *G. max* and *G. hirsutum* had
502 average respective biomass:pot volume ratios of $1.24 \pm 0.07 \text{ g L}^{-1}$ and 1.34 ± 0.13
503 g L^{-1} , when grown under 0% shade cover and received 630 ppm N (Table A2;
504 Table A3; Fig. A1). If growth in this treatment combination was limited by pot
505 volume, then individuals may have had larger carbon costs to acquire nitrogen
506 than would be expected if they were grown in larger pots. This pot volume
507 induced growth limitation could cause a reduction in per-root nitrogen uptake
508 associated with more densely packed roots, which could reduce the positive effect
509 of nitrogen fertilization on whole-plant nitrogen biomass relative to root carbon
510 biomass (Poorter et al. 2012).

511 Growth limitation associated with pot volume provides a possible expla-
512 nation for the marginally insignificant effect of increasing nitrogen fertilization on
513 *G. max* carbon costs to acquire nitrogen when grown under 0% shade cover. This
514 is because the regression line describing the relationship between carbon costs to
515 acquire nitrogen and nitrogen fertilization in *G. max* grown under 0% shade cover
516 would have flattened if growth limitation had caused larger than expected carbon

517 costs to acquire nitrogen in the 0% shade cover, 630 ppm N treatment combi-
518 nation. This may have been exacerbated by the fact that *G. max* likely shifted
519 relative carbon allocation from nitrogen fixation to soil nitrogen acquisition, which
520 could have increased the negative effect of more densely packed roots on nitrogen
521 uptake. These patterns could have also occurred in *G. hirsutum* grown under 0%
522 shade cover; however, there was no change in the effect of nitrogen fertilization on
523 *G. hirsutum* carbon costs to acquire nitrogen grown under 0% shade cover relative
524 to other shade cover treatments. Regardless, the possibility of growth limitation
525 due to pot volume suggests that effects of increasing nitrogen fertilization on car-
526 bon costs to acquire nitrogen in both species grown under 0% shade cover could
527 have been underestimated. Follow-up studies using a similar experimental design
528 with a larger pot volume would be necessary in order to determine whether these
529 patterns were impacted by pot volume-induced growth limitation.

530 2.4.4 *Conclusions*

531 In conclusion, this chapter provides empirical evidence that carbon costs to ac-
532 quire nitrogen are influenced by light availability and soil nitrogen fertilization
533 in a species capable of acquiring nitrogen via symbiotic nitrogen fixation and a
534 species not capable of forming such associations. We show that carbon costs to
535 acquire nitrogen generally increase with increasing light availability and decrease
536 with increasing nitrogen fertilization. This chapter provides important empirical
537 data needed to evaluate the formulation of carbon costs to acquire nitrogen in
538 terrestrial biosphere models, particularly carbon costs to acquire nitrogen that
539 are associated with symbiotic nitrogen fixation. My findings broadly support the

540 general formulation of these carbon costs in the FUN biogeochemical model in
541 response to shifts in nitrogen availability. However, there is a need for future
542 studies to explicitly quantify carbon costs to acquire nitrogen under different en-
543 vironmental contexts, over longer temporal scales, and using larger selections of
544 phylogenetically related species. In addition, I suggest that future studies mini-
545 mize the limitations associated with the metric used here by explicitly measuring
546 belowground carbon fates independently.

547

Chapter 3

548 Soil nitrogen availability modifies leaf nitrogen economies in mature
549 temperate deciduous forests: a direct test of photosynthetic least-cost
550 theory

551 3.1 Introduction

552 Photosynthesis represents the largest carbon flux between the atmosphere and
553 land surface (IPCC 2021), and plays a central role in biogeochemical cycling at
554 multiple spatial and temporal scales (Vitousek and Howarth 1991; LeBauer and
555 Treseder 2008; Kaiser et al. 2015; Wieder et al. 2015). Therefore, carbon and
556 energy fluxes simulated by terrestrial biosphere models are sensitive to the formu-
557 lation of photosynthetic processes (Ziehn et al. 2011; Bonan et al. 2011; Booth
558 et al. 2012; Smith et al. 2016; Smith et al. 2017) and must be represented using
559 robust, empirically tested processes (Prentice et al. 2015; Wieder et al. 2019).
560 Current formulations of photosynthesis vary across terrestrial biosphere models
561 (Smith and Dukes 2013; Rogers et al. 2017), which causes variation in modeled
562 ecosystem processes (Knorr 2000; Knorr and Heimann 2001; Bonan et al. 2011;
563 Friedlingstein et al. 2014) and casts uncertainty on the ability of these models to
564 accurately predict terrestrial ecosystem responses and feedbacks to global change
565 (Zaehle et al. 2005; Schaefer et al. 2012; Davies-Barnard et al. 2020).

566 Terrestrial biosphere models commonly represent C₃ photosynthesis th-
567 rough variants of the Farquhar et al. (1980) biochemical model (Smith and Dukes
568 2013; Rogers 2014; Rogers et al. 2017). This well-tested photosynthesis model
569 estimates leaf-level carbon assimilation, or photosynthetic capacity, as a function
570 of the maximum rate of Ribulose-1,5-bisphosphate carboxylase-oxygenase (Ru-

571 bisco) carboxylation (V_{cmax}) and the maximum rate of Ribulose-1,5-bisphosphate
572 (RuBP) regeneration (J_{max}) (Farquhar et al. 1980). Many terrestrial biosphere
573 models predict these model inputs based on plant functional group specific lin-
574 ear relationships between leaf nutrient content and V_{cmax} (Smith and Dukes 2013;
575 Rogers 2014; Rogers et al. 2017) under the tenet that a large fraction of leaf nutri-
576 ents, and nitrogen in particular, are partitioned toward building and maintaining
577 enzymes that support photosynthetic capacity, such as Rubisco (Brix 1971; Gul-
578 mon and Chu 1981; Evans 1989; Kattge et al. 2009; Walker et al. 2014). Terres-
579 trial biosphere models predict leaf nutrient content from soil nutrient availability
580 based on the assumption that increasing soil nutrients generally increases leaf nu-
581 trients (Firn et al. 2019; Li et al. 2020; Liang et al. 2020) which, in the case of
582 nitrogen, generally corresponds with an increase in photosynthetic processes (Li
583 et al. 2020; Liang et al. 2020).

584 Recent work calls the generality of relationships between soil nutrient avail-
585 ability, leaf nutrient content, and photosynthetic capacity into question, suggest-
586 ing instead that leaf nutrients and photosynthetic capacity are better predicted as
587 an integrated product of aboveground climate, leaf traits, and soil nutrient avail-
588 ability, rather than soil nutrient availability alone (Dong et al. 2017; Dong et al.
589 2020; Dong et al. 2022; Firn et al. 2019; Smith et al. 2019; Peng et al. 2021).
590 It has been reasoned that this result is because plants allocate added nutrients to
591 growth and storage rather than alterations in leaf chemistry (Smith et al. 2019),
592 perhaps as a result of nutrient limitation of primary productivity (LeBauer and
593 Treseder 2008; Fay et al. 2015). Additionally, recent work suggests that relation-
594 ships between leaf nutrient content and photosynthesis vary across environments,

595 and that the proportion of leaf nutrient content allocated to photosynthetic tis-
596 sue varies over space and time with plant acclimation and adaptation responses
597 to light availability, vapor pressure deficit, soil pH, soil nutrient availability, and
598 environmental factors that influence leaf mass per area (Pons and Pearcy 1994;
599 Niinemets and Tenhunen 1997; Evans and Poorter 2001; Hikosaka and Shigeno
600 2009; Ghimire et al. 2017; Onoda et al. 2017; Luo et al. 2021). The use of linear
601 relationships between leaf nutrient content and V_{cmax} to predict photosynthetic
602 capacity, as commonly used in terrestrial biosphere models (Rogers 2014), is not
603 capable of detecting such responses.

604 Photosynthetic least-cost theory provides an alternative framework for un-
605 derstanding relationships between soil nutrient availability, leaf nutrient content,
606 and photosynthetic capacity (Harrison et al. 2021). Leveraging a two-input mi-
607 croeconomics approach (Wright et al. 2003), the theory posits that plants accli-
608 mate to a given environment by optimizing leaf photosynthesis rates at the lowest
609 summed cost of using nutrients and water (Prentice et al. 2014; Wang et al. 2017;
610 Smith et al. 2019; Paillassa et al. 2020). Across resource availability gradients,
611 the theory predicts that optimal photosynthetic rates can be achieved by trading
612 less efficient use of a resource that is less costly to acquire (or more abundant)
613 for more efficient use of a resource more costly to acquire (or less abundant). For
614 example, an increase in soil nutrient availability should reduce the cost of acquir-
615 ing and using nutrients (Bae et al. 2015; Eastman et al. 2021; Perkowski et al.
616 2021), which could increase leaf nutrient investments in photosynthetic proteins to
617 allow similar photosynthetic rates to be achieved with higher nutrient use (lower
618 nutrient use efficiency) but lower water use (greater water use efficiency). The

619 theory suggests similar tradeoffs in response to increasing soil pH (Paillassa et al.
620 2020), specifically, that increasing soil pH should reduce the cost of acquiring soil
621 nutrients due to an increase in plant-available nutrient concentration (Paillassa
622 et al. 2020; Dong et al. 2022). The theory is also capable of reconciling dynamic
623 leaf nutrient-photosynthesis relationships at global scales (Luo et al. 2021).

624 Patterns expected from photosynthetic least-cost theory have recently re-
625 ceived empirical support both in global environmental gradient (Smith et al.
626 2019; Paillassa et al. 2020; Luo et al. 2021; Querejeta et al. 2022; Wester-
627 band et al. 2023) and local manipulative invasion (Bialic-Murphy et al. 2021)
628 studies. However, nutrient addition experiments that directly examine nutrient-
629 water use tradeoffs expected from the theory are rare (but see Guerrieri et al.
630 2011), and only global gradient studies testing the theory have considered soil pH
631 in their analyses. As a result, there is a need to use nutrient addition and soil pH
632 manipulation experiments to test mechanisms driving responses predicted by the
633 theory.

634 In this study, I measured leaf responses to soil nitrogen availability in five
635 deciduous tree species growing in the upper canopy of mature closed canopy tem-
636 perate forests in the northeastern United States. Soil nitrogen availability and pH
637 were manipulated through a nitrogen-by-pH field manipulation experiment with
638 treatments applied since 2011, eight years prior to measurement. Two different
639 soil nitrogen treatments were applied to increase nitrogen availability with op-
640 posing effects on soil pH. An additional N-free acidifying treatment was expected
641 to decrease soil pH. I hypothesized that increased soil nitrogen availability would
642 enable plants to increase nutrient uptake and create more photosynthetic enzymes

643 per leaf, allowing similar photosynthetic rates achieved with lower leaf C_i:C_a and
644 increased leaf nitrogen content allocated to photosynthetic leaf tissue. I expected
645 that this response would be driven by a reduction in the cost of acquiring nitrogen,
646 which would cause trees to sacrifice efficient nitrogen use to enable more efficient
647 use of other limiting resources (i.e., water). Finally, I hypothesized similar leaf
648 responses to increasing soil pH.

649 3.2 Methods

650 3.2.1 *Study site description*

651 I conducted this study in summer 2019 at three stands located within a 20-km ra-
652 dius of Ithaca, NY, USA (42.444 °N, 76.502 °W). All stands contain mature,
653 closed-canopy forests dominated by deciduous tree species. Stands contained
654 abundant sugar maple (*Acer saccharum* Marshall), American beech (*Fagus gran-*
655 *difolia* Ehrh.), and white ash (*Fraxinus americana* L.), accounting for 43%, 15%,
656 and 17% of the total aboveground biomass across the three stands, respectively,
657 with less frequent red maple (*Acer rubrum* L.; 9% of total aboveground biomass)
658 and red oak occurrences (*Quercus rubra* L.; 10% of total aboveground biomass).
659 Soils at each site were broadly classified as a channery silt loam Inceptisols using
660 the USDA NRCS Web Soil Survey data product (Soil Survey Staff 2022). Between
661 2006 and 2020, study sites averaged 972 mm of precipitation per year and had an
662 average temperature of 7.9 °C per a weather station located near the Cornell Uni-
663 versity campus (42.449 °N, 76.449 °W) part of the NOAA NCEI Global Historical
664 Climatology Network (Menne et al. 2012).

665 3.2.2 *Experimental design*

666 Four 40 m x 40 m plots were set up at each site in 2009, each with an additional
667 10 m buffer along plot perimeters (60 m x 60 m total). The plots were set up as a
668 nitrogen-by-pH field manipulation experiment, with one each of four treatments
669 at each site. Two nitrogen treatments were applied, both at $50 \text{ kg N ha}^{-1} \text{ yr}^{-1}$, as
670 either sodium nitrate (NaNO_3) to raise soil pH, or ammonium sulfate ($(\text{NH}_4)_2\text{SO}_4$)
671 to acidify; an elemental sulfur treatment was selected to acidify without nitrogen,
672 applied at the same rate of S addition ($57 \text{ kg S ha}^{-1} \text{ yr}^{-1}$); and control plots
673 received no additions. All amendments were added in pelletized form using hand-
674 held fertilizer spreaders to both the main plots and buffers. Amendments were
675 divided into three equal doses distributed across the growing season from 2011-
676 2017 and added as a single dose from 2018 onward. During 2019, plots were
677 fertilized during the week of May 20.

678 3.2.3 *Leaf gas exchange and trait measurements*

679 I sampled one leaf each from 6 to 10 individuals per plot between June 25 and
680 July 12, 2019 for gas exchange measurements (Table B1). Leaves were collected
681 from deciduous broadleaf trees represented across all sites and plots and were
682 replicated in efforts to mimic the species abundance of each plot at each site.
683 We also attempted to collect leaves from the upper canopy to reduce differential
684 shading effects on leaf physiology. Leaves were accessed by pulling down small
685 branches using an arborist's slingshot and weighted beanbag attached to a throw
686 line. Branches were immediately recut under deionized water and remained sub-
687 merged to reduce stomatal closure and avoid xylem embolism, as done in Smith

688 and Dukes (2018), until gas exchange data were collected.

689 Randomly selected leaves with little to no visible external damage were
690 attached to a Li-COR LI-6800 (Li-COR Bioscience, Lincoln, Nebraska, USA)
691 portable photosynthesis machine to measure net photosynthesis (A_{net} ; $\mu\text{mol m}^{-2}$
692 s^{-1}), stomatal conductance (g_{sw} ; $\text{mol m}^{-2} \text{s}^{-1}$), and intercellular CO_2 concentra-
693 tion (C_i ; $\mu\text{mol mol}^{-1}$) at different reference CO_2 concentrations (C_a ; $\mu\text{mol mol}^{-1}$)
694 concentrations (i.e., an A_{net}/C_i curve) under saturating light conditions (2,000
695 $\mu\text{mol m}^{-2} \text{s}^{-1}$). Reference CO_2 concentrations followed the sequence: 400, 300,
696 200, 100, 50, 400, 400, 600, 800, 1000, 1200, 1500, and 2000 $\mu\text{mol mol}^{-1} \text{CO}_2$. Leaf
697 temperatures were not controlled in the cuvette and ranged from 21.8 °C to 31.7
698 °C (mean±SD: 27.2 ± 2.2 °C). A linear and second order log-polynomial nonlinear
699 regression suggested no effect of temperature on stomatal conductance measured
700 at 400 $\mu\text{mol mol}^{-1} \text{CO}_2$ or net photosynthesis measured at 400 $\mu\text{mol mol}^{-1} \text{CO}_2$
701 (Table B2-B3; Fig. B1). All A_{net}/C_i curves were generated within one hour of
702 branch severance.

703 Leaf morphological and chemical traits were collected on the same leaf used
704 to generate each A_{net}/C_i curve. Images of each leaf were taken using a flat-bed
705 scanner to determine fresh leaf area using the ‘LeafArea’ R package (Katabuchi
706 2015), which automates leaf area calculations using ImageJ software (Schneider
707 et al. 2012). Each leaf was dried at 65°C for at least 48 hours, weighed, and
708 ground using a Retsch MM200 ball mill grinder (Verder Scientific, Inc., Newtown,
709 PA, USA) until homogenized. Leaf mass per area (M_{area} , g m^{-2}) was calculated
710 as the ratio of dry leaf biomass to fresh leaf area. Using a subsample of ground
711 and homogenized leaf biomass, leaf nitrogen content (N_{mass} ; gN g^{-1}) and leaf $\delta^{13}\text{C}$

712 (%₀, relative to Vienna Pee Dee Belemnite international reference standard) were
713 measured at the Cornell Stable Isotope Lab with an elemental analyzer (NC 2500,
714 CE Instruments, Wigan, UK) interfaced to an isotope ratio mass spectrometer
715 (Delta V Isotope Ratio Mass Spectrometer, ThermoFisher Scientific, Waltham,
716 MA, USA). Leaf nitrogen content per unit leaf area (N_{area} ; gN m⁻²) was calculated
717 by multiplying N_{mass} by M_{area} .

718 I used leaf $\delta^{13}\text{C}$ values to estimate χ (unitless), which is an isotope-derived
719 estimate of the leaf $C_i:C_a$ ratio. While intercellular and atmospheric CO₂ con-
720 centrations were directly measured during each A_{net}/C_i curve, deriving χ from
721 $\delta^{13}\text{C}$ provides a more integrative estimate of the $C_i:C_a$ over an individual leaf's
722 lifespan. We derived χ following the approach of Farquhar et al. (1989) described
723 in Cernusak et al. (2013):

$$\chi = \frac{\Delta^{13}\text{C} - a}{b - a} \quad (3.1)$$

724 where $\Delta^{13}\text{C}$ represents the relative difference between leaf $\delta^{13}\text{C}$ (%₀) and air $\delta^{13}\text{C}$
725 (%₀), and is calculated from the following equation:

$$\Delta^{13}\text{C} = \frac{\delta^{13}\text{C}_{\text{air}} - \delta^{13}\text{C}_{\text{leaf}}}{1 + \delta^{13}\text{C}_{\text{leaf}}} \quad (3.2)$$

726 where $\delta^{13}\text{C}_{\text{air}}$ is assumed to be -8%₀ (Keeling et al. 1979; Farquhar et al. 1989), a
727 represents the fractionation between ¹²C and ¹³C due to diffusion in air, assumed
728 to be 4.4%₀, and b represents the fractionation caused by Rubisco carboxylation,
729 assumed to be 27%₀ (Farquhar et al. 1989).

730 3.2.4 A_{net}/C_i curve-fitting and parameter estimation

731 I fit A_{net}/C_i curves of each individual using the ‘fitaci’ function in the ‘plante-
732 cophys’ R package (Duursma 2015). This function estimates the maximum rate
733 of Rubisco carboxylation (V_{cmax} ; $\mu\text{mol m}^{-2} \text{s}^{-1}$) and maximum rate of electron
734 transport for RuBP regeneration (J_{max} ; $\mu\text{mol m}^{-2} \text{s}^{-1}$) based on the Farquhar,
735 von Caemmerer, and Berry biochemical model of C₃ photosynthesis (Farquhar
736 et al. 1980). For each curve fit, I included triose phosphate utilization (TPU)
737 limitation to avoid underestimating J_{max} (Gregory et al. 2021). Curves were
738 visually examined to confirm the likely presence of TPU limitation.

739 I determined Michaelis-Menten coefficients for Rubisco affinity to CO₂ (K_c ;
740 $\mu\text{mol mol}^{-1}$) and O₂ (K_o ; $\mu\text{mol mol}^{-1}$), and the CO₂ compensation point (Γ^* ;
741 $\mu\text{mol mol}^{-1}$) using leaf temperature and equations described in Medlyn et al.
742 (2002) and derived in Bernacchi et al. (2001). Specifically, K_c and K_o were
743 calculated as:

$$K_c = 404.9 * \exp^{\frac{79430(T_k - 298)}{298RT_k}} \quad (3.3)$$

744 and

$$K_o = 278.4 * \exp^{\frac{36380(T_k - 298)}{298RT_k}} \quad (3.4)$$

745 while Γ^* was calculated as:

$$\Gamma^* = 42.75 * \exp^{\frac{37830(T_k - 298)}{298RT_k}} \quad (3.5)$$

746 In all three equations, T_k is the leaf temperature (in Kelvin) during each A_{net}/C_i

747 curve and R is the universal gas constant ($8.314 \text{ J mol}^{-1} \text{ K}^{-1}$).

748 I standardized V_{cmax} and J_{max} estimates to 25°C using a modified Arrhe-

749 nius equation (Kattge and Knorr 2007):

$$k_{25} = \frac{k_{\text{obs}}}{e^{\frac{H_a(T_{\text{obs}} - T_{\text{ref}})}{T_{\text{ref}}RT_{\text{obs}}}} * \frac{1+e^{\frac{T_{\text{ref}}\Delta S - H_d}{T_{\text{obs}}}}}{1+e^{\frac{T_{\text{obs}}\Delta S - H_d}{T_{\text{obs}}}}}} \quad (3.6)$$

750 k_{25} represents the standardized V_{cmax} or J_{max} rate at 25°C , k_{obs} represents the

751 V_{cmax} or J_{max} estimate at the average leaf temperature measured inside the cuvette

752 during the A_{net}/C_i curve. H_a is the activation energy of V_{cmax} ($71,513 \text{ J mol}^{-1}$)

753 Kattge and Knorr (2007) or J_{max} ($49,884 \text{ J mol}^{-1}$) (Kattge and Knorr 2007). H_d

754 represents the deactivation energy of both V_{cmax} and J_{max} ($200,000 \text{ J mol}^{-1}$) (Med-

755 lyn et al. 2002), and R represents the universal gas constant ($8.314 \text{ J mol}^{-1} \text{ K}^{-1}$).

756 T_{ref} represents the standardized temperature of 298.15 K (25°C) and T_{obs} rep-

757 resents the mean leaf temperature (in K) during each A_{net}/C_i curve. ΔS is an

758 entropy term that (Kattge and Knorr 2007) derived as a linear relationship with

759 average growing season temperature (T_g ; $^\circ\text{C}$), where:

$$\Delta S_{v_{\text{cmax}}} = -1.07 T_g + 668.39 \quad (3.7)$$

760 and

$$\Delta S_{j_{\text{max}}} = -0.75 T_g + 659.70 \quad (3.8)$$

761 I estimated T_g in Equations 3.7 and 3.8 based on mean daily (24-hour) air tem-
762 perature of the 30 days leading up to the day of each sample collection using the
763 same weather station reported in the site description. I used V_{cmax25} and J_{max25}
764 estimates to calculate the ratio of J_{max25} to V_{cmax25} ($J_{max25}:V_{cmax25}$; unitless).

765 3.2.5 *Proportion of leaf nitrogen allocated to photosynthesis and structure*

766 I used equations from Niinemets and Tenhunen (1997) to estimate the proportion
767 of leaf nitrogen content allocated to Rubisco and bioenergetics. The proportion of
768 leaf nitrogen allocated to Rubisco ($\rho_{rubisco}$; gN gN⁻¹) was calculated as a function
769 of V_{cmax25} and N_{area} :

$$\rho_{rubisco} = \frac{V_{cmax25} N_r}{V_{cr} N_{area}} \quad (3.9)$$

770 where N_r is the amount of nitrogen in Rubisco, set to 0.16 gN (gN in Rubisco)⁻¹
771 and V_{cr} is the maximum rate of RuBP carboxylation per unit Rubisco protein,
772 set to 20.5 μmol CO₂ (g Rubisco)⁻¹. The proportion of leaf nitrogen allocated to
773 bioenergetics (ρ_{bioe} ; gN gN⁻¹) was similarly calculated as a function of J_{max25} and
774 N_{area} :

$$\rho_{bioe} = \frac{J_{max25} N_b}{J_{mc} N_{area}} \quad (3.10)$$

775 where N_b is the amount of nitrogen in cytochrome f, set to 0.12407 gN (μmol
776 cytochrome f)⁻¹ assuming a constant 1: 1: 1.2 cytochrome f: ferredoxin NADP
777 reductase: coupling factor molar ratio (Evans and Seemann 1989; Niinemets and
778 Tenhunen 1997), and J_{mc} is the capacity of electron transport per cytochrome f,

779 set to 156 μmol electron (μmol cytochrome f) $^{-1}\text{s}^{-1}$.

780 I estimated the proportion of leaf nitrogen content allocated to photosynthetic tissue (ρ_{photo} ; gN gN^{-1}) as the sum of ρ_{rubisco} and ρ_{bioe} . This calculation
781 is an underestimate of the proportion of leaf nitrogen allocated to photosynthetic
782 tissue because it does not include nitrogen allocated to light harvesting proteins.
783 This leaf nitrogen pool was not included because I did not perform chlorophyll
784 extractions on focal leaves. However, the proportion of leaf nitrogen content al-
785 located to light harvesting proteins tends to be small relative to ρ_{rubisco} and ρ_{bioe} ,
786 and may scale with changes in ρ_{rubisco} and ρ_{bioe} (Niinemets and Tenhunen 1997).

788 Finally, I estimated the proportion of leaf nitrogen content allocated to
789 structural tissue ($\rho_{\text{structure}}$; gN gN^{-1}) using an empirical equation from Onoda
790 et al. (2017):

$$N_{\text{cw}} = 0.000355 * M_{\text{area}}^{1.39} \quad (3.11)$$

791 where N_{cw} is the leaf nitrogen content allocated to cell walls (gN m^{-2}). $\rho_{\text{structure}}$
792 was estimated by dividing N_{cw} by N_{area} .

793 3.2.6 *Tradeoffs between nitrogen and water use*

794 Photosynthetic nitrogen use efficiency (PNUE; $\mu\text{mol CO}_2 \text{ mol}^{-1} \text{ N s}^{-1}$) was cal-
795 culated by dividing A_{net} by N_{area} , first converting N_{area} to mol N m^{-2} using the
796 molar mass of nitrogen (14 g mol^{-1}). I used χ as an indicator of water use effi-
797 ciency, which exploratory analyses suggest had similar responses to soil nitrogen
798 availability and pH as intrinsic water use efficiency measured from gas exchange

799 ($A_{\text{net}}/g_{\text{sw}}$). Tradeoffs between nitrogen and water use were determined by cal-
800 culating the ratio of N_{area} to χ ($N_{\text{area}}:\chi$; gN m⁻²) and V_{cmax25} to χ ($V_{\text{cmax25}}:\chi$;
801 $\mu\text{mol m}^{-2} \text{s}^{-1}$). This approach is similar to tradeoff calculations in which nitrogen-
802 water use tradeoffs are measured as the ratio of N_{area} or V_{cmax25} to g_{sw} (Paillassa
803 et al. 2020; Bialic-Murphy et al. 2021). In this chapter, I quantify these rela-
804 tionships using χ in lieu of g_{sw} because g_{sw} rapidly changes with environmental
805 conditions and therefore may have been altered by recent tree branch severance
806 and/or placement in the cuvette.

807 3.2.7 *Soil nitrogen availability and pH*

808 To characterize soil nitrogen availability at the time of our leaf gas exchange
809 measurements, I used mixed bed resin bags to quantify mobile ammonium-N and
810 nitrate-N concentrations in each plot. Lycra mesh bags were filled with 5 g of
811 Dowex® Marathon MR-3 hydrogen and hydroxide form resin (MilliporeSigma,
812 Burlington, MA USA) and sealed with a zip tie. Each bag was activated by
813 soaking in 0.5 M HCl for 20 minutes, then in 2 M NaCl until pH of the saline
814 solution stabilized, as described in Allison et al. (2008). Five resin bags were
815 inserted about 10 cm below the soil surface at each plot on June 25, 2019: one
816 near each of the four plot corners and one near the plot center. All resin bags
817 were collected 24 days later on July 19, 2019 and were frozen until extracted.

818 Prior to anion and cation extraction, each resin bag was rinsed with ul-
819 trapure water (MilliQ IQ 7000; Millipore Sigma, Burlington, MA) to remove any
820 surface soil residues. Anions and cations were extracted from surface-cleaned
821 resin bags by individually soaking and shaking each bag in 100 mL of a 0.1 M

822 HCl/2.0 M NaCl matrix for one hour. Using a microplate reader (Biotek Synergy
823 H1; Biotek Instruments, Winooski, VT USA), I quantified nitrate-N concentra-
824 tions spectrophotometrically at 540 nm with the end product of a single reagent
825 vanadium (III) chloride reaction (Doane and Horwáth 2003), and ammonium-N
826 concentrations quantified at 650 nm with the end product of a modified phenol-
827 hypochlorite reaction (Weatherburn 1967; Rhine et al. 1998). Both the single
828 reagent vanadium (III) chloride and modified phenol-hypochlorite methodologies
829 are well established for determining nitrate-N and ammonium-N concentrations
830 in resin bag extracts (Arnone 1997; Allison et al. 2008). I used a series of negative
831 and positive controls throughout each well plate to verify the accuracy and preci-
832 sion of our measurements, assaying each resin bag extract and control in triplicate.
833 Soil N availability was estimated as the sum of the nitrate-N and ammonium-N
834 concentration in each resin bag, normalized per g of resin and duration in the field
835 ($\mu\text{g N g}^{-1} \text{ resin d}^{-1}$), then subsequently averaged across all resin bags in a plot
836 for a plot-level mean.

837 Soil pH was measured on 0-10 cm mineral soil samples collected prior to
838 fertilization in 2019. Near each of the four plot corners, three 5.5 cm diameter soil
839 cores were collected after first removing the forest floor where present. Each set
840 of three cores was placed in a plastic bag, and later composited by hand mixing
841 and sieved to 4mm. Soil pH was determined for a 1:2 soil:water slurry (10 g field-
842 moist soil to 20 mL DI water) of each sample using an Accumet AB15 pH meter
843 with flushable junction probe (Fisher Scientific; Hampton, NH, USA), and was
844 estimated at the plot level as the mean soil pH within each plot.

845 3.2.8 *Statistical analyses*

846 I built two separate series of linear mixed-effects models to explore effects of soil
847 nitrogen availability, soil pH, species, and leaf nitrogen content on leaf physiolog-
848 ical traits. In the first series of linear mixed-effects models, I explored the effect
849 of soil nitrogen availability, soil pH, and species on leaf nitrogen content, leaf
850 photosynthesis, stomatal conductance, and nitrogen-water use tradeoffs. Models
851 included plot-level soil N availability and plot-level soil pH as continuous fixed ef-
852 fects, species as a categorical fixed effect, and site as a categorical random intercept
853 term. Interaction terms between fixed effects were not included due to the small
854 number of experimental plots. I built a series of separate models with this indepen-
855 dent variable structure to quantify individual effects of soil nitrogen availability,
856 soil pH, and species on N_{area} , M_{area} , N_{mass} , A_{net} , V_{cmax25} , J_{max25} , $J_{\text{max25}}:V_{\text{cmax25}}$,
857 ρ_{rubisco} , $\rho_{\text{bioenergetics}}$, ρ_{photo} , $\rho_{\text{structure}}$, χ , PNUE, $N_{\text{area}}:\chi$, and $V_{\text{cmax25}}:\chi$.

858 A second series of linear mixed-effects models were built to investigate
859 relationships between leaf N content and photosynthetic parameters. Statistical
860 models included N_{area} as a single continuous fixed effect with species and site
861 designated as individual random intercept terms. I used this independent variable
862 structure to quantify individual effects of leaf nitrogen content on A_{net} , V_{cmax25} ,
863 J_{max25} , $J_{\text{max25}}:V_{\text{cmax25}}$, and χ .

864 For all linear mixed-effects models, I used Shapiro-Wilk tests of normality
865 to determine whether linear mixed-effects models satisfied residual normality as-
866 sumptions. If residual normality assumptions were not met, then models were fit
867 using dependent variables that were natural log transformed. If residual normal-
868 ity assumptions were still not met (Shapiro-Wilk: $p < 0.05$), then models were fit

869 using dependent variables that were square root transformed. All residual nor-
870 mality assumptions for both sets of models that did not originally satisfy residual
871 normality assumptions were met with either a natural log or square root data
872 transformation (Shapiro-Wilk: $p>0.05$ in all cases).

873 In the first series of models, models for N_{area} , M_{area} , N_{mass} , $V_{\text{cmax}25}$, $J_{\text{max}25}$,
874 χ , $N_{\text{area}}:\chi$, and $V_{\text{cmax}25}:\chi$, ρ_{rubisco} , $\rho_{\text{bioenergetics}}$, ρ_{photo} , $\rho_{\text{structure}}$ satisfied residual
875 normality assumptions without data transformations (Shapiro-Wilk: $p>0.05$ in
876 all cases). The model for $J_{\text{max}25}:V_{\text{cmax}25}$ satisfied residual normality assumptions
877 with a natural log data transformation, while models for A_{net} and PNUE each
878 satisfied residual normality assumptions with square root data transformations.
879 In the second series of models, models for $V_{\text{cmax}25}$, $J_{\text{max}25}$, χ , and $V_{\text{cmax}25}:\chi$ satis-
880 fied residual normality assumptions without data transformations (Shapiro-Wilk:
881 $p>0.05$ in all cases). The model for $J_{\text{max}25}:V_{\text{cmax}25}$ required a natural log data
882 transformation and the model for A_{net} required a square root data transformation
883 (Shapiro-Wilk: $p>0.05$ in both cases).

884 In all models, I used the ‘lmer’ function in the ‘lme4’ R package (Bates
885 et al. 2015) to fit each model and the ‘Anova’ function in the ‘car’ R package
886 (Fox and Weisberg 2019) to calculate Type II Wald’s χ^2 and determine the signif-
887 icance level ($\alpha=0.05$) of each fixed effect coefficient. Finally, I used the ‘emmeans’
888 R package (Lenth, 2019) to conduct post-hoc comparisons using Tukey’s tests,
889 where degrees of freedom were approximated using the Kenward-Roger approach
890 (Kenward and Roger 1997). All analyses and plots were conducted in R version
891 4.1.1 (R Core Team 2021). All figure regression lines and associated 95% confi-
892 dence interval error bars were plotted using predictions generated across the soil

893 nitrogen availability gradient using the ‘emmeans’ R package (Lenth 2019).

894 3.3 Results

895 3.3.1 *Leaf nitrogen content*

896 Increasing soil nitrogen availability generally increased N_{area} (Table 3.1; Fig. 3.1a).

897 This pattern was driven by an increase in N_{mass} (Table 3.1; Fig. 3.1c) and a

898 marginal increase in M_{area} (Table 3.1; Fig. 3.1e) with increasing soil nitrogen

899 availability. There was no effect of soil pH on N_{area} , N_{mass} , or M_{area} (Table 3.1);

900 however, I also observed strong differences in N_{area} (Fig. 3.1b), N_{mass} (Fig. 3.1d),

901 and M_{area} (Fig. 3.1e) between species (Table 3.1).

Table 3.1. Effects of soil nitrogen availability, soil pH, and species on leaf nitrogen content per unit leaf area (N_{area} ; gN m⁻²), leaf nitrogen content per unit leaf mass (N_{mass} ; gN g⁻¹), and leaf mass per unit leaf area (M_{area} ; g m⁻²)*

	N_{area}			N_{mass}			M_{area}			
	df	Coefficient	χ^2	p	Coefficient	χ^2	p	Coefficient	χ^2	p
Intercept	-	9.03E-01	-	-	1.68E+00	-	-	4.60E+01	-	-
Soil N	1	1.68E-02	11.990	0.001	1.25E-02	6.902	0.009	4.87E-01	4.143	0.042
Soil pH	1	9.28E-02	0.836	0.361	8.08E-02	0.663	0.415	4.05E+00	0.653	0.419
Species	4	-	72.128	<0.001	-	35.074	<0.001	-	29.869	<0.001

902 *Significance determined using Type II Wald χ^2 tests ($\alpha=0.05$). P-values<0.05 are in bold.

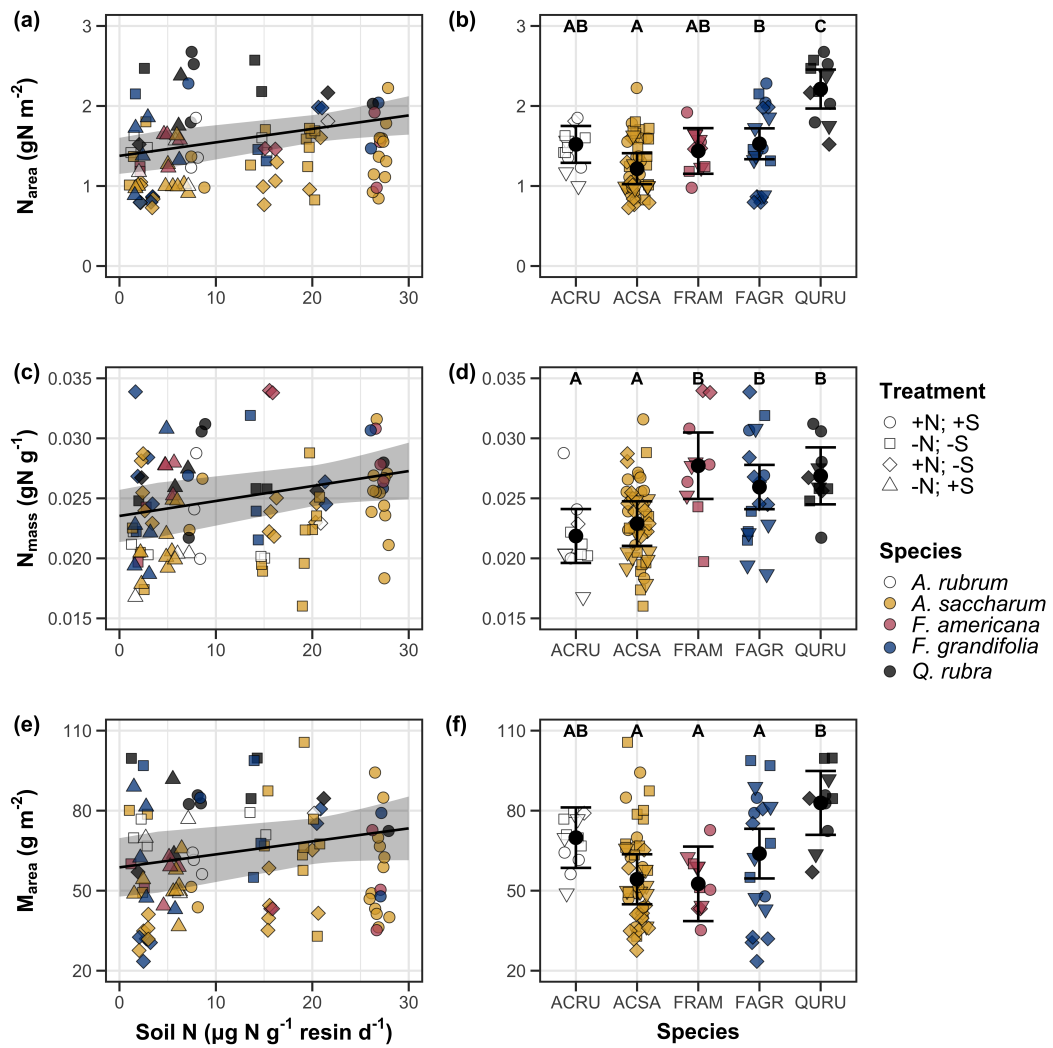


Figure 3.1. Effects of soil N availability and species on leaf nitrogen content per unit leaf area (a-b), leaf nitrogen content per unit leaf biomass (c-d), and leaf mass per unit leaf area (e-f). Soil nitrogen availability is represented on the x-axis in the left column of panels, while species is represented on the x-axis in the right column of panels. Tree species are represented as colored points and treatment plots are represented as shaped points, jittered for visibility. Species are abbreviated in the right column of panels through their assigned NRCS PLANTS Database symbol (USDA NRCS 2022), grouped along the x-axis per common mycorrhizal association, where the first three species commonly associate with arbuscular mycorrhizae (ACRU, ACSA, FAGR) and the second two species with ectomycorrhizae (FAGR, QURU). Trendlines are only included when the regression slope is statistically different from zero ($p < 0.05$).

903 3.3.2 *Net photosynthesis and leaf biochemistry*

904 Increasing soil nitrogen availability generally had no effect on A_{net} , V_{cmax25} , J_{max25} ,
905 or $J_{\text{max25}}:V_{\text{cmax25}}$ (Table 3.2, Figs. 3.2a, 3.2d, 3.2g). I also observed strong species
906 effects on all measured leaf photosynthetic traits (Table 3.2; Figs. 3.2b, 3.2e, 3.2h).
907 Increasing soil pH had a marginal negative effect on A_{net} , but had no effect on
908 V_{cmax25} , J_{max25} , or $J_{\text{max25}}:V_{\text{cmax25}}$ (Table 3.2). There was a weak positive effect of
909 increasing N_{area} on A_{net} (Fig. 3.2c), but quite strong positive effects of increasing
910 N_{area} on V_{cmax25} and J_{max25} (Table 3.2; Fig. 3.2f and 3.2i).

Table 3.2. Effects of soil nitrogen availability, soil pH, species, and N_{area} on net photosynthesis (A_{net} ; $\mu\text{mol m}^{-2} \text{s}^{-1}$), the maximum rate of Rubisco carboxylation (V_{cmax25} ; $\mu\text{mol m}^{-2} \text{s}^{-1}$), the maximum rate of RuBP regeneration (J_{max25} ; $\mu\text{mol m}^{-2} \text{s}^{-1}$), and the ratio of the maximum rate of RuBP regeneration to the maximum rate of Rubisco carboxylation ($J_{\text{max25}}:V_{\text{cmax25}}$; unitless)*

	A_{net}			V_{cmax25}			J_{max25}			
	df	Coefficient	χ^2	p	Coefficient	χ^2	p	Coefficient	χ^2	p
(Intercept)	-	3.29E+00 ^b	-	-	6.38E+01	-	-	1.12E+02	-	-
Soil N	1	-1.23E-03 ^b	1.798	0.180	-3.84E-01	1.745	0.187	-6.70E-01	2.172	0.141
Soil pH	1	-3.09E-01 ^b	3.312	0.069	-4.91E+00	0.655	0.418	-8.18E+00	0.742	0.389
Species	4	-	11.838	0.019	-	31.748	<0.001	-	27.291	<0.001
(N_{area} int.)	-	6.59E-01 ^b	-	-	1.45E-01	-	-	2.86E+01	-	-
N_{area}	4	3.13E-01 ^b	4.790	0.029	2.43E+01	22.616	<0.001	4.04E+01	28.259	<0.001

	$J_{\text{max25}}:V_{\text{cmax25}}$			
	df	Coefficient	χ^2	p
(Intercept)	-	6.59E-01 ^a	-	-
Soil N	1	7.04E-04 ^a	0.088	0.767
Soil pH	1	-7.84E-03 ^a	0.025	0.874
Species	4	-	12.745	0.013
(N_{area} int.)	-	6.69E-01 ^a	-	-
N_{area}	4	-4.69E-02 ^a	1.142	0.285

54

911 *Significance determined using Type II Wald χ^2 tests ($\alpha=0.05$). P-values less than 0.05 are in bold, while p-values
 912 between 0.05 and 0.1 are italicized. Superscript letters indicate model coefficients fit to natural-log (^a) or square-root
 913 (^b) transformed data. Relationships between N_{area} and each response variable were fit using the second series of
 914 bivariate mixed-effects models, so model coefficients and results are independent of model coefficients and results
 915 reported for relationships between soil nitrogen, soil pH, and species for each response variable.

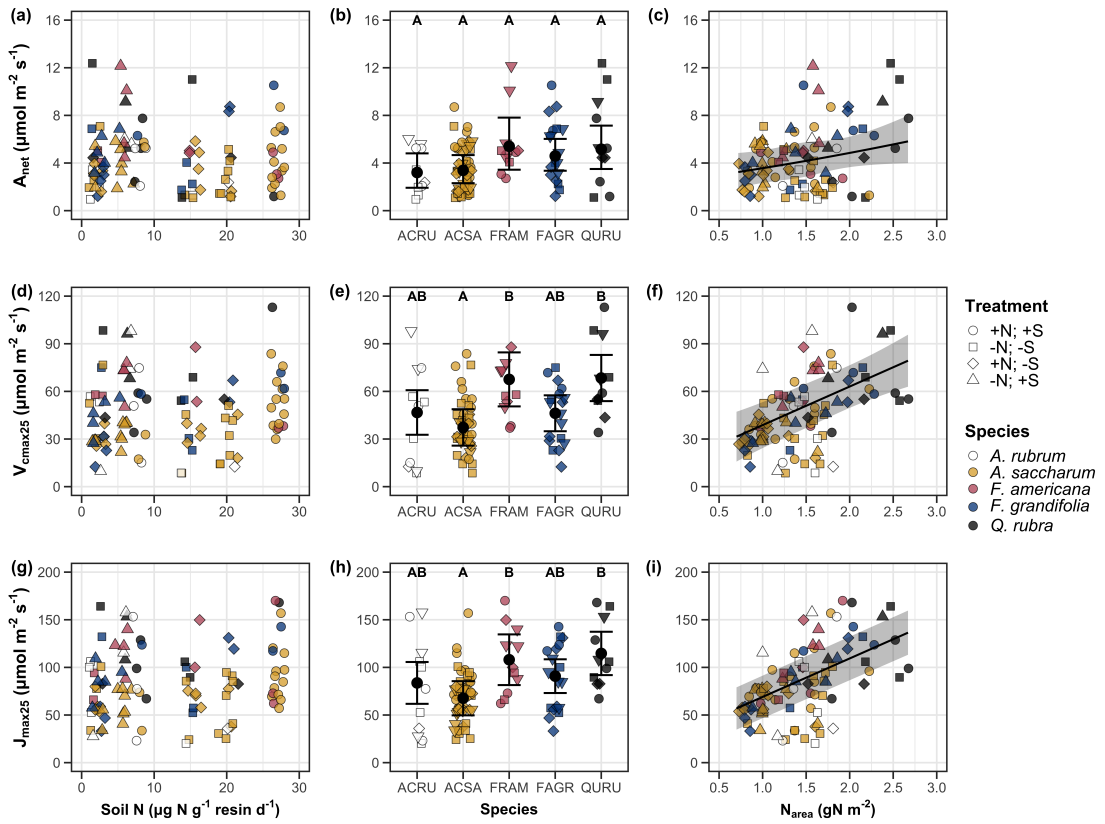


Figure 3.2. Effects of soil nitrogen availability (left column of panels), species (middle column of panels), and leaf nitrogen content per unit leaf area (right column of panels) on net photosynthesis (a-c), maximum Rubisco carboxylation rate (d-f), and maximum RuBP regeneration rate (g-i). Soil nitrogen availability is represented on the x-axis in the left column of panels, species is represented on the x-axis in the middle column of panels, and leaf nitrogen content per unit leaf area is represented continuously on the x-axis in the right column of panels. Species abbreviations and position along the x-axis in the middle column of panels, colored points, shapes, and trendlines are as explained in Figure 3.1.

916 3.3.3 *Leaf nitrogen allocation*

917 Neither soil nitrogen availability nor soil pH affected the proportion of leaf nitro-
918 gen allocated to Rubisco or bioenergetics (Table 3.3; Fig. 3.3a, Fig. 3.3c), nor was
919 there any subsequent effect on the proportion of leaf nitrogen allocated to photo-
920 synthesis (Table 3.3; Fig. 3.3f). I also found no effect of soil nitrogen availability
921 or soil pH on the proportion of leaf nitrogen allocated to structure (Table 3.3;
922 Fig 3.3g). Species varied in the proportion of leaf nitrogen allocated to Rubisco,
923 photosynthesis, and structure (Fig 3.3b, Fig. 3.3d, Fig 3.3h), with no detectable
924 species effect on the proportion of leaf nitrogen allocated to bioenergetics (Table
925 3.3).

Table 3.3. Effects of soil nitrogen availability, soil pH, and species on the proportion of leaf nitrogen content allocated to photosynthesis (ρ_{photo} ; gN gN⁻¹), Rubisco (ρ_{rubisco} ; gN gN⁻¹), bioenergetics (ρ_{bioe} ; gN gN⁻¹), and structure ($\rho_{\text{structure}}$; gN gN⁻¹)*

	ρ_{photo}			ρ_{rubisco}			ρ_{bioe}			
	df	Coefficient	χ^2	p	Coefficient	χ^2	p	Coefficient	χ^2	p
Intercept	-	4.93E-01	-	-	4.17E-01	-	-	7.64E-02	-	-
Soil N	1	-1.23E-03	0.521	0.470	-1.04E-03	0.501	0.479	-1.77E-04	0.557	0.455
Soil pH	1	-4.37E-02	1.581	0.209	-3.70E-02	1.511	0.219	-6.84E-03	1.941	0.164
Species	4	-	13.106	0.011	-	14.152	0.007	-	7.300	0.121

	$\rho_{\text{structure}}$			
	df	Coefficient	χ^2	p
Intercept	-	9.77E-02	-	-
Soil N	1	-2.29E-04	1.165	0.280
Soil pH	1	-1.87E-03	0.179	0.672
Species	4	-	16.428	0.002

926 *Significance determined using Type II Wald χ^2 tests ($\alpha=0.05$). P-values less than 0.05 are in bold.

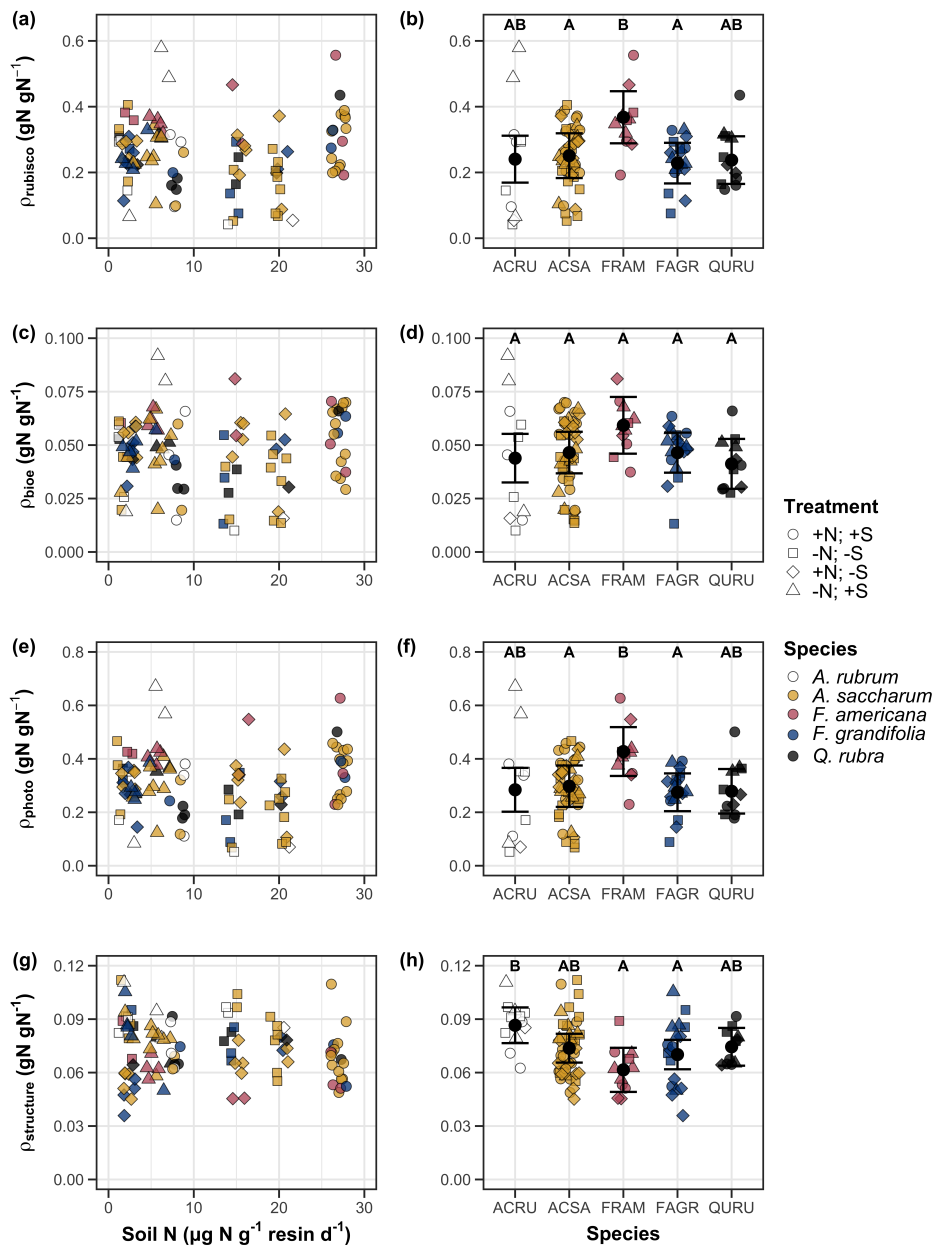


Figure 3.3. Effects of soil nitrogen availability and species on the proportion of leaf nitrogen content allocated to Rubisco (a-b), bioenergetics (c-d), photosynthesis (e-f), and structure (g-h). Soil nitrogen availability is represented on the x-axis in the left column of panels and species are represented on the x-axis in the right column of panels. Species abbreviations and position along the x-axis in the middle column of panels, colored points, shapes, trendlines, error bars, and compact lettering are as explained in Figure 3.1.

927 3.3.4 *Tradeoffs between nitrogen and water use*

928 Although soil nitrogen availability did not affect χ (Table 3.4; Fig. 3.4a), increasing
929 soil nitrogen availability decreased PNUE (Table 3.4; Fig. 3.4d) and increased
930 the ratio of $N_{\text{area}}:\chi$ (Table 3.4; Fig. 3.4f). Specifically, this response yielded a
931 26% reduction in PNUE and 37% stimulation in $N_{\text{area}}:\chi$ across the soil nitrogen
932 availability gradient. There was no apparent effect of soil nitrogen availability on
933 $V_{\text{cmax25}}:\chi$ (Table 3.4; Fig. 3.4h). Increasing soil pH had a weak marginal nega-
934 tive effect on PNUE, but did not influence χ , $N_{\text{area}}:\chi$, or $V_{\text{cmax25}}:\chi$ (Table 3.4). I
935 observed differences in χ (Fig. 3.4b), PNUE (Fig. 3.4e), $N_{\text{area}}:\chi$ (Fig. 3.4g), and
936 $V_{\text{cmax25}}:\chi$ (Fig. 3.4i) between species (Table 3.4). Finally, increasing N_{area} had a
937 strong negative effect on χ (Table 3.4; Fig. 3.4c) and a strong positive effect on
938 $V_{\text{cmax25}}:\chi$ (Table 3.4; Fig. 3.4j).

Table 3.4. Effects of soil nitrogen availability, soil pH, species, and N_{area} on χ (unitless), photosynthetic nitrogen use efficiency (PNUE; $\mu\text{mol CO}_2 \text{ mol}^{-1} \text{ N s}^{-1}$), leaf nitrogen content per unit χ ($N_{\text{area}}:\chi$; gN m^{-2}), and maximum Rubisco carboxylation rate per unit χ ($V_{\text{cmax25}}:\chi$; $\mu\text{mol m}^{-2} \text{ s}^{-1}$)^{*}

	df	χ		PNUE				$N_{\text{area}}:\chi$		
		Coefficient	χ^2	p	Coefficient	χ^2	p	Coefficient	χ^2	p
(Intercept)	-	8.12E-01	-	-	9.57E+00 ^b	-	-	9.19E-01	-	-
Soil N	1	-1.14E-03	1.698	0.193	-6.63E-02 ^b	6.396	0.011	2.60E-02	9.533	0.002
Soil pH	1	-1.91E-02	1.087	0.297	-9.25E-01 ^b	2.843	<i>0.092</i>	2.03E-01	1.321	0.250
Species	4	-	18.843	0.001	-	13.454	0.009	-	52.983	<0.001
(N_{area} int.)	-	8.93E-01	-	-	-	-	-	-	-	-
N_{area}	1	-1.11E-01	80.606	<0.001	-	-	-	-	-	-

	df	$V_{\text{cmax25}}:\chi$		
		Coefficient	χ^2	p
(Intercept)	-	7.20E+01	-	-
Soil N	1	3.99E-01	0.963	0.326
Soil pH	1	-3.12E+00	0.138	0.711
Species	4	-	31.450	<0.001
(N_{area} int.)	-	1.18E+01	-	-
N_{area}	4	3.87E+01	32.797	<0.001

60

939 *Significance determined using Type II Wald χ^2 tests ($\alpha = 0.05$). P -values less than 0.05 are in bold, while p -values
 940 between 0.05 and 0.1 are italicized. Superscript letters indicate model coefficients fit to natural-log (^a) or square-root
 941 (^b) transformed data. Relationships between N_{area} and each response variable were fit using the second series of
 942 bivariate mixed-effects models, so model coefficients and results are independent of model coefficients and results
 943 reported for relationships between soil nitrogen, soil pH, and species for each response variable.

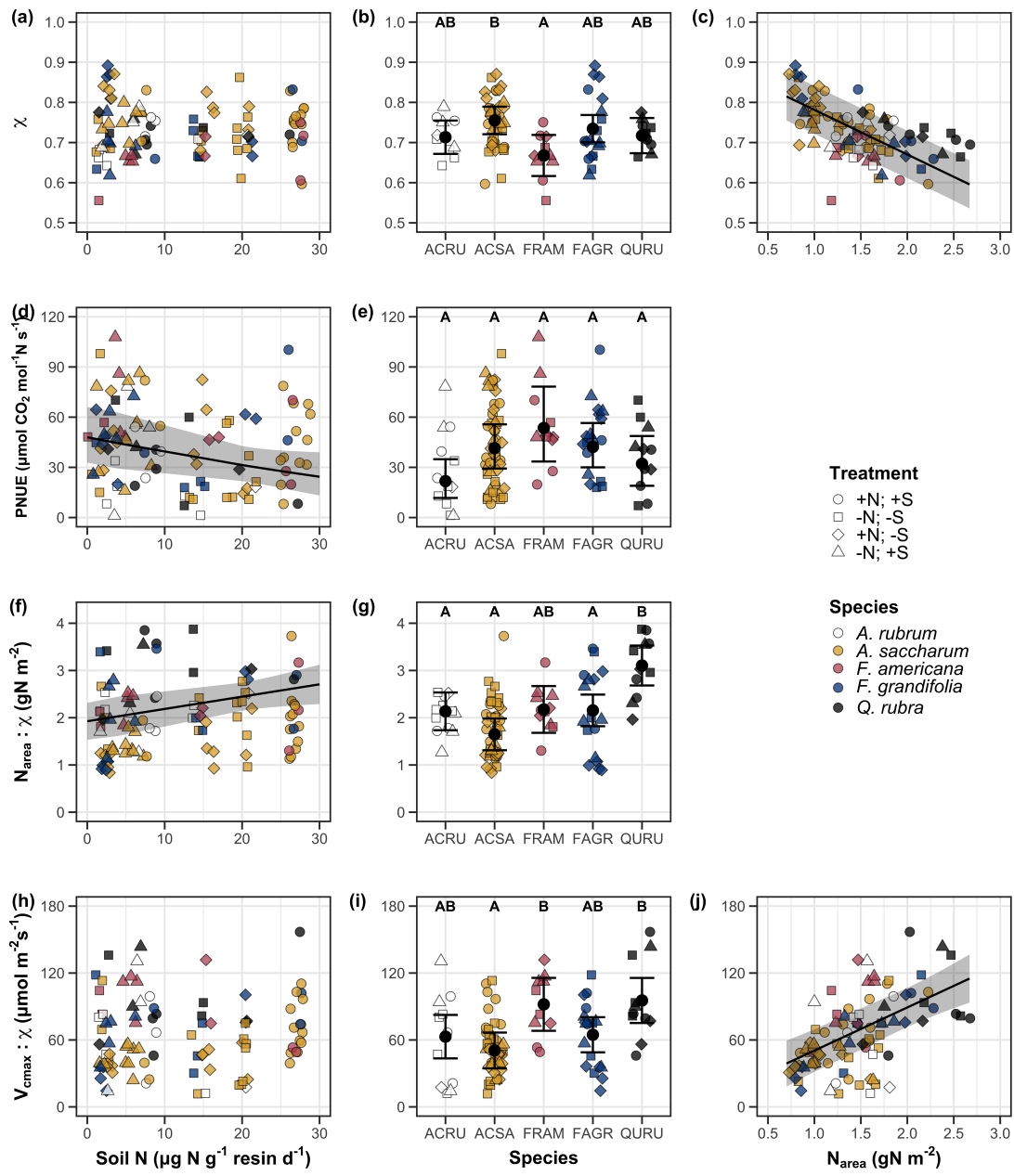


Figure 3.4. Effects of soil nitrogen availability and species on the proportion of leaf nitrogen content allocated to Rubisco (a-b), bioenergetics (c-d), photosynthesis (Rubisco + bioenergetics; e-f), and structure (g-h). Soil nitrogen availability is represented on the x-axis in the left column of panels and species are represented on the x-axis in the right column of panels. Species abbreviations and position along the x-axis in the middle column of panels, colored points, shapes, trendlines, error bars, and compact lettering are as explained in Figure 3.1.

944 3.4 Discussion

945 Photosynthetic least-cost theory provides an explanation for understanding rela-
946 tionships between soil nutrient availability, leaf nutrient allocation, and photosyn-
947 thetic capacity. The theory suggests that plants acclimate to a given environment
948 by optimizing leaf photosynthesis rates at the lowest summed cost of using nu-
949 trients and water (Prentice et al. 2014; Wang et al. 2017; Smith et al. 2019;
950 Paillassa et al. 2020). The theory predicts that an increase in soil nutrient avail-
951 ability should allow similar photosynthesis rates to be achieved with increased leaf
952 nutrient content and photosynthetic capacity (i.e., V_{cmax25} and J_{max25}) at lower
953 leaf $C_i:C_a$ (χ), resulting in an increase in water use efficiency, decrease in nutri-
954 ent use efficiency, and increase in both leaf nutrient content and photosynthetic
955 capacity per unit χ . The theory predicts similar leaf responses to increasing soil
956 pH under acidic conditions, presumably due to generally faster nutrient cycle dy-
957 namics and consequent reductions in the cost of acquiring nutrients relative to
958 water with increasing soil pH (Wang et al. 2017; Paillassa et al. 2020; Dong et al.
959 2020).

960 Supporting the theory, increasing soil nitrogen availability was associated
961 with increased leaf nitrogen content, a pattern that reduced photosynthetic nitro-
962 gen use efficiency and increased leaf N content per unit χ . Increasing soil nitrogen
963 coincided with slight, but non-significant decreases in χ and increases in V_{cmax25}
964 and J_{max25} ($p<0.2$, Table 3.2). The positive trend between soil nitrogen availabil-
965 ity and photosynthetic capacity was supported by the concurrent strong increase
966 in leaf nitrogen content with increasing soil nitrogen availability, which resulted in
967 no change in the proportion of leaf nitrogen content allocated to photosynthesis

968 across the soil nitrogen availability gradient. Additionally, leaf nitrogen content
969 exhibited a strong negative correlation with χ , indicative of strong nitrogen-water
970 use tradeoffs at the leaf level. Responses tended to vary more due to soil ni-
971 trogen availability than soil pH. Overall, these findings are consistent with the
972 nutrient-water use tradeoffs predicted from theory.

973 3.4.1 *Soil nitrogen availability modifies tradeoffs between nitrogen and water use*
974 In support of expected least-cost outcomes and past environmental gradient stud-
975 ies (Dong et al. 2017; Paillassa et al. 2020), increasing soil nitrogen availability
976 was associated with increased leaf nitrogen content. Soil nitrogen availability had
977 smaller impacts on measures of net photosynthesis and χ , which led to reductions
978 in PNUE and increases in leaf nitrogen content per unit χ , as expected from the-
979 ory. Photosynthetic least-cost theory suggests that reductions in PNUE should
980 be driven by an increase in the proportion of leaf nitrogen allocated to photosyn-
981 thetic tissue, a pattern that should allow plants to achieve optimal photosynthetic
982 rates with greater photosynthetic capacity to make better use of available light.
983 Contrasting theory predictions, I found no effect of soil nitrogen availability on
984 photosynthetic capacity. However, photosynthetic capacity did tend to increase
985 with increasing soil nitrogen availability ($p<0.20$; Table 3.2) resulting in no effect
986 of soil nitrogen availability on the relative fraction of leaf nitrogen allocated to
987 photosynthesis, Rubisco, or bioenergetics. These lines of evidence support the
988 idea that trees use additional nitrogen to support increased leaf nitrogen alloca-
989 tion toward photosynthetic tissue and enhance photosynthetic capacity (Wright
990 et al. 2003).

991 Soil nitrogen availability had a stronger effect on leaf nitrogen than pho-
992 tosynthetic capacity. This pattern suggests that additional plant nitrogen up-
993 take due to increased soil nitrogen availability was also being used to support
994 non-photosynthetic nitrogen pools, possibly to structural tissue or stress-induced
995 amino acid and polyamine synthesis (Minocha et al. 2000; Onoda et al. 2004;
996 Bubier et al. 2011). While I found no change in the proportion of leaf nitrogen
997 allocated to leaf structural tissue, the overall stimulation in leaf nitrogen content
998 with increasing soil nitrogen availability suggests an increase in the net amount
999 of nitrogen invested in leaf structural tissue along the N availability gradient.
1000 Importantly, leaf nitrogen allocated to structure was calculated using an empiri-
1001 cal relationship between M_{area} and the amount of leaf nitrogen allocated to cell
1002 walls (Onoda et al. 2017). As the generality of relationships between M_{area} and
1003 the amount of leaf nitrogen allocated to cell walls has been called into question
1004 (Harrison et al. 2009), future work should consider explicitly measuring nitrogen
1005 allocation to cell wall tissue and stress-induced amino acid synthesis to confirm
1006 these patterns.

1007 In opposition to patterns expected from least-cost theory, increasing soil
1008 nitrogen availability had no apparent effect on χ . Interestingly, despite the null
1009 effect of soil nitrogen availability on χ , I observed a strong negative effect of in-
1010 creasing N_{area} on χ , consistent with the nitrogen-water use tradeoffs expected from
1011 theory. The null response of χ to increasing soil nitrogen availability may have
1012 been due to a lack of water limitation in the system, given that the area received
1013 approximately 20% more precipitation (1167 mm) during the 12-month period
1014 leading up to our measurement period than normally expected (972 mm). How-

1015 ever, droughts can and do occur in temperate forests of the northeastern United
1016 States (Sweet et al. 2017), so the observed increase in leaf nitrogen content with
1017 increasing soil nitrogen availability could be a strategy that allows trees to hedge
1018 bets against drier than normal growing seasons (Onoda et al. 2004; Onoda et al.
1019 2017; Hallik et al. 2009). As was suggested in Paillassa et al. (2020), and more
1020 recently by Querejeta et al. (2022), negative effects of soil nitrogen availabil-
1021 ity on χ may increase with increasing aridity. This strategy would be especially
1022 advantageous if it allows individuals growing in arid regions to maintain carbon
1023 assimilation rates with reduced water loss. Future work should attempt to quan-
1024 tify interactive roles of climate and soil nitrogen availability on nitrogen-water use
1025 tradeoffs, which could be done by leveraging coordinated and multifactor nutrient
1026 (Borer et al. 2014) and water (Knapp et al. 2017) manipulation experiments
1027 across broad climatic gradients.

1028 3.4.2 *Soil pH did not modify tradeoffs between nitrogen and water usage*

1029 While the primary purpose of this study was to examine the role of soil nitrogen
1030 availability on nitrogen-water use tradeoffs, this experimental design manipulated
1031 both soil nitrogen and pH, providing an opportunity to isolate the roles of these
1032 variables. Previous correlational studies along environmental gradients have iden-
1033 tified soil pH as a particularly important factor that can modify tradeoffs between
1034 nutrient and water use (Smith et al. 2019; Paillassa et al. 2020; Westerband et al.
1035 2023) and the proportion of leaf nitrogen allocated to photosynthesis (Luo et al.
1036 2021). Such studies implied that these patterns may be driven by reductions in
1037 the cost of acquiring nutrients relative to water with increasing pH, which may

1038 be exacerbated in acidic soils.

1039 Consistent with theory (Wright et al. 2003; Prentice et al. 2014), results
1040 indicate that increasing soil pH was negatively associated with PNUE. However,
1041 there was no effect of soil pH on leaf nitrogen content, χ , or leaf nitrogen content
1042 per unit χ , most likely because the experimental nitrogen additions increased soil
1043 nitrogen supply while both increasing (sodium nitrate) and decreasing (ammo-
1044 nium sulfate) soil pH. These results suggest that soil pH did not play a major
1045 role in modifying expected photosynthetic least-cost theory patterns, contrasting
1046 findings from Paillassa et al. (2020) and other gradient studies that note positive
1047 effects of increasing soil pH on leaf nitrogen content, Rubisco carboxylation, and
1048 χ (Viet et al. 2013; Cornwell et al. 2018; Luo et al. 2021). Instead, null responses
1049 to soil pH show that leaf photosynthetic parameters depend more on soil nitrogen
1050 availability than pH per se, and that inferences from gradient studies might be
1051 confounding covariation between nitrogen availability and soil acidity.

1052 3.4.3 *Species identity explains a large amount of variation in leaf and whole*
1053 *plant traits*

1054 Species generally explained a larger amount of variation in measured leaf traits
1055 than soil nitrogen availability or soil pH. Interspecies variation is an important
1056 factor to consider when deducing mechanisms that drive photosynthetic least-
1057 cost theory, particularly for species that form distinct mycorrhizal associations or
1058 have different photosynthetic pathways, growth forms, or leaf habit (Espelta et al.
1059 2005; Adams et al. 2016; Bialic-Murphy et al. 2021; Scott and Smith 2022). The
1060 need to consider species may also be important when comparing nutrient-water

1061 use tradeoffs in early and late successional species, or in species with different
1062 resource economic strategies (Abrams and Mostoller 1995; Ellsworth and Reich
1063 1996; Wright et al. 2004; Reich 2014; Onoda et al. 2017; Ziegler et al. 2020).

1064 A strength of the study design and sampling effort is that it controls for
1065 many species differences that should modify nitrogen-water use tradeoffs expected
1066 from theory. All tree species measured in this study shared the leaf habit of de-
1067 ciduous broadleaves, were growing in forests of similar successional stage, but
1068 differed in mycorrhizal association and consequent resource economic strategies.
1069 As stands tended to be dominated by trees that associate with arbuscular myc-
1070 orrhizae (*Fraxinus* and both *Acer* species made up roughly 70% of total above-
1071 ground biomass across stands), ecosystem biogeochemical cycle dynamics may be
1072 more closely aligned to the inorganic nutrient economy proposed in Phillips et al.
1073 (2013), which may promote stronger nitrogen-water use tradeoffs in tree species
1074 that associate with arbuscular mycorrhizae. This result was not observed here,
1075 as photosynthetic properties varied as much within as across the two mycorrhizal
1076 associations represented. Given the high variability in measured photosynthetic
1077 traits within and across species, effects of mycorrhizal association likely require
1078 more intensive sampling efforts to detect than were possible here.

1079 3.4.4 *Implications for photosynthetic least-cost theory model development*

1080 In the field, soil nutrient availability is heterogeneous across time and space (Ta-
1081 ble B4). Unaccounted within-plot heterogeneity may have contributed to the low
1082 amount of variation explained by soil nitrogen availability in statistical models,
1083 as resin bags are a coarse surrogate for soil nitrogen availability. Despite this, I

1084 still observed evidence for nutrient-water use tradeoffs, suggesting that observed
1085 responses reported here may be an underestimate toward the net effect of soil ni-
1086 trogen availability on these tradeoffs. While I urge caution in the interpretation of
1087 these results, they do provide a promising baseline for future studies investigating
1088 patterns expected from photosynthetic least-cost theory at finer spatiotemporal
1089 resolutions.

1090 The general stronger relationship between leaf nitrogen content and photo-
1091 synthetic parameters versus between leaf nitrogen content and soil nitrogen avail-
1092 ability suggests that leaf nitrogen content is more directly tied to photosynthesis
1093 than soil nitrogen availability. While this could be due to the high spatiotemporal
1094 heterogeneity of soil nitrogen availability, principles from photosynthetic least-
1095 cost theory suggest that leaf nitrogen content is the downstream product of leaf
1096 nutrient demand to build and maintain photosynthetic machinery, which is set by
1097 aboveground environmental conditions such as light availability, CO₂, tempera-
1098 ture, or vapor pressure deficit (Smith et al. 2019; Paillassa et al. 2020; Peng et al.
1099 2021; Westerband et al. 2023). The stronger relationship between leaf nitrogen
1100 and photosynthetic parameters, paired with the strong negative relationship be-
1101 tween leaf nitrogen and χ , could indicate a relatively stronger effect of climate on
1102 leaf nitrogen-photosynthesis relationships than soil resource availability. However,
1103 the short distance between plots and across sites limited our ability to test this
1104 mechanism.

1105 Variation in soil pH affected least cost responses less than variations in soil
1106 nitrogen availability, in part because experimental treatments directly increased
1107 soil nitrogen and affected soil pH in opposite directions. While soil pH has been

1108 shown to drive nitrogen-water tradeoffs in global gradient analyses (Viet et al.
1109 2013; Paillassa et al. 2020), these responses may be due to covariations between
1110 soil pH and nutrient cycling rather than a role of pH per se. The direct manipu-
1111 lations of soil pH and soil nitrogen availability in this study allowed us to partly
1112 disentangle these factors and show that variation in nitrogen availability matters
1113 more for least-cost tradeoffs than pH alone.

1114 3.4.5 *Conclusions*

1115 Increasing soil nitrogen availability generally increased leaf nitrogen content (both
1116 area- and mass-based), but did not significantly influence χ . This shift in leaf ni-
1117 trogen led to a reduction in PNUE, and an increase in leaf nitrogen per unit
1118 χ with increasing soil nitrogen availability. Despite null effects of soil nitrogen
1119 availability on χ , I observed a strong negative relationship between leaf nitrogen
1120 content and χ . These results provide empirical support for the nutrient-water use
1121 tradeoffs expected from photosynthetic least-cost theory in response to increas-
1122 ing soil nutrient availability, but suggest that all tenets of the theory may not
1123 hold in every environment. These results experimentally test previous work sug-
1124 gesting that leaf nitrogen-water economies vary across gradients of soil nutrient
1125 availability and pH, and show that variations in nutrient availability matter more
1126 for determining variation in leaf photosynthetic traits than soil pH.

1127

Chapter 4

1128 The relative cost of resource use for photosynthesis drives variance in
1129 leaf nitrogen content across a climate and soil resource availability
1130 gradient

1131 4.1 Introduction

1132 Terrestrial biosphere models, which comprise the land surface component of Earth
1133 system models, are sensitive to the formulation of photosynthetic processes (Knorr
1134 and Heimann 2001; Ziehn et al. 2011; Booth et al. 2012; Walker et al. 2021).
1135 This is because photosynthesis is the largest carbon flux between the atmosphere
1136 and terrestrial biosphere (IPCC 2021), and is constrained by ecosystem carbon
1137 and nutrient cycles (Hungate et al. 2003; LeBauer and Treseder 2008; Fay et al.
1138 2015). Many terrestrial biosphere models formulate photosynthesis by parame-
1139 terizing photosynthetic capacity within plant functional groups through empiri-
1140 cal linear relationships between area-based leaf nitrogen content (N_{area}) and the
1141 maximum carboxylation rate of Ribulose-1,5-bisphosphate carboxylase/oxygenase
1142 (V_{cmax}) (Kattge et al. 2009; Rogers 2014; Rogers et al. 2017). Models are also
1143 beginning to include connected carbon-nitrogen cycles (Wieder et al. 2015; Shi
1144 et al. 2016; Davies-Barnard et al. 2020; Braghieri et al. 2022), which allows leaf
1145 photosynthesis to be predicted directly through changes in N_{area} and indirectly
1146 through changes in soil nitrogen availability (e.g., LPJ-GUESS, CLM5.0) (Smith
1147 et al. 2014; Lawrence et al. 2019). Despite recent model developments, open
1148 questions remain regarding the generality of ecological relationships between soil
1149 nitrogen availability, leaf nitrogen content, and leaf photosynthesis across edaphic
1150 and climatic gradients.

1151 Empirical support for positive relationships between soil nitrogen availabil-
1152 ity and N_{area} is abundant (Firn et al. 2019; Liang et al. 2020), and is a result
1153 often attributed to the high nitrogen cost of building and maintaining Rubisco
1154 (Evans 1989; Evans and Seemann 1989; Onoda et al. 2004; Walker et al. 2014;
1155 Onoda et al. 2017; Dong et al. 2020). Such patterns imply that positive relation-
1156 ships between soil nitrogen availability and N_{area} should increase leaf photosyn-
1157 thesis and photosynthetic capacity by increasing the maximum rate of Rubisco
1158 carboxylation through increased investments to Rubisco construction and mainte-
1159 nance. This integrated N_{area} -photosynthesis response to soil nitrogen availability
1160 has been observed both in manipulative experiments and across environmental
1161 gradients (Field and Mooney 1986; Evans 1989; Walker et al. 2014; Li et al.
1162 2020), and is thought to be driven by ecosystem nitrogen limitation, which lim-
1163 its primary productivity globally (LeBauer and Treseder 2008; Fay et al. 2015).
1164 However, this response is not consistently observed, as recent studies note variable
1165 N_{area} -photosynthesis relationships across edaphic and climatic gradients (Liang
1166 et al. 2020; Luo et al. 2021) and that aboveground growing conditions (e.g., light
1167 availability, temperature, vapor pressure deficit) or species identity traits (e.g.,
1168 photosynthetic pathway, nitrogen acquisition strategy) may be more important
1169 for explaining variance in N_{area} and photosynthetic capacity across environmental
1170 gradients (Adams et al. 2016; Dong et al. 2017; Smith et al. 2019; Dong et al.
1171 2020; Peng et al. 2021; Dong et al. 2022; Westerband et al. 2023).

1172 One hypothesized mechanism to explain variance in N_{area} across environ-
1173 mental gradients has been proposed via photosynthetic least-cost theory (Wright
1174 et al. 2003; Prentice et al. 2014; Paillassa et al. 2020; Harrison et al. 2021).

1175 The theory predicts that plants acclimate to environments by optimizing photo-
1176 synthetic assimilation rates at the lowest summed cost of nitrogen and water use
1177 (Wright et al. 2003; Prentice et al. 2014). In a given environment, the theory
1178 suggests that nitrogen and water use can be substituted for each other to maintain
1179 the lowest summed cost of resource use, such that optimal photosynthetic rates
1180 are achieved with less efficient use of the more abundant and less costly resource
1181 to acquire in exchange for more efficient use of the less abundant and more costly
1182 resource to acquire.

1183 Photosynthetic least-cost theory predicts that, all else equal, an increase in
1184 soil nitrogen availability should decrease the cost of acquiring and using nitrogen
1185 relative to water (a ratio referred to herein as β), resulting in optimal photosyn-
1186 thetic rates achieved with greater N_{area} at lower stomatal conductance and lower
1187 leaf $C_i:C_a$ (Wright et al. 2003; Prentice et al. 2014; Paillassa et al. 2020). Alter-
1188 natively, an increase in soil moisture should reduce costs of water acquisition and
1189 use, increasing β (Lavergne et al. 2020), stomatal conductance, and leaf $C_i:C_a$,
1190 resulting in optimal photosynthetic rates achieved with decreased N_{area} . The the-
1191 ory also predicts variability in stomatal conductance and N_{area} in response to
1192 climatic factors, suggesting that the optimal response to increased vapor pressure
1193 deficit (VPD) should be a reduction in stomatal conductance and leaf $C_i:C_a$ that
1194 is counterbalanced by an increase in N_{area} to support the greater photosynthetic
1195 capacity needed to maintain high assimilation at lower conductance (Grossiord
1196 et al. 2020; Dong et al. 2020; López et al. 2021; Westerband et al. 2023).

1197 Leaf nitrogen allocation responses to changing climates or soil resource
1198 availability may also depend on their mode of nutrient acquisition or photo-

1199 synthetic pathway. For example, species that form associations with symbiotic
1200 nitrogen-fixing bacteria (referred as "N-fixing species" from this point forward)
1201 should, in theory, have access to less finite nitrogen supply than species not capa-
1202 ble of forming such associations (referred as "non-fixing species" from this point
1203 forward), which may result in lower β values in N-fixing species than non-fixing
1204 species. This result was previously shown in a greenhouse experiment, where a
1205 leguminous species generally had lower costs of nitrogen acquisition compared to a
1206 non-leguminous species, although these differences were generally stronger under
1207 increased nitrogen limitation (Perkowski et al. 2021). Lower β values could be an
1208 explanation for why N-fixing species commonly have greater leaf nitrogen content
1209 than non-fixing species (Adams et al. 2016; Dong et al. 2017).

1210 Similarly, leaf nitrogen allocation patterns across environmental gradients
1211 may be dependent on photosynthetic pathway. Lower leaf $C_i:C_a$ values in C₄
1212 species suggests that C₄ species should have lower β values than C₃ species (Scott
1213 and Smith 2022), a pattern that could be the result of increased costs associated
1214 with water acquisition and use or reduced costs of nitrogen acquisition and use
1215 relative to C₃ species. Theory predicts that this response in C₄ species will cause
1216 C₄ species to have higher leaf nitrogen content on average compared to C₃ species,
1217 though ample evidence exists documenting general lower leaf nitrogen content in
1218 C₄ species (Schmitt and Edwards 1981; Sage and Pearcy 1987; Ghannoum et al.
1219 2011). No study to date has directly quantified β in C₄ species aside from the
1220 initial parameterization of β in an optimality model for C₄ species (Scott and
1221 Smith 2022) using a global dataset of leaf $\delta^{13}\text{C}$ values (Cornwell et al. 2018).

1222 While photosynthetic least-cost theory provides a unified framework for

1223 understanding integrated effects of climate and soil resource availability on N_{area} ,
1224 empirical tests of the theory are sparse. Previous work shows that increasing
1225 soil nitrogen availability decreases costs of acquiring nutrients (Bae et al. 2015;
1226 Perkowski et al. 2021; Lu et al. 2022), which can induce predictable nutrient-
1227 water use tradeoffs expected from the theory across broad environmental gradients
1228 (Paillassa et al. 2020; Querejeta et al. 2022; Westerband et al. 2023) and in ma-
1229 nipulation experiments (Bialic-Murphy et al. 2021). Additionally, increasing VPD
1230 has been shown to have a positive effect on N_{area} , which is commonly associated
1231 with reduced leaf $C_i:C_a$ (Dong et al. 2017; Dong et al. 2020; Firn et al. 2019;
1232 López et al. 2021).

1233 Despite evidence for patterns expected from photosynthetic least-cost the-
1234 ory, studies have been restricted to exploring these patterns in C₃ species and,
1235 while variance in N_{area} across environmental gradients has been shown to be driven
1236 by strong negative relationships with leaf $C_i:C_a$ (Dong et al. 2017; Paillassa et al.
1237 2020; Westerband et al. 2023), no study has explicitly investigated effects of soil
1238 resource availability or species identity on N_{area} using β as a direct predictor of leaf
1239 $C_i:C_a$. Furthermore, as N_{area} can be broken down into structural (leaf mass per
1240 area; M_{area} ; g m⁻²) and metabolic (mass-based leaf nitrogen content; N_{mass} ; gN
1241 g⁻¹) components (Dong et al. 2017), no study has investigated which component
1242 of N_{area} drives the hypothesized response of N_{area} to leaf $C_i:C_a$. Understanding
1243 whether changes in N_{area} due to leaf $C_i:C_a$ are driven by changes in leaf morphol-
1244 ogy (i.e. M_{area}), stoichiometry (i.e. N_{mass}), or both, is important, particularly
1245 because N_{mass} may negatively covary with M_{area} across environmental gradients
1246 due to tradeoffs between leaf longevity and leaf productivity (Wright et al. 2004;

1247 Reich 2014; Onoda et al. 2017; Wang et al. 2023).

1248 In this study, I measured N_{area} , N_{mass} , M_{area} , leaf $\delta^{13}\text{C}$ -derived estimates
1249 of leaf $C_i:C_a$, and leaf $\delta^{13}\text{C}$ -derived estimates of β in 520 individuals spanning
1250 57 species scattered across 24 grassland sites in Texas, USA (Table C1). Texas
1251 contains a diverse climatic gradient, indicated by 2006-2020 mean annual precipi-
1252 tation totals ranging from 204 to 1803 mm and 2006-2020 mean annual tempera-
1253 ture ranging from 11.8° to 24.6°C. Variability in soil nitrogen availability and soil
1254 moisture was expected across sites, owing to differences in soil texture and above-
1255 ground climate that would drive differential rates of water retention and nitrogen
1256 transformations to plant-available nitrogen substrate. I leveraged the expected
1257 climatic and soil resource variability across sites to test the following hypotheses:

- 1258 1. Soil nitrogen availability will decrease β through a reduction in costs of
1259 nitrogen acquisition and use, while soil moisture will increase β through a
1260 reduction in costs of water acquisition and use. Following previous results, I
1261 expected that N-fixing species would have lower β values and that C_4 species
1262 would have lower β values.
- 1263 2. Leaf $C_i:C_a$ will be positively related to β , a pattern that will result in a
1264 negative indirect effect of increasing soil nitrogen availability on leaf $C_i:C_a$,
1265 a positive indirect effect of increasing soil moisture on leaf $C_i:C_a$, and lower
1266 leaf $C_i:C_a$ in both N-fixing species and C_4 species. I expected that leaf
1267 $C_i:C_a$ would be negatively related to VPD, as increasing atmospheric dryness
1268 would cause plants to close stomata to minimize water loss.
- 1269 3. N_{area} will be negatively related to leaf $C_i:C_a$. This response will result in an

1270 indirect positive and negative effect of increasing soil nitrogen availability
1271 and soil moisture, respectively, on N_{area} , and generally larger N_{area} values
1272 in N-fixing species. While theory predicts that generally lower β values
1273 in C₄ species should yield generally larger N_{area} in C₄ species, I expected
1274 that C₄ species would have lower N_{area} than C₃ species due to generally
1275 greater nitrogen use efficiency in C₄ species. Additionally, I expected VPD
1276 to increase N_{area} , a pattern that would be directly mediated through the
1277 reduction in leaf $C_i:C_a$ with increasing VPD.

1278 4.2 Methods

1279 4.2.1 *Site descriptions and sampling methodology*

1280 I collected leaf and soil samples from 24 open canopy grassland sites scattered
1281 across central and eastern Texas in summer 2020 and summer 2021 (Fig. 4.1).
1282 Twelve sites were visited between June and July 2020 and 14 sites (11 unique from
1283 2020) were visited between May and June 2021 (Table 4.1). I explicitly chose sites
1284 that maximized variability in precipitation and edaphic variability between sites
1285 while minimizing temperature variability across the environmental gradient (Ta-
1286 ble 4.1). No site with personally communicated or anecdotal evidence of grazing
1287 or disturbance (e.g., mowing, feral hog activity, etc.) was used. I collected leaf
1288 material from three individuals each of the five most abundant species at ran-
1289 dom locations at each site, only selecting species that were broadly classified as
1290 graminoid or forb/herb growth habits per the USDA PLANTS database (USDA
1291 NRCS 2022). All collected leaves were fully expanded with no visible herbivory or
1292 other external damage and also free from shading by nearby shrubs or trees. Five

1293 soil samples were collected from 0-15 cm below the soil surface at each site near
1294 the leaf collection sample locations. Soil samples were mixed together by hand to
1295 create one composite soil sample per site.

1296 4.2.2 *Leaf trait measurements*

1297 Images of each leaf were taken immediately following each site visit using a flat-
1298 bed scanner. Fresh leaf area was determined from each image using the ‘LeafArea’
1299 R package (Katabuchi 2015), which automates leaf area calculations using ImageJ
1300 software (Schneider et al. 2012). Each leaf was dried at 65°C for at least 48 hours
1301 to a constant mass, weighed, and manually ground in a mortar and pestle until
1302 homogenized. Leaf mass per area (M_{area} ; g m⁻²) was calculated as the ratio of
1303 dry leaf biomass to fresh leaf area. Subsamples of dried and homogenized leaf
1304 tissue were used to measure leaf nitrogen content (N_{mass} ; gN g⁻¹) through ele-
1305 mental combustion analysis (Costech-4010, Costech Instruments, Valencia, CA).
1306 Leaf nitrogen content per unit leaf area (N_{area} ; gN m⁻²) was calculated as the
1307 product of N_{mass} and M_{area} .

1308 Subsamples of dried and homogenized leaf tissue were sent to the University
1309 of California-Davis Stable Isotope Facility to determine leaf $\delta^{13}\text{C}$. Leaf $\delta^{13}\text{C}$ values
1310 were determined using an elemental analyzer (PDZ Europa ANCA-GSL; Sercon
1311 Ltd., Chestshire, UK) interfaced to an isotope ratio mass spectrometer (PDZ
1312 Europa 20-20 Isotope Ratio Mass Spectrometer, Sercon Ltd., Chestshire, UK).
1313 I used leaf $\delta^{13}\text{C}$ values (‰; relative to Vienna Pee Dee Belemnite international
1314 reference standard) to estimate the ratio of intercellular (C_i) to extracellular (C_a)
1315 CO₂ ratio (leaf $C_i:C_a$; unitless) following the approach of Farquhar et al. (1989)

1316 described in Cernusak et al. (2013). Specifically, I derived leaf $C_i:C_a$ as:

$$C_i : C_a = \frac{\Delta^{13}C - a}{b - a} \quad (4.1)$$

1317 where $\Delta^{13}C$ represents the relative difference between leaf $\delta^{13}\text{C}$ (\textperthousand) and air $\delta^{13}\text{C}$

1318 (\textperthousand), calculated as:

$$\Delta^{13}C = \frac{\delta^{13}C_{air} - \delta^{13}C_{leaf}}{1 + \delta^{13}C_{leaf}} \quad (4.2)$$

1319 $\delta^{13}\text{C}_{air}$, which is commonly assumed to be $-8\text{\textperthousand}$ (Keeling et al. 1979; Farquhar

1320 et al. 1989), was calculated as a function of calendar year t using an empirical

1321 equation derived in Feng (1999):

$$\delta^{13}C_{air} = -6.429 - 0.006e^{0.0217(t-1740)} \quad (4.3)$$

1322 Using this equation, $\delta^{13}\text{C}_{air}$ values were set to $-9.04\text{\textperthousand}$ and $-9.09\text{\textperthousand}$ for 2020 and

1323 2021, respectively. The parameter a represents the fractionation between ^{12}C

1324 and ^{13}C due to diffusion in air, assumed to be $4.4\text{\textperthousand}$, while b represents the

1325 fractionation caused by Rubisco carboxylation, assumed to be $27\text{\textperthousand}$ (Farquhar

1326 et al. 1989). For C_4 species, b in Eqn. 4.1 was set to $6.3\text{\textperthousand}$, and was derived from:

$$b = c + (d \cdot \phi) \quad (4.4)$$

1327 Where c was set to $-5.7\text{\textperthousand}$ and d was set to $30\text{\textperthousand}$ (Farquhar et al. 1989). ϕ , which

1328 is the bundle sheath leakiness term, was set to 0.4. All leaf $C_i:C_a$ values less than

1329 0.1 and greater than 0.95 were assumed to be incorrect and removed from the
1330 analysis.

1331 I derived the unit cost of resource use (β) using leaf $C_i:C_a$ and site climate
1332 data using equations first described in Prentice et al. (2014) and simplified in
1333 Lavergne et al. (2020):

$$\beta = 1.6\eta^*VPD \frac{\chi - (\frac{\Gamma^*}{C_a})^2}{(1 - \chi)^2(K_m + \Gamma^*)} \quad (4.5)$$

1334 where η^* is the viscosity of water relative to 25°C, calculated using elevation and
1335 mean air temperature of the seven days leading up to each site visit following
1336 equations in Huber et al. (2009). VPD represents vapor pressure deficit (Pa), set
1337 to the mean vapor pressure deficit of the seven days leading up to each site visit,
1338 C_a represents atmospheric CO₂ concentration, arbitrarily set to 420 $\mu\text{mol mol}^{-1}$
1339 CO₂. K_m (Pa) is the Michaelis-Menten coefficient for Rubisco affinity to CO₂ and
1340 O₂, calculated as:

$$K_m = K_c \cdot \left(1 + \frac{O_i}{K_o}\right) \quad (4.6)$$

1341 where K_c (Pa) and K_o (Pa) are the Michaelis-Menten coefficients for Rubisco
1342 affinity to CO₂ and O₂, respectively, and O_i is the intercellular O₂ concentration.
1343 Γ^* (Pa) is the CO₂ compensation point in the absence of dark respiration. K_c , K_o ,
1344 and Γ^* were determined using equations described in Medlyn et al. (2002) and
1345 derived in Bernacchi et al. (2001), invoking an elevation correction for atmospheric
1346 pressure as explained in Stocker et al. (2020).

Table 4.1. Site locality information, sampling year, 2006-2020 mean annual precipitation (MAP; mm), mean annual temperature (MAT; °C), and water holding capacity (WHC; mm)*

Site	Latitude	Longitude	Sampling year	MAP	MAT	WHC
Edwards_2019_17	29.95	-100.36	2020	563.5	19.0	224.7
Uvalde_2020_02	29.59	-100.09	2020, 2021	648.5	19.5	224.7
Menard_2020_01	30.91	-99.59	2020	641.9	18.3	220.2
Kerr_2020_03	30.06	-99.34	2021	672.4	18.3	237.5
Bandera_2020_03	29.85	-99.30	2021	789.4	18.8	235.1
Sansaba_2020_01	31.29	-98.62	2020	733.0	18.8	234.3
Comal_2020_21	29.79	-98.43	2020	878.5	19.9	220.7
Blanco_2019_16	29.99	-98.43	2020	833.0	19.2	222.2
Bexar_2019_13	29.24	-98.43	2020	759.3	21.5	206.0
Burnet_2020_14	30.84	-98.34	2021	763.3	19.5	217.8
Comal_2020_19	30.01	-98.32	2021	845.0	19.3	220.4
Hays_2020_54	29.96	-98.17	2021	861.3	20.0	225.6
Burnet_2020_12	30.82	-98.06	2021	815.1	19.4	245.3
Williamson_2019_09	30.71	-97.86	2020	867.7	19.7	270.2
Williamson_2019_10	30.54	-97.77	2020	819.5	19.9	239.8
Bell_2021_08	31.06	-97.55	2021	937.3	19.6	232.3
Fayette_2021_12	29.86	-97.21	2021	985.7	20.4	165.6
Fayette_2019_04	30.09	-96.78	2020	1017.4	20.6	226.9
Fayette_2020_09	29.86	-96.71	2021	1002.7	20.8	187.6
Washington_2020_08	30.28	-96.41	2021	1077.4	20.4	203.9
Austin_2020_03	29.78	-96.24	2021	1108.7	20.6	253.0
Brazos_2020_16	30.93	-96.23	2021	1078.0	20.1	202.2
Brazos_2020_18	30.52	-96.21	2020, 2021	1099.4	20.4	233.5
Harris_2020_03	29.88	-95.31	2020, 2021	1492.0	21.6	265.6

1347 * Rows are arranged by longitude to visualize precipitation variability across sites

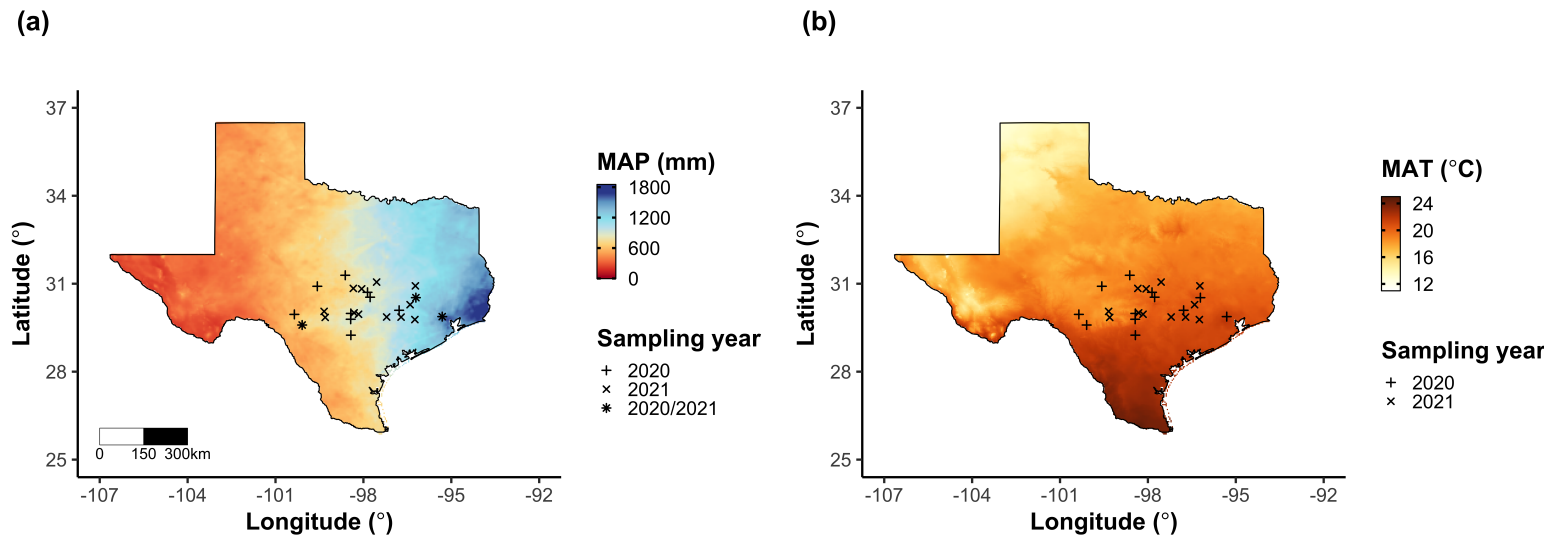


Figure 4.1. Site locations along 2006-2020 mean annual precipitation (a) and mean annual temperature (b) gradients in Texas, USA. Precipitation and temperature data were plotted at a 4-km grid resolution and are masked to include only grid cells that occur within the Texas state boundary of the United States. In both panels, addition signs refer to sites visited in 2020, multiplication signs to sites visited in 2021, and asterisks to sites visited in 2020 and 2021. The scale bar in (a) also applies to (b).

1348 4.2.3 *Site climate data*

1349 I used the Parameter elevation Regressions on Independent Slopes Model (PRISM)
1350 (Daly et al. 2008) climate product to access gridded daily temperature and precip-
1351 itation data for the coterminous United States at a 4-km grid resolution between
1352 January 1, 2006 and July 31, 2021 (PRISM Climate Group, Oregon State Uni-
1353 versity, <https://prism.oregonstate.edu>, data created 4 Feb 2014, accessed 24
1354 Mar 2022). Mean daily air temperature, mean daily VPD, and total daily pre-
1355 cipitation data were extracted from the grid cell that contained the latitude and
1356 longitude of each property using the ‘extract’ function in the ‘terra’ R package
1357 (Hijmans 2022). PRISM data were used in lieu of local weather station data
1358 because several rural sites did not have a local weather station present within a
1359 20-km radius of the site. Daily site climate data were used to estimate mean an-
1360 nual precipitation and mean annual temperature for each site between 2006 and
1361 2020 (Table 4.1). I calculated total precipitation and mean daily VPD for the
1362 prior 1, 2, 3, 4, 5, 6, 7, 8, 9, 10, 15, 20, 25, 30, 60, and 90 days leading up to each
1363 site visit. Temperature was not included in any analysis due to the close range in
1364 mean annual temperature between sites (mean \pm SD: $19.8\pm0.9^{\circ}\text{C}$; Table 4.1).

1365 4.2.4 *Site edaphic characteristics*

1366 Subsamples of composited soil samples were sent to the Texas A&M Soil, Water
1367 and Forage Laboratory to quantify soil nitrate concentration ($\text{NO}_3\text{-N}$; ppm). Soil
1368 $\text{NO}_3\text{-N}$ was determined by extracting composite soil samples in 1 M KCl, measur-
1369 ing absorbance values of extracts at 520 nm using the end product of a $\text{NO}_3\text{-N}$ to
1370 $\text{NO}_2\text{-N}$ cadmium reduction reaction (Kachurina et al. 2000; Keeney and Nelson

1371 1983). Soil texture data from 0-15 cm below the soil surface were accessed using
1372 the SoilGrids2.0 data product (Poggio et al. 2021) through the ‘fetchSoilGrids’
1373 function in the ‘soilDB’ R package (Beaudette et al. 2022). I used SoilGrids2.0
1374 to access soil texture data in lieu of analyses using the composite soil sample due
1375 to a lack of soil material from some sites after sending samples for soil NO₃-N.

1376 Soil moisture was not measured in the field, but was estimated using the
1377 ‘Simple Process-Led Algorithms for Simulating Habitats’ model (SPLASH) (Davis
1378 et al. 2017). This model, derived from the STASH model (Cramer and Prentice
1379 1988), spins up a bucket model using Priestley-Taylor equations (Priestley and
1380 Taylor 1972) to calculate daily soil moisture (W_n ; mm) as a function of the previous
1381 day’s soil moisture (W_{n-1} ; mm), daily precipitation (P_n ; mm), condensation (C_n ;
1382 mm), actual evapotranspiration (E_n^a ; mm), and runoff (RO; mm):

$$W_n = W_{n-1} + P_n + C_n - E_n^a - RO \quad (4.7)$$

1383 Models were spun up by equilibrating the previous day’s soil moisture using succes-
1384 sive model iterations with daily mean air temperature, daily precipitation total,
1385 the number of daily sunlight hours, and latitude as model inputs (Davis et al.
1386 2017). Daily sunlight hours were estimated for each day at each site using the
1387 ‘getSunlightTimes’ function in the ‘suncalc’ R package, which estimated sunrise
1388 and sunset times of each property using date and site coordinates (Thieurmel and
1389 Elmarhraoui 2019). Water holding capacity (mm), or bucket size, was estimated
1390 as a function of soil texture using pedotransfer equations explained in Saxton and
1391 Rawls (2006), as done in Stocker et al. (2020) and Bloomfield et al. (2023). A

1392 summary of these equations is included in Appendix C.1.

1393 Daily soil moisture outputs from the SPLASH model for each site were
1394 used to calculate mean daily soil moisture for the prior 1, 2, 3, 4, 5, 6, 7, 8, 9,
1395 10, 15, 20, 25, 30, 60, and 90 days leading up to each site visit. Mean daily
1396 soil moisture values were then expressed as a fraction of water holding capacity
1397 to normalize across sites with different bucket depths, as done in Stocker et al.
1398 (2018).

1399 4.2.5 *Plant functional group assignments*

1400 Plant functional group was assigned to each species and used as the primary de-
1401 scriptor of species identity. Specifically, plant functional groups were assigned
1402 based on photosynthetic pathway (C_3 , C_4) and ability to form associations with
1403 symbiotic nitrogen-fixing bacteria (legume, non-legume). The ability to form as-
1404 sociations with symbiotic nitrogen-fixing bacteria was assigned based on whether
1405 species were in the *Fabaceae* family, and photosynthetic pathway of each species
1406 was determined from past literature and confirmed through leaf $\delta^{13}C$ values. I
1407 chose these plant functional groups based on *a priori* hypotheses regarding the
1408 functional role of nitrogen fixation and photosynthetic pathway on the sensitivity
1409 of plant nitrogen uptake and leaf nitrogen allocation to soil nitrogen availability
1410 and aboveground growing conditions. These plant functional group classifications
1411 resulted in three distinct plant functional groups within our dataset: C_3 legumes
1412 (n=53), C_3 nonlegumes (n=350), and C_4 nonlegumes (n=117).

1413 4.2.6 *Data analysis*

1414 All analyses and plotting were conducted in R version 4.1.1 (R Core Team 2021).

1415 I constructed a series of separate linear mixed-effects models to investigate en-

1416 vironmental drivers of β , leaf $C_i:C_a$, N_{area} , N_{mass} , and M_{area} , followed by a path

1417 analysis using a piecewise structural equation model to investigate direct and

1418 indirect effects of climate and soil resource availability on N_{area} .

1419 To explore environmental drivers of β , I built a linear mixed-effects model

1420 that included soil moisture, soil nitrogen availability, and plant functional group

1421 as fixed effect coefficients. Species were designated as a random intercept term.

1422 Interaction coefficients between all possible combinations of the three fixed effect

1423 coefficients were also included. β was natural log transformed to linearize data.

1424 I used an information-theoretic model selection approach to determine whether

1425 90-, 60-, 30-, 20-, 15-, 10-, 9-, 8-, 7-, 6-, 5-, 4-, 3-, 2-, or 1-day mean daily soil

1426 moisture conferred the best model fit for β . To do this, I constructed 16 separate

1427 linear mixed-effects models where log-transformed β was included as the response

1428 variable and each soil moisture time step was separately included as a single

1429 continuous fixed effect. Species were included as a random intercept term for all

1430 models. I used corrected Akaike Information Criterion (AICc) to select the soil

1431 moisture timescale that conferred the best model fit, indicated by the model with

1432 the lowest AICc score (Table C4; Fig. C1).

1433 To explore environmental drivers of leaf $C_i:C_a$, I constructed a second linear

1434 mixed effects model that included VPD, soil moisture, soil nitrogen availability,

1435 and plant functional group as fixed effect coefficients. Two-way interactions be-

1436 tween plant functional group and VPD, soil nitrogen availability, or soil moisture

1437 were included as additional fixed effect coefficients, in addition to a three-way
1438 interaction between soil moisture, soil nitrogen availability, and plant functional
1439 group. Species were included as a random intercept term. I used an information-
1440 theoretic model selection approach to determine whether 90-, 60-, 30-, 20-, 15-,
1441 10-, 9-, 8-, 7-, 6-, 5-, 4-, 3-, 2-, or 1-day mean daily VPD conferred the best model
1442 fit for leaf $C_i:C_a$ using the same approach explained above for the soil moisture ef-
1443 fect on β . The soil moisture timescale was set to the same timescale that conferred
1444 the best fit for β .

1445 To explore environmental drivers of N_{area} , N_{mass} , and M_{area} , I constructed
1446 a linear mixed effects model for each trait, including leaf $C_i:C_a$, soil nitrogen
1447 availability, soil moisture, and plant functional group as fixed effect coefficients
1448 for each model. Two-way interactions between plant functional group and β , leaf
1449 $C_i:C_a$, soil nitrogen availability, or soil moisture were included as additional fixed
1450 effect coefficients, in addition to a three-way interaction between soil nitrogen
1451 availability, soil moisture, and plant functional group. Species were included as a
1452 random intercept term, with the soil moisture timescale set to the same timescale
1453 that conferred the best fit for β .

1454 In all linear mixed-effects models explained above, including those to select
1455 relevant timescales, I used the ‘lmer’ function in the ‘lme4’ R package (Bates et al.
1456 2015) to fit each model and the ‘Anova’ function in the ‘car’ R package (Fox and
1457 Weisberg 2019) to calculate Type II Wald’s χ^2 and determine the significance
1458 level ($\alpha=0.05$) of each fixed effect coefficient. I used the ‘emmeans’ R package
1459 (Lenth 2019) to conduct post-hoc comparisons using Tukey’s tests, where degrees
1460 of freedom were approximated using the Kenward-Roger approach (Kenward and

1461 Roger 1997). Trendlines and error ribbons for all plots were drawn using a series
1462 of ‘emmeans’ outputs across the range in plotted x-axis values.

1463 Finally, I conducted a path analysis using a piecewise structural equation
1464 model to examine direct and indirect pathways that determined variance in N_{area} .
1465 Six separate linear mixed effects models were loaded into the piecewise structural
1466 equation model. Models were constructed per *a priori* hypotheses following pat-
1467 terns expected from photosynthetic least-cost theory. The first model regressed
1468 N_{area} against N_{mass} and M_{area} . The second model regressed M_{area} against leaf
1469 $C_i:C_a$. The third model regressed N_{mass} against leaf $C_i:C_a$ and M_{area} (Dong et al.
1470 2017; Dong et al. 2020). The fourth model regressed leaf $C_i:C_a$ against β and
1471 VPD. The fifth model regressed β against soil nitrogen availability, soil moisture,
1472 ability to associate with symbiotic nitrogen-fixing bacteria, and photosynthetic
1473 pathway. The sixth model regressed soil nitrogen availability against soil mois-
1474 ture. All models included the relevant timescale selected in the individual linear
1475 mixed effect models explained above. Models included species as a random inter-
1476 cept term, were built using the ‘lme’ function in the ‘nlme’ R package (Pinheiro
1477 and Bates 2022), and subsequently loaded into the piecewise structural equation
1478 model using the ‘psem’ function in the ‘piecewiseSEM’ R package (Lefcheck 2016).

1479 4.3 Results

1480 4.3.1 *Cost to acquire nitrogen relative to water*

1481 Model selection indicated that 90-day mean soil moisture conferred the best model

1482 fit for β (AICc=1429.14; Table C4; Fig. C1).

1483 Increasing soil nitrogen availability generally decreased β ($p<0.001$; Table

1484 4.2; Fig. 4.2a), a pattern driven by a negative effect of increasing soil nitrogen on

1485 β in C₃ nonlegumes (Tukey: $p=0.002$) and C₃ legumes (Tukey: $p=0.031$) despite

1486 a null effect of soil nitrogen on β in C₄ nonlegumes (Tukey: $p=0.905$). There was

1487 no effect of soil moisture on β ($p=0.902$; Table 4.2; Fig. 4.2b). A functional group

1488 effect ($p<0.001$; Table 4.2) indicated that C₄ nonlegumes generally had lower β

1489 values than both C₃ legumes and C₃ non-legumes (Tukey: $p<0.001$ in both cases),

1490 while β values in C₃ legumes did not differ from C₃ nonlegumes (Tukey: $p=0.804$).

Table 4.2. Effects of soil moisture, soil nitrogen availability, and plant functional group on β (unitless)*

	df	Coefficient	χ^2	p
Intercept	-	3.39E+00	-	-
Soil moisture (SM ₉₀)	1	-2.03E-01	0.015	0.902
Soil N (N)	1	-1.49E-02	13.832	<0.001
PFT	2	-	225.049	<0.001
SM ₉₀ *N	1	-8.86E-04	1.016	0.313
SM ₉₀ *PFT	2	-	0.754	0.686
N*PFT	2	-	5.236	0.073
SM ₉₀ *N*PFT	2	-	3.633	0.163

1491 *Significance determined using Type II Wald χ^2 tests ($\alpha=0.05$). P-values<0.05
1492 are in bold. Model coefficients are expressed on the natural-log scale and are only
1493 included for continuous fixed effects. Key: df=degrees of freedom; χ^2 =Wald Type
1494 II chi-square test statistic

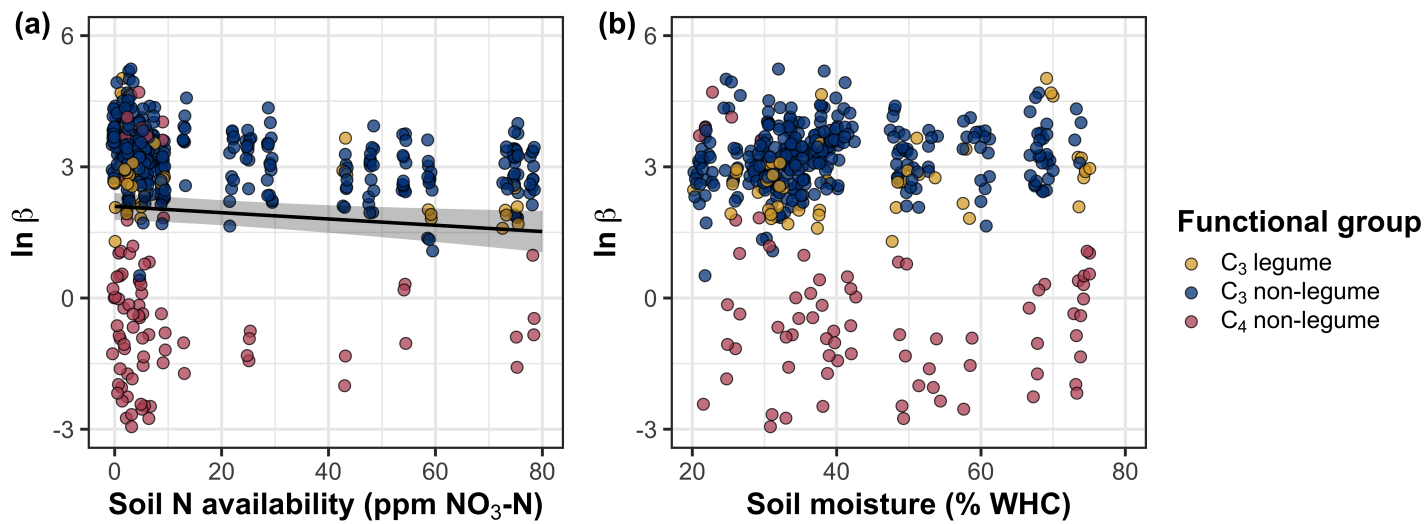


Figure 4.2. Effects of soil nitrogen availability (a) and soil moisture (b) on the cost of acquiring and using nitrogen (β ; unitless). Soil nitrogen availability is represented on the x-axis in (a), soil moisture is represented on the x-axis in (b) as a percent of site water holding capacity, and natural-log transformed β is represented on the y-axis for both panels. Yellow points represent C₃ legumes, blue points represent C₃ nonlegumes, and red points represent C₄ nonlegumes. Throughout, points are jittered for visibility. A black solid trendline is drawn to denote bivariate relationships where the slope is different from zero ($p<0.05$), with error ribbons representing the upper and lower 95% confidence intervals.

1495 4.3.2 *Leaf C_i:C_a*

1496 Model selection indicated that 4-day mean VPD was the timescale that conferred

1497 the best model fit for leaf $C_i:C_a$ (AICc=-793.49; Table C4; Fig. C1).

1498 Model results revealed that increasing VPD generally decreased leaf $C_i:C_a$

1499 ($p<0.001$; Table 4.3; Fig. 4.3a). There was no effect of soil moisture ($p=0.843$;

1500 Table 4.3; Fig. 4.3b) or soil nitrogen availability ($p=0.544$; Table 4.3; Fig. 4.3c) on

1501 leaf $C_i:C_a$. A strong plant functional group effect ($p<0.001$; Table 4.3) indicated

1502 that C₄ nonlegumes had lower leaf $C_i:C_a$ than C₃ legumes and C₃ nonlegumes

1503 (Tukey: $p<0.001$ in both cases), with no difference between C₃ legumes and C₃

1504 nonlegumes (Tukey: $p=0.865$).

Table 4.3. Effects of soil moisture, soil nitrogen availability, and plant functional group on leaf $C_i:C_a$ (unitless)*

	df	Coefficient	χ^2	<i>p</i>
Intercept	-	1.32E+00	-	-
Vapor pressure deficit (VPD_4)	1	-4.53E-01	11.211	<0.001
Soil moisture (SM_{90})	1	-1.71E-01	0.039	0.843
Soil N (N)	1	-3.33E-03	0.369	0.544
PFT	2	-	227.005	<0.001
SM_{90}^*N	1	7.34E-03	2.361	0.124
VPD_4^*PFT	2	-	0.927	0.629
SM_{90}^*PFT	2	-	0.817	0.664
N^*PFT	2	-	4.085	0.130
$SM_{90}^*N^*PFT$	2	-	3.677	0.159

1505 *Significance determined using Type II Wald χ^2 tests ($\alpha=0.05$). *P*-values less
1506 than 0.05 are in bold and *p*-values where $0.05 < p < 0.1$ are italicized. Leaf $C_i:C_a$
1507 was not transformed prior to model fitting, so model coefficients are reported
1508 on the response scale. Model coefficients are only included for continuous fixed
1509 effects. Key: df=degrees of freedom; χ^2 =Wald Type II chi-square test statistic

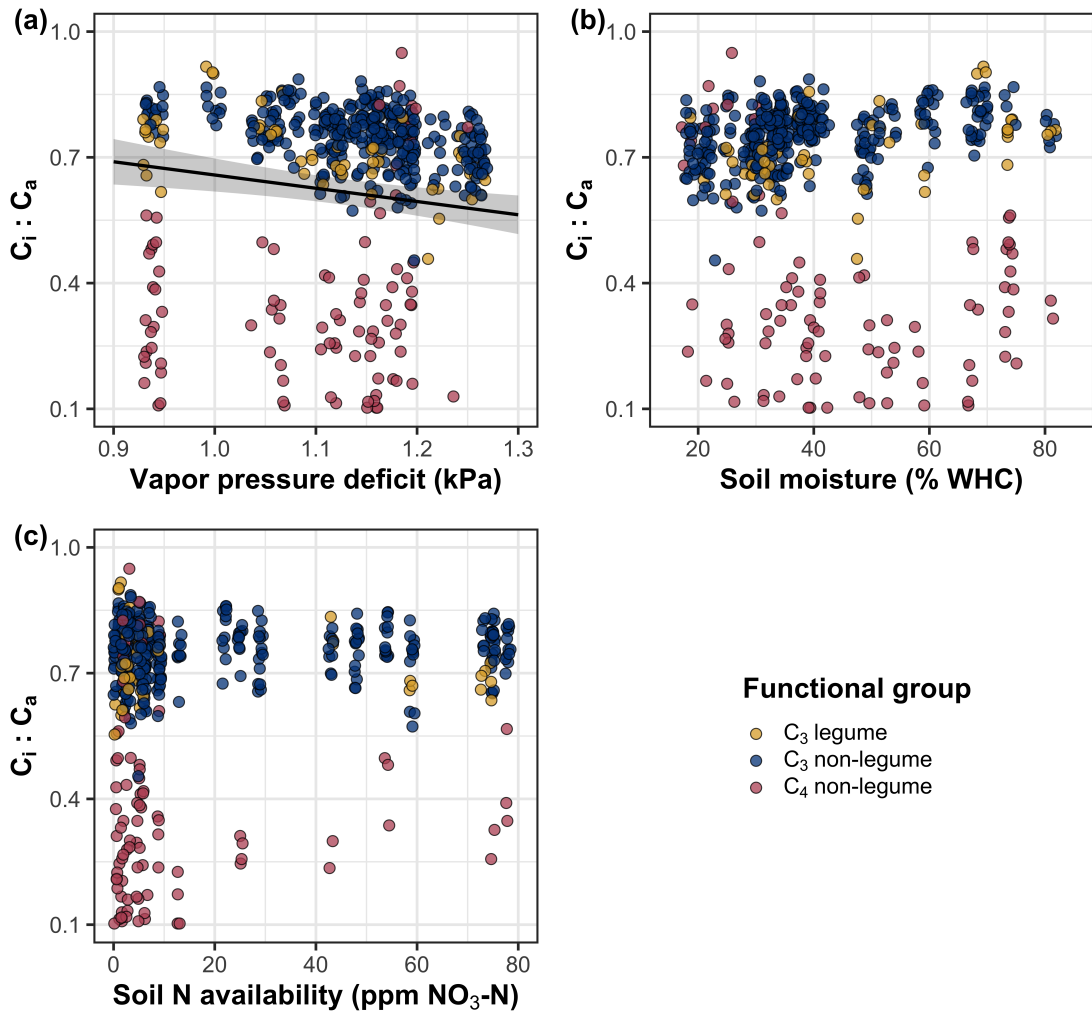


Figure 4.3. Effects of 4-day mean vapor pressure deficit (a), 90-day soil moisture (per water holding capacity; b), and soil nitrogen availability (c) on leaf $C_i:C_a$. Shading and trendlines are as explained in Figure 4.2. Points are jittered for visibility. Variably colored trendlines are only included if there is an interaction between the x-axis and plant functional group, where solid trendlines indicate slopes that are different from zero ($p < 0.05$) and dashed trendlines indicate slopes that are not different from zero ($p > 0.05$). Error ribbons represent the upper and lower 95% confidence intervals of each fitted trendline.

1510 4.3.3 *Leaf nitrogen content*

1511 An interaction between leaf $C_i:C_a$ and plant functional group ($p<0.001$; Table
1512 4.4) revealed that the negative effect of increasing leaf $C_i:C_a$ on N_{area} ($p<0.001$;
1513 Table 4.4) was driven by a negative effect of increasing leaf $C_i:C_a$ on N_{area} in
1514 C_3 nonlegumes (Tukey: $p<0.001$) and C_3 legumes (Tukey: $p=0.002$), but not C_4
1515 nonlegumes (Tukey: $p=0.795$; Fig. 4.4a). An interaction between soil nitrogen
1516 availability and plant functional group ($p=0.041$; Table 4.4) indicated that the
1517 positive effect of increasing soil nitrogen ($p=0.007$; Table 4.4) was only apparent
1518 in C_3 legumes (Tukey: $p<0.001$; Table 4.4; Fig. 4.4d), but not C_3 nonlegumes
1519 (Tukey: $p=0.449$) or C_4 nonlegumes (Tukey: $p=0.680$). Increasing soil moisture
1520 increased N_{area} ($p=0.010$, Table 4.4). A plant functional group effect ($p<0.001$;
1521 Table 4.4) indicated that C_4 nonlegumes had lower N_{area} compared to C_3 legumes
1522 (Tukey: $p<0.001$) and C_3 nonlegumes (Tukey: $p<0.001$), while C_3 legumes had
1523 lower N_{area} compared to C_3 nonlegumes (Tukey: $p=0.030$).

1524 A marginal interaction between soil nitrogen availability and soil moisture
1525 ($p=0.097$; Table 4.4) indicated that the positive effect of increasing soil nitrogen
1526 on N_{mass} ($p<0.001$; Table 4.4; Fig. 4.4e) was only apparent when soil moisture
1527 was less than 50% of the maximum water holding capacity (Tukey: $p<0.05$ in
1528 all cases). There was no effect of leaf $C_i:C_a$ on N_{mass} ($p=0.447$; Table 4.4; Fig.
1529 4.4b). Increasing soil moisture had a positive effect on N_{mass} ($p<0.001$; Table 4.4;
1530 Fig. 4.4h). A plant functional group effect ($p<0.001$; Table 4.4) indicated that
1531 C_4 nonlegumes had lower N_{mass} compared to C_3 legumes (Tukey: $p=0.003$) and
1532 C_3 nonlegumes (Tukey: $p=0.011$), while N_{mass} did not differ between C_3 legumes
1533 and C_3 nonlegumes (Tukey: $p=0.231$).

1534 Variance in M_{area} was driven by a three-way interaction between soil nitro-

1535 gen availability, soil moisture, and plant functional group ($p=0.018$; Table 4.4).

1536 This interaction indicated that increasing soil moisture increased the positive effect

1537 of increasing soil nitrogen availability on M_{area} in C₃ legumes (Tukey: $p=0.030$)

1538 but did not modify the negative effect of increasing soil nitrogen availability on

1539 M_{area} in C₄ nonlegumes (Tukey: $p=0.511$) or C₃ nonlegumes (Tukey: $p>0.999$).

1540 There was otherwise no effect of soil moisture on M_{area} ($p=0.696$; Table 4.4), but

1541 there was a general negative effect of increasing soil nitrogen availability on M_{area}

1542 ($p<0.001$; Table 4.4). An interaction between leaf $C_i:C_a$ and plant functional

1543 group ($p<0.001$; Table 4.4; Fig. 4.4c) indicated that negative effect of increasing

1544 leaf $C_i:C_a$ on M_{area} ($p<0.001$; Table 4.4) was driven by a negative effect of in-

1545 creasing leaf $C_i:C_a$ on M_{area} in C₃ legumes and C₃ nonlegumes (Tukey: $p<0.001$

1546 in both cases), but not C₄ nonlegumes (Tukey: $p=0.343$; Fig. 4.4c).

Table 4.4. Effects of soil moisture, soil nitrogen availability, plant functional group, and leaf $C_i:C_a$ on leaf nitrogen content per unit leaf area (N_{area} ; gN m $^{-2}$), leaf nitrogen content per unit leaf biomass (N_{mass} ; gN g $^{-1}$), and leaf biomass per unit leaf area (M_{area} ; g m $^{-2}$)

		N_{area}			N_{mass}			M_{area}		
	df	Coefficient	χ^2	p	Coefficient	χ^2	p	Coefficient	χ^2	p
(Intercept)	-	2.41E+00	-	-	6.28E-02	-	-	6.90E+00	-	-
$C_i:C_a$	1	-2.32E+00	7.386	0.007	8.04E-01	0.578	0.447	-3.13E+00	15.913	<0.001
Soil N (N)	1	1.26E-02	6.070	0.014	1.12E-02	90.940	<0.001	-2.66E-02	43.529	<0.001
Soil moisture (SM ₉₀)	1	5.60E-01	6.717	0.010	7.81E-01	11.205	<0.001	-2.53E-01	0.153	0.696
PFT	1		-	52.277	<0.001		-	17.184	<0.001	
SM ₉₀ *N	1	5.44E-02	0.444		0.505	-1.91E-02	2.749	0.097	8.16E-02	1.690
$C_i:C_a$ *PFT	1		-	25.631	<0.001		-	4.864	0.078	
N*PFT	1		-	6.389	0.041		-	1.219	0.544	
SM ₉₀ *PFT	1		-	3.548	0.170		-	0.911	0.634	
SM ₉₀ *N*PFT	1		-	3.520	0.172		-	0.092	0.955	

96

1547 *Significance determined using Type II Wald χ^2 tests ($\alpha=0.05$). P-values less than 0.05 are in bold and p-values
 1548 where $0.05 < p < 0.1$ are italicized. Coefficients are reported on the natural-log scale for all traits and are only included
 1549 for continuous fixed effects. Key: df=degrees of freedom; χ^2 =Wald Type II chi-square test statistic

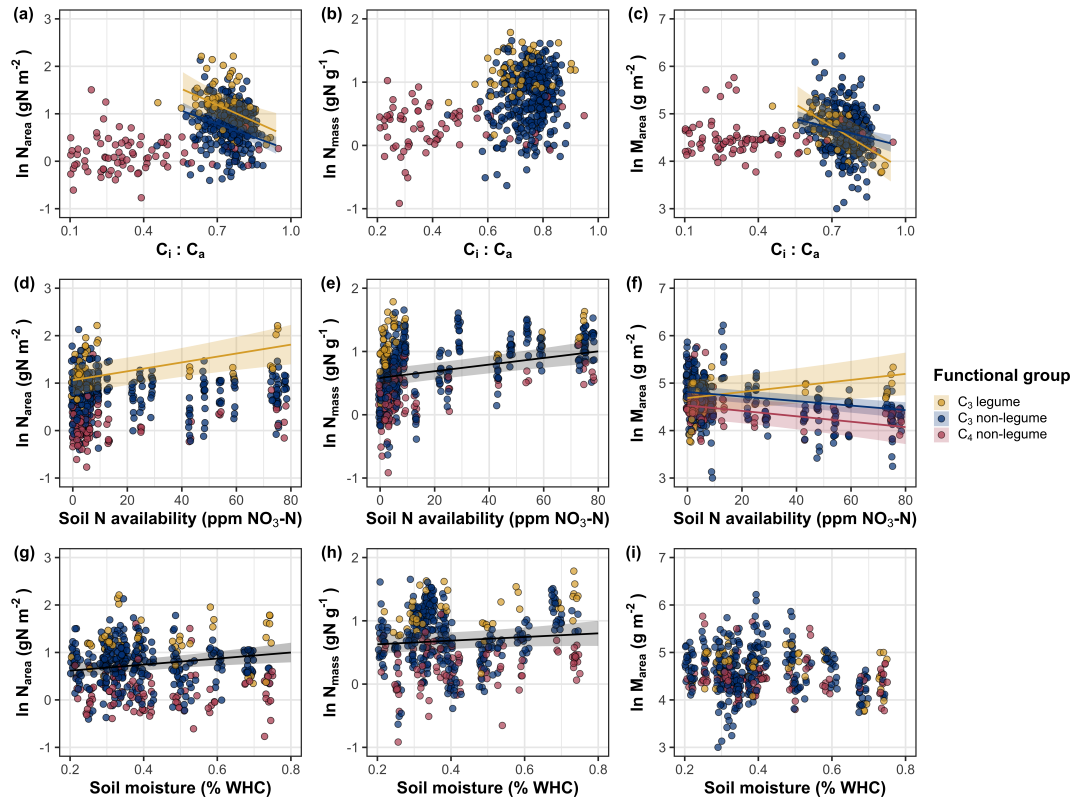


Figure 4.4. Effects of leaf $C_i:C_a$ (a-c), soil nitrogen availability (d-f), and soil moisture (g-i) on leaf nitrogen content per unit leaf area (a, d, g), leaf nitrogen content per unit leaf biomass (b, e, h), and leaf mass per area (c, f, i). Yellow points and trendlines indicate C_3 legumes, blue points and trendlines indicate C_3 nonlegumes, and red points and trendlines indicate C_4 nonlegumes. Points are jittered for visibility. Variably colored trendlines are only included if there is an interaction between plant functional group and the x-axis. Black solid trendlines denote bivariate slopes that are different from zero ($p < 0.05$) where there is no apparent interaction between plant functional group and the x-axis.

1550 4.3.4 *Structural equation model*

1551 The piecewise structural equation model explained 89%, 56%, 77%, 82%, and
1552 37% of variance in N_{area} , N_{mass} , M_{area} , leaf $C_i:C_a$, and β , respectively (Table 4.5; Fig. 4.5). Variance in N_{area} was driven by a positive effect of increasing N_{mass} and
1553 M_{area} ($p < 0.001$ in both cases; Table 4.5; Fig. 4.5). Model results indicated that an
1554 indirect negative effect of $C_i:C_a$ on N_{area} was driven by a strong reduction in M_{area}
1555 with increasing leaf $C_i:C_a$ ($p < 0.001$; Table 4.5) paired with no effect of increasing
1556 $C_i:C_a$ on N_{mass} ($p = 0.111$; Table 4.5). However, there was a strong negative effect of
1557 increasing M_{area} on N_{mass} ($p < 0.001$; Table 4.5; Fig. 4.5). Leaf $C_i:C_a$ increased with
1558 increasing β ($p < 0.001$; Table 4.5) and decreased with increasing VPD ($p < 0.001$; Table 4.5; Fig. 4.5). Variance in β was driven by a negative effect of increasing soil
1559 nitrogen availability ($p < 0.001$; Table 4.5) and was generally higher in C₃ species
1560 ($p < 0.001$; Table 4.5; Fig. 4.5). However, β did not change with soil moisture
1561 ($p = 0.904$; Table 4.5) or with ability to acquire nitrogen via symbiotic nitrogen
1562 fixation ($p = 0.495$; Table 4.5). Finally, soil nitrogen availability was positively
1563 associated with increasing soil moisture ($p = 0.002$; Table 4.5; Fig. 4.5).

Table 4.5. Structural equation model results investigating direct effects of climatic and soil resource availability on leaf nitrogen content*

Predictor	Coefficient	<i>p</i>
N_{area} ($R^2_c=0.89$)		
M_{area}	0.758	<0.001
N_{mass}	0.781	<0.001
N_{mass} ($R^2_c=0.56$)		
Leaf $C_i:C_a$	0.092	0.111
M_{area}	-0.311	<0.001
M_{area} ($R^2_c=0.77$)		
Leaf $C_i:C_a$	-0.237	<0.001
Leaf $C_i:C_a$ ($R^2_c=0.82$)		
β	0.309	<0.001
VPD_4	-0.110	<0.001
β ($R^2_c=0.37$)		
Soil N	-0.213	<0.001
SM_{90}	-0.006	0.904
Photo. pathway	0.446	<0.001
N-fixing ability	-0.056	0.495
Soil N ($R^2_c=0.35$)		
SM_{90}	-0.154	0.002

1566 *Reported coefficients are standardized across the structural equation model. *P*-
1567 values less than 0.05 are noted in bold. Positive coefficients for photosynthetic
1568 pathway indicate generally larger values in C₃ species, while positive coefficients
1569 for N-fixing ability indicate generally larger values in N-fixing species. Key:
1570 df=degrees of freedom; χ^2 =Wald Type II chi-square test statistic; R^2_c =conditional
1571 R² value; N_{area} =leaf nitrogen content per unit leaf area (gN m⁻¹); M_{area} =leaf
1572 mass per unit leaf dry biomass (g m⁻²); N_{mass} =leaf nitrogen content per unit
1573 leaf dry biomass (g g⁻¹); β =cost of acquiring nitrogen relative to water (unitless);
1574 VPD_4 =4-day mean vapor pressure deficit (kPa); SM_{90} =90-day mean soil moisture
1575 (mm)

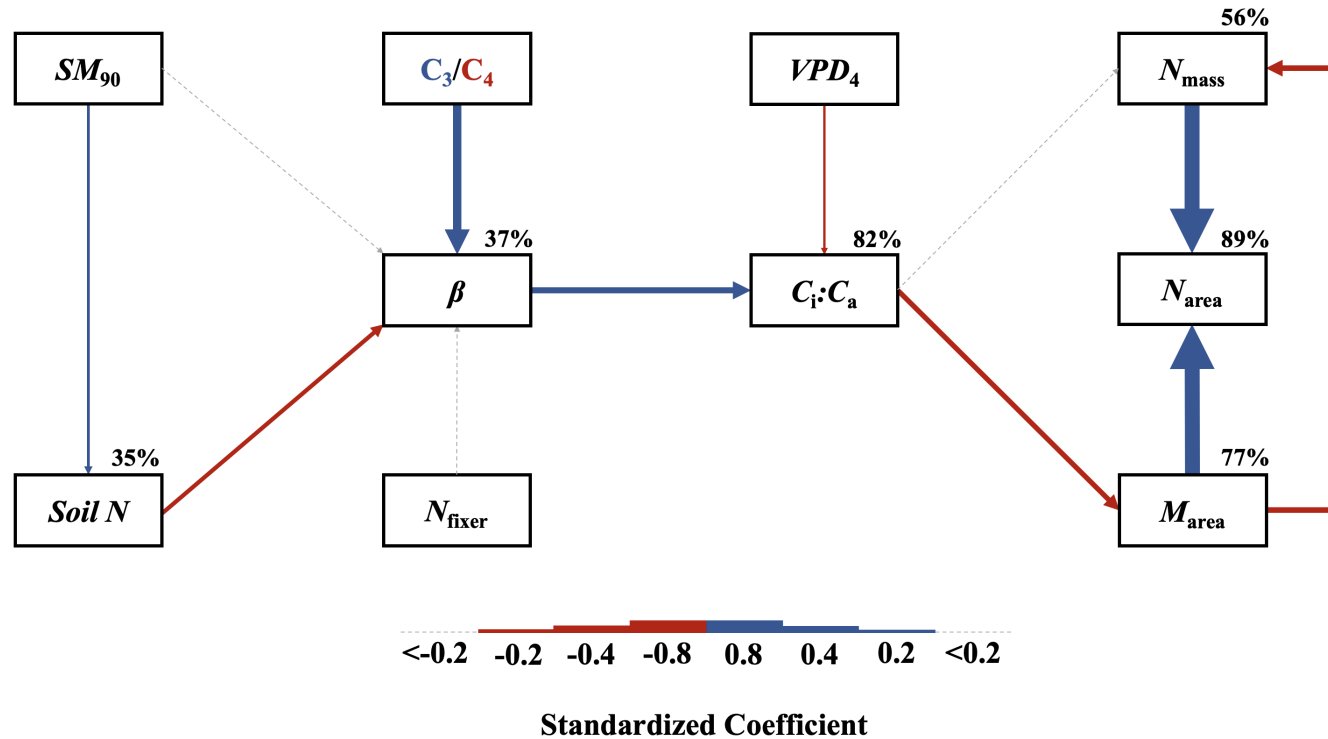


Figure 4.5. Structural equation model results exploring drivers of N_{area} . Boxes indicate measured edaphic factors, climatic factors, and leaf traits. Solid arrows indicate bivariate relationships where $p<0.05$, while dashed arrows indicate relationships where $p>0.05$. Positive model coefficients are indicated through blue arrows, negative model coefficients are indicated through red arrows, and insignificant coefficients are indicated through gray dashed arrows. Arrow thickness scales with the standardized model coefficient of each bivariate relationship. A positive coefficient for photosynthetic pathway indicates larger values in C_3 species, while a positive coefficient for N_{fixer} indicates larger values in N-fixing species. Standardized model coefficients and associated p -values are reported in Table 4.5, with conditional R^2 values for each response variable reported on the top right of each box.

1576 4.4 Discussion

1577 In this study, I quantified direct and indirect effects of edaphic and climatic char-
1578 acteristics on N_{area} and components of N_{area} (N_{mass} and M_{area}) in 520 individuals
1579 spanning across a soil resource availability and climate gradient in Texas, USA.
1580 Strong and consistent patterns emerged in support of those expected from photo-
1581 synthetic least-cost theory, a result driven by a strong direct negative relationship
1582 between leaf $C_i:C_a$ and N_{area} . In further support of patterns expected from theory,
1583 increasing soil nitrogen availability had a strong negative effect on β , resulting in
1584 an indirect stimulation in N_{area} mediated through a positive relationship between
1585 β and $C_i:C_a$. Increasing VPD also indirectly increased N_{area} through a direct
1586 negative effect of increasing VPD on leaf $C_i:C_a$, following hypotheses and pat-
1587 terns expected from theory. Interestingly, a strong positive association between
1588 soil moisture and N_{area} was driven by covariance between soil moisture and soil
1589 nitrogen availability and was not associated with a direct effect of soil moisture
1590 on β . Overall, results provide strong and consistent support for patterns expected
1591 from photosynthetic least-cost theory, showing that both soil resource availability
1592 and climate drive variance in N_{area} through changes in leaf $C_i:C_a$.

1593 4.4.1 *Negative effects of leaf $C_i:C_a$ on N_{area} are driven by reductions in M_{area} ,*
1594 *not N_{mass}*

1595 A strong negative effect of increasing leaf $C_i:C_a$ on N_{area} was detected in both
1596 the linear mixed effect and piecewise structural equation models. The negative
1597 response of N_{area} to increasing leaf $C_i:C_a$ is consistent with previous environmental
1598 gradient (Dong et al. 2017; Querejeta et al. 2022) and manipulation experiments

1599 (3.4c), showing strong support for the nitrogen-water use tradeoffs expected from
1600 photosynthetic least cost theory (Wright et al. 2003; Prentice et al. 2014). Neg-
1601 ative effects of increasing leaf $C_i:C_a$ on N_{area} were driven by a strong negative
1602 effect of increasing $C_i:C_a$ on M_{area} , with no apparent effect of leaf $C_i:C_a$ on N_{mass} ,
1603 suggesting that changes in N_{area} were driven by changes in leaf structure and not
1604 leaf chemistry per se. However, increasing M_{area} was negatively associated with
1605 N_{mass} , indicating that an increase in N_{mass} was associated with larger, thinner
1606 leaves (i.e. lower M_{area}). These results are consistent with patterns reported from
1607 previous studies indicating that variance in N_{area} is driven by changes in M_{area}
1608 across environmental gradients, and that part of this response is due to negative
1609 covariance between M_{area} and N_{mass} (Dong et al. 2017; Dong et al. 2020). I spec-
1610 ulate that this response could be associated with tradeoffs between leaf longevity
1611 and leaf productivity (Wright et al. 2004; Dong et al. 2017; Dong et al. 2022;
1612 Querejeta et al. 2022; Wang et al. 2023).

1613 The negative relationship between leaf $C_i:C_a$ and M_{area} could be a response
1614 that allows leaves to maximize productivity in shorter-lived leaves. Tradeoffs be-
1615 tween leaf longevity and leaf productivity are commonly observed and are included
1616 in a continuum of coordinated leaf traits that position individuals along a fast-
1617 or slow-growing leaf economics spectrum (Wright et al. 2003; Onoda et al. 2004;
1618 Reich 2014; Onoda et al. 2017; Wang et al. 2023). Negative relationships between
1619 leaf $C_i:C_a$ and M_{area} indicate that increased stomatal conductance and reduced
1620 water use efficiency were associated with thinner, larger leaves (i.e., lower M_{area}).
1621 These patterns, combined with the negative covariance between M_{area} and N_{mass}
1622 mentioned above, may have allowed individuals to maximize light interception

1623 and productivity by exploiting high light environments, though this comes at the
1624 expense of increased water loss and decreased water-use efficiency. This strategy
1625 may be especially advantageous for fast-growing species in open canopy systems.
1626 In this study, C₃ legumes and C₃ nonlegumes dominated the dataset (78% of total
1627 sampling effort), of which 22% (17% of total sampling effort) were classified as
1628 annual species with short growing seasons. We observed no effect of leaf C_i:C_a
1629 on N_{area} or M_{area} in C₄ nonlegumes, which made up 22% of the sampling effort
1630 and were generally classified as warm season graminoid species with slower growth
1631 rates and longer growing seasons. These patterns indicate that stronger tradeoffs
1632 between nitrogen and water use may be more apparent in fast-growing species
1633 with high demand for building and maintaining productive leaf tissues.

1634 4.4.2 *Soil nitrogen availability increases N_{area} through changes in β*
1635 The experimental approach used in this study allowed for N_{area} and components
1636 of N_{area} to be quantified as direct and indirect products of soil nitrogen availabil-
1637 ity. Linear mixed effect models revealed a direct positive effect of increasing soil
1638 nitrogen availability on N_{area}, a pattern that was driven by a stronger positive
1639 effect of increasing soil nitrogen availability on N_{mass} than the negative effect of
1640 increasing soil nitrogen availability on M_{area}. Similar patterns were observed in
1641 the structural equation model, where indirect positive effects of increasing soil
1642 nitrogen availability on N_{area} were driven by negative effects of increasing soil
1643 nitrogen availability on β , positive effects of β and leaf C_i:C_a, and negative re-
1644 lationships between leaf C_i:C_a and M_{area}. However, structural equation model
1645 results revealed no direct relationship between leaf C_i:C_a and N_{mass}, and instead

1646 indicated and indirect positive effect of leaf $C_i:C_a$ on N_{mass} mediated through
1647 strong negative covariance between M_{area} and N_{mass} .

1648 Together, results reported here suggest that positive direct effects of in-
1649 creasing soil nitrogen availability on N_{area} are not necessarily the direct product
1650 of increased leaf nitrogen concentration, as has been previously suggested (Firn
1651 et al. 2019; Liang et al. 2020). Instead, effects of increasing soil nitrogen avail-
1652 ability on leaf nitrogen concentration may be driven by costs of nitrogen acquisi-
1653 tion relative to water and negative covariance between M_{area} and N_{mass} , following
1654 patterns predicted by photosynthetic least-cost theory. Findings reported here
1655 suggest that studies quantifying variance in leaf nitrogen content across resource
1656 availability gradients may risk confounding covariance between M_{area} and N_{mass} if
1657 costs of nitrogen acquisition relative to water are not also quantified.

1658 4.4.3 *Soil moisture increases N_{area} by facilitating increases in soil nitrogen
1659 availability*

1660 Increasing soil moisture had a positive effect on N_{area} , a response that was asso-
1661 ciated with a null effect of soil moisture on β . These results contrast patterns
1662 expected from theory, where increasing soil moisture is expected to indirectly de-
1663 crease N_{area} through an increase in β due to a reduction in costs associated with
1664 water acquisition and use (Wright et al. 2003; Prentice et al. 2014; Lavergne
1665 et al. 2020). Interestingly, structural equation model results revealed a strong
1666 positive association between soil moisture and soil nitrogen availability, indicat-
1667 ing an indirect positive effect of increasing soil moisture on N_{area} mediated by
1668 the negative effect of increasing soil nitrogen availability on β . In Texan grass-
1669 lands, productivity and nutrient uptake are often co-limited by precipitation and

1670 nutrient availability (Yahdjian et al. 2011; Wang et al. 2017). Thus, increases
1671 in soil moisture may have facilitated more favorable and productive environments
1672 for soil microbial communities (Reichman et al. 1966; Stark and Firestone 1995;
1673 Paul et al. 2003), or alternatively greater nitrogen mobility in soil solution. As
1674 discussed above, the positive indirect response of N_{area} to increasing soil nitrogen
1675 availability as mediated through reductions in β follow patterns expected from
1676 theory.

1677 4.4.4 *Indirect effects of climate on N_{area} are mediated through changes in leaf*
1678 $C_i:C_a$ *and β*

1679 In support of hypotheses and patterns expected from theory, increasing vapor
1680 pressure deficit indirectly increased N_{area} , mediated through the negative effect
1681 of increasing vapor pressure deficit on leaf $C_i:C_a$. These responses are consistent
1682 with previous work noting strong reductions in stomatal conductance with increas-
1683 ing vapor pressure deficit (Oren et al. 1999; Novick et al. 2016; Sulman et al.
1684 2016; Grossiord et al. 2020; López et al. 2021), a response that allows plants
1685 to minimize water loss as a result of high atmospheric water demand. Results
1686 also support findings from previous experiments across environmental gradients,
1687 where increasing vapor pressure deficit generally increases N_{area} at lower stomatal
1688 conductance across environmental gradients (Dong et al. 2017; Dong et al. 2022;
1689 Paillassa et al. 2020; Westerband et al. 2023). These responses provide another
1690 line of evidence that suggests leaf nitrogen content is a deterministic acclima-
1691 tion response to changing aboveground climate, allowing plants to satisfy demand
1692 to build and maintain photosynthetic enzymes and optimize photosynthetic pro-
1693 cesses by maximizing resource use efficiency (Paillassa et al. 2020; Peng et al.
1694 2021; Dong et al. 2022; Westerband et al. 2023).

1695 4.4.5 *Species identity traits modify effects of the environment on β , leaf $C_i:C_a$,*
1696 *and N_{area}*

1697 N-fixing species generally had higher N_{area} values on average compared to non-
1698 fixing species, a pattern driven by a stronger stimulation in N_{mass} in N-fixing
1699 species coupled with no change in M_{area} between species with different N-fixation
1700 ability. There was no evidence to suggest that N-fixing species had different β or
1701 leaf $C_i:C_a$ values compared to non-fixing species across the environmental gradient.
1702 These results follow patterns from previous environmental gradient experiments
1703 that investigate variance in leaf nitrogen allocation in N-fixing species (Adams
1704 et al. 2016; Dong et al. 2017; Dong et al. 2020), and that increases in N_{mass}
1705 and N_{area} in N-fixing species are not necessarily correlated to increases in water
1706 use efficiency or reductions in leaf $C_i:C_a$ (Adams et al. 2016). While results
1707 are consistent with results from previous environmental gradient experiments,
1708 they do not support hypotheses presented here or patterns expected from theory,
1709 which predicts that stimulations in N_{area} by N-fixing species should be driven
1710 by a reduction in β relative to non-fixing species, and that this response should
1711 decrease stomatal conductance and leaf $C_i:C_a$.

1712 C_4 species generally had lower β , leaf $C_i:C_a$, and N_{area} than C_3 species.
1713 Reduced β and leaf $C_i:C_a$ values in C_4 species follow hypotheses listed above, a
1714 pattern that could be the result of either reduced costs of nitrogen acquisition
1715 and use, increased costs of water acquisition and use, or both (Wright et al. 2003;
1716 Prentice et al. 2014). Results also indicate that β in C_4 nonlegumes was unrespon-
1717 sive to changes in soil nitrogen availability despite an apparent negative effect of
1718 increasing soil nitrogen availability on β in C_3 legumes and C_3 nonlegumes. Com-
1719 bined with a general null response of β to soil moisture regardless of plant func-

1720 tional group, these patterns imply that reduced β values in C₄ species may be the
1721 result of lower costs of nitrogen acquisition and use relative to C₃ species. While
1722 lower β values in C₄ species provides a possible explanation for why C₄ species
1723 often have lower leaf $C_i:C_a$ and greater water use efficiency, theory predicts that
1724 this response should cause C₄ species to have greater N_{area} values compared to
1725 C₃ species, though C₄ species commonly exhibit lower N_{area} and higher nitrogen
1726 use efficiency than C₃ species (Schmitt and Edwards 1981; Sage and Pearcy 1987;
1727 Ghannoum et al. 2011). We speculate that lowered costs of nitrogen acquisition
1728 and use in C₄ species could be driven by more efficient Rubisco carboxylation effi-
1729 ciency in C₄ species associated with CO₂ concentrating mechanisms that eliminate
1730 photorespiration (Ghannoum et al. 2011), which could reduce or eliminate the
1731 need to sacrifice inefficient nitrogen use for efficient water use to achieve optimal
1732 photosynthesis rates.

1733

1734 4.4.6 *Next steps for optimality model development*

1735 Optimality models for both C₃ and C₄ species have been developed using principles
1736 from photosynthetic least-cost theory (Prentice et al. 2014; Wang et al. 2017;
1737 Smith et al. 2019; Stocker et al. 2020; Scott and Smith 2022). In both C₃ and C₄
1738 model variants, β values are held constant using global datasets of leaf $\delta^{13}\text{C}$ (Wang
1739 et al. 2017; Cornwell et al. 2018). Specifically, the C₃ optimality model initially
1740 assumed a constant β value of 240 (Wang et al. 2017), later corrected to 146
1741 (Stocker et al. 2020), while the C₄ optimality model assumes a constant β value of
1742 166 (Scott and Smith 2022). These results, which build on findings from Paillassa
1743 et al. (2020) and Lavergne et al. (2020), demonstrate high variability in calculated

1744 β values across the environmental gradient. Specifically, β values in C₃ species
1745 ranged from 1.7 to 188.0 (mean: 30.2; median: 23.1; standard deviation: 25.4),
1746 while ranged from 0.1 to 110.6 in C₄ species (mean: 7.2; median: 0.7; standard
1747 deviation: 18.6). Mean β values in both C₃ and C₄ species were consistently lower
1748 than values currently implemented in optimality models, though this was likely
1749 the result of increased water limitation across sites relative to global averages.
1750 Regardless, the high degree of β variability across this environmental gradient,
1751 together with findings from Lavergne et al. (2020) and Paillassa et al. (2020),
1752 suggests that the use of constant β values may contribute to erroneous errors when
1753 conducting optimality model simulations. Results from this experiment build
1754 on suggestions from Wang et al. (2017), suggesting that future photosynthetic
1755 least-cost optimality model developments should consider adopting frameworks
1756 for dynamically calculating β .

1757 4.4.7 *Conclusions*

1758 To summarize, variability in N_{area} across an environmental gradient in Texan
1759 grasslands was driven by indirect effects of climate and soil resource availability
1760 mediated. Results from this experiment provide strong and consistent support for
1761 patterns expected from photosynthetic least-cost theory, demonstrating that neg-
1762 ative relationships between $C_i:C_a$ and N_{area} unify expected effects of climatic and
1763 edaphic characteristics on N_{area} across environmental gradients. Results reported
1764 here also demonstrate a need to consider the dynamic nature of the relative cost
1765 of nitrogen versus water uptake (β) across environmental gradients in optimality
1766 models that leverage principles of photosynthetic least-cost theory.

1767

Chapter 5

1768
1769

Optimal resource investment to photosynthetic capacity maximizes
nutrient allocation to whole plant growth under elevated CO₂

1770 5.1 Introduction

1771 Terrestrial ecosystems are regulated by complex carbon and nitrogen cycles. As
1772 a result, terrestrial biosphere models, which are beginning to include coupled
1773 carbon and nitrogen cycles (Shi et al. 2016; Davies-Barnard et al. 2020; Braghieri
1774 et al. 2022), must accurately represent these cycles under different environmental
1775 scenarios to reliably simulate carbon and nitrogen atmosphere-biosphere fluxes
1776 (Hungate et al. 2003; Prentice et al. 2015). While the inclusion of coupled carbon
1777 and nitrogen cycles tends to reduce model uncertainty (Arora et al. 2020), large
1778 uncertainty in role of soil nitrogen availability and nitrogen acquisition strategy
1779 on leaf and whole plant acclimation responses to CO₂ remains (Smith and Dukes
1780 2013; Terrer et al. 2018; Smith and Keenan 2020). This source of uncertainty
1781 likely contributes to the widespread divergence in future carbon and nitrogen flux
1782 simulations across terrestrial biosphere models (Friedlingstein et al. 2014; Zaehle
1783 et al. 2014; Meyerholt et al. 2020).

1784 Plants grown under elevated CO₂ generally have less leaf nitrogen content
1785 than those grown under ambient CO₂, a response that often corresponds with
1786 reductions in photosynthetic capacity and stomatal conductance at the leaf-level
1787 and biomass stimulation over time at the whole plant level (Curtis 1996; Drake
1788 et al. 1997; Ainsworth et al. 2002; Makino 2003; Morgan et al. 2004; Ainsworth
1789 and Long 2005; Ainsworth and Rogers 2007; Smith and Dukes 2013; Poorter et al.
1790 2022). As net primary productivity is generally limited by nitrogen availability

1791 (Vitousek and Howarth 1991; LeBauer and Treseder 2008; Fay et al. 2015), and
1792 soil nitrogen availability is often positively correlated with leaf nitrogen content
1793 and photosynthetic capacity (Field and Mooney 1986; Evans and Seemann 1989;
1794 Evans 1989; Walker et al. 2014; Firn et al. 2019; Liang et al. 2020), some
1795 have hypothesized that leaf and whole plant acclimation responses to CO₂ are
1796 constrained by soil nitrogen availability. The progressive nitrogen limitation hy-
1797 pothesis predicts that elevated CO₂ will increase plant nitrogen demand, which
1798 will increase plant nitrogen uptake and progressively deplete soil nitrogen if soil
1799 nitrogen supply does not exceed plant nitrogen demand (Luo et al. 2004). The
1800 hypothesis predicts that this response should result in strong acute stimulations in
1801 whole plant growth and primary productivity that diminish over time as nitrogen
1802 becomes more limiting. Assuming a positive relationship between soil nitrogen
1803 availability, leaf nitrogen content, and photosynthetic capacity, this hypothesis
1804 also implies that progressive reductions in soil nitrogen availability should be the
1805 mechanism that drives the downregulation in leaf nitrogen content and photosyn-
1806 thetic capacity under elevated CO₂. This hypothesis has received some support
1807 from free air CO₂ enrichment experiments (Reich et al. 2006; Norby et al. 2010),
1808 although is not consistently observed across experiments (Finzi et al. 2006; Moore
1809 et al. 2006; Liang et al. 2016).

1810 While possible that progressive nitrogen limitation may determine leaf and
1811 whole plant acclimation responses to CO₂, growing evidence indicates that leaf ni-
1812 trogen and photosynthetic capacity are more strongly determined through above-
1813 ground growing conditions than by soil resource availability (Dong et al. 2017;
1814 Dong et al. 2020; Dong et al. 2022; Smith et al. 2019; Smith and Keenan 2020;

1815 Paillassa et al. 2020; Peng et al. 2021; Querejeta et al. 2022; Westerband et al.
1816 2023), and satellite-derived chlorophyll fluorescence data indicate that increasing
1817 atmospheric CO₂ may decrease leaf and canopy demand for nitrogen (Dong et al.
1818 2022). Together, results from these studies suggest that the downregulation in
1819 leaf nitrogen content and photosynthetic capacity due to increasing CO₂ may not
1820 be as tightly linked to progressive nitrogen limitation as previously hypothesized.

1821 A unification of optimal coordination and photosynthetic least-cost the-
1822 ories predicts that leaves acclimate to elevated CO₂ by downregulating nitrogen
1823 allocation to Ribulose-1,5-bisphosphate (RuBP) carboxylase/oxygenase (Rubisco)
1824 to optimize resource use efficiencies at the leaf level, which allows for greater re-
1825 source allocation to whole plant growth (Drake et al. 1997; Wright et al. 2003;
1826 Prentice et al. 2014; Smith et al. 2019). The theory predicts that the downregu-
1827 lation in nitrogen allocation to Rubisco results in a stronger downregulation in the
1828 maximum rate of Rubisco carboxylation (V_{cmax}) than the maximum rate of RuBP
1829 regeneration (J_{max}), which maximizes photosynthetic efficiency by allowing net
1830 photosynthesis rates to be equally co-limited by Rubisco carboxylation and RuBP
1831 regeneration (Chen et al. 1993; Maire et al. 2012). This acclimation response
1832 allows plants to make more efficient use of available light while avoiding overin-
1833 vestment in Rubisco, which has high nitrogen and energetic costs of building and
1834 maintaining (Evans 1989; Evans and Clarke 2019). Instead, additional acquired
1835 resources not needed to optimize leaf photosynthesis are allocated to the mainte-
1836 nance of structures that support whole plant growth (e.g., total leaf area, whole
1837 plant biomass, etc.) or to allocation processes not related to leaf photosynthesis
1838 or growth, such as plant defense mechanisms or leaf structural tissue. Regardless,

1839 optimized resource allocation at the leaf level should allow for greater resource
1840 allocation to whole plant growth. The theory indicates that leaf acclimation re-
1841 sponses to CO₂ should be independent of changes in soil nitrogen availability.
1842 While this leaf acclimation response maximizes nitrogen allocation to structures
1843 that support whole plant growth, the theory suggests that the positive effect of
1844 elevated CO₂ on whole plant growth may be further stimulated by soil nitrogen
1845 availability through a reduction in the cost of acquiring nitrogen (Bae et al. 2015;
1846 Perkowski et al. 2021; Lu et al. 2022).

1847 Plants acquire nitrogen by allocating photosynthetically derived carbon be-
1848 lowground in exchange for nitrogen through different nitrogen acquisition strate-
1849 gies. These nitrogen acquisition strategies can include direct uptake pathways
1850 such as mass flow or diffusion (Barber 1962), symbioses with mycorrhizal fungi or
1851 symbiotic nitrogen-fixing bacteria (Vance and Heichel 1991; Marschner and Dell
1852 1994; Smith and Read 2008; Udvardi and Poole 2013), or through the release
1853 of root exudates that prime free-living soil microbial communities (Phillips et al.
1854 2011; Wen et al. 2022). Plants cannot acquire nitrogen without first allocating
1855 carbon belowground, which implies an inherent carbon cost to the plant for acquir-
1856 ing nitrogen regardless of nitrogen acquisition strategy. Carbon costs to acquire
1857 nitrogen often vary in species with different nitrogen acquisition strategies and
1858 are dependent on external environmental factors such as atmospheric CO₂, light
1859 availability, and soil nitrogen availability (Brzostek et al. 2014; Terrer et al. 2016;
1860 Terrer et al. 2018; Allen et al. 2020; Perkowski et al. 2021; Lu et al. 2022), which
1861 suggests that acquisition strategy may be an important factor in determining ef-
1862 fects of soil nitrogen availability on leaf and whole plant acclimation responses to

1863 elevated CO₂.

1864 A recent meta-analysis using data across 20 grassland and forest CO₂ en-
1865 richment experiments suggested that species which acquire nitrogen from sym-
1866 biotic nitrogen-fixing bacteria had reduced costs of nitrogen acquisition under
1867 elevated CO₂ (Terrer et al. 2018). Findings from this meta-analysis indicated
1868 that reductions in costs of nitrogen acquisition in species that form associations
1869 with symbiotic nitrogen-fixing bacteria under elevated CO₂ may drive stronger
1870 stimulations in whole plant growth and downregulations in V_{cmax} than species that
1871 associate with arbuscular mycorrhizal fungi (Smith and Keenan 2020), which gen-
1872 erally have higher costs of nitrogen acquisition under elevated CO₂ (Terrer et al.
1873 2018). However, plant investments in symbiotic nitrogen fixation generally de-
1874 cline with increasing nitrogen availability (Dovrat et al. 2018; Perkowski et al.
1875 2021), a response that has been previously inferred to be the result of a shift in
1876 the dominant mode of nitrogen acquisition to direct uptake pathways as costs of
1877 direct uptake decrease with increasing soil nitrogen availability (Rastetter et al.
1878 2001; Perkowski et al. 2021). Thus, effects of symbiotic nitrogen fixation on plant
1879 acclimation responses to CO₂ should decline with increasing soil nitrogen avail-
1880 ability, although manipulative experiments that directly test these patterns are
1881 rare.

1882 Here, I conducted a 7-week growth chamber experiment using *Glycine max*
1883 L. (Merr.) to examine the effects of soil nitrogen fertilization and inoculation with
1884 symbiotic nitrogen-fixing bacteria on leaf and whole plant acclimation responses
1885 to elevated CO₂. Following patterns expected from theory, I hypothesized that in-
1886 dividual leaves should acclimate to elevated CO₂ by more strongly downregulating

1887 V_{cmax} relative to J_{max} , allowing leaf photosynthesis to approach optimal coordi-
1888 nation. I expected this response to correspond with a stronger downregulation in
1889 leaf nitrogen content than V_{cmax} and J_{max} , which would increase the fraction of
1890 leaf nitrogen content allocated to photosynthesis and photosynthetic nitrogen use
1891 efficiency. At the whole-plant level, I hypothesized that plants would acclimate
1892 to elevated CO₂ by stimulating whole plant growth and productivity, a response
1893 that would be driven by a strong positive response of total leaf area and above-
1894 ground biomass to elevated CO₂. I predicted that leaf acclimation responses to
1895 elevated CO₂ would be independent of soil nitrogen fertilization and inoculation
1896 with symbiotic nitrogen-fixing bacteria; however, I expected that increasing soil
1897 nitrogen fertilization would increase the positive effect of elevated CO₂ on mea-
1898 sures of whole plant growth due to a stronger reduction in the cost of acquiring
1899 nitrogen under elevated CO₂ with increasing fertilization. I also expected stronger
1900 stimulations in whole plant growth due to inoculation, but that this effect would
1901 only be apparent under low fertilization due to a reduction in root nodulation
1902 with increasing fertilization.

1903 5.2 Methods

1904 5.2.1 *Seed treatments and experimental design*

1905 *Glycine max* L. (Merr) seeds were planted in 144 6-liter surface sterilized pots (NS-
1906 600, Nursery Supplies, Orange, CA, USA) containing a steam-sterilized 70:30 v:v
1907 mix of Sphagnum peat moss (Premier Horticulture, Quakertown, PA, USA) to
1908 sand (Pavestone, subsidiary of Quikrete Companies, Atlanta, GA, USA). Before
1909 planting, all *G. max* seeds were surface sterilized in 2% sodium hypochlorite for 3

1910 minutes, followed by three separate 3-minute washes with ultrapure water (MilliQ
1911 7000; MilliporeSigma, Burlington, MA USA). A subset of surface sterilized seeds
1912 were inoculated with *Bradyrhizobium japonicum* (Verdesian N-DureTM Soybean,
1913 Cary, NC, USA) in a slurry following manufacturer recommendations (3.12 g
1914 inoculant and 241 g deionized water per 1 kg seed).

1915 Seventy-two pots were randomly planted with surface-sterilized seeds inoc-
1916 ulated with *B. japonicum*, while the remaining 72 pots were planted with surface-
1917 sterilized uninoculated seeds. Thirty-six pots within each inoculation treatment
1918 were randomly placed in one of two atmospheric CO₂ treatments (ambient and
1919 1000 $\mu\text{mol mol}^{-1}$ CO₂). Pots within each unique inoculation-by-CO₂ treatment
1920 combination randomly received one of nine soil nitrogen fertilization treatments
1921 equivalent to 0, 35, 70, 105, 140, 210, 280, 350, or 630 ppm N. Nitrogen fertil-
1922 ization treatments were created using a modified Hoagland solution (Hoagland
1923 and Arnon 1950) designed to keep concentrations of other macronutrients and
1924 micronutrients equivalent across treatments (Table D1). Pots received the same
1925 fertilization treatment throughout the entire duration experiment, which were ap-
1926 plied twice per week in 150 mL doses as topical agents to the soil surface through-
1927 out the duration of the experiment. This experimental design yielded a fully
1928 factorial experiment with four replicates per unique fertilization-by-inoculation-
1929 by-CO₂ combination.

1930 5.2.2 *Growth chamber conditions*

1931 Upon experiment initiation, pots were randomly placed in one of six Percival
1932 LED-41L2 growth chambers (Percival Scientific Inc., Perry, IA, USA) over two

1933 experimental iterations due to chamber space limitation. Two iterations were
1934 conducted such that one iteration included all elevated CO₂ pots and the second
1935 iteration included all ambient CO₂ pots. Average (\pm SD) CO₂ concentrations
1936 across chambers throughout the experiment were $439 \pm 5 \mu\text{mol mol}^{-1}$ for the am-
1937 bient CO₂ treatment and $989 \pm 4 \mu\text{mol mol}^{-1}$ for the elevated CO₂ treatment.

1938 Daytime growing conditions were simulated using a 16-hour photoperiod,
1939 with incoming light radiation set to chamber maximum (mean \pm SD: 1240 ± 32
1940 $\mu\text{mol m}^{-2} \text{s}^{-1}$ across chambers), air temperature set to 25°C, and relative humid-
1941 ity set to 50%. The remaining 8 hours simulated nighttime growing conditions,
1942 with incoming light radiation set to 0 $\mu\text{mol m}^{-2} \text{s}^{-1}$, chamber temperature set
1943 to 17°C, and relative humidity set to 50%. Transitions between daytime and
1944 nighttime growing conditions were simulated by ramping incoming light radiation
1945 in 45-minute increments and temperature in 90-minute increments over a 3-hour
1946 period (Table D2).

1947 Including the two, 3-hour ramping periods, pots grew under average (\pm SD)
1948 daytime light intensity of $1049 \pm 27 \mu\text{mol m}^{-2} \text{s}^{-1}$. In the elevated CO₂ iteration,
1949 pots grew under $24.0 \pm 0.2^\circ\text{C}$ during the day, $16.4 \pm 0.8^\circ\text{C}$ during the night, and
1950 $51.6 \pm 0.4\%$ relative humidity. In the ambient CO₂ iteration, pots grew under
1951 $23.9 \pm 0.2^\circ\text{C}$ during the day, $16.0 \pm 1.4^\circ\text{C}$ during the night, and $50.3 \pm 0.2\%$
1952 relative humidity. We accounted for climatic differences across the six chambers
1953 by shuffling the same group of pots daily throughout the growth chambers. This
1954 process was done by iteratively moving the group of pots on the top rack of a
1955 chamber to the bottom rack of the same chamber, while simultaneously moving
1956 the group of pots on the bottom rack of a chamber to the top rack of the adjacent

1957 chamber. I moved pots within and across chambers every day throughout the
1958 course of each experiment iteration.

1959 5.2.3 *Leaf gas exchange measurements*

1960 Gas exchange measurements were collected for all individuals on the seventh week
1961 of development. All gas exchange measurements were collected on the center leaf
1962 of the most recent fully expanded trifoliate leaf set. Specifically, I measured net
1963 photosynthesis (A_{net} ; $\mu\text{mol m}^{-2} \text{s}^{-1}$), stomatal conductance (g_{sw} ; $\text{mol m}^{-2} \text{s}^{-1}$),
1964 and intercellular CO_2 (C_i ; $\mu\text{mol mol}^{-1}$) concentrations across a range of atmo-
1965 spheric CO_2 concentrations (i.e., an A_{net}/C_i curve) using the Dynamic Assimila-
1966 tion Technique™. The Dynamic Assimilation Technique™ has been shown to
1967 correspond well with traditional steady-state CO_2 response curves in *G. max*
1968 (Saathoff and Welles 2021). A_{net}/C_i curves were generated along a reference
1969 CO_2 ramp down from $420 \mu\text{mol mol}^{-1} \text{CO}_2$ to $20 \mu\text{mol mol}^{-1} \text{CO}_2$, followed by
1970 a ramp up from $420 \mu\text{mol mol}^{-1} \text{CO}_2$ to $1620 \mu\text{mol mol}^{-1} \text{CO}_2$ after a 90-second
1971 wait period at $420 \mu\text{mol mol}^{-1} \text{CO}_2$. The ramp rate for each curve was set to 200
1972 $\mu\text{mol mol}^{-1} \text{min}^{-1}$, logging every five seconds, which generated 96 data points per
1973 response curve. All A_{net}/C_i curves were generated after A_{net} and g_{sw} stabilized
1974 in a LI-6800 cuvette set to a 500 mol s^{-1} , 10,000 rpm mixing fan speed, 1.5 kPa
1975 vapor pressure deficit, 25°C leaf temperature, $2000 \mu\text{mol m}^{-2} \text{s}^{-1}$ incoming light
1976 radiation, and initial reference CO_2 set to $420 \mu\text{mol mol}^{-1}$.

1977 With the same focal leaf used to generate A_{net}/C_i curves, I measured dark
1978 respiration (R_{d25} ; $\mu\text{mol m}^{-2} \text{s}^{-1}$) following at least a 30-minute period of darkness.
1979 Measurements were collected on a 5-second log interval for 60 seconds after stabi-

1980 lizing in a LI-6800 cuvette set to a 500 mol s^{-1} , 10,000 rpm mixing fan speed, 1.5
1981 kPa vapor pressure deficit, 25°C leaf temperature, and $420 \mu\text{mol mol}^{-1}$ reference
1982 CO₂ concentration (for both CO₂ concentrations), with incoming light radiation
1983 set to $0 \mu\text{mol m}^{-2} \text{ s}^{-1}$. A single dark respiration value was determined for each
1984 focal leaf by calculating the mean dark respiration value (i.e. the absolute value
1985 of A_{net} during the logging period) across the logging interval.

1986 5.2.4 *Leaf trait measurements*

1987 The focal leaf used to generate A_{net}/C_i curves and dark respiration was harvested
1988 immediately following gas exchange measurements. Images of each focal leaf were
1989 curated using a flat-bed scanner to determine wet leaf area using the 'LeafArea' R
1990 package (Katabuchi 2015), which automates leaf area calculations using ImageJ
1991 software (Schneider et al. 2012). Each leaf was dried at 65°C for at least 48
1992 hours, and subsequently weighed and ground until homogenized. Leaf mass per
1993 area (M_{area} ; g m⁻²) was calculated as the ratio of dry leaf biomass to fresh leaf
1994 area. Using subsamples of ground and homogenized leaf tissue, I measured leaf
1995 nitrogen content (N_{mass} ; gN g⁻¹) through elemental combustion analysis (Costech-
1996 4010, Costech, Inc., Valencia, CA, USA). Leaf nitrogen content per unit leaf area
1997 (N_{area} ; gN m⁻²) was calculated by multiplying N_{mass} and M_{area} .

1998 I extracted chlorophyll content from a second leaf in the same trifoliolate
1999 leaf set as the focal leaf used to generate A_{net}/C_i curves. Prior to chlorophyll
2000 extraction, I used a cork borer to punch between 3 and 5 0.6 cm² disks from the
2001 leaf. Separate images of each punched leaf and set of leaf disks were curated using
2002 a flat-bed scanner to determine wet leaf area, again quantified using the 'LeafArea'

2003 R package (Katabuchi 2015). The punched leaf was dried and weighed after at
2004 least 65°C in the drying oven to determine M_{area} of the chlorophyll leaf.
2005 Leaf disks were shuttled into a test tube containing 10mL dimethyl sul-
2006 foxide, vortexed, and incubated at 65degreeC for 120 minutes (Barnes et al.
2007 1992). Incubated test tubes were vortexed again before loaded in 150 μL tri-
2008 licate aliquots to a 96-well plate. Dimethyl sulfoxide was also loaded in a 150
2009 μL triplicate aliquot as a blank. Absorbance measurements at 649.1 nm ($A_{649.1}$)
2010 and 665.1 nm ($A_{665.1}$) were read in each well using a plate reader (Biotek Synergy
2011 H1; Biotek Instruments, Winooski, VT USA) (Wellburn 1994), with triplicates
2012 subsequently averaged and corrected by the mean of the blank absorbance value.
2013 Blank-corrected absorbance values were used to estimate Chl_a ($\mu\text{g mL}^{-1}$) and
2014 Chl_b ($\mu\text{g mL}^{-1}$) following equations from Wellburn (1994):

$$Chl_a = 12.47A_{665.1} - 3.62A_{649.1} \quad (5.1)$$

2015 and

$$Chl_b = 25.06A_{665.1} - 6.50A_{649.1} \quad (5.2)$$

2016 Chl_a and Chl_b were converted to mmol mL^{-1} using the molar mass of chlorophyll a
2017 (893.51 g mol^{-1}) and the molar mass of chlorophyll b (907.47 g mol^{-1}), then added
2018 together to calculate total chlorophyll content in the dimethyl sulfoxide extractant
2019 (mmol mL^{-1}). Total chlorophyll content was multiplied by the volume of the
2020 dimethyl sulfoxide extractant (10 mL) and converted to area-based chlorophyll
2021 content by dividing by the total area of the leaf disks (Chl_{area} ; mmol m^{-2}). Mass-
2022 based chlorophyll content (Chl_{mass} ; mmol g^{-1}) was calculated by dividing Chl_{area}

2023 by the leaf mass per area of the punched leaf.

2024 5.2.5 *A/C_i curve fitting and parameter estimation*

2025 I fit A_{net}/C_i curves of each individual using the ‘fitaci’ function in the ‘planete-

2026 cophys’ R package (Duursma 2015). This function estimates the maximum rate

2027 of Rubisco carboxylation (V_{cmax} ; $\mu\text{mol m}^{-2} \text{s}^{-1}$) and maximum rate of electron

2028 transport for RuBP regeneration (J_{max} ; $\mu\text{mol m}^{-2} \text{s}^{-1}$) based on the Farquhar

2029 biochemical model of C₃ photosynthesis (Farquhar et al. 1980). Triose phosphate

2030 utilization (TPU) limitation was included in all curve fits, and all curve fits in-

2031 cluded measured dark respiration values. As A_{net}/C_i curves were generated using

2032 a common leaf temperature, curves were fit using Michaelis-Menten coefficients

2033 for Rubisco affinity to CO₂ (K_c ; $\mu\text{mol mol}^{-1}$) and O₂ (K_o ; $\mu\text{mol mol}^{-1}$), and the

2034 CO₂ compensation point (Γ^* ; $\mu\text{mol mol}^{-1}$) reported in Bernacchi et al. (2001).

2035 Specifically, K_c was set to 404.9 $\mu\text{mol mol}^{-1}$, K_o was set to 278.4 $\mu\text{mol mol}^{-1}$, and

2036 Γ^* was set to 42.75 $\mu\text{mol mol}^{-1}$. The use of a common leaf temperature across

2037 curves and dark respiration measurements also eliminated the need to manually

2038 temperature standardize rate estimates. For clarity, I reference V_{cmax} , J_{max} , and

2039 R_d estimates throughout the rest of the paper as $V_{\text{cmax}25}$, $J_{\text{max}25}$, and R_{d25} .

2040 5.2.6 Stomatal limitation

2041 I quantified the extent by which stomatal conductance limited photosynthesis (l;

2042 unitless) following equations originally described in Farquhar and Sharkey (1982).

2043 Stomatal limitation was calculated as:

$$l = 1 - \frac{A_{net}}{A_{mod}} \quad (5.3)$$

2044 where A_{mod} represents the photosynthetic rate where $C_i=C_a$. A_{mod} was calculated

2045 as:

$$A_{mod} = V_{cmax25} - \frac{420 - \Gamma^*}{420 + K_m} - R_{d25} \quad (5.4)$$

2046 K_m is the Michaelis-Menten coefficient for Rubisco-limited photosynthesis, calcu-

2047 lated as:

$$K_m = K_c \cdot \left(1 + \frac{O_i}{K_o}\right) \quad (5.5)$$

2048 where O_i refers to leaf intercellular O_2 concentrations, set to $210 \mu\text{mol mol}^{-1}$.

2049 5.2.7 *Proportion of leaf nitrogen allocated to photosynthesis and structure*

2050 I used equations from Niinemets and Tenhunen (1997) to estimate the proportion

2051 of leaf nitrogen content allocated to Rubisco bioenergetics, and light harvesting

2052 proteins. The proportion of leaf N allocated to Rubisco ($\rho_{rubisco}$; gN gN^{-1}) was

2053 calculated as a function of V_{cmax25} and N_{area} :

$$\rho_{rubisco} = \frac{V_{cmax25} N_r}{V_{cr} N_{area}} \quad (5.6)$$

2054 where N_r is the amount of nitrogen in Rubisco, set to $0.16 \text{ gN (gN in Rubisco)}^{-1}$

2055 and V_{cr} is the maximum rate of RuBP carboxylation per unit Rubisco protein,

2056 set to $20.5 \mu\text{mol CO}_2 (\text{g Rubisco})^{-1}$. The proportion of leaf nitrogen allocated to

2057 bioenergetics (ρ_{bioe} ; gN gN^{-1}) was similarly calculated as a function of J_{max25} and

2058 N_{area} :

$$\rho_{\text{bioe}} = \frac{J_{\text{max}25} N_b}{J_{\text{mc}} N_{\text{area}}} \quad (5.7)$$

2059 where N_b is the amount of nitrogen in cytochrome f, set to 0.12407 gN (μmol cytochrome f) $^{-1}$ assuming a constant 1: 1: 1.2 cytochrome f: ferredoxin NADP reductase: coupling factor molar ratio (Evans and Seemann 1989; Niinemets and Tenhunen 1997), and J_{mc} is the capacity of electron transport per cytochrome f, set to 156 μmol electron (μmol cytochrome f) $^{-1}\text{s}^{-1}$.

2064 The proportion of leaf nitrogen allocated to light harvesting proteins (ρ_{light} ; **2065** gN gN $^{-1}$) was calculated as a function of Chl_{mass} and N_{mass} :

$$\rho_{\text{light}} = \frac{Chl_{\text{mass}}}{N_{\text{mass}} c_b} \quad (5.8)$$

2066 where c_b is the stoichiometry of the light-harvesting chlorophyll complexes of **2067** photosystem II, set to 2.75 mmol chlorophyll (gN in chlorophyll) $^{-1}$. We used the **2068** N_{mass} value of the focal leaf used to generate A_{net}/C_i curves instead of the leaf **2069** used to extract chlorophyll content, as the two leaves are from the same trifoliolate **2070** leaf set and are highly correlated with each other (Figure D1).

2071 The proportion of leaf nitrogen content allocated to photosynthetic tissue **2072** (ρ_{photo} ; gN gN $^{-1}$) was estimated as the sum of ρ_{rubisco} , ρ_{bioe} , and ρ_{light} . Finally, **2073** the proportion of leaf N content allocated to structural tissue ($\rho_{\text{structure}}$; gN gN $^{-1}$) **2074** was estimated as:

$$\rho_{\text{structure}} = \frac{N_{\text{cw}}}{N_{\text{area}}} \quad (5.9)$$

2075 where N_{cw} is the leaf nitrogen content allocated to cell walls (gN m $^{-2}$), calculated

2076 as a function of M_{area} using an empirical equation from Onoda et al. (2017):

$$N_{cw} = 0.000355 * M_{area}^{1.39} \quad (5.10)$$

2077 5.2.8 *Whole plant traits*

2078 Seven weeks after experiment initiation and immediately following gas exchange
2079 measurements, I harvested all experimental individuals and separated biomass of
2080 each experimental individual into major organ types (leaves, stems, roots, and
2081 nodules when present). Fresh leaf area of all harvested leaves was measured using
2082 an LI-3100C (Li-COR Biosciences, Lincoln, Nebraska, USA). Total fresh leaf area
2083 (cm^2) was calculated as the sum of all leaf areas, including the focal leaf used to
2084 collect gas exchange data and the focal leaf used to extract chlorophyll content.
2085 All harvested material was dried in an oven set to 65°C for at least 48 hours,
2086 weighed, and ground to homogeneity. Leaves and nodules were manually ground
2087 either with a mortar and pestle, while stems and roots were ground using a Wiley
2088 mill (E3300 Mini Mill; Eberbach Corp., MI, USA). Total dry biomass (g) was
2089 calculated as the sum of dry leaf (including focal leaf for both the A_{net}/C_i curve
2090 and leaf used to extract chlorophyll content), stem, root, and root nodule biomass.
2091 I quantified carbon and nitrogen content of each respective organ type through
2092 elemental combustion (Costech-4010, Costech, Inc., Valencia, CA, USA) using
2093 subsamples of ground and homogenized organ tissue.
2094 Following the approach explained in the first experimental chapter, I calcu-
2095 lated structural carbon costs to acquire nitrogen as the ratio of total belowground
2096 carbon biomass to whole plant nitrogen biomass (N_{cost} ; gC gN^{-1}). Belowground

2097 carbon biomass (C_{bg} ; gC) was calculated as the sum of root carbon biomass
2098 and root nodule carbon biomass. Root carbon biomass and root nodule carbon
2099 biomass was calculated as the product of the organ biomass and the respective
2100 organ carbon content. Whole plant nitrogen biomass (N_{wp} ; gN) was similarly
2101 calculated as the sum of total leaf, stem, root, and root nodule nitrogen biomass,
2102 including the focal leaf used for A_{net}/C_i curve and chlorophyll extractions. Leaf,
2103 stem, root, and root nodule nitrogen biomass was calculated as the product of
2104 the organ biomass and the respective organ nitrogen content. This calculation
2105 only quantifies plant structural carbon costs to acquire nitrogen and does not
2106 include any additional costs of nitrogen acquisition associated with respiration,
2107 root exudation, or root turnover. An explicit explanation of the limitations for
2108 interpreting this calculation can be found in Perkowski et al. (2021) and Terrer
2109 et al. (2018).

2110 Finally, plant investments in nitrogen fixation were calculated as the ra-
2111 tio of root nodule biomass to root biomass, where increasing values indicate an
2112 increase in plant investments to nitrogen fixation (Dovrat et al. 2018; Dovrat
2113 et al. 2020; Perkowski et al. 2021). I also calculated the percent of leaf nitrogen
2114 acquired from the atmosphere (% N_{dfa}) using leaf $\delta^{15}\text{N}$ and the following equation
2115 from Andrews et al. (2011):

$$\%N_{dfa} = \frac{\delta^{15}\text{N}_{reference} - \delta^{15}\text{N}_{sample}}{\delta^{15}\text{N}_{reference} - B} \quad (5.11)$$

2116 where $\delta^{15}\text{N}_{reference}$ refers to a reference plant that exclusively acquires nitrogen via
2117 direct uptake, $\delta^{15}\text{N}_{sample}$ refers to an individual's leaf $\delta^{15}\text{N}$, and B refers to indi-

2118 individuals that are entirely reliant on nitrogen fixation. Within each unique nitrogen
2119 fertilization treatment-by-CO₂ treatment combination, I calculated the mean leaf
2120 δ¹⁵N for individuals growing in the non-inoculated treatment for δ¹⁵N_{reference}. Any
2121 individuals with visual confirmation of root nodule formation or nodule initiation
2122 were omitted from the calculation of δ¹⁵N_{reference}. Following recommendations
2123 from Andrews et al. (2011) I calculated B within each CO₂ treatment using
2124 the mean leaf δ¹⁵N of inoculated individuals that received 0 ppm N. I did not
2125 calculate B within each unique soil nitrogen-by-CO₂ treatment combination, as
2126 previous studies suggest decreased reliance on nitrogen fixation with increasing
2127 soil nitrogen availability (Perkowski et al. 2021). This approach for estimating
2128 nitrogen fixation standardizes values such that approaching 1 indicates increasing
2129 reliance on nitrogen fixation.

2130 5.2.9 *Statistical analyses*

2131 Any uninoculated pots that had substantial root nodule formation (nodule biomass:
2132 root biomass values greater than 0.05 g g⁻¹) were removed from analyses. This was
2133 because they were assumed to have been colonized by symbiotic nitrogen-fixing
2134 bacteria from outside sources. This decision resulted in the removal of sixteen
2135 pots from our analysis: two pots in the elevated CO₂ treatment that received 35
2136 ppm N, three pots in the elevated CO₂ treatment that received 70 ppm N, one pot
2137 in the elevated CO₂ treatment that received 210 ppm N, two pots in the elevated
2138 CO₂ treatment that received 280 ppm N, two pots in the ambient CO₂ treatment
2139 that received 0 ppm N, three pots in the ambient CO₂ treatment that received
2140 70 ppm N, two pots in the ambient CO₂ treatment that received 105 ppm N, and

2141 one pot in the ambient CO₂ treatment that received 280 ppm N.

2142 I built a series of linear mixed effects models to investigate the impacts of
2143 CO₂ concentration, soil nitrogen fertilization, and inoculation with *B. japonicum*
2144 on *G. max* gas exchange, tradeoffs between nitrogen and water use, whole plant
2145 growth, and investment in nitrogen fixation. All models included CO₂ treatment
2146 as a categorical fixed effect, inoculation treatment as a categorical fixed effect,
2147 soil nitrogen fertilization as a continuous fixed effect, with interaction terms be-
2148 tween all three fixed effects. All models also accounted for climatic difference
2149 between chambers across experiment iterations by including a random intercept
2150 term that nested starting chamber rack by CO₂ treatment. Models with this
2151 independent variable structure were created for each of the following dependent
2152 variables: N_{area} , M_{area} , N_{mass} , Chl_{area} , V_{cmax25} , J_{max25} , $J_{\text{max25}}:V_{\text{cmax25}}$, R_{d25} , g_{sw} ,
2153 stomatal limitation, ρ_{rubisco} , ρ_{bioe} , ρ_{light} , ρ_{photo} , $\rho_{\text{structure}}$, N_{cost} , C_{bg} , N_{wp} , total
2154 biomass, total leaf area, nodule biomass, and the ratio of nodule biomass to root
2155 biomass.

2156 I used Shapiro-Wilk tests of normality to determine whether linear mixed
2157 effects models satisfied residual normality assumptions. If residual normality as-
2158 sumptions were not met (Shapiro-Wilk: $p < 0.05$), then models were fit using
2159 dependent variables that were natural log transformed. All residual normality
2160 assumptions that did not originally satisfy residual normality assumptions were
2161 met with either a natural log or square root data transformation (Shapiro-Wilk:
2162 $p > 0.05$ in all cases). Specifically, models for N_{area} , N_{mass} , Chl_{area} , V_{cmax25} ,
2163 J_{max25} , $J_{\text{max25}}:V_{\text{cmax25}}$, g_{sw} , stomatal limitation, ρ_{rubisco} , ρ_{bioe} , ρ_{light} , ρ_{photo} , and to-
2164 tal leaf area satisfied residual normality assumptions without data transformation.

2165 Models for M_{area} , $\rho_{\text{structure}}$, N_{cost} , C_{bg} , N_{wp} , and total biomass satisfied residual
2166 normality assumptions with a natural log data transformation, while models for
2167 nodule biomass and nodule biomass: root biomass satisfied residual normality
2168 assumptions with a square root data transformation.

2169 In all statistical models, I used the 'lmer' function in the 'lme4' R package
2170 (Bates et al. 2015) to fit each model and the 'Anova' function in the 'car' R
2171 package (Fox and Weisberg 2019) to calculate Type II Wald's χ^2 and determine
2172 the significance ($\alpha = 0.05$) of each fixed effect coefficient. I used the 'emmeans'
2173 R package (Lenth 2019) to conduct post-hoc comparisons using Tukey's tests,
2174 where degrees of freedom were approximated using the Kenward-Roger approach
2175 (Kenward and Roger 1997). All analyses and plots were conducted in R version
2176 4.2.0 (R Core Team 2021).

2177 5.3 Results

2178 5.3.1 *Leaf nitrogen and chlorophyll content*

2179 Elevated CO₂ reduced N_{area} , N_{mass} , and Chl_{area} by 29%, 50%, and 31%,
2180 respectively, and stimulated M_{area} by 44% ($p < 0.001$ in all cases; Table 5.1). An
2181 interaction between fertilization and CO₂ (CO₂-by-fertilization interaction: $p_{N_{\text{area}}}$
2182 = 0.017, $p_{N_{\text{mass}}} < 0.001$, $p_{M_{\text{area}}} = 0.006$, $p_{Chl_{\text{area}}} = 0.083$; Table 5.1) indicated
2183 that the general positive effect of increasing fertilization on N_{area} , N_{mass} , and
2184 Chl_{area} ($p < 0.001$ in all cases; Table 5.1) was generally stronger under ambient
2185 CO₂ (Tukey _{N_{area}} : $p = 0.026$; Tukey _{N_{mass}} : $p < 0.001$; Tukey _{M_{area}} : $p = 0.009$;
2186 Tukey _{Chl_{area}} : $p = 0.065$; Table 5.1; Figs. 5.1a-d). This pattern resulted in a
2187 stronger reduction in N_{area} , N_{mass} , and Chl_{area} as well as a stronger stimulation

2188 in M_{area} under elevated CO₂ with increasing fertilization. An additional interac-
2189 tion between inoculation and CO₂ on N_{area} (CO₂-by-inoculation interaction: $p =$
2190 0.030; Table 5.1) indicated that the general positive effect of inoculation on N_{area}
2191 ($p < 0.001$; Table 5.1) was stronger under elevated CO₂ (45% increase; Tukey: p
2192 < 0.001) than under ambient CO₂ (18% increase; Tukey: $p < 0.001$), a result that
2193 increased the reduction in N_{area} in inoculated pots under elevated CO₂. Inocula-
2194 tion treatment did not modify the downregulation in N_{mass} (CO₂-by-inoculation
2195 interaction: $p = 0.148$; Table 5.1) and Chl_{area} ($p = 0.147$; Table 5.1) or the stimu-
2196 lation in M_{area} ($p = 0.866$; Table 5.1) under elevated CO₂. However, interactions
2197 between fertilization and inoculation on N_{area} (fertilization-by-inoculation inter-
2198 action: $p < 0.001$; Table 5.1; Fig. 5.1a), N_{mass} ($p = 0.001$; Table 5.1; Fig. 5.1b),
2199 M_{area} ($p = 0.025$; Table 5.1; Fig. 5.1c), and Chl_{area} ($p < 0.001$; Table 5.1; Fig.
2200 5.1d) indicated that the general positive effect of increasing fertilization on each
2201 trait was stronger in uninoculated pots (Tukey _{N_{area}} : $p < 0.001$; Tukey _{N_{mass}} : $p =$
2202 0.001; Tukey _{M_{area}} : $p = 0.031$; Tukey _{Chl_{area}} : $p < 0.001$).

Table 5.1. Effects of soil nitrogen fertilization, inoculation, and CO₂ treatments on N_{area} , N_{mass} , M_{area} , and Chl_{area}

	N_{area}			N_{mass}			M_{area}^a			
	df	Coefficient	χ^2	p	Coefficient	χ^2	p	Coefficient	χ^2	p
(Intercept)	-	1.10E+00	-	-	3.05E-02	-	-	3.64E+00	-	-
CO ₂	1	-5.67E-01	155.908	<0.001	-1.80E-02	272.362	<0.001	3.04E-01	151.319	<0.001
Inoculation (I)	1	6.21E-01	86.029	<0.001	7.54E-03	15.576	<0.001	1.81E-01	19.158	<0.001
Fertilization (N)	1	3.06E-03	316.408	<0.001	5.78E-05	106.659	<0.001	3.10E-04	21.440	<0.001
CO ₂ *I	1	2.63E-01	4.729	0.030	3.96E-03	2.025	0.155	-3.37E-02	0.029	0.866
CO ₂ *N	1	-3.68E-04	5.723	0.017	-2.85E-05	22.542	<0.001	2.80E-04	7.619	0.006
I*N	1	-1.36E-03	43.381	<0.001	-2.00E-05	11.137	0.001	-3.36E-04	5.022	0.025
CO ₂ *I*N	1	-3.23E-04	0.489	0.484	-2.59E-06	0.041	0.839	1.15E-04	0.208	0.649
	Chl_{area}									
	df	Coefficient	χ^2	p						
(Intercept)	-	2.13E-02	-	-						
CO ₂	1	-1.33E-02	69.233	<0.001						
Inoculation (I)	1	1.24E-01	136.341	<0.001						
Fertilization (N)	1	3.35E-04	163.111	<0.001						
CO ₂ *I	1	-3.18E-02	2.102	0.147						
CO ₂ *N	1	-8.79E-05	2.999	<i>0.083</i>						
I*N	1	-2.65E-04	75.769	<0.001						
CO ₂ *I*N	1	7.68E-05	2.144	0.147						

129

2203 *Significance determined using Type II Wald χ^2 tests ($\alpha = 0.05$). P -values < 0.05 are in bold, while p -values between
 2204 0.05 and 0.1 are italicized. A superscript “a” is included after trait labels to indicate if models were fit with natural
 2205 log transformed response variables. Key: df = degrees of freedom, N_{area} = leaf nitrogen content per unit leaf area,
 2206 N_{mass} = leaf nitrogen content, M_{area} = leaf mass per unit leaf area.

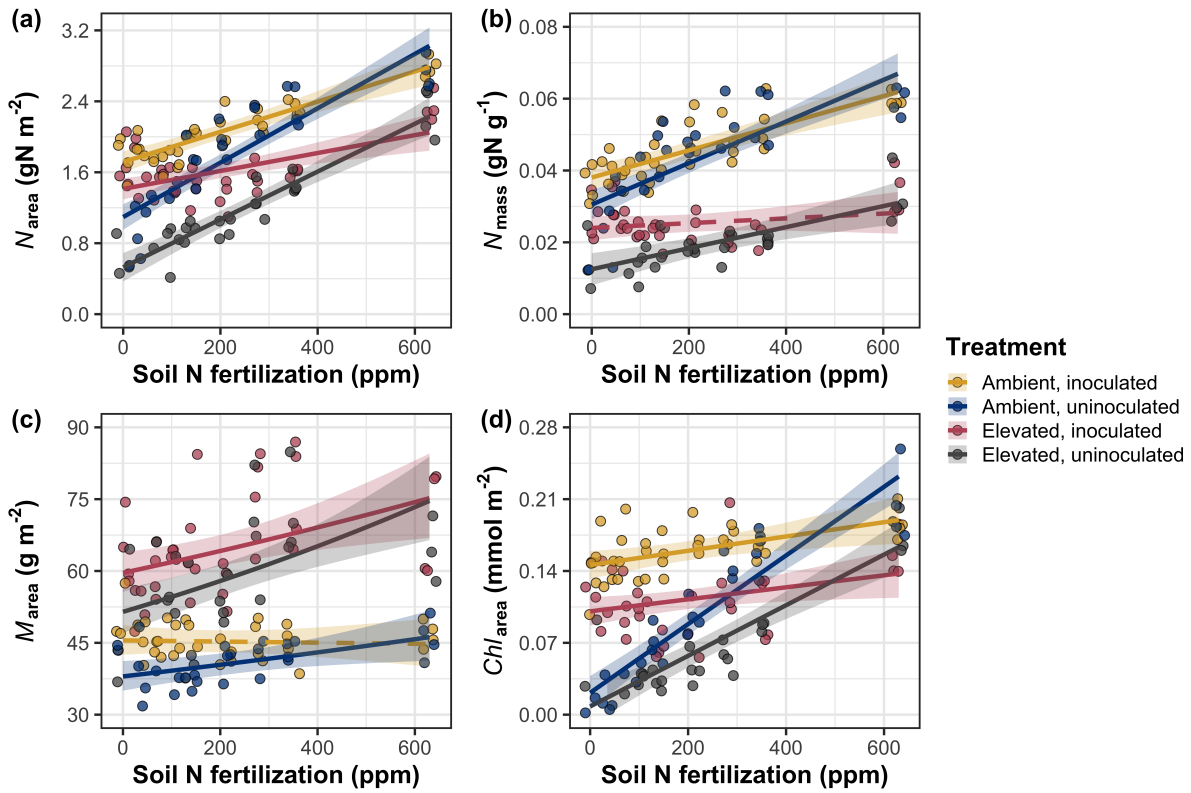


Figure 5.1. Effects of CO_2 , fertilization, and inoculation on leaf nitrogen per unit leaf area (a), leaf nitrogen content (b), leaf mass per unit leaf area (c), and chlorophyll content per unit leaf area (d). Soil nitrogen fertilization is represented on the x-axis in all panels. Yellow points and trendlines indicate inoculated individuals grown under ambient CO_2 , blue points and trendlines indicate uninoculated individuals grown under ambient CO_2 , red points and trendlines indicate inoculated individuals grown under elevated CO_2 , and grey points indicate uninoculated individuals grown under elevated CO_2 . Solid trendlines indicate regression slopes that are different from zero ($p < 0.05$), while dashed trendlines indicate slopes that are not distinguishable from zero ($p > 0.05$).

2207 5.3.2 *Leaf biochemistry and stomatal conductance*

2208 Elevated CO₂ resulted in plants with 16% lower V_{cmax25} ($p < 0.001$; Table
2209 5.2) and 10% lower J_{max25} ($p = 0.014$; Table 5.2) as compared to those grown under
2210 ambient CO₂. However, CO₂ concentration did not influence R_{d25} ($p = 0.613$;
2211 Table 5.2). A relatively stronger downregulation in V_{cmax25} than J_{max25} resulted
2212 in an 8% stimulation in $J_{max25}:V_{cmax25}$ under elevated CO₂ ($p < 0.001$; Table 5.2;
2213 Fig. 2E). The downregulatory effect of CO₂ on V_{cmax25} and J_{max25} was not modified
2214 across the fertilization gradient (CO₂-by-fertilization interaction: $p = 0.185$, $p =$
2215 0.389 for V_{cmax25} and J_{max25} , respectively; Table 5.2; Fig. 5.2a-b) or between
2216 inoculation treatments (CO₂-by-inoculation interaction: $p = 0.799$ and $p = 0.714$
2217 for V_{cmax25} and J_{max25} , respectively; Table 5.2). However, a strong interaction
2218 between fertilization and inoculation (fertilization-by-inoculation interaction: $p \leq$
2219 0.001 in all cases; Table 5.2) indicated that the general positive effect of increasing
2220 fertilization on V_{cmax25} ($p < 0.001$; Table 5.2), J_{max25} ($p < 0.001$; Table 5.2), and
2221 R_{d25} ($p = 0.015$; Table 2) was only observed in uninoculated pots (Tukey: p
2222 ≤ 0.001 in all cases), as there was no apparent effect of fertilization on V_{cmax25}
2223 (Tukey: $p = 0.456$), J_{max25} (Tukey: $p = 0.180$), or R_{d25} (Tukey: $p = 0.443$) in
2224 inoculated pots (Figs. 5.2a-d). A relatively stronger positive effect of increasing
2225 fertilization on V_{cmax25} than J_{max25} resulted in a general reduction in $J_{max25}:V_{cmax25}$
2226 with increasing fertilization ($p < 0.001$), though this pattern was only seen in
2227 uninoculated pots (Tukey: $p = 0.003$) and not inoculated plants (Tukey: $p >$
2228 0.05).

2229 Elevated CO₂ reduced stomatal conductance by 20% ($p < 0.001$; Table
2230 5.2; Fig. 5.2e) compared to ambient CO₂, but this downregulation did not influ-

ence stomatal limitation of photosynthesis ($p = 0.355$; Table 5.2; Fig. 5.2f). As with V_{cmax25} and J_{max25} , the downregulation of stomatal conductance due to elevated CO₂ was not modified across the fertilization gradient (CO₂-by-fertilization interaction: $p = 0.141$; Table 5.2) or between inoculation treatments (CO₂-by-inoculation interaction: $p = 0.179$; Table 5.2). Fertilization also did not modify the general null effect of CO₂ on stomatal limitation (CO₂-by-fertilization interaction: $p = 0.554$; Table 5.2), although an interaction between CO₂ and inoculation (CO₂-by-inoculation interaction: $p = 0.043$; Table 5.2) indicated that inoculation increased stomatal limitation under ambient CO₂ (Tukey: $p = 0.021$), but not under elevated CO₂ (Tukey: $p > 0.999$). An interaction between inoculation and fertilization on stomatal conductance (fertilization-by-inoculation interaction: $p < 0.001$; Table 5.2) indicated that increasing fertilization increased stomatal conductance in uninoculated pots (Tukey: $p = 0.003$) but decreased stomatal conductance in inoculated pots (Tukey: $p = 0.021$). The similar in magnitude, but opposite direction, trend in the effect of increasing fertilization on stomatal conductance between inoculation treatments likely drove a null general response of stomatal conductance to increasing fertilization ($p = 0.642$; Table 5.2).

Table 5.2. Effects of soil nitrogen fertilization, inoculation, and CO₂ on leaf biochemistry

	<i>V_{cmax25}</i>			<i>J_{max25}</i>			<i>R_{d25}</i>			
	df	Coefficient	χ^2	p	Coefficient	χ^2	p	Coefficient	χ^2	p
(Intercept)	-	4.36E+01	-	-	8.30E+01	-	-	1.69E+00	-	-
CO ₂	1	-7.05E+00	18.039	<0.001	-9.11E+00	6.042	0.014	4.53E-01	0.256	0.613
Inoculation (I)	1	5.87E+01	98.579	<0.001	9.62E+01	85.064	<0.001	1.04E+00	3.094	0.079
Fertilization (N)	1	1.32E-01	37.053	<0.001	2.09E-01	25.356	<0.001	2.86E-03	5.965	0.015
CO ₂ *I	1	-4.65E+00	0.065	0.799	7.84E-01	0.667	0.414	-5.71E-01	2.563	0.109
CO ₂ *N	1	-3.58E-02	1.758	0.185	-4.33E-02	0.742	0.389	-1.55E-03	2.675	0.102
I*N	1	-1.35E-01	60.394	<0.001	-2.30E-01	57.410	<0.001	-2.84E-03	12.083	0.001
CO ₂ *I*N	1	2.73E-02	0.748	0.387	3.46E-02	0.377	0.539	7.21E-04	0.244	0.622

	<i>J_{max25}:V_{cmax25}</i>			<i>g_{sw}</i>			Stomatal limitation			
	df	Coefficient	χ^2	p	Coefficient	χ^2	p	Coefficient	χ^2	p
(Intercept)	-	1.92E+00	-	-	1.95E-01	-	-	2.12E-01	-	-
CO ₂	1	5.71E-02	92.010	<0.001	-6.23E-02	9.718	0.002	3.91E-02	0.856	0.355
Inoculation (I)	1	-1.79E-01	27.768	<0.001	1.30E-01	22.351	<0.001	7.87E-02	4.582	0.032
Fertilization (N)	1	-4.61E-04	28.147	<0.001	2.50E-04	0.066	0.797	2.60E-04	32.218	<0.001
CO ₂ *I	1	8.94E-02	2.916	0.088	6.69E-02	1.810	0.179	-7.84E-02	4.093	0.043
CO ₂ *N	1	2.35E-04	3.210	0.073	-8.50E-05	2.165	0.141	-1.24E-04	0.350	0.554
I*N	1	3.27E-04	9.607	0.002	-3.09E-04	14.696	<0.001	-1.67E-04	2.547	0.110
CO ₂ *I*N	1	-1.66E-04	1.102	0.294	-8.89E-05	0.234	0.629	1.67E-04	2.231	0.135

133

2248 *Significance determined using Type II Wald χ^2 tests ($\alpha = 0.05$). *P*-values < 0.05 are in bold, while *p*-values between
 2249 0.05 and 0.1 are italicized. Key: *V_{cmax25}* = maximum rate of Rubisco carboxylation at 25°C; *J_{max25}* = maximum rate
 2250 of electron transport for RuBP regeneration at 25°C, *R_{d25}* = dark respiration at 25°C; *J_{max25}:V_{cmax25}* = the ratio of
 2251 *J_{max25}* to *V_{cmax25}*; *g_{sw}* = stomatal conductance.

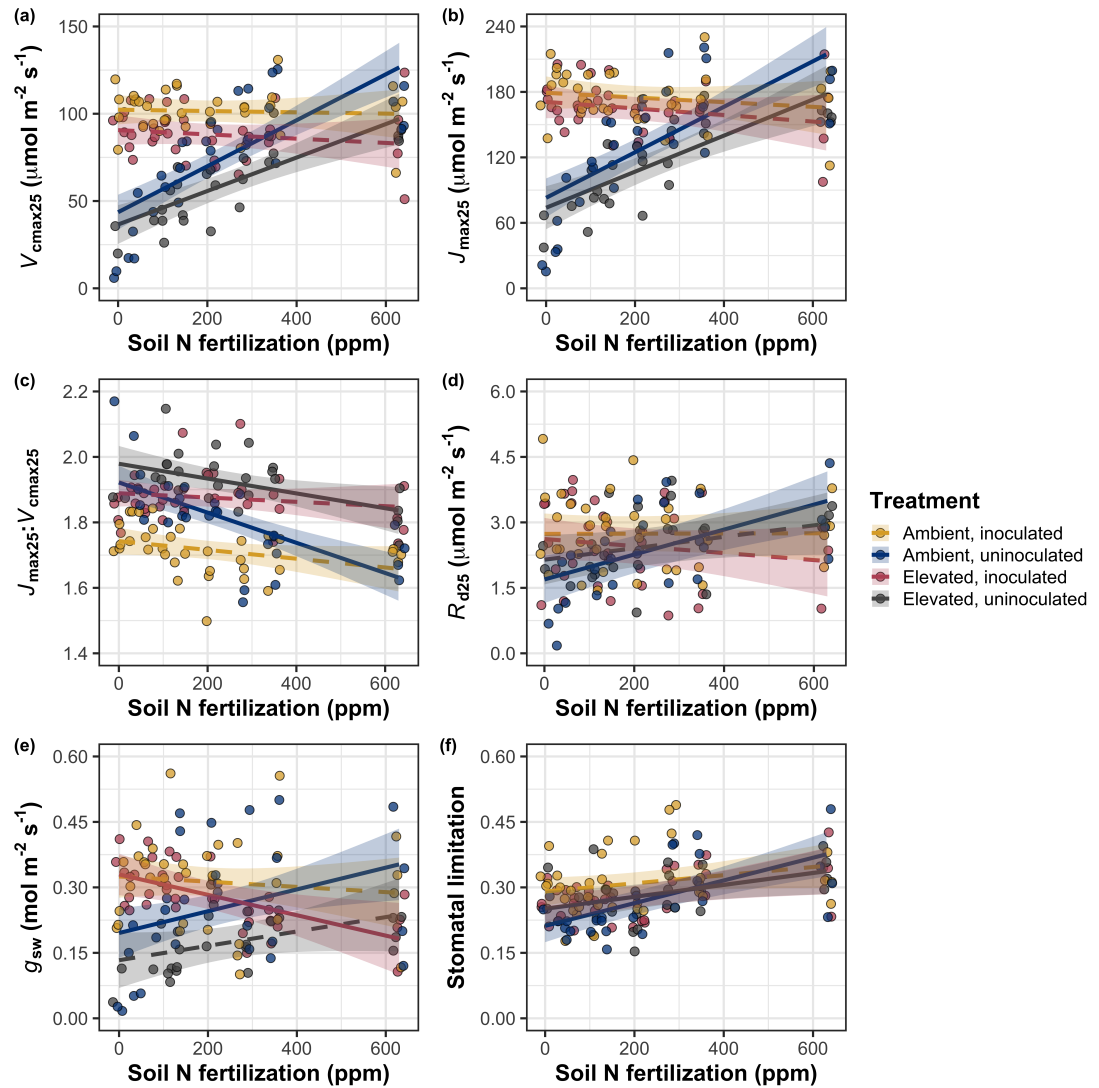


Figure 5.2. Effects of CO₂, fertilization, and inoculation on maximum rate of Rubisco carboxylation (a), the maximum rate of RuBP regeneration (b), and the ratio of the maximum rate of RuBP regeneration to the maximum rate of Rubisco carboxylation leaf mass per unit leaf area (c), dark respiration (d), stomatal conductance (e), and stomatal limitation (f). Soil nitrogen fertilization is represented on the x-axis in all panels. Colored points and trendlines are as explained in Figure 1.

2252 5.3.3 *Leaf nitrogen allocation*

2253 A relatively stronger downregulation in N_{area} than $V_{\text{cmax}25}$ or $J_{\text{max}25}$ resulted
2254 in an 20% and 29% respective stimulation in ρ_{rubisco} and ρ_{bioe} under elevated CO₂
2255 ($p < 0.001$ in both cases; Table 5.3). There was no apparent CO₂ effect on ρ_{light}
2256 ($p = 0.700$; Table 5.3), but the strong stimulation in ρ_{rubisco} and ρ_{bioe} resulted
2257 in a 21% stimulation of ρ_{photo} under elevated CO₂ ($p < 0.001$; Table 5.3; Fig.
2258 5.3a). The stimulation of ρ_{rubisco} , ρ_{bioe} , and ρ_{photo} due to elevated CO₂ was not
2259 modified across the fertilization gradient (CO₂-by-fertilization interaction: p_{rubisco}
2260 = 0.269, $p_{\text{bioe}} = 0.298$, $p_{\text{photo}} = 0.281$; Table 5.3). A marginal interaction between
2261 inoculation and CO₂ on ρ_{rubisco} and ρ_{photo} (CO₂-by-inoculation interaction: p_{rubisco}
2262 = 0.057, $p_{\text{photo}} = 0.057$; Table 5.3) indicated that the general positive effect of
2263 inoculation on ρ_{rubisco} and ρ_{photo} ($p < 0.001$ in both cases; Table 5.3) was only
2264 apparent under ambient CO₂ (Tukey: $p < 0.001$ in both cases), with no apparent
2265 effect of inoculation under elevated CO₂ (Tukey_{rubisco}: $p = 0.200$; Tukey_{photo}: p
2266 = 0.147). Inoculation did not modify the stimulation of ρ_{bioe} under elevated CO₂
2267 (CO₂-by-inoculation interaction: $p = 0.122$; Table 5.3) or the null effect of CO₂ on
2268 ρ_{bioe} (CO₂-by-inoculation interaction: $p = 0.298$; Table 5.3). Strong interactions
2269 between fertilization and inoculation on ρ_{rubisco} , ρ_{bioe} , and ρ_{photo} (fertilization-
2270 by-inoculation interaction: $p < 0.001$ in all cases; Table 5.3) indicated that the
2271 general negative effect of increasing fertilization ($p < 0.001$ in all cases; Table
2272 5.3) was only observed in inoculated pots (Tukey: $p < 0.001$ in all cases), with
2273 no apparent effect of fertilization on ρ_{rubisco} (Tukey: $p = 0.612$), ρ_{bioe} (Tukey:
2274 $p = 0.544$), or ρ_{photo} (Tukey: $p = 0.521$; Fig 5.3a) in uninoculated pots. An
2275 additional interaction between fertilization and inoculation on ρ_{light} (fertilization-

2276 by-inoculation interaction: $p < 0.001$; Table 5.3) indicated a negative effect of
2277 increasing fertilization on ρ_{light} in inoculated pots (Tukey: $p = 0.041$), but a
2278 positive effect of increasing fertilization in uninoculated pots (Tukey: $p < 0.001$).

2279 The stimulation in M_{area} resulted in an 133% stimulation of $\rho_{\text{structure}}$ under
2280 elevated CO₂ ($p < 0.001$; Table 5.3; Fig 5.3b). An interaction between fertiliza-
2281 tion and CO₂ (CO₂-by-fertilization interaction: $p = 0.039$; Table 5.3) indicated
2282 that the general negative effect of increasing fertilization ($p < 0.001$; Table 5.3) on
2283 $\rho_{\text{structure}}$ was marginally stronger under ambient CO₂ (Tukey: $p = 0.055$), resulting
2284 in a stronger stimulation in $\rho_{\text{structure}}$ under elevated CO₂ with increasing fertiliza-
2285 tion. A marginal interaction between inoculation and CO₂ (CO₂-by-inoculation
2286 interaction: $p = 0.057$; Table 5.3) indicated that the general positive effect of
2287 inoculation on $\rho_{\text{structure}}$ ($p < 0.001$; Table 5.3) was only observed under elevated
2288 CO₂ (Tukey: $p < 0.001$), with no apparent inoculation effect observed under am-
2289 bient CO₂ (Tukey: $p = 0.513$). Finally, an interaction between fertilization and
2290 inoculation (fertilization-by-inoculation interaction: $p < 0.001$; Table 5.3) indi-
2291 cated that, while increasing fertilization generally increased $\rho_{\text{structure}}$ ($p < 0.001$;
2292 Table 5.3), this response was generally stronger in uninoculated pots (Tukey: p
2293 = 0.001; Fig. 5.3b).

Table 5.3. Effects of soil N availability, soil pH, species, and N_{area} on leaf nitrogen allocation

		ρ_{rubisco}			ρ_{bioe}			ρ_{light}		
	df	Coefficient	χ^2	p	Coefficient	χ^2	p	Coefficient	χ^2	p
(Intercept)	-	2.70E-01	-	-	5.26E-02	-	-	8.48E-03	-	-
CO_2	1	1.42E-01	23.510	<0.001	3.00E-02	53.899	<0.001	2.03E-03	0.149	0.700
Inoculation (I)	1	1.83E-01	23.475	<0.001	2.80E-02	13.860	<0.001	2.04E-02	147.234	<0.001
Fertilization (N)	1	1.35E-04	16.609	<0.001	1.22E-05	26.827	<0.001	3.22E-05	19.378	<0.001
CO_2*I	1	-1.07E-01	3.629	<i>0.057</i>	-1.67E-02	2.390	0.122	-5.33E-03	0.684	0.408
CO_2*N	1	-2.16E-04	1.223	0.269	-3.59E-05	1.085	0.298	-7.01E-06	0.351	0.553
$I*N$	1	-4.26E-04	20.045	<0.001	-6.87E-05	15.458	<0.001	-4.37E-05	64.042	<0.001
CO_2*I*N	1	2.50E-04	3.327	<i>0.068</i>	4.08E-05	2.651	0.103	1.74E-05	3.735	<i>0.053</i>

		ρ_{photo}			$\rho_{\text{structure}}^a$					
	df	Coefficient	χ^2	p	Coefficient	χ^2	p			
(Intercept)	-	3.32E-01	-	-	-2.93E+00	-	-			
CO_2	1	1.81E-01	27.651	<0.001	8.77E-01	229.571	<0.001			
Inoculation (I)	1	2.31E-01	26.238	<0.001	-2.55E-01	13.872	<0.001			
Fertilization (N)	1	1.76E-04	15.899	<0.001	-1.51E-03	38.128	<0.001			
CO_2*I	1	-1.36E-01	3.671	<i>0.055</i>	-2.99E-01	3.622	<i>0.057</i>			
CO_2*N	1	-2.72E-04	1.163	0.281	3.14E-04	4.266	0.039			
$I*N$	1	-5.37E-04	21.355	<0.001	7.00E-04	11.025	0.001			
CO_2*I*N	1	3.29E-04	4.009	0.045	4.52E-04	0.669	0.413			

137

2294 *Significance determined using Type II Wald χ^2 tests ($\alpha = 0.05$). P-values < 0.05 are in bold, while p -values
 2295 between 0.05 and 0.1 are italicized. A superscript “a” is included after trait labels to indicate if models were fit with
 2296 natural log transformed response variables. Key: df=degrees of freedom, ρ_{rubisco} = proportion of leaf N allocated
 2297 to photosynthesis, ρ_{bioe} = proportion of leaf N allocated to bioenergetics, ρ_{light} = proportion of leaf N allocated to
 2298 light harvesting proteins, ρ_{photo} = proportion of leaf N allocated to photosynthesis, $\rho_{\text{structure}}$ = proportion of leaf N
 2299 allocated to cell wall structural tissue

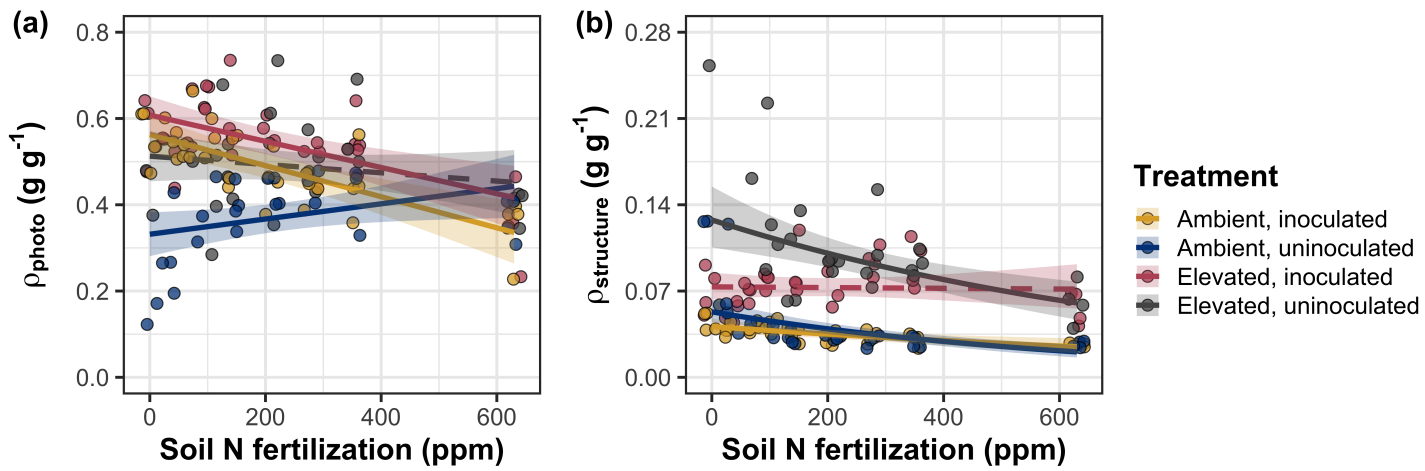


Figure 5.3. Effects of CO_2 , fertilization, and inoculation on the relative fraction of leaf nitrogen allocated to photosynthesis (a) and the fraction of leaf nitrogen allocated to structure (b). Soil nitrogen fertilization is represented on the x-axis in both panels. Colored points and trendlines are as explained in Figure 1.

2300 5.3.4 *Whole plant traits*

2301 Total leaf area was 51% greater and total biomass was 102% greater under
2302 elevated CO₂ ($p < 0.001$ in both cases; Table 5.4), a pattern that was enhanced
2303 by fertilization (CO₂-by-fertilization interaction: $p < 0.001$ in both cases; Table
2304 5.4; Figs. 5.4a-b) but was not modified across inoculation treatments (CO₂-by-
2305 inoculation interaction: $p_{total_leaf_area} = 0.151$, $p_{total_biomass} = 0.472$; Table 5.4).
2306 Specifically, the general positive effect of increasing fertilization on total leaf area
2307 and whole plant biomass ($p < 0.001$ in both cases; Table 5.4) was stronger under
2308 elevated CO₂ (Tukey: $p < 0.001$ in both cases). The general positive effect of
2309 increasing fertilization on total leaf area was modified by inoculation treatment
2310 (fertilization-by-inoculation interaction: $p < 0.001$ in both cases; Table 5.4), in-
2311 dicating a stronger positive effect of increasing fertilization in uninoculated pots
2312 (Tukey: $p_{total_leaf_area} = 0.002$, $p_{total_biomass} = 0.001$, Fig. 5.4a).

2313 A 62% stimulation in N_{cost} under elevated CO₂ was modified through a
2314 strong three-way interaction between CO₂, fertilization, and inoculation (CO₂-
2315 by-inoculation-by-fertilization interaction: $p < 0.001$; Table 5.4; Fig. 5.4). This
2316 interaction revealed a general negative effect of increasing fertilization on N_{cost}
2317 ($p < 0.001$; Table 5.4) that was observed in all treatment combinations (Tukey:
2318 $p < 0.001$ in all cases) except for inoculated pots grown under elevated CO₂
2319 (Tukey: $p = 0.779$; Fig. 5.4c). This response also resulted in generally stronger
2320 negative effects of increasing fertilization on N_{cost} in uninoculated pots grown
2321 under elevated CO₂ than uninoculated pots grown under ambient CO₂ (Tukey:
2322 $p = 0.001$) and inoculated pots grown under either ambient CO₂ (Tukey: $p <$
2323 0.001) or elevated CO₂ (Tukey: $p < 0.001$), while uninoculated pots grown under

2324 ambient CO₂ had generally stronger negative effects of increasing fertilization on
2325 N_{cost} than inoculated pots grown under elevated CO₂ (Tukey: $p = 0.002$), but
2326 not inoculated pots grown under ambient CO₂ (Tukey: $p = 0.216$; Fig. 5.4).
2327 The general reduction in N_{cost} with increasing fertilization and in uninoculated
2328 pots were driven by a stronger positive effect of increasing fertilization on N_{wp}
2329 (denominator of N_{cost}) than C_{bg} (numerator of N_{cost}), while the general stimulation
2330 in N_{cost} under elevated CO₂ was driven by a stronger positive effect of elevated
2331 CO₂ on C_{bg} than N_{wp} (Table 5.4).

Table 5.4. Effects of soil N availability, soil pH, species, and N_{area} on total leaf area, whole plant biomass, and carbon costs to acquire nitrogen

	Total leaf area			Total biomass			N_{cost}			
	df	Coefficient	χ^2	p	Coefficient	χ^2	p	Coefficient	χ^2	p
(Intercept)	-	8.78E+01	-	-	9.96E-01	-	-	8.67E+00	-	-
CO_2	1	3.36E+01	69.291	<0.001	5.07E-01	131.477	<0.001	8.75E+00	88.189	<0.001
Inoculation (I)	1	1.88E+02	35.715	<0.001	7.96E-01	34.264	<0.001	-1.68E+00	136.343	<0.001
Fertilization (N)	1	9.35E-01	274.199	<0.001	3.14E-03	269.046	<0.001	-8.50E-03	80.501	<0.001
$\text{CO}_2 * \text{I}$	1	6.44E+01	2.064	0.151	-7.69E-02	0.518	0.472	-8.38E+00	85.237	<0.001
$\text{CO}_2 * \text{N}$	1	5.05E-01	18.655	<0.001	1.61E-03	16.877	<0.001	-9.17E-03	1.050	0.306
$\text{I} * \text{N}$	1	-3.84E-01	10.804	0.001	-1.45E-03	15.779	<0.001	4.20E-03	46.489	<0.001
$\text{CO}_2 * \text{I} * \text{N}$	1	-2.97E-03	<0.001	0.990	-1.14E-04	0.023	0.880	1.32E-02	18.125	<0.001

	C_{bg}			N_{wp}			
	df	Coefficient	χ^2	p	Coefficient	χ^2	p
(Intercept)	-	-1.70E+00	-	-	1.24E-01	-	-
CO_2	1	9.21E-01	84.134	<0.001	-3.41E-03	23.890	<0.001
Inoculation (I)	1	1.18E+00	41.030	<0.001	1.68E-01	134.460	<0.001
N fertilization (N)	1	3.38E-03	152.248	<0.001	6.69E-04	529.021	<0.001
$\text{CO}_2 * \text{I}$	1	-6.18E-01	8.965	0.003	3.68E-02	1.190	0.275
$\text{CO}_2 * \text{N}$	1	-3.66E-05	1.188	0.276	1.58E-04	5.915	0.015
$\text{I} * \text{N}$	1	-2.22E-03	22.648	<0.001	-3.20E-04	55.562	<0.001
$\text{CO}_2 * \text{I} * \text{N}$	1	8.09E-04	1.109	0.292	-7.54E-05	0.620	0.431

141

2332 *Significance determined using Type II Wald χ^2 tests ($\alpha = 0.05$). P-values < 0.05 are in bold, while p-values between
 2333 0.05 and 0.1 are italicized. Key: df = degrees of freedom; N_{cost} = structural carbon cost to acquire nitrogen; C_{bg} =
 2334 belowground carbon biomass; N_{wp} = whole plant nitrogen biomass

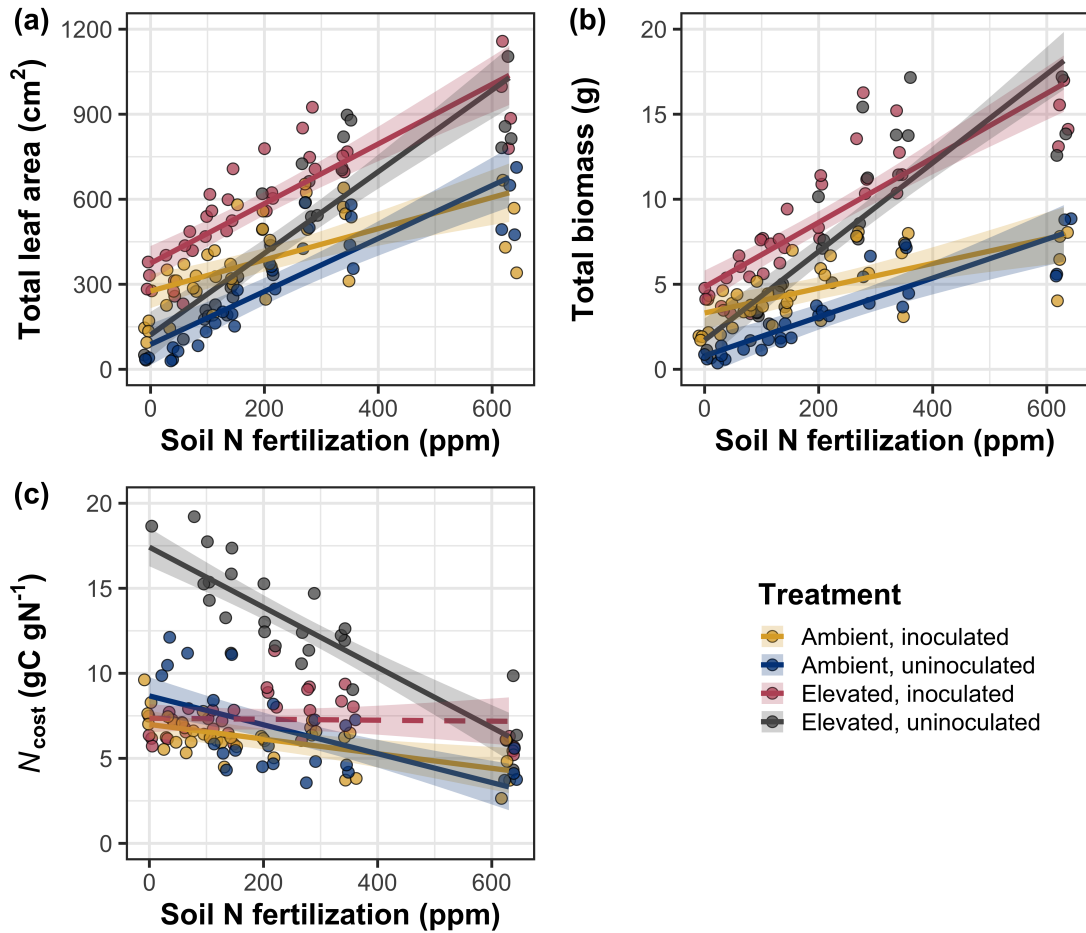


Figure 5.4. Effects of CO_2 , fertilization, and inoculation on total leaf area (a), total biomass (b), and structural carbon costs to acquire nitrogen (c). Soil nitrogen fertilization is represented continuously on the x-axis in all panels. Colored points and trendlines are as explained in Figure 1.

2335 5.3.5 Nitrogen fixation

2336 Nodule biomass was stimulated by 30% under elevated CO₂ ($p < 0.001$;
2337 Table 5.5), a pattern that was modified across the fertilization gradient (CO₂-
2338 by-fertilization interaction: $p = 0.479$; Table 5.5), but not between inoculation
2339 treatments (CO₂-by-inoculation interaction: $p = 0.404$; Table 5.5). Specifically,
2340 the general negative effect of increasing fertilization on nodule biomass ($p < 0.001$;
2341 Table 5.5) was stronger under elevated CO₂ than ambient CO₂ (Tukey: $p <$
2342 0.001; Fig. 5.5a), which reduced the stimulation in nodule biomass under elevated
2343 CO₂ with increasing fertilization. A strong interaction between fertilization and
2344 inoculation (fertilization-by-inoculation interaction: $p < 0.001$; Table 5.5) was
2345 driven by a stronger negative effect of increasing fertilization in inoculated pots
2346 (Tukey: $p < 0.001$; Fig. 5.5a).

2347 There was no effect of CO₂ on nodule: root biomass ($p = 0.767$; Table
2348 5.5), although an interaction between CO₂ and inoculation (CO₂-by-inoculation
2349 interaction: $p < 0.001$; Table 5.5) indicated that the general positive effect of in-
2350 oculation on nodule: root biomass ($p < 0.001$; Table 5.5) was stronger under am-
2351 bient CO₂ (3129% increase; Tukey: $p < 0.001$) than elevated CO₂ (379% increase;
2352 Tukey: $p < 0.001$; Fig. 5.5b). The null effect of CO₂ on nodule: root biomass
2353 was consistently observed across the fertilization gradient ($p = 0.183$; Table 5.5;
2354 Fig. 5.5b). An interaction between fertilization and inoculation (fertilization-by-
2355 inoculation interaction: $p < 0.001$; Table 5.5) indicated that the general negative
2356 effect of increasing fertilization on nodule: root biomass ($p < 0.001$; Table 5.5)
2357 was stronger in inoculated pots (Tukey: $p < 0.001$; Fig. 5.5b).

2358 There was no effect of CO₂ on %N_{dfa} ($p = 0.472$; Table 5.5), a pattern

2359 that was not modified by inoculation (CO_2 -by-inoculation interaction: $p = 0.156$;
2360 Table 5.5) or fertilization (CO_2 -by-fertilization interaction: $p = 0.099$; Table 5.5).
2361 An interaction between fertilization and inoculation (fertilization-by-inoculation
2362 interaction: $p < 0.001$; Table 5.5) indicated that the general negative effect of
2363 increasing fertilization on $\%N_{dfa}$ ($p < 0.001$; Table 5.5) was only observed in
2364 inoculated pots (Tukey: $p < 0.001$), with no apparent effect of fertilization on
2365 $\%N_{dfa}$ in uninoculated pots (Tukey: $p = 0.651$; Table 5.5; Fig. 5.5c).

Table 5.5. Effects of soil N availability, soil pH, species, and N_{area} on root nodule biomass and plant investments in symbiotic nitrogen fixation

	Root nodule biomass ^b			Root nodule: root biomass ^b			% N_{dfa}^b			
	df	Coefficient	χ^2	p	Coefficient	χ^2	p	Coefficient	χ^2	p
(Intercept)	-	9.41E-03	-	-	1.33E-02	-	-	7.48E-01	-	-
CO ₂	1	1.20E-01	19.258	<0.001	9.94E-02	0.087	0.768	-1.00E-01	0.518	0.472
Inoculation (I)	1	5.74E-01	755.020	<0.001	5.40E-01	903.691	<0.001	9.01E+00	955.570	<0.001
Fertilization (N)	1	7.71E-06	84.376	<0.001	-5.99E-06	258.099	<0.001	3.64E-04	292.938	<0.001
CO ₂ *I	1	-4.68E-02	0.950	0.330	-1.38E-01	20.614	<0.001	-1.44E-01	2.010	0.156
CO ₂ *N	1	-1.59E-04	2.106	0.147	-1.73E-04	1.773	0.183	-6.21E-05	2.716	0.099
I*N	1	-5.82E-04	44.622	<0.001	-7.45E-04	133.918	<0.001	-1.58E-02	231.290	<0.001
CO ₂ *I*N	1	7.26E-05	0.196	0.658	1.76E-04	2.359	0.125	2.77E-03	2.119	0.145

2366 *Significance determined using Type II Wald χ^2 tests ($\alpha = 0.05$). P-values < 0.05 are in bold, while p-values between
2367 0.05 and 0.1 are italicized. Superscript letters indicate model coefficients fit to square-root (^b) transformed data.
2368 Key: df = degrees of freedom % N_{dfa} = percent nitrogen fixed from the atmosphere.

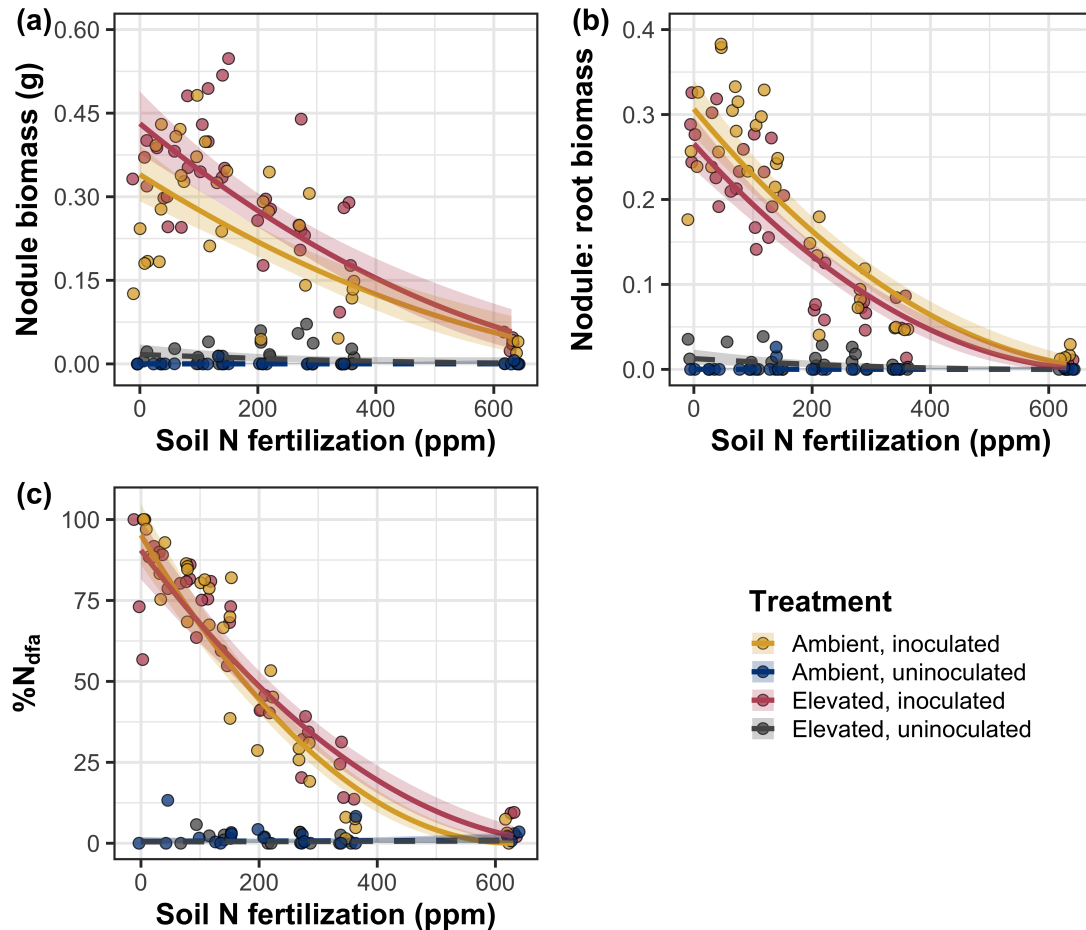


Figure 5.5. Effects of CO_2 , fertilization, and inoculation on nodule biomass (a), nodule: root biomass (b), and percent nitrogen fixed from the atmosphere (c). Soil nitrogen fertilization is represented on the x-axis. Yellow points and trendlines indicate inoculated individuals grown under ambient CO_2 , blue points and trendlines indicate uninoculated individuals grown under ambient CO_2 , red points and trendlines indicate inoculated individuals grown under elevated CO_2 , and grey points indicate uninoculated individuals grown under elevated CO_2 . Solid trendlines indicate slopes that are different from zero ($p < 0.05$), while dashed trendlines indicate slopes that are not different from zero ($p > 0.05$). Curvilinear trendlines occur as a result of back-transforming models where response variables received either a natural log or square root transformation prior to fitting.

2369 5.4 Discussion

2370 In this study, I determined leaf and whole plant acclimation responses of
2371 7-week *G. max* seedlings grown under two CO₂ concentrations, two inoculation
2372 treatments, and nine soil nitrogen fertilization treatments in a full-factorial growth
2373 chamber experiment. In support of my hypotheses and patterns expected from
2374 theory, elevated CO₂ reduced N_{area} , V_{cmax25} , and J_{max25} . The relatively stronger
2375 downregulation in V_{cmax25} than J_{max25} under elevated CO₂ resulted in a stimulation
2376 in $J_{\text{max25}}:V_{\text{cmax25}}$ under elevated CO₂. The downregulation of V_{cmax25} and J_{max25}
2377 under elevated CO₂ was similar across fertilization and inoculation treatments,
2378 indicating that the CO₂ responses were not due to nitrogen limitation. Interest-
2379 ingly, results indicate that elevated CO₂ increased the fraction of leaf nitrogen
2380 allocated to photosynthesis and structure, leading to a stimulation in nitrogen
2381 use efficiency under elevated CO₂ despite the apparent downregulation in N_{area} ,
2382 V_{cmax25} , and J_{max25} . The downregulation in leaf photosynthetic processes under
2383 elevated CO₂ also corresponded with a strong stimulation in total leaf area and to-
2384 tal biomass. Strong stimulations in whole plant growth due to elevated CO₂ were
2385 generally enhanced with increasing fertilization and were negatively related to
2386 structural carbon costs to acquire nitrogen. Inoculation generally did not modify
2387 whole plant responses to elevated CO₂ across the fertilization gradient, likely due
2388 to a strong reduction in root nodulation with increasing fertilization. However,
2389 strong positive effects of inoculation on whole plant growth were observed under
2390 low fertilization, consistent with our hypothesis. Overall, observed leaf and whole
2391 plant acclimation responses to CO₂ support hypotheses and patterns expected
2392 from photosynthetic least-cost theory, showing that leaf acclimation responses to

2393 CO₂ were decoupled from soil nitrogen availability and ability to acquire nitro-
2394 gen via symbiotic nitrogen fixation. Instead, leaf and whole plant acclimation
2395 responses to CO₂ were driven by optimal resource investment to photosynthetic
2396 capacity, where optimal resource investment at the leaf level maximized nitrogen
2397 allocation to structures that support whole plant growth.

2398 5.4.1 *Soil nitrogen fertilization has divergent effects on leaf and whole plant*
2399 *acclimation responses to CO₂*

2400 Elevated CO₂ reduced N_{area} , V_{cmax25} , J_{max25} , and stomatal conductance by
2401 29%, 16%, 10%, and 20%, respectively (Table 5.2). The larger downregulation in
2402 V_{cmax25} than J_{max25} led to an 8% stimulation in $J_{\text{max25}}:V_{\text{cmax25}}$ (Table 5.2), while
2403 the larger downregulation in N_{area} than V_{cmax25} resulted in a 21% stimulation
2404 in the fraction of leaf nitrogen allocated to photosynthesis under elevated CO₂.
2405 These acclimation responses are directionally consistent with previous studies that
2406 have investigated or reviewed leaf acclimation responses to CO₂ (Drake et al.
2407 1997; Makino et al. 1997; Ainsworth et al. 2002; Ainsworth and Long 2005;
2408 Ainsworth and Rogers 2007; Smith and Dukes 2013; Smith and Keenan 2020;
2409 Poorter et al. 2022), and follow patterns expected from photosynthetic least-cost
2410 theory (Wright et al. 2003; Prentice et al. 2014; Smith et al. 2019; Smith and
2411 Keenan 2020). Together, the stimulation in $J_{\text{max25}}:V_{\text{cmax25}}$ and the fraction of leaf
2412 nitrogen allocated to photosynthesis, and nitrogen use efficiency under elevated
2413 CO₂ provide strong support for the idea that leaves were downregulating V_{cmax25}
2414 in response to elevated CO₂ in order to optimally coordinate photosynthesis such
2415 that net photosynthesis rates approached becoming equally co-limited by Rubisco

2416 carboxylation and RuBP regeneration (Chen et al. 1993; Maire et al. 2012).

2417 Increasing fertilization and inoculation induced strong positive effects on
2418 N_{area} (Fig. 1a), $V_{\text{cmax}25}$ (Fig. 5.2a), $J_{\text{max}25}$ (Fig. 5.2b). The general positive
2419 response of N_{area} to increasing fertilization and in inoculated pots was enhanced
2420 under ambient CO₂, which, paired with the general downregulation in N_{area} un-
2421 der elevated CO₂, resulted in a stronger downregulation of N_{area} under elevated
2422 CO₂ with increasing fertilization and in inoculated pots (Fig. 5.1a). These pat-
2423 terns suggest that N_{area} responses to CO₂ were at least partially dependent on
2424 soil nitrogen fertilization and nitrogen acquisition strategy. However, the general
2425 stimulation in the fraction of leaf nitrogen allocated to Rubisco, bioenergetics,
2426 or photosynthesis under elevated CO₂ was not modified across the fertilization
2427 gradient and was only marginally enhanced in inoculated pots. These patterns
2428 suggest that the increased downregulation of Narea under elevated CO₂ with in-
2429 creasing fertilization was not associated with a change in relative investment to
2430 photosynthetic tissue. Instead, a stronger downregulation in the fraction of leaf
2431 nitrogen allocated to structure under ambient CO₂ resulted in a stronger stim-
2432 ulation in $\rho_{\text{structure}}$ under elevated CO₂ with increasing fertilization (Fig. 5.3b),
2433 indicating that fertilization shifted relative investment in leaf structural tissue un-
2434 der elevated CO₂. These results, combined with a stimulation in PNUE (Fig. SX)
2435 and iWUE (Fig. SX) under elevated CO₂ that was independent of fertilization
2436 or inoculation treatment, provide additional support for the hypothesis that leaf
2437 acclimation photosynthetic responses to CO₂ were independent of fertilization;
2438 though fertilization may contribute to changes in leaf morphology under elevated
2439 CO₂ through shifts in M_{area} (Onoda et al. 2017; Wang et al. 2017; Dong et al.

2440 2022).

2441 The downregulation in N_{area} , $V_{\text{cmax}25}$, and $J_{\text{max}25}$ under elevated CO₂ cor-
2442 responded with a respective 62% and 100% stimulation in total leaf area (Fig.
2443 5.4a) and total biomass (Fig. 5.4b). The stimulation in total leaf area and total
2444 biomass under elevated CO₂ also corresponded with generally higher structural
2445 carbon costs to acquire nitrogen (Fig. 5.4c), a pattern driven by a stimulation
2446 in belowground carbon biomass and reduction in whole plant nitrogen biomass.
2447 Alone, this result suggests that elevated CO₂ reduces plant nitrogen uptake effi-
2448 ciency, which does not explain why plants grown under elevated CO₂ generally had
2449 higher biomass and total leaf area. However, a strong negative effect of increasing
2450 fertilization on structural carbon costs to acquire nitrogen, which were generally
2451 similar between CO₂ concentrations, was driven by a stronger increase in whole
2452 plant nitrogen biomass than belowground carbon biomass. Thus, increases in the
2453 positive response of whole plant growth and total leaf area under elevated CO₂
2454 with increasing fertilization were likely driven by an increase in nitrogen uptake
2455 efficiency, allowing plants to satisfy any increase in whole plant nitrogen demand
2456 associated with increased CO₂.

2457 Interestingly, these results indicate that the general stimulation in total
2458 leaf area and whole plant growth under elevated CO₂ was not modified by inoc-
2459 ulation despite an apparent general negative effect of inoculation on N_{cost} . This
2460 response could have been due to strong negative effect of increasing fertilization on
2461 nodulation (Fig. 5.5), which may have caused the strong increase in the positive
2462 effect of elevated CO₂ on whole plant growth with increasing fertilization to mask
2463 any increase in the positive effect of elevated CO₂ on whole plant growth due to

2464 inoculation. Reductions in nodulation with increasing fertilization are commonly
2465 observed patterns that have been inferred to be a response that allows species
2466 optimize nitrogen uptake efficiency as costs to acquire nitrogen via direct uptake
2467 become more similar (Fig. 5.4c) (Gibson and Harper 1985; Rastetter et al. 2001).
2468 In this study, pairwise comparisons indicated strong positive effects of inocula-
2469 tion on total leaf area and total biomass (158% increase in total leaf area, 119%
2470 increase in total biomass) under elevated CO₂ at 0 ppm N, but no observable
2471 inoculation effect on total leaf area or total biomass under elevated CO₂ at 350
2472 ppm N or 630 ppm N. While these responses did not generally differ from those
2473 observed under ambient CO₂, they do confirm the hypothesis that positive effects
2474 of inoculation on whole plant growth responses to elevated CO₂ would decrease
2475 with increasing fertilization.

2476 Combined, results reported here suggest that soil nitrogen availability has
2477 a divergent role in modifying leaf and whole plant acclimation responses to CO₂.
2478 Leaf acclimation responses were generally decoupled from fertilization, while whole
2479 plant acclimation responses relied heavily on an increase in nitrogen uptake ef-
2480 ficiency and consequent reduction in costs of acquiring nitrogen associated with
2481 increasing fertilization. However, whole plant responses to CO₂ indicated that
2482 fertilization may play a more important role in determining whole plant acclima-
2483 tion responses to CO₂ than nitrogen acquisition strategy, although these patterns
2484 were likely driven by reductions in nodulation with increasing fertilization. These
2485 results suggest that plants acclimate to CO₂ in nitrogen-limited systems by mini-
2486 mizing the number of optimally coordinated leaves, and that the downregulation
2487 in leaf nitrogen content under elevated CO₂ is not a direct response to changes in

2488 soil nitrogen availability as previously implied.

2489 5.4.2 *Implications for future model development*

2490 Many terrestrial biosphere models predict photosynthetic capacity through
2491 plant functional group-specific linear regressions between N_{area} and V_{cmax} (Rogers
2492 2014; Rogers et al. 2017), which assumes that leaf nitrogen-photosynthesis rela-
2493 tionships are constant across growing environments. Our results build on previ-
2494 ous work suggesting that leaf nitrogen-photosynthesis relationships dynamically
2495 change across growing environments (Luo et al. 2021; Dong et al. 2022). Specif-
2496 ically, results from this experiment indicate that CO_2 concentration increased
2497 the fraction of leaf nitrogen content allocated to photosynthesis, while a general
2498 negative effect of increasing fertilization on the fraction of leaf nitrogen content
2499 allocated to photosynthesis was dependent on inoculation treatment. Similar in-
2500 creases in N_{area} , $V_{\text{cmax}25}$, and $J_{\text{max}25}$ with increasing fertilization resulted in no
2501 change in the fraction of leaf nitrogen allocated to photosynthesis in uninoculated
2502 pots, while larger increases in N_{area} than $V_{\text{cmax}25}$ and $J_{\text{max}25}$ with increasing fertil-
2503 ization decreased the fraction of leaf nitrogen allocated to photosynthesis in inoc-
2504 ulated pots (Fig. 5.3a). As inoculated pots were able to access less finite supply of
2505 nitrogen across the fertilization gradient, these patterns suggest that constant leaf
2506 nitrogen-photosynthesis relationships may only apply in environments where ni-
2507 trogen is limiting and will likely change with increasing CO_2 concentrations. Thus,
2508 terrestrial biosphere models that parameterize photosynthetic capacity through
2509 linear relationships between N_{area} and V_{cmax} (Rogers 2014; Rogers et al. 2017)
2510 may be overestimating photosynthetic capacity in systems where nitrogen is not

2511 as limiting and may contribute to erroneous model simulations under future CO₂
2512 concentrations.

2513 These results also demonstrate that optimal resource investment to photo-
2514 synthetic capacity defines leaf acclimation responses to elevated CO₂, and that
2515 these responses were independent of fertilization or inoculation treatment. Cur-
2516 rent approaches for simulating photosynthetic responses to CO₂ generally invoke
2517 patterns expected from progressive nitrogen limitation, where the downregulation
2518 in N_{area} , and therefore photosynthetic capacity, due to elevated CO₂ are com-
2519 monly a function of progressive reductions in soil nitrogen availability. Results
2520 reported here contradict this formulation, suggesting that the leaf acclimation re-
2521 sponse is driven by optimal resource investment to photosynthetic capacity and
2522 is independent of soil resource supply. Optimality models that leverage prin-
2523 ciples from optimal coordination and photosynthetic least-cost theories (Wang
2524 et al. 2017; Stocker et al. 2020; Scott and Smith 2022) are capable of capturing
2525 such acclimation responses to CO₂ (Smith and Keenan 2020), suggesting that the
2526 implementation of these models may improve the simulation of photosynthetic
2527 processes in terrestrial biosphere models under increasing CO₂ concentrations.

2528 5.4.3 *Study limitations and future directions*

2529 There are two study limitations that must be addressed to contextualize
2530 patterns observed in this study. First, restricting the volume of belowground
2531 substrate via a potted experiment does not adequately replicate belowground en-
2532 vironments of natural systems, and therefore may modify effects of soil resource
2533 availability and inoculation on plant nitrogen uptake, particularly if pot size limits

2534 whole plant growth (Poorter et al. 2012). I attempted to minimize the extent of
2535 pot size limitation experienced in the first experimental chapters while account-
2536 ing for the expected stimulation in whole plant growth under elevated CO₂ by
2537 using 6-liter pots. Despite attempts to minimize growth limitation imposed by
2538 pot volume, fertilization and CO₂ treatments increased the biomass: pot volume
2539 ratio such that all treatment combinations to exceed 1 g L⁻¹ biomass: pot volume
2540 under high fertilization. The 1 g L⁻¹ biomass: pot volume recommendation from
2541 Poorter et al. (2012) was designated to avoid growth limitation imposed by pot
2542 volume. However, if pot size limitation indeed limited whole plant growth, then
2543 structural carbon costs to acquire nitrogen, belowground carbon biomass, whole
2544 plant nitrogen biomass, and whole plant biomass should each exhibit strong sat-
2545 uration points with increasing fertilization, which was not observed here. Addi-
2546 tionally, a second set of photosynthetic measurements from one week prior to the
2547 harvest (6 weeks post-germination) revealed ... As pot limitation is expected
2548 to decrease net photosynthesis, and focal leaves were of similar ages between the
2549 sixth and seventh week, one might expect growth limitation induced by constricted
2550 pot volume to result in a dampened effect of inoculation and fertilization on net
2551 photosynthesis, V_{cmax} , and J_{max25} . Analyses from the sixth week of development
2552 revealed ... Additionally, analyses revealed a stronger/weaker downregulation in
2553 V_{cmax25} and J_{max25} on week 7, though disentangling the causality of this response
2554 (i.e. whether due to pot size limitation or simply a stronger acclimation response)
2555 would be difficult.

2556 Second, this study evaluated leaf and whole plant responses to CO₂ in 7-
2557 week seedlings. Given the long-term scale of the progressive nitrogen limitation

2558 hypothesis, patterns observed here should be validated in longer-term nitrogen
2559 manipulation experiments. Previous work in free air CO₂ enrichment experiments
2560 show some support for patterns expected from the progressive nitrogen limitation
2561 hypothesis (Reich et al. 2006; Norby et al. 2010), although results are not consis-
2562 tent across experimental sites (Finzi et al. 2006; Moore et al. 2006; Liang et al.
2563 2016). We found some support for patterns expected by the progressive nitrogen
2564 limitation hypothesis, namely an increase in plant nitrogen uptake under elevated
2565 CO₂ (Luo et al. 2004), though leaf acclimation responses to CO₂ were strongly
2566 indicative of optimal resource investment to photosynthetic capacity as expected
2567 from photosynthetic least-cost theory (Prentice et al. 2014; Smith et al. 2019;
2568 Smith and Keenan 2020).

2569 5.4.4 *Conclusions*

2570 This study provides strong evidence suggesting that leaf acclimation re-
2571 sponds to elevated CO₂ did not vary with soil nitrogen fertilization or ability
2572 to acquire nitrogen through symbiotic nitrogen fixation. However, whole plant
2573 acclimation responses to CO₂ were dependent on fertilization, where increasing
2574 fertilization increased the positive effect of whole plant growth under elevated
2575 CO₂. Results also indicate that fertilization played a relatively more important
2576 role in modifying whole plant responses to CO₂, perhaps due to a reduction in
2577 nodulation across the fertilization gradient. These patterns strongly support the
2578 hypothesis that leaf and whole plant acclimation responses are driven by opti-
2579 mal resource investment to photosynthetic capacity, and that leaf acclimation
2580 responses to CO₂ were not modified by changes in soil nitrogen availability. Ad-

2581 ditionally, strong interactions between fertilization and inoculation on leaf and
2582 whole plant traits indicated positive effects of fertilization on leaf and whole plant
2583 traits in uninoculated pots, but null effects of fertilization on leaf and whole plant
2584 traits in inoculated pots. These results build on previous work suggesting that
2585 constant leaf nitrogen-photosynthesis relationships are dynamic and change across
2586 growing environments, calling the use of constant relationships by terrestrial bio-
2587 sphere models into question.

2588

Chapter 6

2589

Conclusions

2590 The experiments included in this dissertation were designed to test mechanisms
2591 that drive patterns expected from photosynthetic least-cost theory across various
2592 edaphic and climatic gradients. Specifically, I evaluate the context dependency
2593 of carbon costs to acquire nitrogen across soil nitrogen availability and how vari-
2594 ance in carbon costs to acquire nitrogen scales to influence leaf and whole plant
2595 acclimation responses to changing environments.

2596 In the first experimental chapter, I quantified carbon costs to acquire ni-
2597 trogen in a species capable of forming associations with symbiotic nitrogen-fixing
2598 bacteria (*Glycine max*) and a species not capable of forming such associations
2599 (*Gossypium hirsutum*) grown under four soil nitrogen fertilization treatments and
2600 four light availability treatments in a full factorial greenhouse experiment. I found
2601 that increasing light availability increased carbon costs to acquire nitrogen in both
2602 species due to a larger increase in belowground carbon biomass than whole plant
2603 nitrogen biomass. These patterns were observed in both species. I also found
2604 that increasing fertilization decreased carbon costs to acquire nitrogen due to a
2605 larger increase in whole plant nitrogen biomass than belowground carbon biomass.
2606 While these patterns were observed in both species, carbon costs to acquire nitro-
2607 gen in *G. max* were less responsive to increasing fertilization than *G. hirsutum*,
2608 providing some support for my second hypothesis. Root nodulation data indicated
2609 that *G. max* shifted relative carbon allocation from nitrogen fixation to direct up-
2610 take with increasing fertilization, which may explain the reduced responsiveness

2611 of *G. max* carbon costs to acquire nitrogen across the fertilization gradient.

2612 Despite evidence that reductions in the response of *G. max* carbon costs
2613 to acquire nitrogen to increasing fertilization may have been driven by shifts away
2614 from nitrogen fixation with increasing fertilization, I urge caution in assigning
2615 causality to the differential response of carbon costs to acquire nitrogen between
2616 species. This is because *G. max* and *G. hirsutum* are not phylogenetically related
2617 and have different life histories. Specifically, *G. max* is a herbaceous annual species,
2618 while *G. hirsutum* is a woody perennial species. Differences in life history between
2619 the two species limit my ability to assess whether reductions in the negative effect
2620 of increasing fertilization on carbon costs to acquire nitrogen in *G. max* were
2621 driven by shifts to direct uptake with increasing fertilization. However, these
2622 patterns were later confirmed in the fourth experimental chapter, where I quantify
2623 similar weaker negative effects of increasing fertilization on carbon costs to acquire
2624 nitrogen in *G. max* that were inoculated with symbiotic nitrogen-fixing bacteria
2625 compared to *G. max* that were left uninoculated across a similar soil nitrogen
2626 fertilization gradient.

2627 In the second experimental chapter, I assessed whether changes in soil
2628 nitrogen availability or soil pH drove changes in nitrogen-water use tradeoffs pre-
2629 dicted by photosynthetic least-cost theory. I measured leaf traits of mature upper
2630 canopy deciduous trees growing in a nine-year nitrogen-by-sulfur field manipula-
2631 tion experiment, where experimental sulfur additions were added with intent to
2632 acidify plots. Following patterns expected from the theory, increasing soil nitrogen
2633 availability was associated with increased leaf nitrogen content, but not net pho-
2634 tosynthesis, resulting in an increase in photosynthetic nitrogen use efficiency. In

2635 further support of theory, increasing soil nitrogen availability exhibited slight, but
2636 nonsignificant, decreases in leaf $C_i:C_a$ and increases in measures of photosynthetic
2637 capacity. Perhaps the strongest evidence for the theory was a strong negative
2638 relationship between leaf nitrogen content and leaf $C_i:C_a$, of which increased with
2639 increasing soil nitrogen availability through a stronger increase in leaf nitrogen
2640 content than leaf $C_i:C_a$.

2641 I found no effect of soil pH on nitrogen-water use tradeoffs aside from a
2642 marginal reduction in net photosynthesis rates that marginally reduced photosyn-
2643 thetic nitrogen use efficiency with increasing soil pH. Directionally, reductions in
2644 photosynthetic nitrogen use efficiency with increasing soil pH were as expected per
2645 theory; however, this response was driven by no change in leaf nitrogen content
2646 and a reduction in net photosynthesis. Theory predicts that these tradeoffs should
2647 be driven by no change in net photosynthesis and an increase in leaf nitrogen con-
2648 tent. Regardless, the general null leaf response to changing soil pH may have
2649 been due to experimental treatments directly increased soil nitrogen availability
2650 and affected soil pH in opposite patterns, suggesting that soil nitrogen availability
2651 may be more important in dictating nitrogen-water use tradeoffs than soil pH per
2652 se.

2653 In the third experimental chapter, I quantified variance in leaf nitrogen
2654 content across a precipitation and soil resource availability gradient in Texan
2655 grasslands. Specifically, I measured area-based leaf nitrogen content, components
2656 of area-based leaf nitrogen content (leaf mass per unit leaf area, leaf nitrogen per
2657 unit dry biomass), leaf $C_i:C_a$, and the unit cost of acquiring nitrogen relative to
2658 water in 520 individuals comprising 57 species. I found that variance in area-

2659 based leaf nitrogen content was positively associated with increasing soil nitrogen
2660 availability, soil moisture, vapor pressure deficit, and was negatively related to
2661 increasing leaf $C_i:C_a$. Following patterns expected from theory, a path analysis
2662 revealed that the positive soil nitrogen-leaf nitrogen relationship was driven by a
2663 positive relationship between soil nitrogen availability and the unit cost of acquir-
2664 ing and using nitrogen relative to water, a positive relationship between the unit
2665 cost of acquiring and using nitrogen relative to water, and negative relationship
2666 between leaf $C_i:C_a$ and leaf mass per unit leaf area. Interestingly, there was no
2667 effect of $C_i:C_a$ on leaf nitrogen content per unit dry biomass, indicating that vari-
2668 ance in area-based leaf nitrogen content across the environmental gradient was
2669 driven by a change in leaf morphology and not leaf chemistry.

2670 In the fourth experimental chapter, I quantified leaf and whole plant accli-
2671 mation responses in *G. max* grown under two atmospheric CO₂ levels, with and
2672 without inoculation with *Bradyrhizobium japonicum*, and across nine nitrogen fer-
2673 tilization treatments in a full factorial growth chamber experiment. I found strong
2674 evidence that leaf nitrogen content, V_{cmax} , and J_{max} were each downregulated un-
2675 der elevated CO₂. A stronger downregulation in V_{cmax} than J_{max} and stronger
2676 downregulation in leaf nitrogen content than V_{cmax} or J_{max} provided strong sup-
2677 port suggesting that leaves were acclimating to elevated CO₂ by optimizing leaf
2678 photosynthetic resource use efficiency to achieve optimal coordination. In striking
2679 support of my hypotheses, I find strong evidence suggesting that leaf acclimation
2680 responses to elevated CO₂ were decoupled from soil nitrogen fertilization and in-
2681 oculation treatment, despite apparent strong increases in leaf nitrogen content,
2682 V_{cmax} , and J_{max} with increasing fertilization and in inoculated pots. These find-

2683 ings contrast the current formulation of photosynthetic processes in terrestrial
2684 biosphere models, where many models simulate downregulations in leaf nitrogen
2685 content under elevated CO₂ schemes as a function of progressive nitrogen limita-
2686 tion.

2687 There are currently two iterations of optimality models that employ the
2688 use of patterns expected from photosynthetic least-cost theory, one for C₃ species
2689 (Wang et al. 2017; Smith et al. 2019; Stocker et al. 2020) and one more recently
2690 developed for C₄ species (Scott and Smith 2022). In both model variants, costs to
2691 acquire and use nitrogen relative to water are held constant using a global dataset
2692 of δ¹³C (Cornwell et al. 2018). The C₃ optimality model initially assumed a
2693 constant cost to acquire and use nitrogen relative to water value of 240 (Wang et al.
2694 2017), later corrected to 146 (Stocker et al. 2020), while the C₄ optimality model
2695 assumes a constant value of 166 (Scott and Smith 2022). Throughout experiments,
2696 I show strong evidence suggesting that costs to acquire and use nitrogen are
2697 dynamic and vary predictably across environmental gradients, and that changes
2698 in these costs yield predictable changes in leaf nitrogen-water use tradeoffs and
2699 acclimation responses to changing environments. Thus, optimality models that
2700 hold unit costs of resource use constant may contribute to erroneous errors in
2701 model simulations. Future iterations of optimality models that leverage patterns
2702 expected from photosynthetic least-cost theory should consider development of
2703 explicit schemes for dynamically calculating costs to acquire and use nitrogen
2704 relative to water, or be coupled with previously established plant nitrogen uptake
2705 models (e.g., FUN) (Fisher et al. 2010; Brzostek et al. 2014; Allen et al. 2020).

2706 First principles of photosynthetic least-cost theory suggest that plants can

2707 optimize photosynthesis rates by sacrificing inefficient use of a relatively more
2708 abundant (and less costly to acquire) resource for more efficient use of a relatively
2709 less abundant (and more costly to acquire) resource. I show strong support for
2710 these patterns across experiments, where increasing soil nitrogen fertilization gen-
2711 erally decreased the cost of acquiring nitrogen relative to water, a pattern that
2712 scaled to influence leaf nitrogen-water use tradeoffs. These findings provide im-
2713 portant empirical validation of photosynthetic least-cost theory needed to further
2714 develop optimality models and eventually implement in terrestrial biosphere model
2715 products. Many current terrestrial biosphere model products do not include ro-
2716 bust frameworks for simulating acclimation responses to changing environmental
2717 conditions, and empirical findings shown here provide some support that optimal-
2718 ity models that leverage photosynthetic least-cost theory predictions may improve
2719 the ability of terrestrial biosphere models to accurately simulate photosynthetic
2720 processes. Future work should leverage data collected from these experiments,
2721 particularly the environmental gradient experiment across Texan grasslands, to
2722 conduct model-data comparisons to evaluate optimality model performance.

2723 Many terrestrial biosphere models predict photosynthetic capacity through
2724 plant functional group-specific linear regressions between area-based leaf nitrogen
2725 content and V_{cmax} (Rogers 2014; Rogers et al. 2017), which assumes that leaf
2726 nitrogen-photosynthesis relationships are constant across growing environments.
2727 I found constant leaf nitrogen-photosynthesis relationships with increasing soil ni-
2728 trogen availability in the nitrogen-by-sulfur field manipulation experiment. How-
2729 ever, results from the CO₂-by-nitrogen-by-inoculation manipulation experiment
2730 indicated that leaf nitrogen-photosynthesis responses to soil nitrogen availability

2731 were dependent on whether nitrogen was limiting. Specifically, similar increases in
2732 area-based leaf nitrogen content, $V_{\text{cmax}25}$, and $J_{\text{max}25}$ with increasing fertilization
2733 resulted in no change in the fraction of leaf nitrogen allocated to photosynthesis in
2734 uninoculated pots, while larger increases in area-based leaf nitrogen content than
2735 $V_{\text{cmax}25}$ and $J_{\text{max}25}$ with increasing fertilization decreased the fraction of leaf nitro-
2736 gen allocated to photosynthesis in inoculated pots. As inoculated pots were able
2737 to access less finite supply of nitrogen across the fertilization gradient, these pat-
2738 terns suggest that constant leaf nitrogen-photosynthesis relationships may only
2739 apply in environments where nitrogen is limiting. Further investigation is cer-
2740 tainly warranted regarding the effect of soil nitrogen availability in modifying leaf
2741 nitrogen-photosynthesis relationships, but findings from these experiments suggest
2742 that representing photosynthetic processes through positive relationships between
2743 soil nitrogen availability, leaf nitrogen, and photosynthetic capacity are likely con-
2744 tributing to erroneous errors in model simulations and may be an explanation for
2745 the high degree of divergence between carbon and nutrient flux simulations across
2746 terrestrial biosphere model products (Friedlingstein et al. 2014; Davies-Barnard
2747 et al. 2020).

2748 The experiments included in this dissertation have provided a strong foun-
2749 dation for me to continue growing as a plant physiological ecologist. I envision
2750 five primary avenues for future research that build on the work presented here,
2751 which are briefly summarized below:

2752 1. Manipulative and environmental gradient experiments included in this dis-
2753 sertation were designed to provide empirical data needed to test photosyn-
2754 thetic least-cost theory assumptions. While these results show promising

- 2755 patterns for patterns expected from photosynthetic least-cost theory, they
2756 do not necessarily address whether these patterns follow those simulated by
2757 optimality models that leverage photosynthetic least-cost principles. Thus,
2758 a clear future direction of this research could be to conduct model-data
2759 comparisons using data collected here (or similar experiments) to compare
2760 against optimality model simulations.
- 2761 2. Experiments included in this dissertation explicitly quantify effects of sym-
2762 biotic nitrogen fixation on carbon costs to acquire nitrogen, nitrogen-water
2763 use tradeoffs, and leaf nitrogen-photosynthesis relationships. However, car-
2764 bon costs to acquire nitrogen also vary in species that associate with dif-
2765 ferent mycorrhizal types (Brzostek et al. 2014; Terrer et al. 2018), and
2766 dominant mycorrhizal type in an ecosystem may dictate net biogeochemical
2767 cycle dynamics (Phillips et al. 2013). Thus, future work should consider
2768 conducting similar experiments while manipulating mycorrhizal association
2769 to comprehensively understand how microbial symbioses modify leaf and
2770 whole plant acclimation responses to changing environments. This avenue
2771 of research would be particularly useful in forested ecosystems, as previous
2772 work suggests that dominant mycorrhizal type in hardwood forests dictate
2773 net biogeochemical cycle dynamics
- 2774 3. Recent work indicates a high degree of variance in symbiotic nitrogen fixa-
2775 tion rates across terrestrial biosphere models (Davies-Barnard et al. 2020;
2776 Meyerholt et al. 2016), perhaps due to nitrogen fixation rates that are im-
2777 plemented across terrestrial biosphere models as a function of temperature
2778 (Houlton et al. 2008). While energetic costs of nitrogen fixation are cer-

2779 tainly temperature dependent, I show that structural costs of nitrogen fix-
2780 ation are driven by shifts in soil resource availability. The light-by-nitrogen
2781 greenhouse experiment was recently published in *Journal of Experimental*
2782 *Botany*, and a reviewer encouraged future work to include a model-data
2783 comparison comparing carbon costs to acquire nitrogen measured in the
2784 experiment to carbon costs to acquire nitrogen simulated by the FUN bio-
2785 geochemical model (Fisher et al. 2010; Brzostek et al. 2014; Allen et al.
2786 2020). Conveniently, FUN calculates carbon costs to acquire nitrogen follow-
2787 ing the same calculation used in the first and fourth experimental chapter,
2788 and doing this would be a useful next step toward understanding why ni-
2789 trogen fixation simulations in terrestrial biosphere models might deviate to
2790 such a large degree between products.

2791 4. Carbon costs to acquire nitrogen relative to water were quantified at the
2792 leaf level as a function of $\delta^{13}\text{C}$ and vapor pressure deficit, while structural
2793 carbon costs to acquire nitrogen were quantified at the whole plant level
2794 as the ratio of belowground carbon allocation per unit whole plant nitro-
2795 gen biomass. As increasing soil nitrogen availability decreases both leaf and
2796 whole plant estimates of costs to acquire and use nitrogen, one might expect
2797 leaf and whole plant carbon cost to acquire nitrogen estimates to covary. Fu-
2798 ture work should consider investigating if leaf and whole plant estimates of
2799 carbon costs to acquire nitrogen covary and evaluate whether environmental
2800 conditions (or species acquisition strategy) modifies any of this possible co-
2801 variance. Strong covariance between leaf and whole plant costs of nitrogen
2802 acquisition could be a possible avenue to implement frameworks for allowing

2803 costs of nitrogen acquisition to vary in optimality models, as the FUN model
2804 calculates carbon costs of nitrogen acquisition at the whole plant level.

2805 5. While experiments included in this dissertation target effects of soil nitrogen
2806 availability on carbon costs to acquire nitrogen and associated leaf nitrogen-
2807 water use tradeoffs, photosynthetic least-cost theory predicts that costs of
2808 nutrient use, not just nitrogen, relative to water are substitutable. Recent
2809 iterations of the FUN biogeochemical cycle includes the carbon and nitro-
2810 gen cost of acquiring and using phosphorus, which similarly varies in species
2811 with different nutrient acquisition strategies (Allen et al. 2020). The im-
2812 plementation of this model in a terrestrial biosphere model (E3SM) was
2813 recently shown to improve model performance of ecosystem nutrient lim-
2814 itation (Braghiere et al. 2022). As phosphorus commonly co-limits leaf
2815 photosynthesis and primary productivity, extending experiments reported
2816 here to investigate carbon and nitrogen costs of phosphorus use may be a
2817 useful next step in understanding extensions and limitations of photosyn-
2818 thetic least-cost theory.

2819 I conclude this dissertation with a brief word of thanks to all who have
2820 shaped me into the plant physiological ecologist that I am today. Specifically,
2821 I am thankful for the incredible mentorship of my advisor and committee chair,
2822 Dr. Nick Smith, who provided invaluable insight for each of these experimental
2823 chapters, and for my committee members for their helpful advise and support
2824 throughout these experiments. I am excited to continue growing as a plant phys-
2825 iological ecologist, look forward to continuing to understand nutrient acquisition
2826 and allocation responses to global change, and am excited to help mentor future

2827 generations of young researchers.

2828

References

- 2829 Abrams, M. D. and S. A. Mostoller (1995). Gas exchange, leaf structure and
2830 nitrogen in contrasting successional tree species growing in open and under-
2831 story sites during a drought. *Tree Physiology* 15(6), 361–370.
- 2832 Adams, M. A., T. L. Turnbull, J. I. Sprent, and N. Buchmann (2016). Legumes
2833 are different: Leaf nitrogen, photosynthesis, and water use efficiency. *Pro-
2834 ceedings of the National Academy of Sciences of the United States of Amer-
2835 ica* 113(15), 4098–4103.
- 2836 Ainsworth, E. A., P. A. Davey, C. J. Bernacchi, O. C. Dermody, E. A. Heaton,
2837 D. J. Moore, P. B. Morgan, S. L. Naidu, H. S. Y. Ra, X. G. Zhu, P. S. Curtis,
2838 and S. P. Long (2002). A meta-analysis of elevated [CO₂] effects on soybean
2839 (*Glycine max*) physiology, growth and yield. *Global Change Biology* 8(8),
2840 695–709.
- 2841 Ainsworth, E. A. and S. P. Long (2005). What have we learned from 15 years of
2842 free-air CO₂ enrichment (FACE)? A meta-analytic review of the responses
2843 of photosynthesis, canopy properties and plant production to rising CO₂.
2844 *New Phytologist* 165(2), 351–372.
- 2845 Ainsworth, E. A. and A. Rogers (2007). The response of photosynthesis and
2846 stomatal conductance to rising [CO₂]: mechanisms and environmental in-
2847 teractions. *Plant, Cell and Environment* 30(3), 258–270.
- 2848 Allen, K., J. B. Fisher, R. P. Phillips, J. S. Powers, and E. R. Brzostek (2020).
2849 Modeling the carbon cost of plant nitrogen and phosphorus uptake across
2850 temperate and tropical forests. *Frontiers in Forests and Global Change* 3,

- 2851 1–12.
- 2852 Allison, S. D., C. I. Czimczik, and K. K. Treseder (2008). Microbial activity
2853 and soil respiration under nitrogen addition in Alaskan boreal forest. *Global
2854 Change Biology* 14(5), 1156–1168.
- 2855 Andersen, M. K., H. Hauggaard-Nielsen, P. Ambus, and E. S. Jensen (2005).
2856 Biomass production, symbiotic nitrogen fixation and inorganic N use in dual
2857 and tri-component annual intercrops. *Plant and Soil* 266(1-2), 273–287.
- 2858 Andrews, M., E. K. James, J. I. Sprent, R. M. Boddey, E. Gross, and F. B. dos
2859 Reis (2011). Nitrogen fixation in legumes and actinorhizal plants in natural
2860 ecosystems: Values obtained using ^{15}N natural abundance. *Plant Ecology
2861 and Diversity* 4(2-3), 117–130.
- 2862 Arndal, M. F., A. Tolver, K. S. Larsen, C. Beier, and I. K. Schmidt (2018). Fine
2863 root growth and vertical distribution in response to elevated CO₂, warming
2864 and drought in a mixed heathland–grassland. *Ecosystems* 21(1), 15–30.
- 2865 Arnone, J. A. (1997). Indices of plant N availability in an alpine grassland under
2866 elevated atmospheric CO₂. *Plant and Soil* 190(1), 61–66.
- 2867 Arora, V. K., A. Katavouta, R. G. Williams, C. D. Jones, V. Brovkin,
2868 P. Friedlingstein, J. Schwinger, L. Bopp, O. Boucher, P. Cadule, M. A.
2869 Chamberlain, J. R. Christian, C. Delire, R. A. Fisher, T. Hajima, T. Ilyina,
2870 E. Joetzjer, M. Kawamiya, C. D. Koven, J. P. Krasting, R. M. Law, D. M.
2871 Lawrence, A. Lenton, K. Lindsay, J. Pongratz, T. Raddatz, R. Séférian,
2872 K. Tachiiri, J. F. Tjiputra, A. Wiltshire, T. Wu, and T. Ziehn (2020).
2873 Carbon-concentration and carbon-climate feedbacks in CMIP6 models and
2874 their comparison to CMIP5 models. *Biogeosciences* 17(16), 4173–4222.

- 2875 Bae, K., T. J. Fahey, R. D. Yanai, and M. Fisk (2015). Soil nitrogen availability affects belowground carbon allocation and soil respiration in northern
2876 hardwood forests of New Hampshire. *Ecosystems* 18(7), 1179–1191.
- 2877
- 2878 Barber, S. A. (1962). A diffusion and mass-flow concept of soil nutrient availability. *Soil Science* 93(1), 39–49.
- 2879
- 2880 Barnes, J. D., L. Balaguer, E. Manrique, S. Elvira, and A. W. Davison (1992).
2881 A reappraisal of the use of DMSO for the extraction and determination
2882 of chlorophylls a and b in lichens and higher plants. *Environmental and
2883 Experimental Botany* 32(2), 85–100.
- 2884 Bates, D., M. Mächler, B. Bolker, and S. Walker (2015). Fitting linear mixed-
2885 effects models using lme4. *Journal of Statistical Software* 67(1), 1–48.
- 2886 Beaudette, D., J. Skovlin, S. Roeker, and A. Brown (2022). soilDB: Soil
2887 Database Interface.
- 2888 Bengtson, P., J. Barker, and S. J. Grayston (2012). Evidence of a strong cou-
2889 pling between root exudation, C and N availability, and stimulated SOM
2890 decomposition caused by rhizosphere priming effects. *Ecology and Evolu-
2891 tion* 2(8), 1843–1852.
- 2892 Bernacchi, C. J., E. L. Singsaas, C. Pimentel, A. R. Portis, and S. P. Long
2893 (2001). Improved temperature response functions for models of Rubisco-
2894 limited photosynthesis. *Plant, Cell and Environment* 24(2), 253–259.
- 2895 Bialic-Murphy, L., N. G. Smith, P. Voothuluru, R. M. McElderry, M. D.
2896 Roche, S. T. Cassidy, S. N. Kivlin, and S. Kalisz (2021). Invasion-induced
2897 root–fungal disruptions alter plant water and nitrogen economies. *Ecology*

- 2898 *Letters* 24(6), 1145–1156.
- 2899 Bloom, A. J., F. S. Chapin, and H. A. Mooney (1985). Resource limitation
2900 in plants - an economic analogy. *Annual Review of Ecology and Systemat-*
2901 *ics* 16(1), 363–392.
- 2902 Bloomfield, K. J., B. D. Stocker, T. F. Keenan, and I. C. Prentice (2023).
2903 Environmental controls on the light use efficiency of terrestrial gross primary
2904 production. *Global Change Biology* 29(4), 0–2.
- 2905 Bonan, G. B., M. D. Hartman, W. J. Parton, and W. R. Wieder (2013). Eval-
2906 uating litter decomposition in earth system models with long-term litter
2907 bag experiments: an example using the Community Land Model version 4
2908 (CLM4). *Global Change Biology* 19(3), 957–974.
- 2909 Bonan, G. B., P. J. Lawrence, K. W. Oleson, S. Levis, M. Jung, M. Reich-
2910 stein, D. M. Lawrence, and S. C. Swenson (2011). Improving canopy pro-
2911 cesses in the Community Land Model version 4 (CLM4) using global flux
2912 fields empirically inferred from FLUXNET data. *Journal of Geophysical Re-*
2913 *search* 116(G2), G02014.
- 2914 Booth, B. B. B., C. D. Jones, M. Collins, I. J. Totterdell, P. M. Cox, S. Sitch,
2915 C. Huntingford, R. A. Betts, G. R. Harris, and J. Lloyd (2012). High sen-
2916 sitivity of future global warming to land carbon cycle processes. *Environ-*
2917 *mental Research Letters* 7(2), 024002.
- 2918 Borer, E. T., W. S. Harpole, P. B. Adler, E. M. Lind, J. L. Orrock, E. W.
2919 Seabloom, and M. D. Smith (2014). Finding generality in ecology: A model
2920 for globally distributed experiments. *Methods in Ecology and Evolution* 5(1),
2921 65–73.

- 2922** Braghieri, R. K., J. B. Fisher, K. Allen, E. Brzostek, M. Shi, X. Yang, D. M.
- 2923** Ricciuto, R. A. Fisher, Q. Zhu, and R. P. Phillips (2022). Modeling global
- 2924** carbon costs of plant nitrogen and phosphorus acquisition. *Journal of Ad-*
- 2925** *vances in Modeling Earth Systems* 14(8), 1–23.
- 2926** Brix, H. (1971). Effects of nitrogen fertilization on photosynthesis and respi-
- 2927** ration in Douglas-fir. *Forest Science* 17(4), 407–414.
- 2928** Brzostek, E. R., J. B. Fisher, and R. P. Phillips (2014). Modeling the carbon
- 2929** cost of plant nitrogen acquisition: Mycorrhizal trade-offs and multipath
- 2930** resistance uptake improve predictions of retranslocation. *Journal of Geo-*
- 2931** *physical Research: Biogeosciences* 119, 1684–1697.
- 2932** Bubier, J. L., R. Smith, S. Juutinen, T. R. Moore, R. Minocha, S. Long, and
- 2933** S. Minocha (2011). Effects of nutrient addition on leaf chemistry, morphol-
- 2934** ogy, and photosynthetic capacity of three bog shrubs. *Oecologia* 167(2),
- 2935** 355–368.
- 2936** Cernusak, L. A., N. Ubierna, K. Winter, J. A. M. Holtum, J. D. Marshall, and
- 2937** G. D. Farquhar (2013). Environmental and physiological determinants of
- 2938** carbon isotope discrimination in terrestrial plants. *New Phytologist* 200(4),
- 2939** 950–965.
- 2940** Chen, J.-L., J. F. Reynolds, P. C. Harley, and J. D. Tenhunen (1993). Coor-
- 2941** dination theory of leaf nitrogen distribution in a canopy. *Oecologia* 93(1),
- 2942** 63–69.
- 2943** Clark, D. B., L. M. Mercado, S. Sitch, C. D. Jones, N. Gedney, M. J. Best,
- 2944** M. Pryor, G. G. Rooney, R. L. H. Essery, E. Blyth, O. Boucher, R. J.
- 2945** Harding, C. Huntingford, and P. M. Cox (2011). The Joint UK Land Envi-

- 2946 ronment Simulator (JULES), model description. Part 2: Carbon fluxes and
2947 vegetation dynamics. *Geoscientific Model Development* 4(3), 701–722.
- 2948 Cornwell, W. K., J. H. C. Cornelissen, K. Amatangelo, E. Dorrepaal, V. T.
2949 Eviner, O. Godoy, S. E. Hobbie, B. Hoorens, H. Kurokawa, N. Pérez-
2950 Harguindeguy, H. M. Quested, L. S. Santiago, D. A. Wardle, I. J. Wright,
2951 R. Aerts, S. D. Allison, P. van Bodegom, V. Brovkin, A. Chatain, T. V.
2952 Callaghan, S. Díaz, E. Garnier, D. E. Gurvich, E. Kazakou, J. A. Klein,
2953 J. Read, P. B. Reich, N. A. Soudzilovskaia, M. V. Vaieretti, and M. Westoby
2954 (2008). Plant species traits are the predominant control on litter decompo-
2955 sition rates within biomes worldwide. *Ecology Letters* 11(10), 1065–1071.
- 2956 Cornwell, W. K., I. J. Wright, J. Turner, V. Maire, M. M. Barbour, L. A.
2957 Cernusak, T. E. Dawson, D. S. Ellsworth, G. D. Farquhar, H. Griffiths,
2958 C. Keitel, A. Knohl, P. B. Reich, D. G. Williams, R. Bhaskar, J. H. C. Cor-
2959 nelissen, A. Richards, S. Schmidt, F. Valladares, C. Körner, E.-D. Schulze,
2960 N. Buchmann, and L. S. Santiago (2018). Climate and soils together regulate
2961 photosynthetic carbon isotope discrimination within C₃ plants worldwide.
2962 *Global Ecology and Biogeography* 27(9), 1056–1067.
- 2963 Cramer, W. and I. C. Prentice (1988). Simulation of regional soil moisture
2964 deficits on a European scale. *Norsk Geografisk Tidsskrift - Norwegian Jour-*
2965 *nal of Geography* 42(2-3), 149–151.
- 2966 Curtis, P. S. (1996). A meta-analysis of leaf gas exchange and nitrogen in trees
2967 grown under elevated carbon dioxide. *Plant, Cell and Environment* 19(2),
2968 127–137.
- 2969 Daly, C., M. Halbleib, J. I. Smith, W. P. Gibson, M. K. Doggett, G. H. Taylor,

- 2970** J. Curtis, and P. P. Pasteris (2008). Physiographically sensitive mapping
2971 of climatological temperature and precipitation across the conterminous
2972 United States. *International Journal of Climatology* 28(15), 2031–2064.
- 2973** Davies-Barnard, T., J. Meyerholt, S. Zaehle, P. Friedlingstein, V. Brovkin,
2974 Y. Fan, R. A. Fisher, C. D. Jones, H. Lee, D. Peano, B. Smith, D. Wårlind,
2975 and A. J. Wiltshire (2020). Nitrogen cycling in CMIP6 land surface models:
2976 progress and limitations. *Biogeosciences* 17(20), 5129–5148.
- 2977** Davis, T. W., I. C. Prentice, B. D. Stocker, R. T. Thomas, R. J. Whitley,
2978 H. Wang, B. J. Evans, A. V. Gallego-Sala, M. T. Sykes, and W. Cramer
2979 (2017). Simple process-led algorithms for simulating habitats (SPLASH
2980 v.1.0): robust indices of radiation, evapotranspiration and plant-available
2981 moisture. *Geoscientific Model Development* 10, 689–708.
- 2982** Delaire, M., E. Frak, M. Sigogne, B. Adam, F. Beaujard, and X. Le Roux
2983 (2005). Sudden increase in atmospheric CO₂ concentration reveals strong
2984 coupling between shoot carbon uptake and root nutrient uptake in young
2985 walnut trees. *Tree Physiology* 25(2), 229–235.
- 2986** Doane, T. A. and W. R. Horwáth (2003). Spectrophotometric determination of
2987 nitrate with a single reagent. *Analytical Letters* 36(12), 2713–2722.
- 2988** Dong, N., I. C. Prentice, B. J. Evans, S. Caddy-Retalic, A. J. Lowe, and I. J.
2989 Wright (2017). Leaf nitrogen from first principles: field evidence for adaptive
2990 variation with climate. *Biogeosciences* 14(2), 481–495.
- 2991** Dong, N., I. C. Prentice, I. J. Wright, B. J. Evans, H. F. Togashi, S. Caddy-
2992 Retalic, F. A. McInerney, B. Sparrow, E. Leitch, and A. J. Lowe (2020).
2993 Components of leaf-trait variation along environmental gradients. *New Phy-*

- 2994** *tologist* 228(1), 82–94.
- 2995** Dong, N., I. C. Prentice, I. J. Wright, H. Wang, O. K. Atkin, K. J. Bloomfield,
- 2996** T. F. Domingues, S. M. Gleason, V. Maire, Y. Onoda, H. Poorter, and N. G.
- 2997** Smith (2022). Leaf nitrogen from the perspective of optimal plant function.
- 2998** *Journal of Ecology* 110(11), 2585–2602.
- 2999** Dong, N., I. J. Wright, J. M. Chen, X. Luo, H. Wang, T. F. Keenan, N. G.
- 3000** Smith, and I. C. Prentice (2022). Rising CO₂ and warming reduce global
- 3001** canopy demand for nitrogen. *New Phytologist* 235(5), 1692–1700.
- 3002** Dovrat, G., H. Bakhshian, T. Masci, and E. Sheffer (2020). The nitrogen eco-
- 3003** nomic spectrum of legume stoichiometry and fixation strategy. *New Phytol-*
- 3004** *ogist* 227(2), 365–375.
- 3005** Dovrat, G., T. Masci, H. Bakhshian, E. Mayzlish Gati, S. Golan, and E. Shef-
- 3006** fer (2018). Drought-adapted plants dramatically downregulate dinitrogen
- 3007** fixation: Evidences from Mediterranean legume shrubs. *Journal of Ecol-*
- 3008** *ogy* 106(4), 1534–1544.
- 3009** Drake, B. G., M. A. Gonzàlez-Meler, and S. P. Long (1997). More efficient
- 3010** plants: a consequence of rising atmospheric CO₂? *Annual Review of Plant*
- 3011** *Biology* 48, 609–639.
- 3012** Duursma, R. A. (2015). Plantecophys - An R package for analyzing and mod-
- 3013** elling leaf gas exchange data. *PLOS ONE* 10(11), e0143346.
- 3014** Eastman, B. A., M. B. Adams, E. R. Brzostek, M. B. Burnham, J. E. Carrara,
- 3015** C. Kelly, B. E. McNeil, C. A. Walter, and W. T. Peterjohn (2021). Altered
- 3016** plant carbon partitioning enhanced forest ecosystem carbon storage after 25

- 3017** years of nitrogen additions. *New Phytologist* 230(4), 1435–1448.
- 3018** Ellsworth, D. S. and P. B. Reich (1996). Photosynthesis and leaf nitrogen in five
- 3019** Amazonian tree species during early secondary succession. *Ecology* 77(2),
- 3020** 581–594.
- 3021** Espelta, J. M., P. Cortés, M. Mangirón, and J. Retana (2005). Differences
- 3022** in biomass partitioning, leaf nitrogen content, and water use efficiency δ^{13}
- 3023** result in similar performance of seedlings of two Mediterranean oaks with
- 3024** contrasting leaf habit. *Ecoscience* 12(4), 447–454.
- 3025** Evans, J. R. (1989). Photosynthesis and nitrogen relationships in leaves of C₃
- 3026** plants. *Oecologia* 78(1), 9–19.
- 3027** Evans, J. R. and V. C. Clarke (2019). The nitrogen cost of photosynthesis.
- 3028** *Journal of Experimental Botany* 70(1), 7–15.
- 3029** Evans, J. R. and H. Poorter (2001). Photosynthetic acclimation of plants to
- 3030** growth irradiance: the relative importance of specific leaf area and nitrogen
- 3031** partitioning in maximizing carbon gain. *Plant, Cell and Environment* 24(8),
- 3032** 755–767.
- 3033** Evans, J. R. and J. R. Seemann (1989). The allocation of protein nitrogen in
- 3034** the photosynthetic apparatus: costs, consequences, and control. *Photosyn-*
- 3035** *thesis* 8, 183–205.
- 3036** Exbrayat, J.-F., A. A. Bloom, P. Falloon, A. Ito, T. L. Smallman, and
- 3037** M. Williams (2018). Reliability ensemble averaging of 21st century projec-
- 3038** tions of terrestrial net primary productivity reduces global and regional
- 3039** uncertainties. *Earth System Dynamics* 9(1), 153–165.

- 3040** Farquhar, G. D., J. R. Ehleringer, and K. T. Hubick (1989). Carbon isotope
3041 discrimination and photosynthesis. *Annual Review of Plant Physiology and*
3042 *Plant Molecular Biology* 40(1), 503–537.
- 3043** Farquhar, G. D. and T. D. Sharkey (1982). Stomatal conductance and photo-
3044 synthesis. *Annual Review of Plant Physiology* 33(1), 317–345.
- 3045** Farquhar, G. D., S. von Caemmerer, and J. A. Berry (1980). A biochemical
3046 model of photosynthetic CO₂ assimilation in leaves of C₃ species.
3047 *Planta* 149(1), 78–90.
- 3048** Fay, P. A., S. M. Prober, W. S. Harpole, J. M. H. Knops, J. D. Bakker, E. T.
3049 Borer, E. M. Lind, A. S. MacDougall, E. W. Seabloom, P. D. Wragg, P. B.
3050 Adler, D. M. Blumenthal, Y. M. Buckley, C. Chu, E. E. Cleland, S. L.
3051 Collins, K. F. Davies, G. Du, X. Feng, J. Firn, D. S. Gruner, N. Hagenah,
3052 Y. Hautier, R. W. Heckman, V. L. Jin, K. P. Kirkman, J. A. Klein, L. M.
3053 Ladwig, Q. Li, R. L. McCulley, B. A. Melbourne, C. E. Mitchell, J. L. Moore,
3054 J. W. Morgan, A. C. Risch, M. Schütz, C. J. Stevens, D. A. Wedin, and
3055 L. H. Yang (2015). Grassland productivity limited by multiple nutrients.
3056 *Nature Plants* 1(7), 15080.
- 3057** Feng, X. (1999). Trends in intrinsic water-use efficiency of natural trees for the
3058 past 100-200 years: A response to atmospheric CO₂ concentration. *Geochim-
3059* *ica et Cosmochimica Acta* 63(13-14), 1891–1903.
- 3060** Field, C. B. and H. A. Mooney (1986). The photosynthesis-nitrogen relationship
3061 in wild plants. In T. J. Givnish (Ed.), *On the Economy of Plant Form and*
3062 *Function*, pp. 25–55. Cambridge: Cambridge University Press.
- 3063** Finzi, A. C., D. J. P. Moore, E. H. DeLucia, J. Lichter, K. S. Hofmockel, R. B.

- 3064 Jackson, H. S. Kim, R. Matamala, H. R. McCarthy, R. Oren, J. S. Pippen,
3065 and W. H. Schlesinger (2006). Progressive nitrogen limitation of ecosystem
3066 processes under elevated CO₂ in a warm-temperate forest. *Ecology* 87(1),
3067 15–25.
- 3068 Firn, J., J. M. McGree, E. Harvey, H. Flores Moreno, M. Schutz, Y. M. Buckley,
3069 E. T. Borer, E. W. Seabloom, K. J. La Pierre, A. M. MacDougall, S. M.
3070 Prober, C. J. Stevens, L. L. Sullivan, E. Porter, E. Ladouceur, C. Allen,
3071 K. H. Moromizato, J. W. Morgan, W. S. Harpole, Y. Hautier, N. Eisen-
3072 hauer, J. P. Wright, P. B. Adler, C. A. Arnillas, J. D. Bakker, L. Biederman,
3073 A. A. D. Broadbent, C. S. Brown, M. N. Bugalho, M. C. Caldeira, E. E. Cle-
3074 land, A. Ebeling, P. A. Fay, N. Hagenah, A. R. Kleinhesselink, R. Mitchell,
3075 J. L. Moore, C. Nogueira, P. L. Peri, C. Roscher, M. D. Smith, P. D. Wragg,
3076 and A. C. Risch (2019). Leaf nutrients, not specific leaf area, are consistent
3077 indicators of elevated nutrient inputs. *Nature Ecology and Evolution* 3(3),
3078 400–406.
- 3079 Fisher, J. B., S. Sitch, Y. Malhi, R. A. Fisher, C. Huntingford, and S.-Y. Tan
3080 (2010). Carbon cost of plant nitrogen acquisition: A mechanistic, globally
3081 applicable model of plant nitrogen uptake, retranslocation, and fixation.
3082 *Global Biogeochemical Cycles* 24(1), 1–17.
- 3083 Fox, J. and S. Weisberg (2019). *An R companion to applied regression* (Third
3084 edit ed.). Thousand Oaks, California: Sage.
- 3085 Franklin, O., R. E. McMurtrie, C. M. Iversen, K. Y. Crous, A. C. Finzi, D. Tis-
3086 sue, D. S. Ellsworth, R. Oren, and R. J. Norby (2009). Forest fine-root
3087 production and nitrogen use under elevated CO₂: contrasting responses

- 3088** in evergreen and deciduous trees explained by a common principle. *Global
3089 Change Biology* 15(1), 132–144.
- 3090** Friedlingstein, P., M. Meinshausen, V. K. Arora, C. D. Jones, A. Anav, S. K.
3091 Liddicoat, and R. Knutti (2014). Uncertainties in CMIP5 climate projections
3092 due to carbon cycle feedbacks. *Journal of Climate* 27(2), 511–526.
- 3093** Friel, C. A. and M. L. Friesen (2019). Legumes modulate allocation to rhizobial
3094 nitrogen fixation in response to factorial light and nitrogen manipulation.
3095 *Frontiers in Plant Science* 10, 1316.
- 3096** Fujikake, H., A. Yamazaki, N. Ohtake, K. Sueoshi, S. Matsuhashi, T. Ito,
3097 C. Mizuniwa, T. Kume, S. Hoshimoto, N.-S. Ishioka, S. Watanabe, A. Osa,
3098 T. Sekine, H. Uchida, A. Tsuji, and T. Ohyama (2003). Quick and reversible
3099 inhibition of soybean root nodule growth by nitrate involves a decrease in
3100 sucrose supply to nodules. *Journal of Experimental Botany* 54(386), 1379–
3101 1388.
- 3102** Ghannoum, O., J. R. Evans, and S. von Caemmerer (2011). Nitrogen and water
3103 use efficiency of C₄ plants. In A. S. Raghavendra and R. F. Sage (Eds.), *C₄
3104 Photosynthesis and Related CO₂ Concentrating Mechanisms*, Chapter 8, pp.
3105 129–146. Springer.
- 3106** Ghimire, B., W. J. Riley, C. D. Koven, J. Kattge, A. Rogers, P. B. Reich, and
3107 I. J. Wright (2017). A global trait-based approach to estimate leaf nitrogen
3108 functional allocation from observations:. *Ecological Applications* 27(5),
3109 1421–1434.
- 3110** Giardina, C. P., M. D. Coleman, J. E. Hancock, J. S. King, E. A. Lilleskov,
3111 W. M. Loya, K. S. Pregitzer, M. G. Ryan, and C. C. Trettin (2005). The

- 3112** response of belowground carbon allocation in forests to global change. In
3113 D. Binkley and O. Manyailo (Eds.), *Tree Species Effects on Soils: Implica-*
3114 *tions for Global Change* (Volume 55 ed.), Chapter Chapter 7, pp. 119–154.
3115 Berlin/Heidelberg: Springer-Verlag.
- 3116** Gibson, A. H. and J. E. Harper (1985). Nitrate effect on nodulation of soybean
3117 by *Bradyrhizobium japonicum*. *Crop Science* 25(3), 497–501.
- 3118** Gill, A. L. and A. C. Finzi (2016). Belowground carbon flux links biogeochemical
3119 cycles and resource-use efficiency at the global scale. *Ecology Letters* 19(12),
3120 1419–1428.
- 3121** Goll, D. S., V. Brovkin, B. R. Parida, C. H. Reick, J. Kattge, P. B. Reich, P. M.
3122 van Bodegom, and Ü. Niinemets (2012). Nutrient limitation reduces land
3123 carbon uptake in simulations with a model of combined carbon, nitrogen
3124 and phosphorus cycling. *Biogeosciences Discussions* 9(3), 3173–3232.
- 3125** Gregory, L. M., A. M. McClain, D. M. Kramer, J. D. Pardo, K. E. Smith, O. L.
3126 Tessmer, B. J. Walker, L. G. Ziccardi, and T. D. Sharkey (2021, oct). The
3127 triose phosphate utilization limitation of photosynthetic rate: Out of global
3128 models but important for leaf models. *Plant, Cell and Environment* 44(10),
3129 3223–3226.
- 3130** Grossiord, C., T. N. Buckley, L. A. Cernusak, K. A. Novick, B. Poulter, R. T. W.
3131 Siegwolf, J. S. Sperry, and N. G. McDowell (2020). Plant responses to rising
3132 vapor pressure deficit. *New Phytologist* 226(6), 1550–1566.
- 3133** Gulmon, S. L. and C. C. Chu (1981). The effects of light and nitrogen on pho-
3134 tosynthesis, leaf characteristics, and dry matter allocation in the chaparral
3135 shrub, *Diplacus aurantiacus*. *Oecologia* 49(2), 207–212.

- 3136** Gutschick, V. P. (1981). Evolved strategies in nitrogen acquisition by plants.
- 3137** *The American Naturalist* 118(5), 607–637.
- 3138** Hallik, L., Ü. Niinemets, and I. J. Wright (2009). Are species shade and drought
- 3139** tolerance reflected in leaf-level structural and functional differentiation in
- 3140** Northern Hemisphere temperate woody flora? *New Phytologist* 184(1), 257–
- 3141** 274.
- 3142** Harrison, M. T., E. J. Edwards, G. D. Farquhar, A. B. Nicotra, and J. R.
- 3143** Evans (2009). Nitrogen in cell walls of sclerophyllous leaves accounts for
- 3144** little of the variation in photosynthetic nitrogen-use efficiency. *Plant, Cell*
- 3145** and *Environment* 32(3), 259–270.
- 3146** Harrison, S. P., W. Cramer, O. Franklin, I. C. Prentice, H. Wang,
- 3147** Å. Bränström, H. de Boer, U. Dieckmann, J. Joshi, T. F. Keenan,
- 3148** A. Lavergne, S. Manzoni, G. Mengoli, C. Morfopoulos, J. Peñuelas,
- 3149** S. Pietsch, K. T. Rebel, Y. Ryu, N. G. Smith, B. D. Stocker, and I. J.
- 3150** Wright (2021). Eco-evolutionary optimality as a means to improve vegeta-
- 3151** tion and land-surface models. *New Phytologist* 231(6), 2125–2141.
- 3152** Henneron, L., P. Kardol, D. A. Wardle, C. Cros, and S. Fontaine (2020). Rhizo-
- 3153** sphere control of soil nitrogen cycling: a key component of plant economic
- 3154** strategies. *New Phytologist* 228(4), 1269–1282.
- 3155** Hijmans, R. J. (2022). terra: Spatial Data Analysis.
- 3156** Hikosaka, K. and A. Shigeno (2009). The role of Rubisco and cell walls in the
- 3157** interspecific variation in photosynthetic capacity. *Oecologia* 160(3), 443–
- 3158** 451.

- 3159** Hoagland, D. R. and D. I. Arnon (1950). The water culture method for growing
3160 plants without soil. *California Agricultural Experiment Station: 347* 347(2),
3161 1–32.
- 3162** Hobbie, E. A. (2006). Carbon allocation to ectomycorrhizal fungi correlates
3163 with belowground allocation in culture studies. *Ecology* 87(3), 563–569.
- 3164** Hobbie, E. A. and J. E. Hobbie (2008). Natural abundance of ^{15}N in nitrogen-
3165 limited forests and tundra can estimate nitrogen cycling through mycorrhizal
3166 fungi: a review. *Ecosystems* 11(5), 815–830.
- 3167** Hoek, T. A., K. Axelrod, T. Biancalani, E. A. Yurtsev, J. Liu, and J. Gore
3168 (2016). Resource availability modulates the cooperative and competitive na-
3169 ture of a microbial cross-feeding mutualism. *PLOS Biology* 14(8), e1002540.
- 3170** Höglberg, M. N., M. J. I. Briones, S. G. Keel, D. B. Metcalfe, C. Campbell, A. J.
3171 Midwood, B. Thornton, V. Hurry, S. Linder, T. Näsholm, and P. Höglberg
3172 (2010). Quantification of effects of season and nitrogen supply on tree below-
3173 ground carbon transfer to ectomycorrhizal fungi and other soil organisms in
3174 a boreal pine forest. *New Phytologist* 187(2), 485–493.
- 3175** Höglberg, P., M. N. Höglberg, S. G. Göttlicher, N. R. Betson, S. G. Keel, D. B.
3176 Metcalfe, C. Campbell, A. Schindlbacher, V. Hurry, T. Lundmark, S. Linder,
3177 and T. Näsholm (2008). High temporal resolution tracing of photosynthate
3178 carbon from the tree canopy to forest soil microorganisms. *New Phytolo-*
3179 *gist* 177(1), 220–228.
- 3180** Houlton, B. Z., Y.-P. Wang, P. M. Vitousek, and C. B. Field (2008). A uni-
3181 fying framework for dinitrogen fixation in the terrestrial biosphere. *Na-*
3182 *ture* 454(7202), 327–330.

- 3183** Huber, M. L., R. A. Perkins, A. Laesecke, D. G. Friend, J. V. Sengers, M. J.
3184 Assael, I. N. Metaxa, E. Vogel, R. Mareš, and K. Miyagawa (2009). New
3185 international formulation for the viscosity of H₂O. *Journal of Physical and*
3186 *Chemical Reference Data* 38(2), 101–125.
- 3187** Hungate, B. A., J. S. Dukes, M. R. Shaw, Y. Luo, and C. B. Field (2003).
3188 Nitrogen and climate change. *Science* 302(5650), 1512–1513.
- 3189** IPCC (2021). *Climate Change 2021: The Physical Science Basis. Contribution*
3190 *of Working Group I to the Sixth Assessment Report of the Intergovernmental*
3191 *Panel on Climate Change*, Volume In Press. Cambridge, United Kingdom
3192 and New York, NY, USA: Cambridge University Press.
- 3193** Johnson, N. C., J. H. Graham, and F. A. Smith (1997). Functioning of mycor-
3194 rhizal associations along the mutualism-parasitism continuum. *New Phytol-*
3195 *ogist* 135(4), 575–585.
- 3196** Kachurina, O. M., H. Zhang, W. R. Raun, and E. G. Krenzer (2000). Simul-
3197 taneous determination of soil aluminum, ammonium- and nitrate- nitrogen
3198 using 1 M potassium chloride. *Communications in Soil Science and Plant*
3199 *Analysis* 31(7-8), 893–903.
- 3200** Kaiser, C., M. R. Kilburn, P. L. Clode, L. Fuchslueger, M. Koranda, J. B. Cliff,
3201 Z. M. Solaiman, and D. V. Murphy (2015). Exploring the transfer of recent
3202 plant photosynthates to soil microbes: mycorrhizal pathway vs direct root
3203 exudation. *New Phytologist* 205(4), 1537–1551.
- 3204** Katabuchi, M. (2015). LeafArea: An R package for rapid digital analysis of leaf
3205 area. *Ecological Research* 30(6), 1073–1077.

- 3206** Kattge, J. and W. Knorr (2007). Temperature acclimation in a biochemical
3207 model of photosynthesis: a reanalysis of data from 36 species. *Plant, Cell*
3208 and *Environment* 30(9), 1176–1190.
- 3209** Kattge, J., W. Knorr, T. Raddatz, and C. Wirth (2009). Quantifying photosyn-
3210 thetic capacity and its relationship to leaf nitrogen content for global-scale
3211 terrestrial biosphere models. *Global Change Biology* 15(4), 976–991.
- 3212** Kayler, Z., A. Gessler, and N. Buchmann (2010). What is the speed of link
3213 between aboveground and belowground processes? *New Phytologist* 187(4),
3214 885–888.
- 3215** Kayler, Z., C. Keitel, K. Jansen, and A. Gessler (2017). Experimental evidence
3216 of two mechanisms coupling leaf-level C assimilation to rhizosphere CO₂
3217 release. *Environmental and Experimental Botany* 135, 21–26.
- 3218** Keeling, C. D., W. G. Mook, and P. P. Tans (1979, jan). Recent trends in the
3219 ¹³C:¹²C ratio of atmospheric carbon dioxide. *Nature* 277(5692), 121–123.
- 3220** Keeney, D. R. and D. W. Nelson (1983). Nitrogen—Inorganic Forms. In A. L.
3221 Page (Ed.), *Methods of Soil Analysis* (2nd ed.), Chapter 33, pp. 643–698.
3222 Madison, WI, USA: ASA and SSSA.
- 3223** Kenward, M. G. and J. H. Roger (1997). Small sample inference for fixed effects
3224 from restricted maximum likelihood. *Biometrics* 53(3), 983.
- 3225** Knapp, A. K., M. L. Avolio, C. Beier, C. J. W. Carroll, S. L. Collins, J. S.
3226 Dukes, L. H. Fraser, R. J. Griffin-Nolan, D. L. Hoover, A. Jentsch, M. E.
3227 Loik, R. P. Phillips, A. K. Post, O. E. Sala, I. J. Slette, L. Yahdjian, and
3228 M. D. Smith (2017). Pushing precipitation to the extremes in distributed

- 3229 experiments: recommendations for simulating wet and dry years. *Global
3230 Change Biology* 23(5), 1774–1782.
- 3231 Knorr, W. (2000). Annual and interannual CO₂ exchanges of the
3232 terrestrial biosphere: process-based simulations and uncertainties. *Global
3233 Ecology and Biogeography* 9(3), 225–252.
- 3234 Knorr, W. and M. Heimann (2001). Uncertainties in global terrestrial biosphere
3235 modeling: 1. A comprehensive sensitivity analysis with a new photosynthesis
3236 and energy balance scheme. *Global Biogeochemical Cycles* 15(1), 207–225.
- 3237 Kulmatiski, A., P. B. Adler, J. M. Stark, and A. T. Tredennick (2017). Water
3238 and nitrogen uptake are better associated with resource availability than
3239 root biomass. *Ecosphere* 8(3), e01738.
- 3240 Lavergne, A., D. Sandoval, V. J. Hare, H. Graven, and I. C. Prentice (2020).
3241 Impacts of soil water stress on the acclimated stomatal limitation of pho-
3242 tosynthesis: Insights from stable carbon isotope data. *Global Change Biol-
3243 ogy* 26(12), 7158–7172.
- 3244 Lawrence, D. M., R. A. Fisher, C. D. Koven, K. W. Oleson, S. C. Swen-
3245 son, G. B. Bonan, N. Collier, B. Ghimire, L. Kampenhout, D. Kennedy,
3246 E. Kluzek, P. J. Lawrence, F. Li, H. Li, D. L. Lombardozzi, W. J. Riley,
3247 W. J. Sacks, M. Shi, M. Vertenstein, W. R. Wieder, C. Xu, A. A. Ali,
3248 A. M. Badger, G. Bisht, M. Broeke, M. A. Brunke, S. P. Burns, J. Buzan,
3249 M. Clark, A. Craig, K. M. Dahlin, B. Drewniak, J. B. Fisher, M. Flanner,
3250 A. M. Fox, P. Gentine, F. M. Hoffman, G. Keppel-Aleks, R. Knox, S. Ku-
3251 mar, J. Lenaerts, L. R. Leung, W. H. Lipscomb, Y. Lu, A. Pandey, J. D.
3252 Pelletier, J. Perket, J. T. Randerson, D. M. Ricciuto, B. M. Sanderson,

- 3253 A. Slater, Z. M. Subin, J. Tang, R. Q. Thomas, M. Val Martin, and X. Zeng
3254 (2019). The Community Land Model Version 5: description of new features,
3255 benchmarking, and impact of forcing uncertainty. *Journal of Advances in*
3256 *Modeling Earth Systems* 11(12), 4245–4287.
- 3257 LeBauer, D. S. and K. K. Treseder (2008). Nitrogen limitation of net primary
3258 productivity. *Ecology* 89(2), 371–379.
- 3259 Lefcheck, J. S. (2016). piecewiseSEM: Piecewise structural equation modelling
3260 in r for ecology, evolution, and systematics. *Methods in Ecology and Evolu-*
3261 *tion* 7(5), 573–579.
- 3262 Lenth, R. (2019). emmeans: estimated marginal means, aka least-squares
3263 means.
- 3264 Li, W., H. Zhang, G. Huang, R. Liu, H. Wu, C. Zhao, and N. G. McDowell
3265 (2020). Effects of nitrogen enrichment on tree carbon allocation: A global
3266 synthesis. *Global Ecology and Biogeography* 29(3), 573–589.
- 3267 Liang, J., X. Qi, L. Souza, and Y. Luo (2016). Processes regulating progressive
3268 nitrogen limitation under elevated carbon dioxide: a meta-analysis. *Biogeosciences*
3269 13(9), 2689–2699.
- 3270 Liang, X., T. Zhang, X. Lu, D. S. Ellsworth, H. BassiriRad, C. You, D. Wang,
3271 P. He, Q. Deng, H. Liu, J. Mo, and Q. Ye (2020). Global response patterns of
3272 plant photosynthesis to nitrogen addition: A meta-analysis. *Global Change*
3273 *Biology* 26(6), 3585–3600.
- 3274 López, J., D. A. Way, and W. Sadok (2021). Systemic effects of rising atmo-
3275 spheric vapor pressure deficit on plant physiology and productivity. *Global*

- 3276** *Change Biology* 27(9), 1704–1720.
- 3277** Lu, J., J. Yang, C. Keitel, L. Yin, P. Wang, W. Cheng, and F. A. Dijkstra
3278 (2022). Belowground carbon efficiency for nitrogen and phosphorus acqui-
3279 sition varies between *Lolium perenne* and *Trifolium repens* and depends on
3280 phosphorus fertilization. *Frontiers in Plant Science* 13, 1–9.
- 3281** Luo, X., T. F. Keenan, J. M. Chen, H. Croft, I. C. Prentice, N. G. Smith,
3282 A. P. Walker, H. Wang, R. Wang, C. Xu, and Y. Zhang (2021). Global
3283 variation in the fraction of leaf nitrogen allocated to photosynthesis. *Nature*
3284 *Communications* 12(1), 4866.
- 3285** Luo, Y., W. S. Currie, J. S. Dukes, A. C. Finzi, U. A. Hartwig, B. A. Hungate,
3286 R. E. McMurtrie, R. Oren, W. J. Parton, D. E. Pataki, R. M. Shaw, D. R.
3287 Zak, and C. B. Field (2004). Progressive nitrogen limitation of ecosystem
3288 responses to rising atmospheric carbon dioxide. *BioScience* 54(8), 731–739.
- 3289** Maire, V., P. Martre, J. Kattge, F. Gastal, G. Esser, S. Fontaine, and J.-F.
3290 Soussana (2012). The coordination of leaf photosynthesis links C and N
3291 fluxes in C₃ plant species. *PLoS ONE* 7(6), e38345.
- 3292** Makino, A. (2003). Rubisco and nitrogen relationships in rice: leaf photosyn-
3293 thesis and plant growth. *Soil Science and Plant Nutrition* 49(3), 319–327.
- 3294** Makino, A., M. Harada, T. Sato, H. Nakano, and T. Mae (1997). Growth and N
3295 Allocation in Rice Plants under CO₂ Enrichment. *Plant Physiology* 115(1),
3296 199–203.
- 3297** Markham, J. H. and C. Zekveld (2007). Nitrogen fixation makes biomass al-
3298 location to roots independent of soil nitrogen supply. *Canadian Journal of*

- 3299** *Botany* (9), 787–793.
- 3300** Marschner, H. and B. Dell (1994). Nutrient uptake in mycorrhizal symbiosis.
- 3301** *Plant and Soil* 159(1), 89–102.
- 3302** Matamala, R. and W. H. Schlesinger (2000). Effects of elevated atmospheric
- 3303** CO₂ on fine root production and activity in an intact temperate forest
- 3304** ecosystem. *Global Change Biology* 6(8), 967–979.
- 3305** Medlyn, B. E., E. Dreyer, D. S. Ellsworth, M. Forstreuter, P. C. Harley,
- 3306** M. U. F. Kirschbaum, X. Le Roux, P. Montpied, J. Strassmeyer, A. Wal-
- 3307** croft, K. Wang, and D. Loustau (2002). Temperature response of parameters
- 3308** of a biochemically based model of photosynthesis. II. A review of experimen-
- 3309** tal data. *Plant, Cell and Environment* 25(9), 1167–1179.
- 3310** Menge, D. N. L., S. A. Levin, and L. O. Hedin (2008). Evolutionary tradeoffs can
- 3311** select against nitrogen fixation and thereby maintain nitrogen limitation.
- 3312** *Proceedings of the National Academy of Sciences* 105(5), 1573–1578.
- 3313** Menne, M. J., I. Durre, R. S. Vose, B. E. Gleason, and T. G. Houston (2012).
- 3314** An overview of the global historical climatology network-daily database.
- 3315** *Journal of Atmospheric and Oceanic Technology* 29(7), 897–910.
- 3316** Meyerholt, J., K. Sickel, and S. Zaehle (2020). Ensemble projections elucidate
- 3317** effects of uncertainty in terrestrial nitrogen limitation on future carbon up-
- 3318** take. *Global Change Biology* 26(7), 3978–3996.
- 3319** Meyerholt, J., S. Zaehle, and M. J. Smith (2016). Variability of projected ter-
- 3320** restrial biosphere responses to elevated levels of atmospheric CO₂ due to
- 3321** uncertainty in biological nitrogen fixation. *Biogeosciences* 13(5), 1491–1518.

- 3322** Minocha, R., S. Long, A. H. Magill, J. D. Aber, and W. H. McDowell (2000).
- 3323** Foliar free polyamine and inorganic ion content in relation to soil and soil
- 3324** solution chemistry in two fertilized forest stands at the Harvard Forest,
- 3325** Massachusetts. *Plant and Soil* 222(1-2), 119–137.
- 3326** Moore, D. J., S. Aref, R. M. Ho, J. S. Pippen, J. G. Hamilton, and E. H. De
- 3327** Lucia (2006). Annual basal area increment and growth duration of *Pinus*
- 3328** *taeda* in response to eight years of free-air carbon dioxide enrichment. *Global*
- 3329** *Change Biology* 12(8), 1367–1377.
- 3330** Morgan, J. A., D. E. Pataki, C. Körner, H. Clark, S. J. Del Grosso, J. M.
- 3331** Grünzweig, A. K. Knapp, A. R. Mosier, P. C. D. Newton, P. A. Niklaus,
- 3332** J. B. Nippert, R. S. Nowak, W. J. Parton, H. W. Polley, and M. R. Shaw
- 3333** (2004). Water relations in grassland and desert ecosystems exposed to ele-
- 3334** vated atmospheric CO₂. *Oecologia* 140(1), 11–25.
- 3335** Muñoz, N., X. Qi, M. W. Li, M. Xie, Y. Gao, M. Y. Cheung, F. L. Wong, and
- 3336** H.-M. Lam (2016). Improvement in nitrogen fixation capacity could be part
- 3337** of the domestication process in soybean. *Heredity* 117(2), 84–93.
- 3338** Nadelhoffer, K. J. and J. W. Raich (1992). Fine root production estimates and
- 3339** belowground carbon allocation in forest ecosystems. *Ecology* 73(4), 1139–
- 3340** 1147.
- 3341** Niinemets, Ü. and J. D. Tenhunen (1997). A model separating leaf structural
- 3342** and physiological effects on carbon gain along light gradients for the shade-
- 3343** tolerant species *Acer saccharum*. *Plant, Cell and Environment* 20(7), 845–
- 3344** 866.
- 3345** Norby, R. J., J. Ledford, C. D. Reilly, N. E. Miller, and E. G. O'Neill

- 3346** (2004). Fine-root production dominates response of a deciduous forest to
3347 atmospheric CO₂ enrichment. *Proceedings of the National Academy of Sci-
ences* 101(26), 9689–9693.
- 3349** Norby, R. J., J. M. Warren, C. M. Iversen, B. E. Medlyn, and R. E. Mc-
3350 Murtrie (2010). CO₂ enhancement of forest productivity constrained by
3351 limited nitrogen availability. *Proceedings of the National Academy of Sci-
ences* 107(45), 19368–19373.
- 3353** Novick, K. A., D. L. Ficklin, P. C. Stoy, C. A. Williams, G. Bohrer, A. C.
3354 Oishi, S. A. Papuga, P. D. Blanken, A. Noormets, B. N. Sulman, R. L.
3355 Scott, L. Wang, and R. P. Phillips (2016). The increasing importance of
3356 atmospheric demand for ecosystem water and carbon fluxes. *Nature Climate
Change* 6(11), 1023–1027.
- 3358** Noyce, G. L., M. L. Kirwan, R. L. Rich, and J. P. Megonigal (2019). Asyn-
3359 chronous nitrogen supply and demand produce nonlinear plant allocation re-
3360 sponds to warming and elevated CO₂. *Proceedings of the National Academy
of Sciences* 116(43), 21623–21628.
- 3362** Onoda, Y., K. Hikosaka, and T. Hirose (2004). Allocation of nitrogen to
3363 cell walls decreases photosynthetic nitrogen-use efficiency. *Functional Ecol-
ogy* 18(3), 419–425.
- 3365** Onoda, Y., I. J. Wright, J. R. Evans, K. Hikosaka, K. Kitajima, Ü. Niinemets,
3366 H. Poorter, T. Tosens, and M. Westoby (2017). Physiological and structural
3367 trade-offs underlying the leaf economics spectrum. *New Phytologist* 214(4),
3368 1447–1463.
- 3369** Oren, R., J. S. Sperry, G. G. Katul, D. E. Pataki, B. E. Ewers, N. Phillips,

- 3370 and K. V. R. Schäfer (1999). Survey and synthesis of intra- and interspecific
3371 variation in stomatal sensitivity to vapor pressure deficit. *Plant, Cell and*
3372 *Environment* 22(12), 1515–1526.
- 3373 Oreskes, N., K. Shrader-Frechette, and K. Belitz (1994). Verification, vali-
3374 dation, and confirmation of numerical models in the Earth sciences. *Sci-
3375 ence* 263(5147), 641–646.
- 3376 Paillassa, J., I. J. Wright, I. C. Prentice, S. Pepin, N. G. Smith, G. Ethier,
3377 A. C. Westerband, L. J. Lamarque, H. Wang, W. K. Cornwell, and V. Maire
3378 (2020). When and where soil is important to modify the carbon and water
3379 economy of leaves. *New Phytologist* 228(1), 121–135.
- 3380 Parvin, S., S. Uddin, S. Tausz Posch, R. Armstrong, and M. Tausz (2020). Car-
3381 bon sink strength of nodules but not other organs modulates photosynthesis
3382 of faba bean (*Vicia faba*) grown under elevated [CO₂] and different water
3383 supply. *New Phytologist* 227(1), 132–145.
- 3384 Paul, K. I., P. J. Polglase, A. M. O'Connell, J. C. Carlyle, P. J. Smethurst, and
3385 P. K. Khanna (2003). Defining the relation between soil water content and
3386 net nitrogen mineralization. *European Journal of Soil Science* 54(1), 39–48.
- 3387 Peng, Y., K. J. Bloomfield, L. A. Cernusak, T. F. Domingues, and I. C. Pren-
3388 tice (2021). Global climate and nutrient controls of photosynthetic capacity.
3389 *Communications Biology* 4(1), 462.
- 3390 Perkowski, E. A., E. F. Waring, and N. G. Smith (2021). Root mass carbon
3391 costs to acquire nitrogen are determined by nitrogen and light availabil-
3392 ity in two species with different nitrogen acquisition strategies. *Journal of*
3393 *Experimental Botany* 72(15), 5766–5776.

- 3394** Phillips, R. P., E. R. Brzostek, and M. G. Midgley (2013). The mycorrhizal-
3395 associated nutrient economy: a new framework for predicting carbon-
3396 nutrient couplings in temperate forests. *New Phytologist* 199(1), 41–51.
- 3397** Phillips, R. P., A. C. Finzi, and E. S. Bernhardt (2011). Enhanced root ex-
3398 udation induces microbial feedbacks to N cycling in a pine forest under
3399 long-term CO₂ fumigation. *Ecology Letters* 14(2), 187–194.
- 3400** Pinheiro, J. and D. Bates (2022). nlme: linear and nonlinear mixed effects
3401 models.
- 3402** Poggio, L., L. M. De Sousa, N. H. Batjes, G. B. M. Heuvelink, B. Kempen,
3403 E. Ribeiro, and D. Rossiter (2021). SoilGrids 2.0: Producing soil information
3404 for the globe with quantified spatial uncertainty. *Soil* 7(1), 217–240.
- 3405** Pons, T. L. and R. W. Pearcy (1994). Nitrogen reallocation and photosynthetic
3406 acclimation in response to partial shading in soybean plants. *Physiologia
3407 Plantarum* 92(4), 636–644.
- 3408** Poorter, H., J. Bühler, D. Van Dusschoten, J. Climent, and J. A. Postma (2012).
3409 Pot size matters: A meta-analysis of the effects of rooting volume on plant
3410 growth. *Functional Plant Biology* 39(11), 839–850.
- 3411** Poorter, H., O. Knopf, I. J. Wright, A. A. Temme, S. W. Hogewoning, A. Graf,
3412 L. A. Cernusak, and T. L. Pons (2022). A meta-analysis of responses of C₃
3413 plants to atmospheric CO₂: dose-response curves for 85 traits ranging from
3414 the molecular to the whole-plant level. *New Phytologist* 233(4), 1560–1596.
- 3415** Prentice, I. C., N. Dong, S. M. Gleason, V. Maire, and I. J. Wright (2014).
3416 Balancing the costs of carbon gain and water transport: testing a new theo-

- 3417 retical framework for plant functional ecology. *Ecology Letters* 17(1), 82–91.
- 3418 Prentice, I. C., X. Liang, B. E. Medlyn, and Y.-P. Wang (2015). Reliable, ro-
- 3419 bust and realistic: The three R's of next-generation land-surface modelling.
- 3420 *Atmospheric Chemistry and Physics* 15, 5987–6005.
- 3421 Priestley, C. H. B. and R. J. Taylor (1972). On the Assessment of Surface
- 3422 Heat Flux and Evaporation Using Large-Scale Parameters. *Monthly Weather*
- 3423 *Review* 100(2), 81–92.
- 3424 Querejeta, J. I., I. Prieto, C. Armas, F. Casanoves, J. S. Diémé, M. Diouf,
- 3425 H. Yossi, B. Kaya, F. I. Pugnaire, and G. M. Rusch (2022). Higher leaf
- 3426 nitrogen content is linked to tighter stomatal regulation of transpiration
- 3427 and more efficient water use across dryland trees. *New Phytologist* 235(4),
- 3428 1351–1364.
- 3429 R Core Team (2021). R: A language and environment for statistical computing.
- 3430 Raich, J. W., D. A. Clark, L. Schwendenmann, and T. E. Wood (2014). Above-
- 3431 ground tree growth varies with belowground carbon allocation in a tropical
- 3432 rainforest environment. *PLoS ONE* 9(6), e100275.
- 3433 Rastetter, E. B., P. M. Vitousek, C. B. Field, G. R. Shaver, D. Herbert, and
- 3434 G. I. Ågren (2001). Resource optimization and symbiotic nitrogen fixation.
- 3435 *Ecosystems* 4(4), 369–388.
- 3436 Reich, P. B. (2014). The world-wide 'fast-slow' plant economics spectrum: a
- 3437 traits manifesto. *Journal of Ecology* 102(2), 275–301.
- 3438 Reich, P. B., S. E. Hobbie, T. Lee, D. S. Ellsworth, J. B. West, D. Tilman,
- 3439 J. M. H. Knops, S. Naeem, and J. Trost (2006). Nitrogen limitation con-

- 3440** strains sustainability of ecosystem response to CO₂. *Nature* 440(7086), 922–
3441 925.
- 3442** Reichman, G. A., D. L. Grunes, and F. G. Viets (1966). Effect of soil moisture
3443 on ammonification and nitrification in two Northern Plains soils. *Soil Science
3444 Society of America Journal* 30(3), 363–366.
- 3445** Rhine, E. D., R. L. Mulvaney, E. J. Pratt, and G. K. Sims (1998). Improving
3446 the Berthelot reaction for determining ammonium in soil extracts and water.
3447 *Soil Science Society of America Journal* 62(2), 473.
- 3448** Rogers, A. (2014). The use and misuse of V_{cmax} in Earth System Models. *Photo-
3449 synthesis Research* 119(1-2), 15–29.
- 3450** Rogers, A., B. E. Medlyn, J. S. Dukes, G. B. Bonan, S. Caemmerer, M. C.
3451 Dietze, J. Kattge, A. D. B. Leakey, L. M. Mercado, Ü. Niinemets, I. C.
3452 Prentice, S. P. Serbin, S. Sitch, D. A. Way, and S. Zaehle (2017). A roadmap
3453 for improving the representation of photosynthesis in Earth system models.
3454 *New Phytologist* 213(1), 22–42.
- 3455** Saathoff, A. J. and J. Welles (2021). Gas exchange measurements in the un-
3456 steady state. *Plant Cell and Environment* 44(11), 3509–3523.
- 3457** Sage, R. F. and R. W. Pearcy (1987). The nitrogen use efficiency of C₃ and C₄
3458 plants: I. Leaf nitrogen, growth, and biomass partitioning in *Chenopodium
3459 album* (L.) and *Amaranthus retroflexus* (L.). *Plant Physiology* 84(3), 954–
3460 958.
- 3461** Saleh, A. M., M. Abdel-Mawgoud, A. R. Hassan, T. H. Habeeb, R. S. Yehia,
3462 and H. AbdElgawad (2020). Global metabolic changes induced by arbuscular

- 3463** mycorrhizal fungi in oregano plants grown under ambient and elevated levels
3464 of atmospheric CO₂. *Plant Physiology and Biochemistry* 151, 255–263.
- 3465** Saxton, K. E. and W. J. Rawls (2006). Soil water characteristic estimates by
3466 texture and organic matter for hydrologic solutions. *Soil Science Society of*
3467 *America Journal* 70(5), 1569–1578.
- 3468** Schaefer, K., C. R. Schwalm, C. Williams, M. A. Arain, A. Barr, J. M. Chen,
3469 K. J. Davis, D. Dimitrov, T. W. Hilton, D. Y. Hollinger, E. Humphreys,
3470 B. Poulter, B. M. Racza, A. D. Richardson, A. Sahoo, P. Thornton, R. Var-
3471 gas, H. Verbeeck, R. Anderson, I. Baker, T. A. Black, P. Bolstad, J. Chen,
3472 P. S. Curtis, A. R. Desai, M. C. Dietze, D. Dragoni, C. M. Gough, R. F.
3473 Grant, L. Gu, A. K. Jain, C. Kucharik, B. E. Law, S. Liu, E. Lokipitiya,
3474 H. A. Margolis, R. Matamala, J. H. McCaughey, R. Monson, J. W. Munger,
3475 W. Oechel, C. Peng, D. T. Price, D. Ricciuto, W. J. Riley, N. Roulet,
3476 H. Tian, C. Tonitto, M. Torn, E. Weng, and X. Zhou (2012). A model-
3477 data comparison of gross primary productivity: Results from the North
3478 American Carbon Program site synthesis. *Journal of Geophysical Research:*
3479 *Biogeosciences* 117(G3), G03010.
- 3480** Schmitt, M. R. and G. E. Edwards (1981). Photosynthetic capacity and nitrogen
3481 use efficiency of maize, wheat, and rice: A comparison between C₃ and C₄
3482 photosynthesis. *Journal of Experimental Botany* 32(3), 459–466.
- 3483** Schneider, C. A., W. S. Rasband, and K. W. Eliceiri (2012). NIH Image to
3484 ImageJ: 25 years of image analysis. *Nature Methods* 9(7), 671–675.
- 3485** Scott, H. G. and N. G. Smith (2022). A Model of C₄ photosynthetic acclima-
3486 tion based on least-cost optimality theory suitable for Earth system model

- 3487 incorporation. *Journal of Advances in Modeling Earth Systems* 14(3), 1–16.
- 3488 Shi, M., J. B. Fisher, E. R. Brzostek, and R. P. Phillips (2016). Carbon cost
3489 of plant nitrogen acquisition: Global carbon cycle impact from an improved
3490 plant nitrogen cycle in the Community Land Model. *Global Change Biology*
3491 *22*(3), 1299–1314.
- 3492 Shi, M., J. B. Fisher, R. P. Phillips, and E. R. Brzostek (2019). Neglecting
3493 plant–microbe symbioses leads to underestimation of modeled climate im-
3494 pacts. *Biogeosciences* 16(2), 457–465.
- 3495 Smith, B., D. Wärldin, A. Arneth, T. Hickler, P. Leadley, J. Siltberg, and
3496 S. Zaehle (2014). Implications of incorporating N cycling and N limitations
3497 on primary production in an individual-based dynamic vegetation model.
3498 *Biogeosciences* 11(7), 2027–2054.
- 3499 Smith, N. G. and J. S. Dukes (2013). Plant respiration and photosynthesis in
3500 global-scale models: incorporating acclimation to temperature and CO₂.
3501 *Global Change Biology* 19(1), 45–63.
- 3502 Smith, N. G. and J. S. Dukes (2018). Drivers of leaf carbon exchange capacity
3503 across biomes at the continental scale. *Ecology* 99(7), 1610–1620.
- 3504 Smith, N. G. and T. F. Keenan (2020). Mechanisms underlying leaf photosyn-
3505 thetic acclimation to warming and elevated CO₂ as inferred from least-cost
3506 optimality theory. *Global Change Biology* 26(9), 5202–5216.
- 3507 Smith, N. G., T. F. Keenan, I. C. Prentice, H. Wang, I. J. Wright, Ü. Niinemets,
3508 K. Y. Crous, T. F. Domingues, R. Guerrieri, F. oko Ishida, J. Kattge, E. L.
3509 Kruger, V. Maire, A. Rogers, S. P. Serbin, L. Tarvainen, H. F. Togashi,

- 3510 P. A. Townsend, M. Wang, L. K. Weerasinghe, and S.-X. Zhou (2019).
3511 Global photosynthetic capacity is optimized to the environment. *Ecology*
3512 *Letters* 22(3), 506–517.
- 3513 Smith, N. G., D. L. Lombardozzi, A. Tawfik, G. B. Bonan, and J. S. Dukes
3514 (2017). Biophysical consequences of photosynthetic temperature acclimation
3515 for climate. *Journal of Advances in Modeling Earth Systems* 9(1), 536–547.
- 3516 Smith, N. G., S. L. Malyshev, E. Shevliakova, J. Kattge, and J. S. Dukes
3517 (2016). Foliar temperature acclimation reduces simulated carbon sensitivity
3518 to climate. *Nature Climate Change* 6(4), 407–411.
- 3519 Smith, S. E. and D. J. Read (2008). *Mycorrhizal Symbiosis*. Academic Press.
- 3520 Soil Survey Staff (2022). Web Soil Survey.
- 3521 Soudzilovskaia, N. A., J. C. Douma, A. A. Akhmetzhanova, P. M. van Bode-
3522 gom, W. K. Cornwell, E. J. Moens, K. K. Treseder, and J. H. C. Cornelissen
3523 (2015). Global patterns of plant root colonization intensity by mycorrhizal
3524 fungi explained by climate and soil chemistry. *Global Ecology and Biogeog-
3525 raphy* 24(3), 371–382.
- 3526 Stark, J. M. and M. K. Firestone (1995). Mechanisms for soil moisture ef-
3527 fects on activity of nitrifying bacteria. *Applied and Environmental Microbi-
3528 ology* 61(1), 218–221.
- 3529 Stocker, B. D., H. Wang, N. G. Smith, S. P. Harrison, T. F. Keenan, D. San-
3530 doval, T. Davis, and I. C. Prentice (2020). P-model v1.0: An optimality-
3531 based light use efficiency model for simulating ecosystem gross primary pro-
3532 duction. *Geoscientific Model Development* 13(3), 1545–1581.

- 3533** Stocker, B. D., J. Zscheischler, T. F. Keenan, I. C. Prentice, J. Peñuelas, and
3534 S. I. Seneviratne (2018). Quantifying soil moisture impacts on light use
3535 efficiency across biomes. *New Phytologist* 218(4), 1430–1449.
- 3536** Sulman, B. N., D. T. Roman, K. Yi, L. Wang, R. P. Phillips, and K. A.
3537 Novick (2016). High atmospheric demand for water can limit forest car-
3538 bon uptake and transpiration as severely as dry soil. *Geophysical Research*
3539 *Letters* 43(18), 9686–9695.
- 3540** Sulman, B. N., E. Shevliakova, E. R. Brzostek, S. N. Kivlin, S. L. Malyshev,
3541 D. N. L. Menge, and X. Zhang (2019). Diverse mycorrhizal associations
3542 enhance terrestrial C storage in a global model. *Global Biogeochemical Cy-
cles* 33(4), 501–523.
- 3544** Sweet, S. K., D. W. Wolfe, A. DeGaetano, and R. Benner (2017). Anatomy
3545 of the 2016 drought in the Northeastern United States: Implications for
3546 agriculture and water resources in humid climates. *Agricultural and Forest*
3547 *Meteorology* 247, 571–581.
- 3548** Taylor, B. N. and D. N. L. Menge (2018). Light regulates tropical symbiotic
3549 nitrogen fixation more strongly than soil nitrogen. *Nature Plants* 4(9), 655–
3550 661.
- 3551** Terrer, C., S. Vicca, B. A. Hungate, R. P. Phillips, and I. C. Prentice (2016).
3552 Mycorrhizal association as a primary control of the CO₂ fertilization effect.
3553 *Science* 353(6294), 72–74.
- 3554** Terrer, C., S. Vicca, B. D. Stocker, B. A. Hungate, R. P. Phillips, P. B. Reich,
3555 A. C. Finzi, and I. C. Prentice (2018). Ecosystem responses to elevated CO₂
3556 governed by plant–soil interactions and the cost of nitrogen acquisition. *New*

- 3557 *Phytologist* 217(2), 507–522.
- 3558 Thieurmel, B. and A. Elmarhraoui (2019). suncalc: Compute sun position,
- 3559 sunlight phases, moon position, and lunar phase.
- 3560 Thomas, R. Q., E. N. J. Brookshire, and S. Gerber (2015). Nitrogen limita-
- 3561 tion on land: how can it occur in Earth system models? *Global Change*
- 3562 *Biology* 21(5), 1777–1793.
- 3563 Thomas, R. Q., S. Zaehle, P. H. Templer, and C. L. Goodale (2013). Global pat-
- 3564 terns of nitrogen limitation: confronting two global biogeochemical models
- 3565 with observations. *Global Change Biology* 19(10), 2986–2998.
- 3566 Thornton, P. E., J.-F. Lamarque, N. A. Rosenbloom, and N. M. Mahowald
- 3567 (2007). Influence of carbon-nitrogen cycle coupling on land model response
- 3568 to CO₂ fertilization and climate variability. *Global Biogeochemical Cy-*
- 3569 *cles* 21(4), GB4018.
- 3570 Tingey, D. T., D. L. Phillips, and M. G. Johnson (2000). Elevated CO₂ and
- 3571 conifer roots: effects on growth, life span and turnover. *New Phytolo-*
- 3572 *gist* 147(1), 87–103.
- 3573 Udvardi, M. and P. S. Poole (2013). Transport and metabolism in legume-
- 3574 rhizobia symbioses. *Annual Review of Plant Biology* 64, 781–805.
- 3575 USDA NRCS (2022). The PLANTS Database.
- 3576 Uselman, S. M., R. G. Qualls, and R. B. Thomas (2000). Effects of increased
- 3577 atmospheric CO₂, temperature, and soil N availability on root exudation
- 3578 of dissolved organic carbon by an N-fixing tree (*Robinia pseudoacacia* L.).
- 3579 *Plant and Soil* 222, 191–202.

- 3580 van Diepen, L. T. A., E. A. Lilleskov, K. S. Pregitzer, and R. M. Miller (2007).
- 3581 Decline of arbuscular mycorrhizal fungi in northern hardwood forests ex-
- 3582 posed to chronic nitrogen additions. *New Phytologist* 176(1), 175–183.
- 3583 Vance, C. P. and G. H. Heichel (1991). Carbon in N₂ fixation: Limitation or
- 3584 exquisite adaptation. *Annual Review of Plant Physiology and Plant Molec-*
- 3585 *ular Biology* 42(1), 373–392.
- 3586 Viet, H. D., J.-H. Kwak, K.-S. Lee, S.-S. Lim, M. Matsushima, S. X. Chang,
- 3587 K.-H. Lee, and W.-J. Choi (2013). Foliar chemistry and tree ring δ¹³C of
- 3588 *Pinus densiflora* in relation to tree growth along a soil pH gradient. *Plant*
- 3589 *and Soil* 363(1-2), 101–112.
- 3590 Vitousek, P. M., K. Cassman, C. C. Cleveland, T. Crews, C. B. Field, N. B.
- 3591 Grimm, R. W. Howarth, R. Marino, L. Martinelli, E. B. Rastetter, and
- 3592 J. I. Sprent (2002). Towards an ecological understanding of biological nitro-
- 3593 gen fixation. In *The Nitrogen Cycle at Regional to Global Scales*, pp. 1–45.
- 3594 Springer Netherlands.
- 3595 Vitousek, P. M. and R. W. Howarth (1991). Nitrogen limitation on land and in
- 3596 the sea: How can it occur? *Biogeochemistry* 13(2), 87–115.
- 3597 Vitousek, P. M., S. Porder, B. Z. Houlton, and O. A. Chadwick (2010).
- 3598 Terrestrial phosphorus limitation: mechanisms, implications, and nitro-
- 3599 gen–phosphorus interactions. *Ecological Applications* 20(1), 5–15.
- 3600 Walker, A. P., A. P. Beckerman, L. Gu, J. Kattge, L. A. Cernusak, T. F.
- 3601 Domingues, J. C. Scales, G. Wohlfahrt, S. D. Wullschleger, and F. I. Wood-
- 3602 ward (2014). The relationship of leaf photosynthetic traits - V_{cmax} and J_{max}
- 3603 - to leaf nitrogen, leaf phosphorus, and specific leaf area: a meta-analysis

- 3604** and modeling study. *Ecology and Evolution* 4(16), 3218–3235.
- 3605** Walker, A. P., A. L. Johnson, A. Rogers, J. Anderson, R. A. Bridges, R. A.
- 3606** Fisher, D. Lu, D. M. Ricciuto, S. P. Serbin, and M. Ye (2021). Multi-
- 3607** hypothesis comparison of Farquhar and Collatz photosynthesis models re-
- 3608** veals the unexpected influence of empirical assumptions at leaf and global
- 3609** scales. *Global Change Biology* 27(4), 804–822.
- 3610** Wang, H., I. C. Prentice, T. F. Keenan, T. W. Davis, I. J. Wright, W. K.
- 3611** Cornwell, B. J. Evans, and C. Peng (2017). Towards a universal model for
- 3612** carbon dioxide uptake by plants. *Nature Plants* 3(9), 734–741.
- 3613** Wang, H., I. C. Prentice, I. J. Wright, D. I. Warton, S. Qiao, X. Xu, J. Zhou,
- 3614** Kikuzawa, and N. C. Stenseth (2023). Leaf economics fundamentals ex-
- 3615** plained by optimality principles. *Science Advances* 9(3), eadd566.
- 3616** Wang, J., J. M. Knops, C. E. Brassil, and C. Mu (2017). Increased productivity
- 3617** in wet years drives a decline in ecosystem stability with nitrogen additions
- 3618** in arid grasslands. *Ecology* 98(7), 1779–1786.
- 3619** Wang, W., Y. Wang, G. Hoch, Z. Wang, and J. Gu (2018). Linkage of root mor-
- 3620** phology to anatomy with increasing nitrogen availability in six temperate
- 3621** tree species. *Plant and Soil* 425(1-2), 189–200.
- 3622** Weatherburn, M. W. (1967). Phenol-hypochlorite reaction for determination of
- 3623** ammonia. *Analytical Chemistry* 39(8), 971–974.
- 3624** Wellburn, A. R. (1994). The spectral determination of chlorophylls a and b, as
- 3625** well as total carotenoids, using various solvents with spectrophotometers of
- 3626** different resolution. *Journal of Plant Physiology* 144(3), 307–313.

- 3627** Wen, Z., P. J. White, J. Shen, and H. Lambers (2022). Linking root exudation to belowground economic traits for resource acquisition. *New Phytologist* 233(4), 1620–1635.
- 3630** Westerband, A. C., I. J. Wright, V. Maire, J. Paillassa, I. C. Prentice, O. K.
- 3631** Atkin, K. J. Bloomfield, L. A. Cernusak, N. Dong, S. M. Gleason, C. Guilherme Pereira, H. Lambers, M. R. Leishman, Y. Malhi, and R. H. Nolan
- 3632**
- 3633** (2023). Coordination of photosynthetic traits across soil and climate gradients. *Global Change Biology* 29(3), 1–29.
- 3634**
- 3635** Wieder, W. R., C. C. Cleveland, W. K. Smith, and K. Todd-Brown (2015).
- 3636** Future productivity and carbon storage limited by terrestrial nutrient availability. *Nature Geoscience* 8(6), 441–444.
- 3637**
- 3638** Wieder, W. R., D. M. Lawrence, R. A. Fisher, G. B. Bonan, S. J. Cheng, C. L.
- 3639** Goodale, A. S. Grandy, C. D. Koven, D. L. Lombardozzi, K. W. Oleson,
- 3640** and R. Q. Thomas (2019). Beyond static benchmarking: using experimental
- 3641** manipulations to evaluate land model assumptions. *Global Biogeochemical*
- 3642** *Cycles* 33(10), 1289–1309.
- 3643** Wright, I. J., P. B. Reich, and M. Westoby (2003). Least-cost input mixtures
- 3644** of water and nitrogen for photosynthesis. *The American Naturalist* 161(1),
- 3645** 98–111.
- 3646** Wright, I. J., P. B. Reich, M. Westoby, D. D. Ackerly, Z. Baruch, F. Bongers,
- 3647** J. Cavender-Bares, T. Chapin, J. H. C. Cornelissen, M. Diemer, J. Flexas,
- 3648** E. Garnier, P. K. Groom, J. Gulias, K. Hikosaka, B. B. Lamont, T. Lee,
- 3649** W. Lee, C. Lusk, J. J. Midgley, M.-L. Navas, Ü. Niinemets, J. Oleksyn,
- 3650** N. Osada, H. Poorter, P. Poot, L. Prior, V. I. Pyankov, C. Roumet, S. C.

- 3651** Thomas, M. G. Tjoelker, E. J. Veneklaas, and R. Villar (2004). The world-wide leaf economics spectrum. *Nature* 428(6985), 821–827.
- 3653** Xu-Ri and I. C. Prentice (2017). Modelling the demand for new nitrogen fixation by terrestrial ecosystems. *Biogeosciences* 14(7), 2003–2017.
- 3655** Yahdjian, L., L. A. Gherardi, and O. E. Sala (2011). Nitrogen limitation in arid-subhumid ecosystems: A meta-analysis of fertilization studies. *Journal of Arid Environments* 75(8), 675–680.
- 3658** Zaehle, S., B. E. Medlyn, M. G. De Kauwe, A. P. Walker, M. C. Dietze, T. Hickler, Y. Luo, Y. P. Wang, B. El-Masri, P. Thornton, A. Jain, S. Wang, D. Warlind, E. Weng, W. Parton, C. M. Iversen, A. Gallet-Budynek, H. McCarthy, A. C. Finzi, P. J. Hanson, I. C. Prentice, R. Oren, and R. J. Norby (2014). Evaluation of 11 terrestrial carbon-nitrogen cycle models against observations from two temperate Free-Air CO₂ Enrichment studies. *New Phytologist* 202(3), 803–822.
- 3665** Zaehle, S., S. Sitch, B. Smith, and F. Hatterman (2005). Effects of parameter uncertainties on the modeling of terrestrial biosphere dynamics. *Global Biogeochemical Cycles* 19(3), GB3020.
- 3668** Zhu, Q., W. J. Riley, J. Tang, N. Collier, F. M. Hoffman, X. Yang, and G. Bisht (2019). Representing nitrogen, phosphorus, and carbon interactions in the E3SM land model: development and global benchmarking. *Journal of Advances in Modeling Earth Systems* 11(7), 2238–2258.
- 3672** Ziegler, C., M. E. Dusenge, B. Nyirambangutse, E. Zibera, G. Wallin, and J. Uddling (2020). Contrasting dependencies of photosynthetic capacity on leaf nitrogen in early- and late-successional tropical montane tree species.

- 3675** *Frontiers in Plant Science* 11, 1–12.
- 3676** Ziehn, T., J. Kattge, W. Knorr, and M. Scholze (2011). Improving the pre-
3677 dictability of global CO₂ assimilation rates under climate change. *Geophys-
3678 ical Research Letters* 38(10), L10404.

3679 Appendix A: Supplemental material for "Structural carbon costs to
3680 acquire nitrogen are determined by nitrogen and light availability in
3681 two species with different nitrogen acquisition strategies"

Table A1. Summary table containing volumes of compounds used to create modified Hoagland's solutions for each soil nitrogen fertilization treatment. All volumes are expressed as milliliters per liter (mL/L)

Compound	0 ppm N	70 ppm N	210 ppm N	630 ppm N
1 M NH ₄ H ₂ PO ₄	0	0.33	1	1
2 M KNO ₃	0	0.67	2	2
2 M Ca(NO ₃) ₂	0	0.67	2	2
1 M NH ₄ NO ₃	0	0.33	1	0
8 M NH ₄ NO ₃	0	0	0	2
1 M KH ₂ PO ₄	1	0.67	0	0
1 M KCl	4	1.33	0	0
1 M CaCO ₃	4	3	0	0
2 M MgSO ₄	1	1	1	1
10% Fe-EDTA	1	1	1	1
Trace Elements	1	1	1	1

Table A2. Analysis of variance results exploring species-specific effects of light availability, nitrogen fertilization, and their interactions on the ratio of whole plant biomass to pot volume

	df	Biomass:pot volume		
		Coefficient	χ^2	p
<i>G. hirsutum</i>				
Intercept		0.740	-	-
Light (L)	1	-4.23E-03	189.581	<0.001
Nitrogen (N)	1	7.86E-04	17.927	<0.001
L*N	1	-6.61E-06	4.709	0.030
<i>G. max</i>				
Intercept		-0.233	-	-
Light (L)	1	-1.12E-02	69.500	<0.001
Nitrogen (N)	1	8.29E-04	40.297	<0.001
L*N	1	-8.51E-06	5.548	0.019

3682 *Significance determined using Wald's χ^2 tests ($P = 0.05$). P -values < 0.05 are
3683 in bold and p -values between 0.05 and 0.1 are italicized. Negative coefficients
3684 for light treatments indicate a positive effect of increasing light availability on
3685 all response variables, as light availability is treated as percent shade cover in all
3686 linear mixed-effects models.

Table A3. Slopes of the regression line describing the relationship between each dependent variable and nitrogen fertilization at each light level*

	Shade cover	Slope
<i>G. hirsutum</i>		
0%		8.29E-04^a
30%		5.74E-04^a
50%		4.03E-04^a
80%		1.48E-04 ^a
<i>G. max</i>		
0%		7.86E-04
30%		5.87E-04
50%		4.55E-04
80%		<i>2.57E-05</i>

207

3687 *Slopes represent estimated marginal mean slopes from linear mixed-effects models described in the Methods. Slopes
 3688 were calculated using the ‘emmeans’ R package (Lenth 2019). Superscripts indicate slopes fit to natural-log (^a) or
 3689 square root (^b) transformed data. Slopes statistically different from zero (Tukey: $p < 0.05$) are indicated in bold.
 3690 Marginally significant slopes (Tukey: $0.05 < p < 0.1$) are italicized.

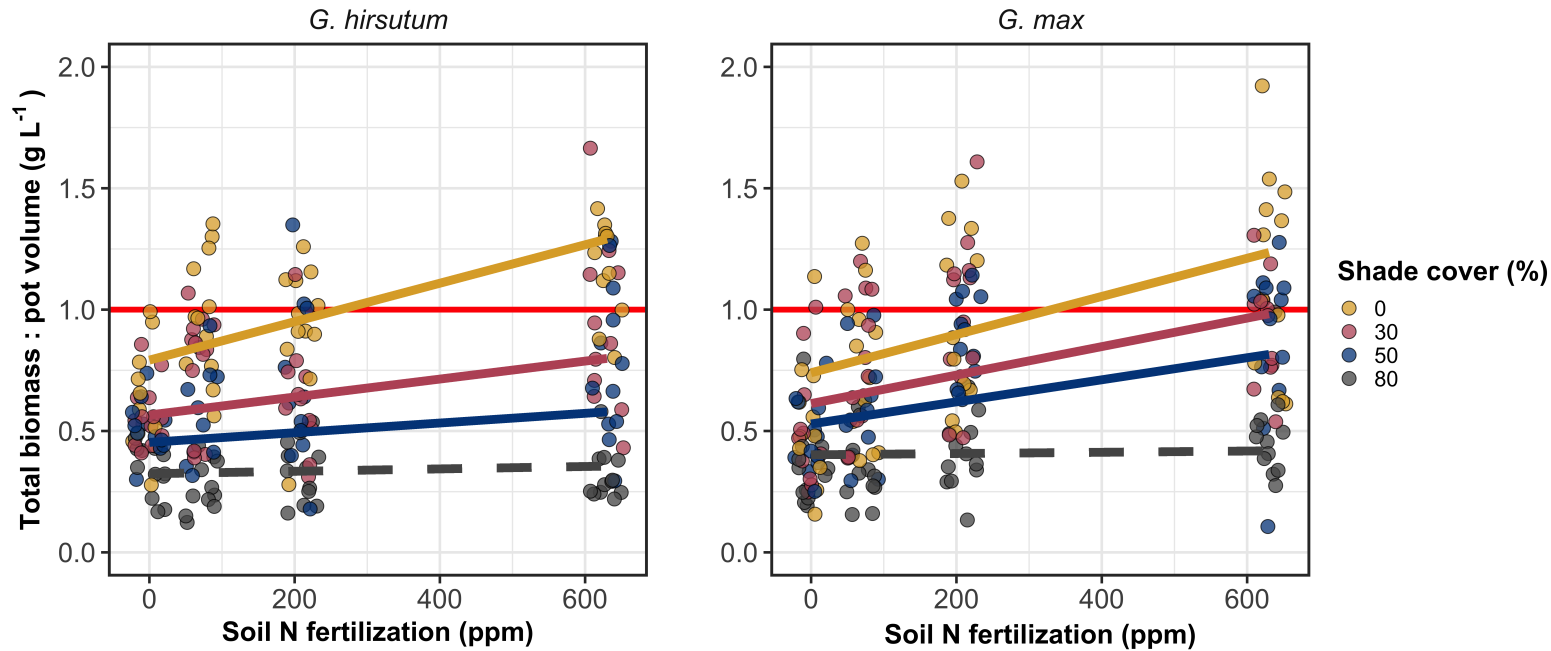


Figure A1. Effects of shade cover and nitrogen fertilization on the ratio of plant biomass to rooting volume in *G. hirsutum* (left panel) and *G. max* (right panel). The red horizontal line indicates the recommended 1 g L^{-1} threshold for BVR recommended by Poorter et al. (2012) to avoid pot size-induced growth limitation. Nitrogen fertilization treatments are represented on the x-axis. Shade cover treatments are represented through colored points and trendlines. Trendlines were created by back-transforming marginal mean slopes and intercepts from species-specific linear mixed-effects models. These values were calculated using the 'emtrends' and 'emmmeans' functions in the 'emmmeans' R package (Lenth 2019). Points are jittered for visibility. Yellow points and trendlines represent the 0% shade cover treatment, blue points and trendlines represent the 30% shade cover treatment, green points and trendlines represent the 50% shade cover treatment, and purple points and trendlines represent the 80% shade cover treatment. Solid trendlines indicate slopes that are significantly different from zero (Tukey: $p < 0.05$), while dashed trendlines indicate slopes that are not statistically different from zero.

3691 Appendix B: Supplemental material for "Soil nitrogen availability
3692 modifies leaf nitrogen economies in mature temperate deciduous
3693 forests: a direct test of photosynthetic least-cost theory"

Table B1. Sample sizes of each species, abbreviated by their USDA NRCS PLANTS database code, within each plot at each site

	ACRU	ACSA	FAGR	FRAM	QURU	N_{plot}
Bald Hill						
+N; +S	0	6	1	0	1	8
+N; -S	1	2	2	0	1	6
-N; +S	2	2	0	0	2	6
-N; -S	2	3	3	0	2	10
Carter Creek						
+N; +S	0	6	1	2	0	9
+N; -S	0	4	0	2	0	6
-N; +S	0	5	1	4	0	10
-N; -S	0	7	0	0	0	7
Mount Pleasant						
+N; +S	3	2	1	0	3	9
+N; -S	0	5	4	1	0	10
-N; +S	1	2	4	0	0	7
-N; -S	3	3	1	2	1	10
N_{spp}	12	47	18	11	10	98

3694 *Plots within each site are represented based on nitrogen and sulfur addition
3695 status. The final column on the right depicts total sample size per plot in each
3696 site (N_{plot}) and the final row on the bottom represents cumulative species sample
3697 size across all plots and all sites (N_{spp}). Key: ACRU = *A. rubrum*; ACSA = *A.*
3698 *saccharum*; FAGR = *F. grandifolia*; FRAM = *F. americana*; QURU = *Q. rubra*

Table B2. Analysis of variance results exploring the linear effect of leaf temperature on net photosynthesis rate and stomatal conductance measured at 400 $\mu\text{mol mol}^{-1}$ CO₂

		A_{net}		g_s	
	df	χ^2	p	χ^2	p
Leaf temperature	1	1.287	0.257	1.716	0.190

3699 Results detail linear mixed effects model where temperature was regressed against
3700 net photosynthesis or stomatal conductance, with site and species designated as
3701 random intercept terms. Significance was determined using Type II Wald χ^2
3702 tests ($\alpha = 0.05$). Key: A_{net} = net photosynthesis rate at 400 $\mu\text{mol mol}^{-1}$ CO₂;
3703 g_s =stomatal conductance measured at 400 $\mu\text{mol mol}^{-1}$ CO₂

Table B3. Second order log-polynomial regression coefficients that described the effect of leaf temperature on net photosynthesis and stomatal conductance measured at 400 $\mu\text{mol mol}^{-1}$ CO₂

	a	b	c
A_{net}	9.422	-0.573	0.010
g_s	-0.170	-0.186	0.003

3704 Net photosynthesis and stomatal conductance values were fit to the log-polynomial
3705 equation $\log(y) = a + bx + cx^2$, where x is leaf temperature. Key: A_{net} = net
3706 photosynthesis rate at 400 $\mu\text{mol mol}^{-1}$ CO₂; g_s = stomatal conductance measured
3707 at 400 $\mu\text{mol mol}^{-1}$ CO₂

Table B4. Mean, standard error, and 95% confidence interval ranges of soil nitrogen availability estimates across all measured plots. All units are expressed as $\mu\text{g N g}^{-1}$ resin d^{-1}

Site	Treatment	Mean	SE	Lower 95% CI	Upper 95% CI
Bald Hill	Ammonium sulfate	27.11	6.14	15.08	39.13
Bald Hill	Control	14.41	5.02	4.56	24.26
Bald Hill	Sodium nitrate	20.65	3.15	14.46	26.83
Bald Hill	Sulfur	6.33	2.19	2.04	10.62
Carter Creek	Ammonium sulfate	26.94	5.36	16.43	37.44
Carter Creek	Control	19.87	1.92	16.10	23.64
Carter Creek	Sodium nitrate	15.51	4.16	7.36	23.65
Carter Creek	Sulfur	5.50	1.40	2.75	8.25
Mount Pleasant	Ammonium sulfate	8.02	2.31	3.49	12.56
Mount Pleasant	Control	2.00	0.57	0.89	3.11
Mount Pleasant	Sodium nitrate	2.52	0.68	1.19	3.85
Mount Pleasant	Sulfur	2.42	0.39	1.66	3.17

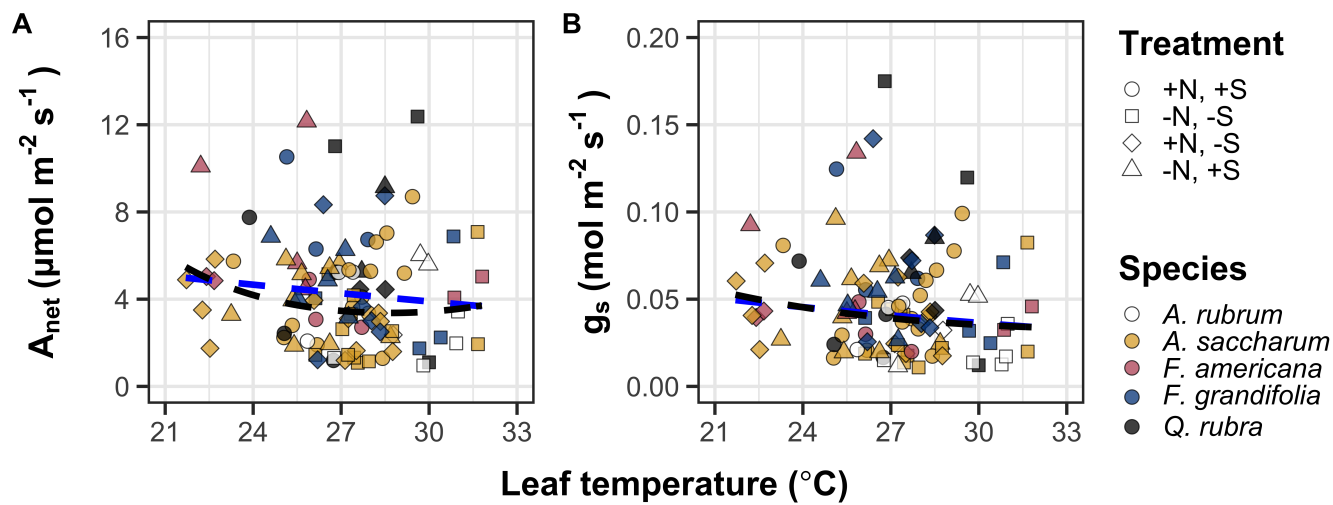


Figure B1. Effects of leaf temperature on net photosynthesis rate (panel A) and stomatal conductance (panel B) values when measured at $400 \mu\text{mol mol}^{-1} \text{CO}_2$. Leaf temperature is represented continuously on the x-axis, while species are represented as colored points. Colored points and shapes are as explained in Figure 3.1. The dashed blue trendline describes the linear relationship between leaf temperature and each response variable, while the dashed black trendline describes the same relationship with a log-polynomial regression equation.

**3708 Appendix C: Supplemental material for "The relative cost of resource
3709 use for photosynthesis drives variance in leaf nitrogen content across a
3710 climate and soil resource availability gradient"**

3711 C.1 Calculations for soil water holding capacity

3712 Water holding capacity (θ_{WHC} ; mm) was calculated as a function of the
3713 volumetric soil water storage at field capacity (W_{FC} ; m³ m⁻³), and the volumetric
3714 soil water storage at wilting point (W_{PWP} ; m³ m⁻³):

$$\theta_{WHC} = (W_{FC} - W_{PWP})(1 - f_{gravel}) * \min(z_{bedrock}, z_{max}) \quad (\text{C4.1})$$

3715 where f_{gravel} (%) is the fraction of gravel content in soil, $z_{bedrock}$ (mm) is the
3716 distance to bedrock, and z_{max} (mm) is the maximum allowable distance to bedrock,
3717 set to 2000mm. W_{FC} is calculated as:

$$\theta_{FC} = k_{fc} + (1.283 * (k_{fc})^2 - 0.374 * k_{fc} - 0.015) \quad (\text{C4.2})$$

3718 where

$$\begin{aligned} k_{fc} = & -0.251 * f_{sand} + 0.195 * f_{clay} + 0.011 * f_{OM} \\ & + 0.006 * (f_{sand} * f_{OM}) - 0.027 * (f_{clay} \\ & * f_{OM}) + 0.452 * (f_{sand} * f_{clay}) + 0.299 \end{aligned} \quad (\text{C4.3})$$

3719 W_{PWP} is calculated as:

$$W_{PWP} = k_{pwp} + (0.14 * k_{pwp} - 0.02) \quad (\text{C4.4})$$

3720 where

$$\begin{aligned} k_{pwp} = & -0.024 * f_{sand} + 0.487 * f_{clay} + 0.006 * f_{OM} \\ & + 0.005 * (f_{sand} * f_{OM}) - 0.013 * (f_{clay} \\ & * f_{OM}) + 0.068 * (f_{sand} * f_{clay}) + 0.031 \end{aligned} \quad (\text{C4.5})$$

3721 In Equations C4.4 and C4.5, f_{sand} (%) is the fraction of sand content in soil (%),
3722 f_{clay} (%) is the fraction of clay content in soil (%), and f_{OM} is the fraction of
3723 organic matter in soil (%). Organic matter in the soil was calculated in this study
3724 by converting soil organic carbon data extracted from SoilGrids 2.0 to soil organic
3725 matter using the van Bemmelen factor (1.724 conversion factor).

Table C1. List of sampled species and their plant functional group assignment

Symbol	Species	Photo. pathway	Growth duration	Growth habit	N-fixer?	Plant functional group	Number sampled
ACAN11	<i>Acaciella angustissima</i>	c3	perennial	forb	yes	c3_legume	3
AMAR2	<i>Ambrosia artemisiifolia</i>	c3	annual	forb	no	c3_nonlegume	25
AMPS	<i>Ambrosia psilostachya</i>	c3	perennial	forb	no	c3_nonlegume	32
ARAL3	<i>Argemone albiflora</i>	c3	annual	forb	no	c3_nonlegume	3
ARPU9	<i>Aristida purpurea</i>	c4	perennial	graminoid	no	c4_nonlegume	2
ASAS	<i>Asclepias asperula</i>	c3	perennial	forb	no	c3_nonlegume	3
ASLA4	<i>Asclepias latifolia</i>	c3	perennial	forb	no	c3_nonlegume	3
ASSY	<i>Asclepias syriaca</i>	c3	perennial	forb	no	c3_nonlegume	18
BASA	<i>Baccharis salicina</i>	c3	perennial	shrub	no	c3_nonlegume	3
BOIS	<i>Bothriochloa ischaemum</i>	c4	perennial	graminoid	no	c4_nonlegume	6
BOSA	<i>Bothriochloa saccharoides</i>	c4	perennial	graminoid	no	c4_nonlegume	6
CAAM2	<i>Callicarpa americana</i>	c3	perennial	shrub	no	c3_nonlegume	3
CAPL3	<i>Carex planostachys</i>	c4	perennial	graminoid	no	c4_nonlegume	3
CAREX	<i>Carex</i> spp.	c4	perennial	graminoid	no	c4_nonlegume	16
CHFE3	<i>Chamaesyce fendleri</i>	c3	perennial	forb	no	c3_nonlegume	2
CHPI8	<i>Chrysopsis pilosa</i>	c3	annual	forb	no	c3_nonlegume	3
COCO13	<i>Conoclinium coelestinum</i>	c3	perennial	forb	no	c3_nonlegume	3
COER	<i>Commelina erecta</i>	c3	perennial	forb	no	c3_nonlegume	3
CRGLL	<i>Croton glandulosus</i>	c3	annual	forb	no	c3_nonlegume	22
CYDA	<i>Cynodon dactylon</i>	c4	perennial	graminoid	no	c4_nonlegume	15
DATE3	<i>Dasyllirion texanum</i>	c3	perennial	shrub	no	c3_nonlegume	3
DIAN	<i>Dichanthium annulatum</i>	c4	perennial	graminoid	no	c4_nonlegume	8
ENPE4	<i>Engelmannia peristenia</i>	c3	perennial	forb	no	c3_nonlegume	6
EUMA8	<i>Euphorbia marginata</i>	c3	annual	forb	no	c3_nonlegume	6
GAPU	<i>Gaillardia pulchella</i>	c3	annual	forb	no	c3_nonlegume	16
GLGO	<i>Glandularia gooddingii</i>	c3	perennial	forb	no	c3_nonlegume	2
HEAN3	<i>Helianthus annuus</i>	c3	annual	forb	no	c3_nonlegume	6

Table C2. List of sampled species and their plant functional group assignment (cont.)

Symbol	Species	Photo. pathway	Growth duration	Growth habit	N-fix?	Plant functional group	Number sampled
HECA8	<i>Heterotheca canescens</i>	c3	perennial	forb	no	c3_nonlegume	2
HETE3	<i>Heliotropium tenellum</i>	c3	annual	forb	no	c3_nonlegume	3
IVAX	<i>Iva axillaris</i>	c3	perennial	forb	no	c3_nonlegume	4
LIAT	<i>Lilaeopsis attenuata</i>	c3	perennial	forb	no	c3_nonlegume	3
LIPU	<i>Liatris punctata</i>	c3	perennial	forb	no	c3_nonlegume	3
LOPE	<i>Lolium perenne</i>	c3	perennial	graminoid	no	c3_nonlegume	9
MIQU2	<i>Mimosa quadrivalvis</i>	c3	perennial	forb	yes	c3_legume	15
NALE3	<i>Nassella leucotricha</i>	c3	perennial	graminoid	no	c3_nonlegume	19
OECU2	<i>Oenothera curtiflora</i>	c3	annual	forb	no	c3_nonlegume	3
OENOT	<i>Oenothera</i> spp.	c3	annual	forb	no	c3_nonlegume	1
PAVI2	<i>Panicum virgatum</i>	c4	perennial	graminoid	no	c4_nonlegume	12
PRGL2	<i>Prosopis glandulosa</i>	c3	perennial	shrub	yes	c3_legume	33
QUHA3	<i>Quercus harvardii</i>	c3	perennial	shrub	no	c3_nonlegume	3
QUMO	<i>Quercus mohriana</i>	c3	perennial	shrub	no	c3_nonlegume	1
RACO3	<i>Ratibida columnifera</i>	c3	perennial	forb	no	c3_nonlegume	40
RHAM	<i>Rhamnus</i> spp.	c3	perennial	shrub	yes	c3_legume	1
RHSET	<i>Rhynchosia senna</i>	c3	perennial	forb	yes	c3_legume	1
RUHI2	<i>Rudbeckia hirta</i>	c3	perennial	forb	no	c3_nonlegume	3
RUNU	<i>Ruellia nudiflora</i>	c3	perennial	forb	no	c3_nonlegume	15
RUTR	<i>Rubus trivialis</i>	c3	perennial	vine	no	c3_nonlegume	3
SAFA2	<i>Salvia farinacea</i>	c3	perennial	forb	no	c3_nonlegume	7
SCHIZ4	<i>Schizachyrium</i> spp.	c4	perennial	graminoid	no	c4_nonlegume	8
SCSC	<i>Schizachyrium scoparium</i>	c4	perennial	graminoid	no	c4_nonlegume	3
SODI	<i>Solanum dimidiatum</i>	c3	perennial	forb	no	c3_nonlegume	1
SOEL	<i>Solanum elaeagnifolium</i>	c3	perennial	forb	no	c3_nonlegume	53
SOHA	<i>Sorghum halapense</i>	c4	perennial	graminoid	no	c4_nonlegume	38
STTE3	<i>Stillingia texana</i>	c3	perennial	forb	no	c3_nonlegume	3

Table C3. List of sampled species and their plant functional group assignment (cont.)

Symbol	Species	Photo. pathway	Growth duration	Growth habit	N-fixer?	Plant functional group	Number sampled
VEOC	<i>Verbesina occidentalis</i>	c3	perennial	forb	no	c3_nonlegume	3
VEST	<i>Verbena stricta</i>	c3	perennial	forb	no	c3_nonlegume	3
WEAC	<i>Wedelia acapulcensis</i>	c3	perennial	shrub	no	c3_nonlegume	6

Table C4. Model selection results for soil moisture, air temperature, and vapor pressure deficit. Soil moisture was used in a bivariate regression against β , while vapor pressure deficit was used in bivariate regressions against leaf $C_i:C_a$ *

Day	Soil moisture		VPD	
	AICc	RMSE	AICc	RMSE
1	1431.77	0.8400	-772.71	0.0853
2	1431.76	0.8400	-775.47	0.0849
3	1431.78	0.8400	-770.86	0.0854
4	1431.79	0.8401	-793.49	0.0839
5	1431.79	0.8401	-771.66	0.0853
6	1431.78	0.8401	-771.66	0.0853
7	1431.78	0.8401	-771.05	0.0854
8	1431.76	0.8401	-770.94	0.0854
9	1431.75	0.8401	-770.11	0.0854
10	1431.74	0.8401	-770.08	0.0855
15	1431.54	0.8401	-768.64	0.0856
20	1431.40	0.8401	-769.77	0.0855
30	1431.23	0.8400	-772.18	0.0853
60	1429.84	0.8391	-779.06	0.0848
90	1429.14	0.8385	-773.99	0.0852

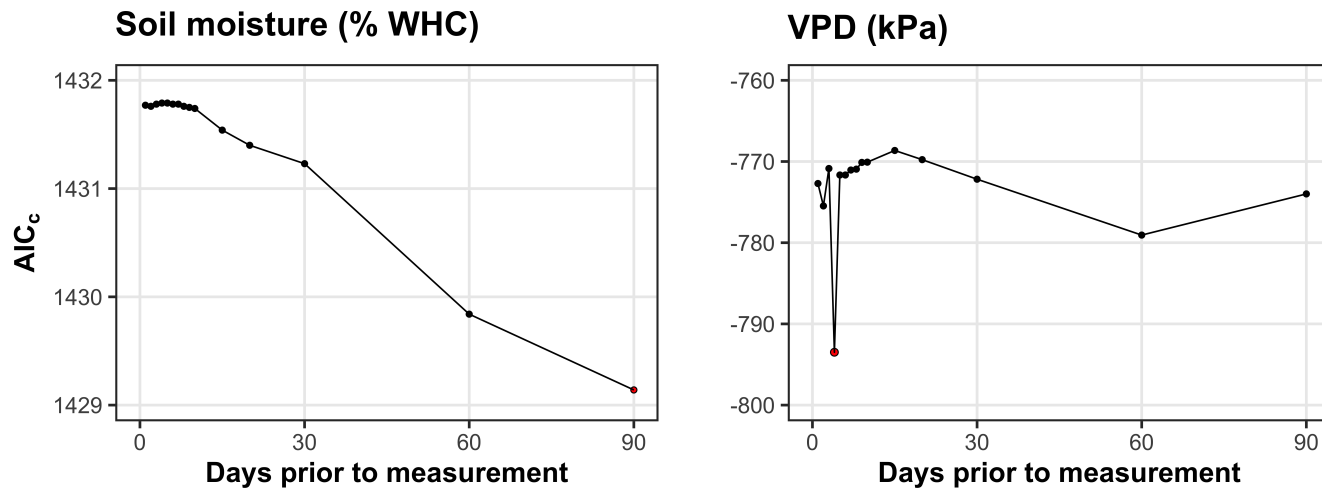


Figure C1. Model selection results exploring relevant timescales for soil moisture (left panel) and vapor pressure deficit (right panel). The x-axis indicates the number of days before each site visit and the y-axis notes the corrected Akaike Information Criterion value. The timescale with the lowest AIC_c value, and therefore most relevant timescale to include in statistical models, is noted as a red point.

**3726 Appendix D: Supplemental material for "Optimal resource investment
 3727 to photosynthetic capacity maximizes nutrient allocation to whole
 3728 plant growth under elevated CO₂"**

Table D1. Summary table containing volumes of compounds used to create modified Hoagland's solutions for each soil nitrogen fertilization treatment. All volumes are expressed as milliliters per liter (mL/L)

Compound	0 ppm N	35 ppm N	70 ppm N	105 ppm N	140 ppm N
1 M NH ₄ H ₂ PO ₄	0	0.165	0.33	0.5	0.67
2 M KNO ₃	0	0.335	0.67	1	1.33
2 M Ca(NO ₃) ₂	0	0.335	0.67	1	1.33
1 M NH ₄ NO ₃	0	0.165	0.33	0.5	0.67
8 M NH ₄ NO ₃	0	0	0	0	0
1 M KH ₂ PO ₄	1	0.85	0.67	0.5	0.33
1 M KCl	3	2.45	2	1.5	1
1 M CaCO ₃	4	3.33	2.67	2	1.33
2 M MgSO ₄	1	1	1	1	1
10% Fe-EDTA	1	1	1	1	1
Trace elements	1	1	1	1	1

Compound	210 ppm N	280 ppm N	350 ppm N	630 ppm N
1 M NH ₄ H ₂ PO ₄	1	1	1	1
2 M KNO ₃	2	2	2	2
2 M Ca(NO ₃) ₂	2	2	2	2
1 M NH ₄ NO ₃	1	3.5	0	0
8 M NH ₄ NO ₃	0	0	0.75	2
1 M KH ₂ PO ₄	0	0	0	0
1 M KCl	0	0	0	0
1 M CaCO ₃	0	0	0	0
2 M MgSO ₄	1	1	1	1
10% Fe-EDTA	1	1	1	1
Trace elements	1	1	1	1

Table D2. Summary of the daily growth chamber growing condition program

Time	Air temperature (°C)	Light (%)
09:00	21	25
09:45		50
10:30	25	75
11:15		100
22:45	21	75
23:30		50
00:15	17	25
01:00		0

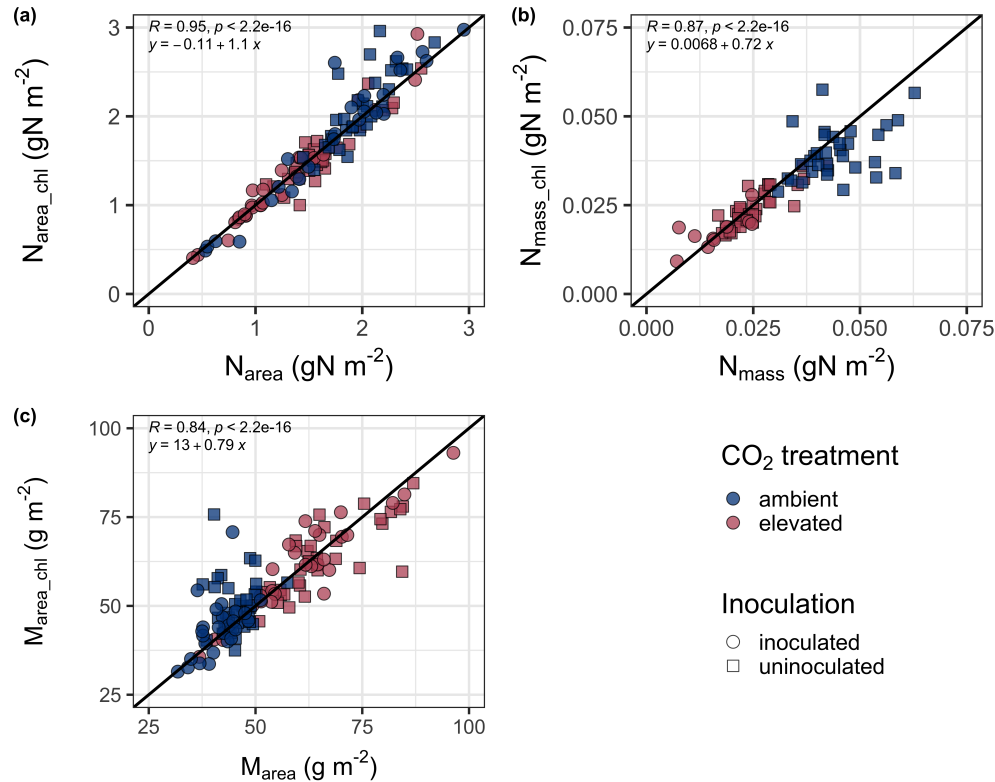


Figure D1. Relationships between area-based leaf nitrogen content (a), mass-based leaf nitrogen content (b), and leaf mass per unit leaf area (c) measured on the focal leaf used to generate A_{net}/C_i curves and leaf nitrogen content measured on the leaf used for chlorophyll extractions. Blue points refer to leaves grown under ambient CO₂ and red points refer leaves grown under elevated CO₂. Square points indicate uninoculated pots and circular points indicate inoculated pots. Pearson's correlation, associated p -values, and the line of the regression line that described each bivariate are included in the top left corner of each plot. The solid black line visualizes the trend given a 1:1 bivariate relationship.

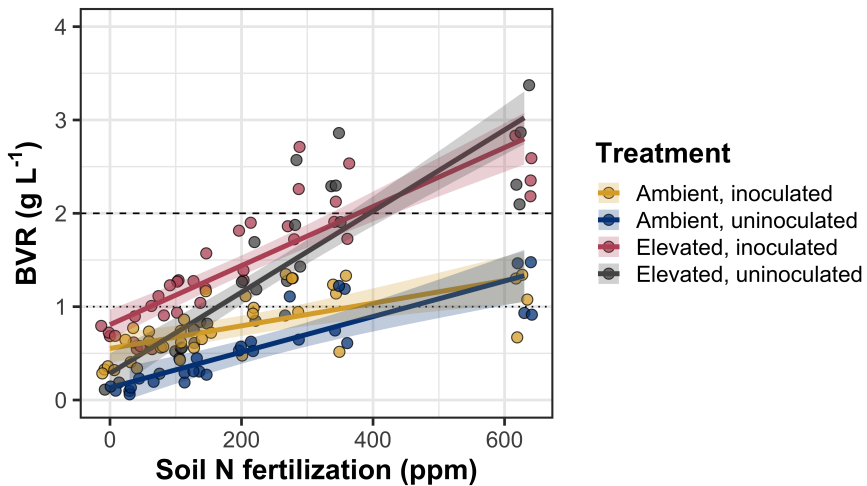


Figure D2. Effects of CO₂, fertilization, and inoculation on the ratio of whole plant biomass to pot volume. Soil nitrogen fertilization is represented on the x-axis in all panels. Yellow points and trendlines indicate inoculated individuals grown under ambient CO₂, blue points and trendlines indicate uninoculated individuals grown under ambient CO₂, red points and trendlines indicate inoculated individuals grown under elevated CO₂, and grey points indicate uninoculated individuals grown under elevated CO₂. Solid trendlines indicate regression slopes that are different from zero ($p < 0.05$), while dashed trendlines indicate slopes that are not distinguishable from zero ($p > 0.05$). The dotted horizontal line indicates the point where biomass:pot volume exceeds 1 g L⁻¹, and the dashed line indicates the point where biomass:pot volume exceeds 2 g L⁻¹.